Regulation of the microenvironment and chemoresistance in liver therapy

Blanca Cucarull Martínez

UNIVERSITAT DE BARCELONA

Faculty of Medicine and Health Sciences

Doctoral Programme in Biomedicine

REGULATION OF THE MICROENVIRONMENT AND CHEMORESISTANCE IN LIVER THERAPY

Doctoral thesis conducted at:

Department of Cell Death and Proliferation

Institute of Biomedical Research of Barcelona (IIBB)

Spanish National Research Council (CSIC)

Blanca Cucarull Martínez

PhD candidate

Dr. Albert Morales Muñoz

Director

Dr. Montserrat Marí Garcia

Co-director

Dr. Carles Enrich Bastús

Tutor

IibB

CSIC

CONSEJO SUPERIOR DE INVESTIGACIONES CIENTÍFICAS

Acknowledgements

I wish to express my sincere appreciation to my supervisor, Dr. Albert Morales for giving me the unique opportunity to carry out my doctoral thesis in his lab. Without his support and help, this project would not have been realized. I would also like to thank Dr. Montserrat Marí and Dr. Anna Colell for all their support and invaluable advice. I am grateful to Dr. Carles Enrich for being my tutor.

I would like to acknowledge Dr. Jordi Bruix and Dr. Maria Reig and all members of the BCLC group from Hospital Clínic de Barcelona for their collaboration. In addition, I am grateful to all the lecturers from the Biomedicine Department at UB for facilitating the completion of my PhD.

I am indebted to the Ministry of Science, Innovation and Universities of the Spanish Government and to the Agency for Management of University and Research Grants (AGAUR) of the Catalan Government for funding my PhD studies.

I would like to recognize the assistance and guidance of my lab colleagues. Anna Tutusaus, who is always ready to help, Estefanía de Gregorio, who is always willing to talk as well as to have some drinks, Vicente Roca, who has taught us how to enjoy every little moment, and Cristina de Dios, on whom everyone can rely. I would like to thank Dr. Milica Stefanovic and other former members of our group. I am grateful to Dr. Pablo García de Frutos for his collaboration and Dr. Cristina Aresté for her guidance and advice. Moreover, I would like to pay my special regards to Dr. Roser Cortés and all personnel from IIBB and CSIC who have aided me in scientific and non-scientific matters. I must admit that the work environment could not have been better.

I would also like to mention my friends, specially Álvaro and Andreu, with whom I have spent many good times. I could not thank enough the greatest support in my life, my mother Paqui, for always being there and helping me throughout my life. Thanks to her I have come this far. And to all my family. I would also like to thank my partner, Nacho, for his everyday support and patience since the day we met. A lot of new adventures lie ahead for us. And to all my in-laws, for all their support.

Overall, I would like to show my gratitude to everyone who has made this work possible.

Abstract

Hepatocellular carcinoma (HCC) is the most common liver cancer and currently the fourth cause of cancer-related death. Since its appearance, the multityrosine kinase inhibitor (MKI) sorafenib has been the standard systemic treatment for HCC patients. Recently, novel MKI have become available, such as lenvatinib, regorafenib and cabozantinib, as well as immune-based therapies. Still, the efficacy of MKI should be improved. On the other hand, the BCL-2 family of proteins tightly regulate programmed cell death. Therefore, BH3 mimetics, small molecules which mimic BCL-2 proteins, have been proposed as chemotherapeutic compounds to trigger cell death, although their efficacy against solid tumors has not been widely explored.

Firstly, we identified that regorafenib upregulated the mRNA expression of the anti-apoptotic BCL-xL in murine liver tumors. Taking these results into account, we proposed that regorafenib anti-tumor action could be enhanced by the addition of the BH3 mimetic A-1331852, which specifically targets the BCL-xL protein. When hepatoma cells were treated with this combination of agents, a potent cytotoxic effect was observed. Contrarily, ABT-199 administration, which blocks BCL-2, did not cooperate with regorafenib to increase cell death in liver cancer cells. The dual treatment of regorafenib and A-1331852 induced a loss in mitochondrial membrane potential, the release of cytochrome c and an increase in caspase-3 activity, indicating that the mitochondrial pathway of apoptosis was activated in liver cancer cells. Furthermore, regorafenib treatment was found to decrease MCL-1 protein levels in hepatoma cells. Hence, a specific inhibitor of MCL-1 together with A-1331852 was administered to HCC cells, resulting in strong cell death. Regorafenib and A-1331852 also reduced tumor liver spheroids growth. In a PDX mouse model, the co-administration of regorafenib and the BCL-xL antagonist A-1331852 reduced tumor volume and decreased its proliferation. This combination also proved to be effective even in regorafenib-resistant cells and animal models. Clinical data showed that the ratio of BCL-xL/MCL-1 was increased in HCC patients, including early and advanced stages of the disease. In short, the dual treatment of regorafenib and the BH3 mimetic A-1331852 was highly effective against HCC preclinical models.

MKI therapy has been described to increase reactive oxygen species (ROS) production. We wondered whether the employment of a pro-oxidant compound, like BSO, which

provokes an intracellular GSH depletion, could aid in sorafenib, regorafenib and cabozantinib effectiveness, or, on the contrary, the use of antioxidant supplements might counteract its efficacy. We observed that BSO-treated hepatoma cells were much more sensible to the administration of sorafenib and regorafenib. Both MKIs increased mitochondrial ROS generation in HCC cells, and that effect was enhanced with BSO pre-treatment. Likewise, the cytotoxic capacity of regorafenib and A-1331852 was found to be ROS-mediated. Hepatoma cells were treated with two different MKIs and BH3 mimetic combinations and the addition of the antioxidants MnTBAP and GSHe increased cell viability, suggesting that their use could considerably interfere with chemotherapy effectiveness. Liver cancer spheroids displayed an increase in mitochondrial ROS production when treated with BSO and sorafenib. Again, the use of MnTBAP and GSHe blocked sorafenib effect on tumor liver spheroids. Finally, an induction of mitophagy was observed with the depletion of GSH and sorafenib/regorafenib treatment in hepatoma cells. In conclusion, MKIs exert their cytotoxicity via a mitochondrial ROS generation and antioxidants supplementation may restrain MKI chemotherapeutic effect in liver cancer cells.

Resumen

El carcinoma hepatocelular (CHC) es el tipo de cáncer hepático más común y actualmente la cuarta causa de muerte por cáncer en el mundo. Desde su aparición, el inhibidor de receptores tirosina quinasa sorafenib ha sido el tratamiento sistémico estándar para los pacientes con CHC. Recientemente han surgido nuevos inhibidores multiquinasa, como el lenvatinib, el regorafenib y el cabozantinib, así como terapias inmunológicas. Con todo, la eficacia de los inhibidores multiquinasa debería ser mejorada. Por otra parte, la familia de proteínas de BCL-2 es clave en la regulación de la muerte celular programada. Así pues, los miméticos de BH3, moléculas que imitan la estructura de las proteínas BCL-2, han sido propuestos como agentes quimioterápicos para desencadenar la muerte celular, aunque su eficacia contra tumores sólidos no ha sido ampliamente explorada.

Inicialmente, identificamos que el regorafenib incrementó la expresión a nivel de ARNm del miembro pro-apoptótico BCL-xL en tumores hepáticos de ratón. Teniendo en cuenta estos primeros resultados, hipotetizamos que la acción antitumoral del regorafenib podría ser potenciada con la adición del mimético de BH3 A-1331852, que bloquea específicamente la proteína BCL-xL. Cuando las células tumorales hepáticas fueron tratadas con esta combinación de fármacos, se observó un potente efecto citotóxico. Por el contrario, la administración de ABT-199, que antagoniza la proteína BCL-2, no contribuyó a aumentar el efecto antiproliferativo del regorafenib en las células tumorales hepáticas. El tratamiento dual de regorafenib y A-1331852 provocó una pérdida de potencial de la membrana mitocondrial, la liberación del citocromo c en el citosol y un aumento de la actividad de caspasa-3, indicando la activación de la vía mitocondrial de la apoptosis en estas células. Además, el tratamiento con regorafenib disminuyó los niveles proteicos de MCL-1. En consecuencia, se administró un inhibidor específico de MCL-1 junto con A-1331852 a las células tumorales hepáticas, resultando en una muerte celular intensa. El regorafenib y el compuesto A-1331852 también redujeron el crecimiento de los esferoides de tumores hepáticos. En un modelo PDX de ratón, la co-administración de regorafenib y del antagonista de BCL-xL disminuyó el volumen tumoral y su proliferación. Esta combinación demostró ser efectiva también en células tumorales hepáticas resistentes a regorafenib y en modelos animales. Los datos clínicos mostraron que el ratio BCL-xL/MCL-1 está incrementado en pacientes con CHC,

incluyendo tanto estadios tempranos como tardíos de la enfermedad. En conjunto, el tratamiento dual del regorafenib y el mimético de BH3 A-1331852 fue altamente efectivo frente a modelos preclínicos de CHC.

Se ha descrito que la terapia con inhibidores multiquinasa incrementa la producción de especies reactivas del oxígeno (EROs). Nos preguntamos si el uso de un compuesto pro-oxidante, como el BSO, que provoca una disminución de los niveles intracelulares de GSH, podría incrementar la efectividad de sorafenib, regorafenib y cabozantinib, o, por el contrario, el empleo de suplementos antioxidantes podría contrarrestar su eficacia. Observamos que las células de hepatoma tratadas con BSO fueron mucho más sensibles al tratamiento con sorafenib y regorafenib. Estos dos inhibidores multiquinasa aumentaron la generación de EROs mitocondriales y este efecto fue potenciado con un tratamiento previo con BSO. Así mismo, la capacidad citotóxica del regorafenib y A-1331852 demostró estar mediada por EROs. En células de hepatoma que se trataron con dos combinaciones distintas de inhibidores multiquinasa y miméticos de BH3, los antioxidantes MnTBAP y GSHe incrementaron la viabilidad celular, sugiriendo que su uso podría interferir considerablemente con la efectividad de la quimioterapia. Los esferoides tumorales hepáticos mostraron un aumento en la producción de EROs mitocondriales cuando se trataron con BSO y sorafenib. De nuevo, el suplemento de MnTBAP y GSHe bloqueó la acción de sorafenib en los esferoides tumorales hepáticos. Finalmente, se observó una inducción de la mitofagia con la disminución de GSH y el tratamiento con sorafenib/regorafenib en las células de hepatoma. En conclusión, los inhibidores multiquinasa ejercen su acción citotóxica vía la generación de EROs mitocondriales y la suplementación con antioxidantes podría impedir el efecto quimioterapéutico de los inhibidores multiquinasa en las células tumorales hepáticas.

Contents

List of figures

List of abbreviations

Abbreviation	Explanation
AFP	Alpha fetoprotein
AKT	Protein Kinase B
AIF	Apoptosis-inducing factor
ALBI	Albumin-bilirubin
ALL	Acute lymphoblastic leukemia
ALP	Alkaline phosphatase
ALT	Alanine transaminase
AML	Acute myeloid leukemia
Ang-1/2	Angiopoietin-1/-2
AOPP	Advanced oxidation protein products
APAF1	Apoptotic protease-activating factor 1
α-SMA	Alpha-smooth muscle actin
ATG	Autophagy-related
ATO	Arsenic trioxide
BAD	BCL-2-associated agonist of cell death
BAFs	BRG1- or HRBM-associated factors
BAX	BCL-2-associated X protein
BCL-2	B-cell lymphoma 2
BCLC	Barcelona Clinic Liver Cancer
BH	BCL-2 Homology
BID	BH3 interacting domain death agonist (BID)
BIK	BCL-2-interacting killer
BMF	BCL-2-modifiying factor
BNIP3	BCL2/adenovirus E1B 19 kDa protein-interacting protein 3
BSO	Buthionine sulfoximine
CAFs	Cancer-associated fibroblasts
CAT	Catalase
CLL	Chronic lymphocytic leukemia
CRC	Colorectal cancer
CSC	Cancer stem cell

DLBCL	Diffuse large B-cell lymphoma
DRP1	Dynamin-related protein 1
EC	Endothelial cells
ECM	Extracellular matrix components
EGF	Epidermal growth factor
EMT	Epithelial-mesenchymal transition
ERK	Extracellular signal regulated kinase
FABP4	Fatty acid binding protein 4
FAK	Focal adhesion kinase
FGF	Fibroblast growth factor
FL	Follicular lymphoma
FLT-3	Fms like tyrosine kinase 3
FUNDC1	FUN14 Domain Containing 1
GCS	Gamma-glutamylcysteine synthetase
GPx	Glutathione peroxidase
GR	Glutathione reductase
GRX2	Glutaredoxin 2
GSH	Glutathione
GST	Glutathione S-transferase
HBV	Hepatitis B virus
HBx	Hepatitis B viral x
HCC	Hepatocellular carcinoma
HCV	Hepatitis C virus
HGDNs	High-grade dysplastic nodules
HGF	Hepatocyte growth factor
HIF-1α	Hypoxia-inducible factor 1-alpha
HR	Hazard ratio
HRK	Activator of apoptosis harakiri
HSCs	Hepatic stellate cells
HUVEC	Human umbilical vein endothelial cell
IAPs	Inhibitors of apoptosis proteins
IFNγ	Interferon gamma
IMM	Inner mitochondrial membrane

KEAP1	Kelch-like ECH-associated protein 1
K_i	Inhibition constant
LA	Lysophosphatidic acid
LGDNs	Low-grade dysplastic nodules
MAPK	Mitogen-activated protein kinase
MCL	Mantle cell lymphoma
MCL-1	Myeloid cell leukemia sequence 1
MDA	Malondialdehyde
MDS	Myelodysplastic syndrome
MDSCs	Myeloid-derived suppressor cells
MEF	Mouse embryonic fibroblasts
MEK	MAPK/ERK kinase
MFN	Mitofusin
MKI	Multikinase inhibitor
MM	Multiple myeloma
MMP	Mitochondrial membrane potential
MMPs	Metalloproteinases
MnTBAP	Mn(III)tetrakis(4-benzoic acid) porphyrin
MOMP	Mitochondrial outer membrane permeabilization
mTOR	Mammalian target of rapamycin
NAFLD	Non-alcoholic fatty liver disease
NASH	Non-alcoholic steatohepatitis
NF-κB	Nuclear factor kappa-light-chain-enhancer of activated B cells
NFR2	Nuclear factor erythroid 2-related factor 2
NHL	Non-Hodgkin lymphoma
NIX	BNIP3-like
NK cells	Natural killer cells
NSCLC	Non-small-cell lung cancer
OGC	2-oxoglutarate carrier
OPTN	Optineurin
OXPHOS	Oxidative phosphorylation
PBAF	Polybromo-associated BAF
PD-1	Programmed cell death 1

PD-L1	Programmed cell death 1 ligand 1
PDGF	Platelet-derived growth factor
PDX	Patient-derived xenografts
PI3K	Phosphatidylinositol-3-kinase
PINK1	PTEN-induced putative kinase 1
PUMA	p53 upregulated modulator of apoptosis
RNS	Reactive nitrogen species
ROS	Reactive oxygen species
SCLC	Small cell lung cancer
SOD	Superoxide dismutase
STAT3	Signal transducer and activator of transcription 3
TAMs	Tumor-associated macrophages
TGF-β	Transforming growth factor beta
TIE2	Angiopoietin-1 receptor
TKI	Tyrosine kinase inhibitor
TME	Tumor microenvironment
TNF	Tumor necrosis factor
TNM	Tumor, Node, Metastasis
TRAIL	TNF-related apoptosis-inducing ligand
Tregs	Regulatory T cells
TRX2	Thioredoxin 2
TRXPs	Thioredoxin peroxidase
VDAC1	Voltage-dependent anion-selective channel 1
VEGF	Vascular endothelial growth factor
VEGFA	Vascular endothelial growth factor A
xCT	Cysteine/glutamate transporter
ZEB1	Zinc finger E-box-binding homeobox 1

Introduction

1. Hepatocellular carcinoma

1.1. Epidemiology

Liver cancer is the sixth most frequent neoplasm and the fourth cause of cancer-related death, with 841,080 new cases and 781,631 deaths annually[1]. Among liver cancers, hepatocellular carcinoma (HCC) accounts for 90% of primary liver tumors[2]. HCC develops in a context of chronic liver disease in most cases and is more frequent in men than in women in a ratio 2:1[1].

Common risk factors of HCC are chronic infection with hepatitis B virus (HBV) and aflatoxin B1 exposure in eastern Asia and sub-Saharan Africa, while in Europe, Japan and North America the main risk factors are hepatitis C virus (HCV) and alcohol use[3]. These causes together with haemochromatosis and alpha-1-antitrypsin deficiency can also lead to cirrhosis, another well-known factor in the development of HCC. Tobacco and HIV infection also increase the risk of developing HCC. Non-alcoholic fatty liver disease (NAFLD) and non-alcoholic steatohepatitis (NASH), including metabolic syndrome, diabetes and obesity, are emerging as HCC causes[4], particularly in women, possibly driving the increase in overall HCC cases[5].

HCC can be prevented by vaccination against the infection with HBV[6]. In patients with HCV, interferon and direct-acting antivirals might reduce the risk of HCC development[7]. Coffee consumption and statins use have also been linked to a decrease in HCC incidence[8,9].

1.2. Molecular pathogenesis

1.2.1. Cellular origin

The cell of origin of HCC remains unclear. It has been suggested, as in numerous cancer types, that liver stem cells may be responsible for initiating HCC, but also a transit-amplifying population or mature hepatocytes. Some preclinical murine models of HCC support the likelihood of mature hepatocytes being the origin of HCC. Other models reinforce the idea that HCC may arise from liver stem cells[10,11]. Intrahepatic cholangiocarcinomas, tumors that are present in bile ducts, or mixed HCC and cholangiocarcinomas frequently derive from mature hepatocytes, suggesting cell plasticity[12,13].

1.2.2. Molecular drivers

70-80% of HCC develop in a context of cirrhosis that involves a complex multistep process[3,14]. In the cirrhotic liver, HCC starts with the presence of pre-cancerous cirrhotic nodules, called low-grade dysplastic nodules (LGDNs) that can transform into high-grade dysplastic nodules (HGDNs), and, in turn, into early-stage HCC and progress to advanced HCC[3]. Without underlying cirrhosis (20-30% cases), HCC can develop mainly on a background of HBV infection or NASH[15] or, less frequently, adenomas[16].

HCC arises from the accumulation of somatic mutations and epigenomic alterations. While most of them occur in 'passenger' genes, a few of them are regarded as 'drivers' responsible for the activation of key signaling pathways leading to hepatocarcinogenesis[17]. In dysplastic nodules and established HCC, mutations of *TERT* promoter, which encodes the synthesis of telomere reverse transcriptase, are frequent (6% in LGDNs, 20% in HGDNs and 60% in HCC)[18,19]. The WNT-β-catenin pathway is frequently activated in HCC due to mutations in *AXIN1* and *CTNNB1* (11-37% cases)[20,21]. p53 inactivation and cell cycle control alterations (*CDKN2A*) are also common in HCC, especially in aflatoxin B1 exposure and HBV infection[22,23]. Furthermore, defects in chromatin remodeling complexes and epigenetic regulators are often found in HCC, including mutations in the BRG1- or HRBM-associated factors (BAFs) and polybromo-associated BAF (PBAF) chromatin complex (*ARID1A* and *ARID2*, being 10% and 5% of cases, respectively)[15,19,24]. Receptor tyrosine kinase (RAS-RAF-MAPK) and phosphatidylinositol-3-Kinase, Protein Kinase B and mammalian target of rapamycin (PI3K-AKT-mTOR) pathways are usually activated in HCC, owing to the amplification of a region that includes *FGF19* (5% tumors) and mutations in *RPS6KA3* and *RSK2* (5-9% cases)[25,26]. Oxidative stress signaling pathway is also activated through activating mutations in nuclear factor erythroid 2-related factor 2 (*NFE2L2* or NFR2) or inactivation of Kelch-like ECH-associated protein 1 (*KEAP1*)[27]. DNA amplifications take place in chromosome regions 11q13 and 6p21, affecting the oncogene cyclin D1 (*CCND1*) and neoangiogenic vascular endothelial growth factor A (*VEGFA*) respectively, inducing the latter the secretion of macrophage-mediated hepatocyte growth factor (HGF) secretion and thus, tumor proliferation[28,29]. However, many of the aforementioned mutations in HCC are still not druggable[26,30].

1.2.3. Molecular classes

Genomic, transcriptomic and epigenomic profiling analyses have allowed establishing a molecular classification of HCC. Despite the fact this classification is not used yet in clinical practice, it correlates with clinical features[14,31]. Two molecular subtypes have been identified: the proliferation class and the nonproliferation class[32]. Cell proliferation and survival pathways, such as PI3K-AKT-mTOR, RAS-MAPK and MET, chromosomal instability, *TP53* inactivation, *FGF19* and *CCND1* amplifications and α-fetoprotein overexpression characterize the proliferation class. It is related to HBV infection and has a poor clinical outcome[33]. However, tumors that belong to the nonproliferation class have often an activation of *CTNNB1* and more *TERT* promoter mutations. Transcriptionally, those tumors are similar to normal hepatocytes and are related to alcohol use and HCV infection etiologies and have better outcomes[15,34].

Tumor microenvironment (TME) is considered to play a fundamental role in all steps of carcinogenesis[35]. HCC has an inflammatory milieu due to, viral hepatitis, alcohol abuse and NAFLD or NASH. Immune cells, such as lymphocytes and macrophages, stellate cells and endothelial cells interact with hepatocytes in the chronically inflamed liver[3,17]. HCC that have high immune cell infiltration, activation of programmed cell death protein 1 (PD-1)/programmed cell death 1 ligand 1 (PD-L1), activation of IFNγ signaling pathway and granzyme B and perforin 1 expression could be grouped into an 'immune class' and constitute the 30% of tumors. Two different subclasses can be found within the 'immune class', an adaptive T cell response can identify the 'active immune' subtype, whereas the 'exhausted subclass' exhibits TGFβ-mediated immunosuppression and T cell exhaustion[36]. On the other hand, 25% of HCC lack of the infiltration of immune cells.

1.3. Surveillance

Patients with HCC at early stages may benefit the most from surveillance, since the symptoms caused by HCC are often detected at advanced stages of the disease and, therefore, those patients are not eligible for curative treatment[3].

Survival benefits of HCC surveillance have been shown in several publications that include mathematical models, a clinical trial and a meta-analysis of cohort studies[37,38]. Surveillance could be useful for patients with cirrhosis (having more of 1.5% incidence of HCC per year), as well as patients who are candidates for liver transplant[39]. Patients with chronic HBV infection have different risk of developing HCC depending on their

geographic region. Age, male sex, liver fibrosis, high viral replication, genotype C and a family history of HCC also increase such risk[40]. While patients with chronic HCV infection and fibrosis should be enrolled on a surveillance program, patients who have developed NAFLD in absence of cirrhosis are not eligible for surveillance, since the risk of HCC is likely to be rather low[15]. Abdominal ultrasonography every six months is the preferred test for surveillance. It has a sensitivity of 60-80% and a specificity of more than 90%[41]. The most common serological tumor marker is α-fetoprotein (AFP), although its sensitivity is around 60%[42]. Recent advances in this area have uncovered that liquid biopsy and the analysis of circulating tumor DNA may provide a novel tool for early detection of HCC[43].

1.4. Diagnosis

Diagnostic algorithms based on nodule size and detection have been described elsewhere[2,44]. Imaging techniques allow the distinction of a pattern of hyperenhancement in the arterial phase and washout in venous or delayed phases on contrast-enhanced CT or MRI. This is because, in patients with cirrhosis, during malignant transformation of hepatocytes, benign lesions receive blood supply from the portal system while malignant nodules are supplied from the hepatic artery[45]. Immunohistochemical markers such as glypigan 3, heat shock protein 70, glutamine synthetase and clathrin heavy chain can increase the accuracy at the time of diagnosis[46].

1.5. Staging

Most patients with HCC have concomitant liver disease. For this reason, the prognosis evaluation must include tumor stage, the degree of liver dysfunction and performance status[15,44]. Furthermore, the prognostic prediction should be linked to treatment indication[47]. Among others, the most relevant staging systems are the "Cancer of the Liver Italian Program" (CLIP score), the "Hong Kong Liver Cancer" (HKLC) staging system, and the "Tumor, Node, Metastasis" (TNM)[48]. Worth mentioning, the "Barcelona Clinic Liver Cancer" (BCLC) algorithm is the staging system most widely applied for HCC. Since 1999, when it was first introduced, it has been updated according to clinical data[49].

The BCLC system quantifies tumor burden depending on the number and size of lesions and the presence/absence of macrovascular tumor invasion. In addition, the Child-Pugh

grade assesses liver function impairment, although it has limited predictive power[2]. The albumin-bilirubin (ALBI) score stratifies patients across BCLC stages, but its role in clinical decision making or stratification in trials is yet to be defined[2,44].

High AFP serum levels are linked to a poorer prognosis. Some studies have described that increased AFP levels can predict risk of tumor relapse after surgical resection[50] or response to loco-regional treatment and survival in HCC[51,52]. Vascular endothelial growth factor (VEGF), angiopoietin 2 (Ang2) or KIT may improve prognostic prediction, but these markers are still to be implemented on the individual assessment of a specific patient[44,52].

1.6. Tumor microenvironment in HCC

The interaction of the microenvironment with the tumor plays a relevant role in HCC pathogenesis. The tumor microenvironment is directly implicated in the modulation of liver fibrosis, the process of hepatocarcinogenesis, the epithelial-mesenchymal transition (EMT), invasion and metastasis[53,54].
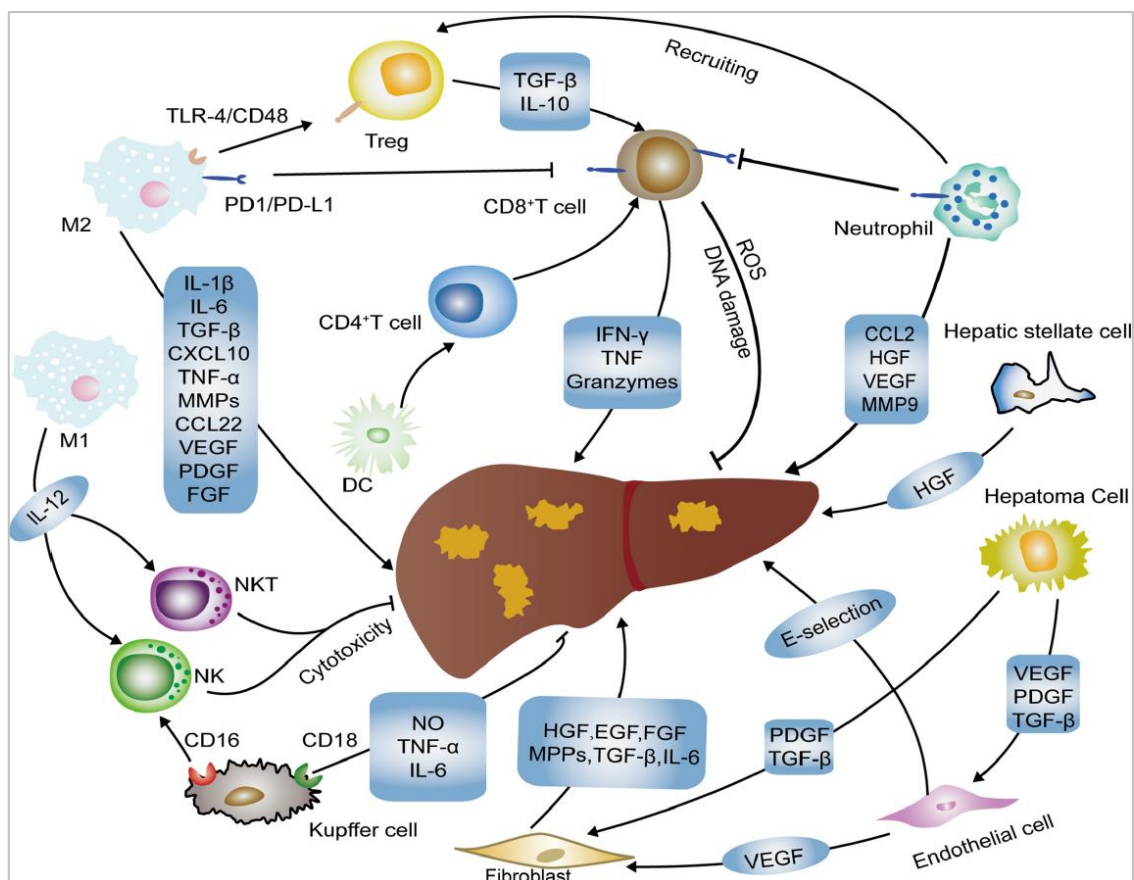
Figure 1. Components of tumor microenvironment implicated in the onset and progression of HCC. Extracted from Qin et al., 2020, Ref 54.

1.6.1. Hepatic Stellate Cells

Hepatic stellate cells (HSCs) are major components of liver connective tissue. They are localized in the basolateral surface of hepatocytes and the anti-luminal side of sinusoidal cells[55]. HSCs are in charge of vitamin A storage, synthesis of matrix metalloproteinases (MMPs) and extracellular matrix components (ECM, collagen), release of cytokines (IL-6 and IL-1β), defensin-1, chemokines (CCL5, CCL2) and growth factors (TGF-α/β, EGF, PDGF, bFGF)[55,56]. Normally, HSCs are in a quiescent state. Upon liver injury, they become activated, their cytoskeleton becomes remodeled through an increased expression of alpha-smooth muscle actin (α-SMA) and there is also a rise in cytokines, ECM components and growth factors production[55]. In the activated state, HSCs transdifferentiate into myofibroblast-like cells. This phenotype makes them more contractile, so they can infiltrate the HCC stroma and localize around fibrous septa, sinusoids and capsules[57,58].

Conditioned media from tumoral hepatocytes has been found to increase the proliferation of rat HSCs and induce the expression of HSCs activation markers[59,60]. Similarly, another study demonstrated that collected media from HSCs potentiated the tumorigenic capacity of HCC cancer cell lines[61]. The co-culture of hepatoma cells and activated HSCs also revealed the activation of genes related to inflammation, chemotaxis, angiogenesis and metalloproteinase from microarray analysis data[62,63]. Regarding *in vivo* studies, the co-implantation of HCC and HSCs cells in nude mice increased tumor growth via NF-κB and extracellular signal regulated kinase (ERK) pathways activation[61,64]. In this sense, a previous study from our group showed that angiogenin was responsible for the crosstalk between HCC and HSCs cells both *in vitro* and in mice models[65].

HSCs are also involved in the promotion of angiogenesis in HCC, diverse mechanism are responsible for this, among them the secretion of angiopoietin-1[66], or IL-8[67]. Moreover, PDGF secreted by tumor and endothelial cells has been described to attract HSCs, while at the same time, HSCs secrete VEGF thus promoting angiogenesis[68].

Several studies have pointed out that the secretion of IL-6 by HSCs may promote HCC progression[69,70]. In an HCC murine model with obesity, insulin resistance, and dyslipidemia, fatty acid binding protein 4 (FABP4) was enriched in intra-tumoral HSCs, contributing to hepatocarcinogenesis[71]. Co-culture of HSCs with HCC cells demonstrated that overexpression miR-1246 secreted by HSCs or the silencing of its target RORα increased proliferation, invasion and metastasis of HCC cells, with the involvement of Wnt/β-catenin pathway[72]. Zinc finger E-box-binding homeobox 1 (ZEB1)

was also described to target Wnt/β-catenin pathway and activate HSCs that, in turn, promoted HCC cells progression[73].

HSCs have been described to promote tumor chemoresistance. The laminin-332/α3 integrin axis and the ubiquitination of focal adhesion kinase (FAK) by HSCs were demonstrated to be involved in sorafenib chemoresistance[74]. FGF9, expressed only by HSCs, promoted the tumorigenic capacity of HCC cells and the resistance to sorafenib. FGF9 overexpression was associated to poor prognosis in patients with HCC[75].

While most studies favor a role for HSCs in promoting HCC, HSCs have also been found to detain HCC progression. In particular, endosialin secreted by HSCs was reported to negatively regulate HCC proliferation in inducible mouse models of HCC[76].

1.6.2. Cancer-associated fibroblasts

Fibroblasts are present in the fibrillar matrix of connective tissue. They are responsible for wound healing, formation of ECM, tissue maturation and the inflammatory response[77]. Cancer-associated fibroblasts (CAFs) are a sub-group of fibroblasts that are activated and implicated in cancer progression. Although CAFs arise from normal fibroblasts, CAFs can also derive from epithelial cells, endothelial cells, smooth muscle cells, bone marrow-derived progenitor cells and pre-adipocytes[78]. An interesting work showed that HCC cells secrete lysophosphatidic acid (LA). LA is involved in tumor initiation, progression, invasion and metastasis[79]. LA is believed to promote fibroblast differentiation into CAFs through a paracrine mechanism[80]. Additionally, HCC tumors frequently develop on a cirrhotic liver in which there is a great amount of activated fibroblasts[81]. Therefore, CAFs may contribute to HCC tumor progression by producing growth factors (EGF, FGF, HGF and TGF-β), chemokines (SDF-1), cytokines (IL-6) and metalloproteinases (MMP-3 and MMP-9)[82–84]. Moreover, the exosomal miR-1228-3p released by CAFs and directed to HCC cells was described to be involved in chemoresistance[85].

Interestingly, there is a growing number of evidence showing that the crosstalk between CAFs and HCC tumors could be mediated by miRNAs contained in exosomes. For example, low miR-150-3p levels secreted by CAFs have been discovered to be involved in HCC migration and invasiveness as well as poor clinical outcome[86]. Interestingly, the upregulation of mirR-335-5p by CAFs inhibited HCC tumor cells proliferation *in vitro* and *in vivo*[87]. Moreover, HCC tumor cells were found to induce the conversion of HSCs into

CAFs through the secretion of miR-21, that promoted cancer progression via the secretion of the angiogenic factors VEGF, MMP2, MMP9, bFGF and TGF-β[88].

CAFs have also been shown to maintain cancer stem cell(CSC)-like features by inducing the expression of Notch3 and the activation of chromatin modification factor lysine-specific demethylase 1 (LSD1)[89]. Another work also found that the release of IL-6 by CAFs induced stem cell phenotype in HCC cells through Notch signaling as well[90].

1.6.3. Tumor-Associated Macrophages

Macrophages around the tumor site are called tumor-associated macrophages (TAMs). Macrophages can display M1 (classic) or M2 (alternative) phenotype depending on their tumor-suppressing or tumor-promoting role[91]. M1 macrophages produce Th1-cytokines, such as IFN-γ, and are activated by LPS and other microbial antigens. They exhibit high antigen-presenting capacity and increased cytotoxic activity thereby producing reactive oxygen species (ROS)[92]. On the contrary, M2 macrophages are polarized by Th2-type cytokines IL-4, IL-13, glucocorticoids and TGF-β. Their antigen-presenting capacity is low. M2 macrophages decrease inflammation, suppress the adaptive immune system and promote tumor progression, angiogenesis and tissue repair[93].

In HCC, M2 macrophages have been found to promote tumor progression and metastasis with the involvement of glypican-3, a member of the glypican family of heparin-sulfate proteoglycans reported to be highly expressed in the majority (>70%) of HCC[94]. In addition, TGF-β1 secretion by TAMs promoted cancer progression, CSC-like phenotype and EMT in HCC[95,96], and moreover, TAM-production of IL-6, via STAT3, also promoted stemness in HCC[97]. Moreover, in a murine model of HCC, intra-tumoral macrophages expressing MMP-9 were involved in ECM remodeling, thus favoring tumor progression[98]. While in another study the presence of TAMs correlated with tumor vascularity, pointing towards the ability of TAMs in promoting angiogenesis[99].

It has been shown, in Hepa1-6 HCC tumors, that in the early phase of tumor development infiltrated macrophages displayed a tumor suppressing phenotype, while at advanced stages the TAM population increases and is associated to tumor progression[100]. Interestingly, a novel work has found that M2 macrophage-derived exosomes facilitate HCC metastasis by transferring α(M) β(2) integrin to tumor cells[101]. At the same time, tumor cells have been found to release Wnt ligands that promoted M2 polarization of macrophages and, in turn, promoted tumor growth, invasion and immunosuppression in

HCC[102]. In this regard, treatment of HCC with sorafenib has been shown to induce the repolarization of alternative macrophages to M1 phenotype through IGF-1 signaling[103].

Additionally, in HCC human samples, TAM infiltration was linked with PD-L1 overexpression[104]. Although M1 macrophages have been considered to exert an anti-tumor role, a new study has demonstrated that M1 macrophages promoted PD-L1 expression in HCC tumor cells, highlighting the potential role of M1 macrophages in tumor promotion through IL-1β pathway[105]. In fact, Kupffer cells, resident macrophages in the liver, have been reported to mediate tumor growth in HCC by producing PD-1 receptor that interacts with PD-L1 in CD8$^+$ T cells, impairing CD8$^+$ T cell response[106]. In addition, Kupffer cells produce osteopontin that is involved in inflammation, tumor progression and mestastasis[107].

1.6.4. Endothelial cells

Endothelial cells (ECs) are present in the interior face of blood vessels. Other cells, such as HSCs, stabilize the layer that they conform and control the vessel size and elasticity[108]. The interactions of ECs with the ECM and basement membrane proteins play a role in proliferation, stability and neoangiogenesis. When the basement membrane degrades, ECs become exposed to collagen, which triggers the formation of new blood vessels[109]. Neovascularization favors tumor proliferation, invasion and metastasis, since the new blood supply provides oxygen and nutrients to the tumor[110]. Tumor blood vessels have structural abnormality and increased permeability. ECs carry angiogenic receptors, for instance VEGFR, EGFR, PDGFR and CXCR[111]. Additionally, hypoxia is a known driver of tumor angiogenesis. Many studies conducted in HCC preclinical models have shown that hypoxia-inducible factor (HIF) proteins led to the activation of VEGF that promote angiogenesis[112–114]. VEGF and VEGFRs are crucial for HCC development[115,116]. The binding of VEGF ligands to their receptors elicits downstream phosphorylation that results in EC proliferation and the formation of new branches of blood vessels[117]. High VEGF levels in serum have been found to associate with bad prognosis in HCC patients who underwent surgical resection[118], since sVEGF concentration has been showed to correlate with angiogenesis, invasion and metastasis of HCC[119]. The interaction of platelet-derived growth factors (PDGF) with PDGF receptors (PDGFR) triggers the activation of the same signaling pathways as the binding of VEGF and VEGFRs not only in ECs but also in fibroblasts, smooth muscle cells and HSCs[120]. In this sense, PDGFRα expression was associated to microvascular invasion[121].

Additionally, fibroblast growth factor (FGF) and fibroblast growth factor receptors (FGFR) regulate also cell growth and angiogenesis[122]. Basic fibroblast growth factor (bFGF) fostered VEGF expression and their synergistic effect contributed to HCC development and neovascularization[123]. Of interest, Angiopoietin-1 (Ang-1) and 2 (Ang-2) bind to their receptor, Tie2, to stimulate angiogenesis[124]. Ang-1 and Ang-2 expression was detected in hepatoma, HSCs, ECs and smooth muscle cells, while Tie2 receptor was only identified in ECs, HSCs, smooth muscle cells and monocytes[125,126]. Ang-2 serum levels were high in patients with cirrhosis and HCC[127], being a prognosis marker[128]. Ang-2 exhibited a synergistic effect with VEGF in the development of angiogenesis in HCC in mice, through the activation of MMP-2 and MMP-9[129]. Ang-2 was included in a five-gene signature that effectively predicted HCC rapid growth[130]. As other pro-angiogenic factors, Ang-2 was also played a role in the promotion of HCC invasion and metastasis[131].

Another angiogenic marker of HCC in ECs is CD105 (endoglin), whose expression correlated with tumor recurrence and metastasis[132]. Furthermore, CD105+ tumor-derived ECs isolated from HCC displayed higher angiogenic activity and were more resistant to chemotherapeutic agents[133].

1.6.5. Tumor-Associated cells of the innate immune system

Innate immune mechanisms, known drivers of liver disease progression in pre-HCC conditions such as fibrosis or cirrhosis, may either support or counteract tumor-related immune activation. Intensive research has been performed to decipher the immunological mechanisms that are involved in initiation and progression of liver cancer. In the context of HCC, various studies on the effects of immunotherapies have been conducted with partially conflicting results, which might be explained by the fact that the efficacy of immunotherapies depends on very complex and only poorly understood interactions between many different immune cells, tumor cells and cells of the tumor environment. For reviews on the subject see[134,135].

In recent years, tumor-infiltrating immune cells have been intensively analyzed and characterized[135]. For numerous solid tumors, including primary liver cancer, associations between certain immune cell populations and response to therapy as well as on prognosis have been proposed. Although the precise significance of the tumor immune microenvironment is still not fully understood, a high density of myeloid cells including TAMs (already commented in section 1.6.3), and myeloid-derived suppressor cells

(MDSCs) are abundant in the HCC microenvironment and are often associated with poor prognosis. This is because, generally, myeloid cells in HCC play a vital role in supporting tumor initiation, progression, angiogenesis, metastasis, and therapeutic resistance[136]. On the other hand, a high density of infiltrating T-effector cells is often associated with a good prognosis[137]. In general terms, a 'pro-inflammatory' tumor microenvironment and infiltrating natural killer (NK) cells, and CD8-expressing T cells are associated with improved clinical outcomes in a broad range of tumor types[138]. Natural killer (NK) cells account for 25-50% of the total number of hepatic lymphocytes, which implicates that NK cells play an important role in liver immunity. The frequencies of both circulating and tumor infiltrating NK cells are positively correlated with survival benefit in hepatocellular cancer (HCC)[139]. The inhibitory function of other immune cells, for example, MDSCs and regulatory T cells, appear to have a major role in disrupting the capacity for the immune control of cancers[137].

1.7. Systemic therapies for HCC

Clinical treatment of HCC includes surgical therapies, resection or tumor ablation, transplantation, transarterial chemoembolization (TACE), therapies that have been extensively revised[2,15,44].

HCC patients with a solitary tumor and preserved liver function are candidates for resection. Liver transplantation benefits patients who are not good candidates for surgical resection, and present with a solitary tumor ≤5 cm or up to three nodules ≤3 cm. Image-guided ablation is the most frequently used therapeutic strategy, but its efficacy is limited by the size of the tumor and its localization. TACE has survival benefit in asymptomatic patients with multifocal disease without vascular invasion or extrahepatic spread[44]. Finally, systemic therapies are only recommended in advanced HCC and with well-preserved liver function[44]. No systemic drugs were available for patients with advanced stage of HCC until 2007, when sorafenib was approved[2]. Sorafenib increased the available treatment options for patients with extrahepatic spread and vascular invasion and improved survival in patients with advanced HCC.

Nonetheless, various limitations such as low response rates, resistance to sorafenib, or adverse effects (e.g., hand-foot skin reaction) prompted concerted efforts aimed at developing new molecular targeted agents to provide more treatment options and second-line agents for patients with disease progression or intolerance to sorafenib.

Of importance, during the past five years many trials have been made in search for novel and more effective systemic treatments for advanced HCC, not only as first-line but also in second-line, as recently reviewed in an EASL position paper aimed at helping clinicians provide the best possible care for patients today[140]. Therefore, as of today, drugs licensed in some countries include four oral multi-tyrosine kinase inhibitors (MKIs) (sorafenib, lenvatinib, regorafenib and cabozantinib), one anti-angiogenic antibody (ramucirumab) and four immune checkpoint inhibitors, alone or in combination (atezolizumab in combination with bevacizumab, ipilimumab in combination with nivolumab, nivolumab and pembrolizumab in monotherapy).

According to this updated guidelines, in the next paragraph we will introduce the systemic treatments approved in recommended order of use.
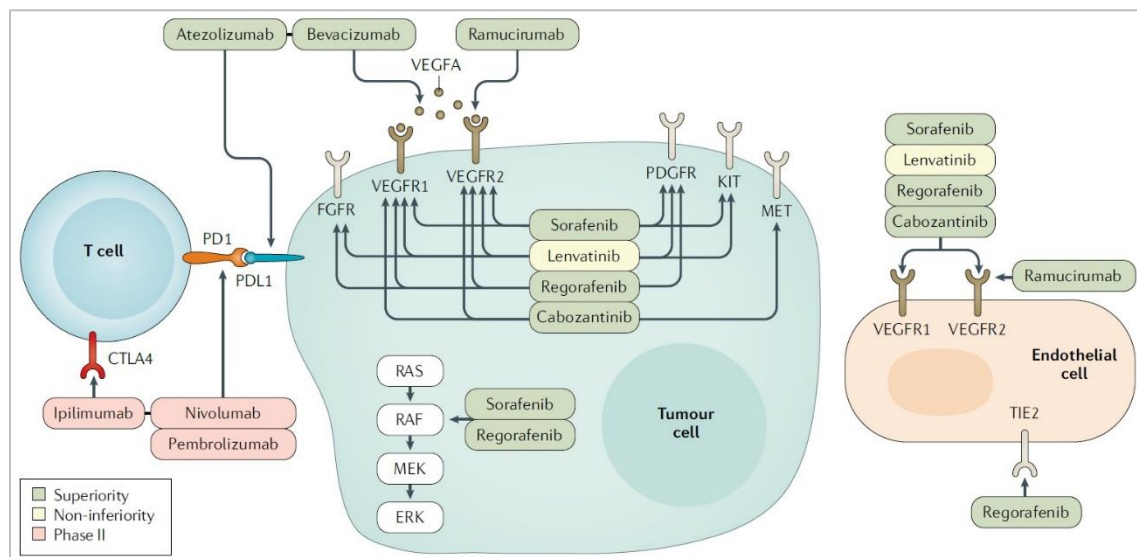
Figure 2. Main systemic therapies and their mechanism of action. Main systemic therapies currently available with their molecular and cellular targets. First and second line drugs are depicted. Extracted from Llovet et al. 2021, Ref 13.

1.7.1. First-line therapies

1.7.1.1. Atezolizumab-bevacizumab (atezo-bev)

To date, atezolizumab and bevacizumab combination is the first treatment superior to sorafenib demonstrating prolonged overall survival (67.2% vs. 54.6%; hazard ratio [HR] 0.58) and progression free survival (6.8 months vs. 4.3 months; HR 0.59)[141]. The success of IMbrave 150 clinical trial has changed the paradigm of HCC treatment and

atezo-bev has become the recommended systemic therapy if no contraindications are present [140].

Atezolizumab (Tecentriq™) is a humanized IgG1 monoclonal antibody that targets PD-L1 to prevent its binding with PD-1 and B7-1 receptors, thus reversing T-cell suppression[142].Bevacizumab (Avastin™) is a monoclonal antibody that targets vascular endothelial growth factor (VEGF), inhibiting angiogenesis and tumor growth[115]. Anti-VEGF therapy also enhances anti- PD-1/PD-L1 activity by reducing VEGF-mediated immunosuppression and promoting T-cell infiltration in tumors[143]. Of note, as single-agent, others immune checkpoint inhibitors[144,145], as well as atezolizumab monotherapy[146], did not reach better outcome in HCC patients highlighting the synergistic efficacy of immunotherapy and anti-angiogenic combination.

Regarding adverse effects, hypertension and increased AST or ALT are grade 3 or 4 adverse events frequently observed after atezo–bev treatment. Moreover, bleeding, a life-threatening risk for cirrhotic patients, is a common reaction to bevacizumab. In this sense, risk of bleeding, comorbidities such as arterial hypertension and cardiovascular disease, and prior autoimmune conditions may become limiting parameters for the indication of atezo-bev. If the patient has contraindications to atezolizumab-bevacizumab, alternative therapies should be considered, such as sorafenib or lenvatinib.

1.7.1.2. Sorafenib

Sorafenib (Nexavar®) is a small molecule that inhibits the phosphorylation of up to 40 tyrosine kinases, including VEGFR1, 2 and 3, PDGFRβ, KIT and RET. This tyrosine kinase inhibitor (TKI) also suppresses Raf kinase isoforms, such as wild-type Raf1, B-Raf and mutant b-raf V600E. It has been shown to target MAPK pathway as well. Sorafenib displayed anti-proliferative, anti-angiogenic and pro-apoptotic properties in HCC cell lines[147], anti-tumor activity in tumor xenograft nude mice[148], and anti-metastatic effect in preventing postsurgical recurrence in an orthotopic mouse model[149]. The efficacy of sorafenib possibly lays on its capacity to target both tumor cells and their microenvironment[3]. As an example, it has been described that sorafenib also had an impact on HSCs proliferation by the suppression of α-SMA and PDGF-related pathways, which decreased HCC cell viability[150]. Moreover, sorafenib was described to promote

immunosuppression through the induction of PD-L1 expression in infiltrating immune cells[151].

Sorafenib was the first compound that demonstrated survival benefit in HCC in a phase 3, double-blind trial versus placebo (SHARP trial). The median overall survival for patients in the sorafenib arm was 10.7 months compared to 7.9 months in the control group (HR 0.69, 95% confidence interval 0.55-0.87, P<0.001)[152]. In a parallel trial conducted in the Asian-Pacific population, sorafenib showed a similar survival benefit[153]. The most common adverse effects are diarrhea (8-9% patients) and hand-foot skin reaction (8-16% patients)[152]. Sorafenib is recommended as the standard systemic therapy for HCC in the first line setting in patients with well-preserved liver function (Child-Pugh A class), with advanced tumors, BCLC-C, or tumors that progressed after loco-regional therapies[2]. The appearance of dermatologic reactions has been linked to a better survival following sorafenib administration[154]. Among the molecular mechanisms responsible for sorafenib effectivity in HCC cells is the activation of programmed cell death, apoptosis, provoked by the downregulation of myeloid cell leukemia sequence 1 (MCL-1) expression, an anti-apoptotic member of the BCL-2 family[155]. Sorafenib has also been described to be involved in the autophagy pathway. The administration of autophagy inhibitors, such as chloroquine or pemetrexed, improved sorafenib efficacy in tumor cells and nude mice hepatoma tumors[156]. Additionally, MCL-1 downregulation was found to disrupt MCL-1:Beclin 1 complex and induce autophagic cell death in HCC cell lines[157].

However, it has been observed in a large number of patients that sorafenib effectiveness is hampered by drug resistance. HCC is highly heterogeneous, within the tumor and among individuals, and this influences disease progression, classification, prognosis, and naturally, cellular susceptibility to drug resistance. In this sense, long-term exposure to sorafenib of hepatoma cells provoked the acquisition of chemoresistance as well as EMT features[158,159]. Hypoxia has been described to be involved in sorafenib resistance due to HIF-1α and NF-κB activation[160]. Also, M2 macrophages have been found to participate in sorafenib resistance by the release of HGF[161].

1.7.1.3. Lenvatinib

Lenvatinib (Lenvima®) is an inhibitor of VEGFRs, RET, KIT, PDGFRα and FGFR1-FGFR4[162]. It also displayed anti-angiogenic properties and anti-FGFRs activity in

hepatoma cells and xenografts[163,164]. Lenvatinib has been described to exert an immunomodulatory effect through the increase of CD8$^+$ T cell population while diminishing macrophages and monocytes populations in HCC cells[165].

In a phase 3 clinical trial, lenvatinib showed to be non-inferior to sorafenib in terms of overall survival. Hypertension, diarrhea or a decrease in appetite or weight were among the most common adverse events[166]. In a small group of patients, the levels of AFP were found to decrease in the next two weeks following treatment, suggesting that AFP levels could be predictive of patients response[167]. Furthermore, circulating FGF-19 and Ang-2 have been proposed as predictors of clinical response to lenvatinib in HCC patients[168,169] as well as an early tumor shrinkage[170].

However, like sorafenib, HCC has been described to display resistance against lenvatinib. The HGF/c-MET signaling activation was identified as one mechanism of lenvatinib tolerance[171].

1.7.2. Second-line therapies

1.7.2.1. Regorafenib

Regorafenib (Stivarga®) is a multikinase inhibitor (MKI) against VEGFR-2, VEGFR-3, KIT, RET, wild-type and mutant (V600E) B-Raf, PDGFR, FGFR1, angiopoietin 1 receptor (TIE2), RET and p-38-alpha. Its inhibitory profile is slightly different from sorafenib, since regorafenib has stronger potency targeting VEGFR and TIE2, KIT and RET[172]. Like sorafenib, regorafenib inhibits angiogenesis, oncogenesis and tumor microenvironment. Regorafenib was shown to block cell growth and invasion in hepatoma cell lines[173]. This MKI also targeted MAPK pathway, induced caspase cleavage and activated the autophagic pathway[174,175]. Moreover, both intrinsic and extrinsic apoptotic pathways were activated by regorafenib[176]. The treatment with regorafenib provoked a decrease in the expression of metastasis-related proteins in HCC cells[177]. Regorafenib was demonstrated to block EMT activation and overcome the acquired resistance to sorafenib[178].

The RESORCE trial was the first phase 3 clinical trial that showed that patients who progressed on sorafenib benefited from oral regorafenib administration versus placebo in a second line setting[179]. Median survival was 10.6 months for the regorafenib arm while 7.8 months for the control group (HR 0.63; 95% 0.50-0.79; p<0.0001). Manageable

adverse events consisted in hand-foot-skin-reaction, hypertension and fatigue. Additional analyses of RESORCE trial have suggested that the administration of regorafenib following sorafenib may extend survival[180].

1.7.2.2. Cabozantinib

Cabozantinib (Cometriq®, Cabometyx™) is a small molecule with tyrosine kinase inhibitory prolife against VEGFR-2, RET, KIT, FLT-3, TIE2, and AXL. Cabozantinib differs from sorafenib and regorafenib in that it is capable to also block c-Met[181]. Cabozantinib has demonstrated anti-tumor activity in HCC cells by inhibiting tumor growth, angiogenesis, invasion and migration. It also reduced the number of HCC metastatic nodules in the lungs and liver in mice[182]. In a phase two clinical trial, cabozantinib demonstrated effectivity in HCC patients[183]. Those promising results led to the conduction of a phase 3 clinical trial in patients who progressed after sorafenib treatment. Cabozantinib increased overall survival (10.2 months) compared to placebo (8.0 months, HR 0.76; 95% CI, 0.63-0.92; $p = 0.005$). The most frequent side effects were palmar-plantar erythrodysesthesia, hypertension, increase AST, fatigue and diarrhea[184].

1.7.2.3. Nivolumab

Nivolumab (Opdivo®) is a human monoclonal antibody that targets programmed cell death protein 1 (PD-1). It is an immune checkpoint inhibitor, since nivolumab impedes the signaling that blocks T cell anti-tumor activity[185]. A phase 1/2 dose escalation study performed with advanced HCC with or without previous sorafenib treatment showed the potential of nivolumab for the treatment of HCC (CheckMate 040 trial)[186]. A further analysis of the CheckMate 040 trial highlighted that some inflammatory biomarkers trended with improved survival and an anti-tumor immune response[187]. Nevertheless, a subset of patients with hyperprogressive disease (HPD) was identified after nivolumab treatment in HCC patients[188]. Furthermore, administration of nivolumab plus ipilimumab, which targets CTLA-4, a inhibitory T-cell receptor, also showed to be a promising therapeutic strategy in HCC patients who progressed on sorafenib[189].

1.7.2.4. Pembrolizumab

The humanized monoclonal antibody pembrolizumab (Keytruda®) blocks PD-1 as well. In a non-randomized phase 2 clinical trial pembrolizumab was effective in patients who were treated previously with sorafenib (KEYNOTE-224)[190]. These results led to test pembrolizumab compared to placebo in a phase 3 randomized clinical trial. Although median overall survival was longer for the pembrolizumab arm, 13.9 months (95% CI, 11.6 to 16.0 months) and 10.6 months (95% CI, 8.3 to 13.5 months) for placebo, results were not statistically significant[144].

1.7.2.5. Ramucirumab

Regarding antiangiogenic therapies, ramucirumab (Cyramza®), a monoclonal antibody against VEGFR2[191–193], failed to improve survival in the REACH trial in patients treated previously with sorafenib. However, the authors identified AFP serum levels as a prognostic marker showing that patients with high levels of AFP (≥400ng/ml) benefit from ramucirumab treatment. These observations were validated in REACH-2, a double-blind phase III trial where only patient treated with sorafenib with high AFP levels were included. Ramucirumab improved overall survival (8.5 versus 7.3 months HR 0.710, 95% CI 0.531–0.949; P = 0.0199) and has become the first HCC therapy with biomarker-guided patient selection. Hypertension, liver failure and hyponatraemia were the most common grade 3–4 adverse events.

1.7.2.6. Combination therapies

Regarding ongoing clinical studies, several combinations of treatment regimens are being tested in patients with HCC in both first line and second line: the RENOBATE study (combination of regorafenib and nivolumab administered as first-line therapy in unresectable HCC), the REGOMUNE trial (avelumab, that targets PD-L1, will be studied together with regorafenib), the GOING trial (second-line treatment with regorafenib followed by nivolumab treatment in patients who have progressed on sorafenib administration), the ACTION trial (will evaluate the effectivity of cabozantinib in patients who are sorafenib-intolerant or do not meet the RESORCE criteria), and the COSMIC-312 clinical trial (administration of cabozantinib in combination with the immune checkpoint inhibitor atezolizumab), among some others.
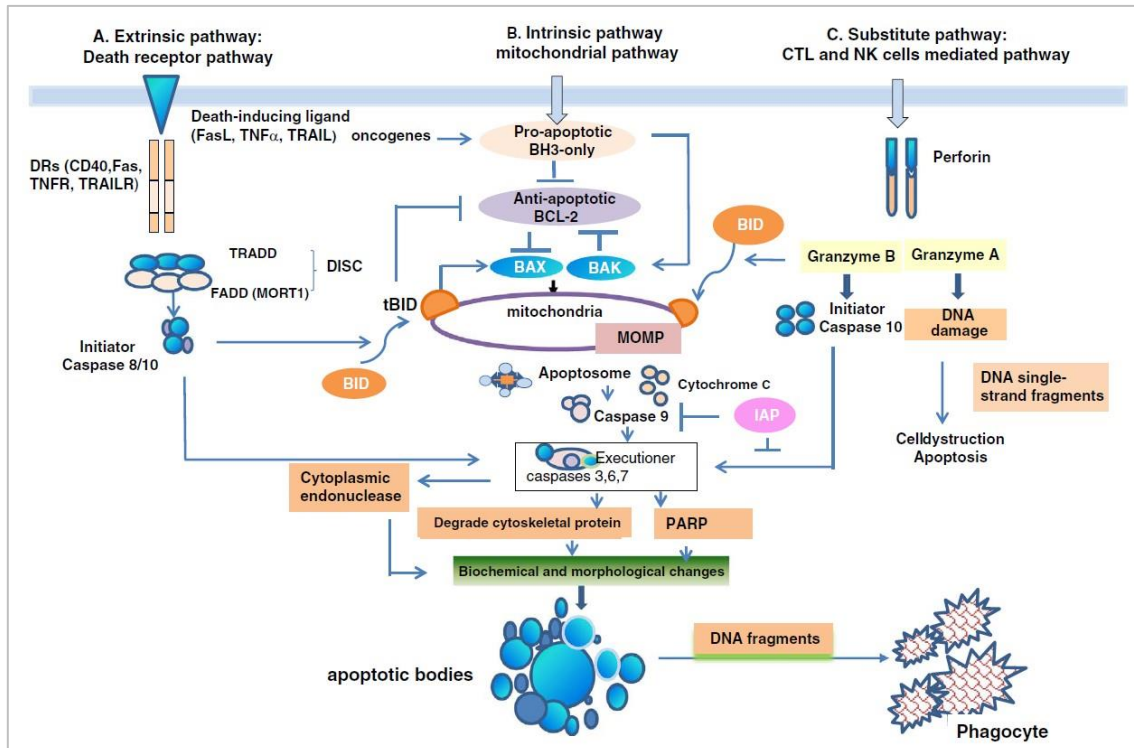
2. Apoptosis

2.1. Introduction to apoptosis

Apoptosis is the most common form of "programmed cell death" and consists in the elimination of cells in an organized manner[194]. Programmed cell death and apoptosis play an important role during embryonic development and aging. Apoptosis also acts to keep cell populations in tissues and as homeostatic machinery. Moreover, apoptosis acts as a defense mechanism to remove damaged cells due to pathogens or noxious agents. The apoptotic process eliminates tumor cells or auto-aggressive immune cells as well[195]. Both physiological and pathological conditions can trigger apoptosis, although not all cell types will undergo cell death depending on a given stimulus. Apoptosis can be activated intrinsically or extrinsically, but both pathways converge at the activation of caspases[195,196].

Apoptotic cells can be distinguished from non-apoptotic cells owing to cell shrinkage, which occurs in the early steps of apoptosis[197]. Cell shrinkage is characterized by cellular smaller size, dense cytoplasm and tightly packed organelles. Besides, another important feature of apoptosis is chromatin condensation or pyknosis, which can be observed by bright field or fluorescence microscopy. Then, the blebbing of the plasma membrane and the fragmentation of the nucleus occur, processes which lead to the formation of apoptotic bodies. These apoptotic bodies will be phagocytized by macrophages, but also by parenchymal or neoplastic cells. Within the phagocytes, apoptotic bodies will be eliminated inside phagolysosomes[198].

Importantly, apoptosis is not accompanied by an inflammatory reaction, since apoptotic cells do not release their cellular components to their surrounding milieu. Besides, apoptotic bodies are rapidly engulfed by phagocytic cells thereby preventing necrosis. Finally, no inflammatory cytokines are produced by the engulfing cells[198,199].

2.2. Pathways of apoptosis

Apoptosis can occur through three signaling pathways: the extrinsic pathway, the intrinsic pathway and the cytotoxic T-cell and NK cell-mediated and peforin-granzyme-dependent killing pathway[200].

Figure 3. Apoptosis pathways. Extrinsic, intrinsic and CTL/NK cells mediated pathways of apoptosis. The three pathways converge on the executioner caspases -3, -6 and -7. Extracted from Wu et al., 2018, Ref. 197.

2.2.1. The extrinsic pathway

The extrinsic pathway of apoptosis is activated when specific ligands bind to their cell-surface death receptors, receptors that belong to the tumor necrosis factor (TNF) superfamily (TNFRSF) and have both an extracellular domain and intracellular death domains[201,202]. The intracellular death domains are key for the transmission of the death signal from the cell surface to intracellular pathways. The well-known couples of ligands, present on the cell surface of T cells, and death receptors are FasL (CD95 ligand)/FasR, TNF-α/TNFR1, Apo3L/DR3, TNF-related apoptosis-inducing ligand (TRAIL)/DR4 and TRAIL/DR5[202]. When ligands bind to their death receptors, FADD (Fas-associated death domain protein) adapter protein is recruited. FADD, in turn, recruits inactive forms of caspase-8 through the dimerization of the death effector domain, forming a "death-inducing signaling complex" (DISC) and activates caspases-8[203]. With the activation of caspase-8, apoptosis is triggered. The executioner caspases-3, and -7 become activated and perform the cleavage of the proteins of the cytoskeleton, promoting cell death. The activation of the extrinsic pathway can be inhibited by c-FLIP protein, which binds to FADD and caspase-8 and blocks them[204]. Interestingly, upon the activation of caspase-

8, BID protein, which takes part in the intrinsic pathways of apoptosis, is cleaved and translocates to mitochondria, resulting in BCL-2-associated X protein (BAX) and BAK activation and oligomerization and the intrinsic pathway continuation[205].

2.2.2 . The intrinsic pathway

The intrinsic or mitochondrial pathway of apoptosis is initiated by different stimuli that provoke an intracellular response, activating and promoting the interaction between the BCL-2 family of proteins, the key regulators of the intrinsic apoptosis pathway, that cause mitochondrial outer membrane permeabilization (MOMP), and consequently cell death by apoptosis[206]. MOMP triggers the release of intermembrane space mitochondrial proteins into the cytosol: cytochrome c, Smac/DIABLO and HtrA2/Omi. Cytochrome c binds to apoptotic protease-activating factor 1 (APAF1) in order to form the apoptosome or caspase activation complex, whereas Smac and Omi block inhibitors of apoptosis proteins (IAPs), which inactivate caspase-9, -3 and -7[207]. HtrA2/Omi accumulates in the nucleus where activates the transcription of p73, an upregulator of several proapoptotic genes, such as Bax and Bak[208]. The apoptosome activates procaspase-9, which forms clusters that activate caspase-9. Furthermore, the release of apoptosis-inducing factor (AIF), endonuclease G (EndoG) and CAD from the mitochondria induces their translocation into the nucleus, where they promote DNA fragmentation and chromatin condensation[209]. The activation of caspase-9 induces the activation of executioner caspases 3, 6 and 7. At this point, the extrinsic and intrinsic pathways of apoptosis converge in the execution phase. Executioner caspases promote cytoplasmic endonuclease activation, which produces the degradation of the nucleus, and proteases that cleave cytoskeletal and nuclear proteins, including PARP, cytokeratins, the plasma membrane cytoskeletal protein alpha fodrin, NuMA and others. Specifically, caspase-3 is one of the main executioner caspases and can be activated by caspase-8, -9 or -10. Caspase-3 induces the activation of the endonuclease CAD, which, in turn, degrades nuclear DNA and promotes chromatin condensation. Caspase-3 promotes cytoskeletal reorganization. One of its targets is gelsolin, which is a core protein for actin polymerization. The cleaved gelsolin fragments promote the cleavage of actin filaments, resulting in the disintegration of cytoskeleton, cell division, signal transduction and intracellular traffic, all contributing to the collapse of the cell[198,210].These protein and nucleic acid degradation processes confer the biochemical and morphological features that exhibit apoptotic cells, like chromatin condensation, DNA fragmentation, plasma

membrane blebbing, and formation of apoptotic bodies, which will be engulfed by a phagocytic cell[211]. The distinguishing mark of this step is phospholipid asymmetry and the externalization of phosphatidylserine on the cell surface of apoptotic cells. This exposure of phosphatidylserine on the cell membrane favors phagocytic recognition by engulfing cells. The destruction of the cellular content is fast and no inflammatory response is triggered, as no cell constituents are released[212].

2.2.3. The perforin/granzyme pathway

Cytotoxic T lymphocytes are capable of killing cells through the extrinsic pathway, being FasL/FasR binding the most common mechanism of apoptosis induced by cytotoxic T lymphocytes[213]. T cells can also execute their cytotoxic function of eliminating tumor cells or cells with viral infections through the secretion of perforin, a molecule that forms transmembrane pores, and the release of cytoplasmic granules that go through the pore and into the tumor or virus-infected cell. The major components of those granules are the serine proteases granzyme A and B[214,215].

Through the cleavage of aspartate residues, granzyme B activates pro-caspase-10. Furthermore, granzyme B has been reported to activate the intrinsic pathway in order to amplify the death signal by Bid cleavage and induce cytochrome c release[216]. Granzyme B can cleave and activate procaspase-3 and -7[217]. In contrast, Granzyme A has been described to activate apoptosis in a caspase-independent mechanism. Granzyme A impairs both mitochondrial function and mitochondrial potential. As a result, superoxide anion is generated, activating the SET complex, an ER-associated oxidative stress response complex that is in charge of maintaining chromatin structure and DNA repair[218]. Therefore, DNA repair mechanisms and chromatin structure maintenance become blocked due to granzyme A action, leading to apoptotic DNA degradation.

2.3. The BCL-2 family

The B-cell lymphoma 2, BCL-2, family of proteins regulate the intrinsic or mitochondrial pathway of apoptosis. They contain between one and four BCL-2 Homology (BH) domains, named BH1 to BH4. Depending on these domains, they can be classified into three categories: anti-apoptotic members, multi-domain pro-apoptotic members and BH3-only proteins[206].

2.3.1. Structure and function of BCL-2 family

BCL-2 is a fundamental constituent of BCL-2 family. BCL-2 is considered as a novel class of oncogene that prevents cells from suffering apoptosis instead of promoting cell proliferation and accelerated transformation induced by MYC[206]. High levels of BCL-2 are expressed in numerous hematologic malignances. Furthermore, BCL-2 has been found to protect cells against many cytotoxic stimuli, e.g. anti-cancer compounds. BCL-2 knock-out mice displayed an impairment in the maturation and activation of B and T cells[219].

Anti-apoptotic proteins bear four BH domains, BH1-BH4, and comprise BCL-2, BCL-X$_L$, MCL-1, BCL-W, A1 (BFL1) and BCL-B. The members of this family display a hydrophobic groove that joins the BH3 domain of their pro-apoptotic counterparts. The BH4 domain was discovered to be crucial for the anti-apoptotic function of BCL-2 proteins, since the loss of that domain, located in the N-terminus of BCL-2, abrogates its anti-apoptotic activity while the ability to bind to BH3-only proteins is not influenced[220].

Multi-domain pro-apoptotic members are BAX, BAK and BOK and contain all BH domains. These multi-domain pro-apoptotic proteins are considered 'effectors', as they straightforward produce conformational changes in themselves and oligomerize, that lead to the formation of the MOMP complex and trigger the onset of apoptosis[220].

BH3-only members are pro-apoptotic and contain solely the BH3 domain. They include BH3 interacting domain death agonist (BID), BIM, PUMA, NOXA, BCL-2-associated agonist of cell death (BAD), activator of apoptosis harakiri (HRK), BCL-2-interacting killer (BIK), BCL-2-modifying factor (BMF), BNIP3 and NIX[220]. The BH3 domain consists of 9-15 amino acids that allow the binding of anti-apoptotic BCL-2 through their hydrophobic groove[221]. BH3-only proteins can be subdivided into two groups. The 'activators' (tBID, active and truncated form of BID, BIM and PUMA) can directly interplay with 'effectors', whereas BAD, BIK, BMK, HRK and NOXA are considered 'sensitizers/derepressors' and interact with anti-apoptotic members and liberate the activators to combine with BAX and BAK[221].
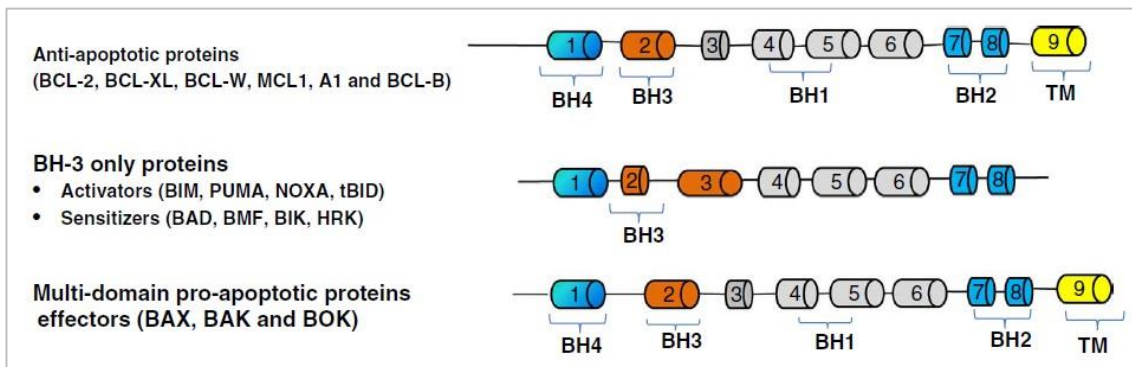
Figure 4. BCL-2 family members. Anti-apoptotic proteins, BH3-only proteins and multi-domain pro-apoptotic effectors with the BH3 domains represented. Extracted from Wu et al., 2018, Ref. 197.

The affinity of binding varies depending on the pro-survival and pro-apoptotic proteins, relying on the differences of the sequence of the groove and the BH3 domain[220,222]. PUMA, tBID and BIM bind to all pro-survival proteins, while BAD engages merely BCL-2, BCL-X$_L$ and BCL-W and NOXA binds MCL-1 or A1. Therefore, BH3-only proteins with the ability to bind all pro-survival members are considered to be more effective in killing than BH3-only proteins with a more restricted binding profile. Moreover, activated BAX binds to all pro-survival proteins, but BAK is mostly controlled by BCL-X$_L$, MCL-1 and A1[223].

Anti-apoptotic members are found on the mitochondrial outer membrane (MOM), the endoplasmic reticulum membrane and the nuclear membrane. The MOM integrity is preserved thanks to anti-apoptotic proteins, which counteract pro-apoptotic ones. Many BCL-2 proteins, such as BCL-2 and BAK, possess a transmembrane domain that links them to the membrane of mitochondria or other organelles. On the contrary, BAX is mostly present in the cytosol[224].

Aspects regarding protein structure, specific binding partners and localization of the BCL-2 family of proteins have been extensively reviewed[224].

To trigger apoptosis, pro-apoptotic proteins or activated BAX and BAK must overwhelm pro-survival ones[206]. Then, activated BAX and BAK homo-oligomerize and promote MOM pore formation and MOMP.

2.3.2. Apoptotic priming

The expression levels of BCL-2 family proteins are distinct depending on the tissue, developmental stage, cell type, organismal age and experimented cell damage or stress[225]. A cell that is 'primed' towards apoptosis easily experiences MOMP in the presence of a pro-apoptotic stimulus. In contrast, a cell that bears a high load of pro-survival proteins is considered 'less primed' or 'unprimed' and counteracts easily pro-apoptotic signaling. Whether a cell fails to express sufficient levels of effectors BAX and BAK, the cell will not be capable of dying through the intrinsic pathway. In that case, that cell can also die by the extrinsic pathway and it is considered 'apoptosis refractory[222]. Thus, apoptotic priming shows how easily a cell will undergo apoptosis. The BH3 profiling assay measures apoptotic priming[226]. By using peptides that mimic BH3-only proteins, aka BH3 mimetics, their binding to the pro-survival members activates the loss of cytochrome c, which is measured. This assay has been used to determine the dependency level of pro-survival proteins of chronic lymphocytic leukemias (CLL), certain acute myeloid leukemias (AML), healthy/transformed T cells and multiple myelomas (MM). The BH3 profiling has allowed uncovering new interactions between BCL-2 family proteins. Importantly, apoptotic priming may predict the response to chemotherapy in cancer patients[227].
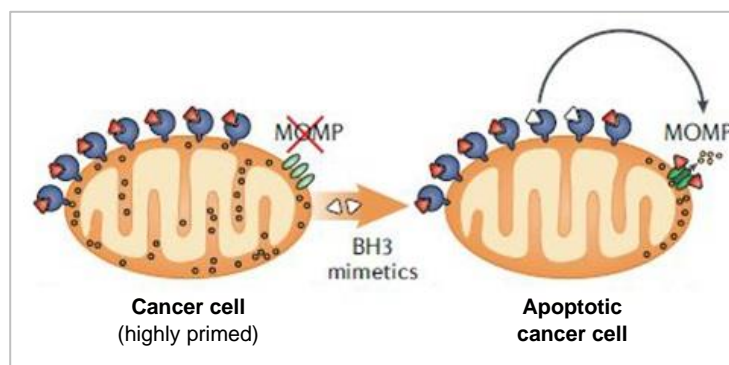
Figure 5. Apoptotic priming. Highly primed cancer cells undergo apoptosis with the addition of BH3 mimetics. Modified from Singh et al., 2019, Ref 722.

2.3.3. Apoptosis in cancer cells

Apoptosis is a crucial process that regulates homeostasis thereby eliminating excessive or defective cells and must be tightly controlled[206]. An increase in apoptosis can lead to, for instance, an augment in neuronal death in neurodegenerative diseases or acute brain injuries after cerebral ischemia. Moreover, pathogens are capable of inducing excessive

cell death. On the other hand, a defective apoptotic mechanism can produce numerous pathologic conditions such as cancer, autoimmune diseases or propagation of intracellular pathogens[206]. The malignant transformation of a cell is a process that involves DNA damage, pressure to favor cell growth and abnormal proliferation signals. In many cancers, the oncogene MYC appears to be deregulated and the expression of several pro-apoptotic genes is under the transcriptional control of MYC[228]. Therefore, cells undergoing oncogenic transformation often express high levels of pro-apoptotic proteins. However, selective pressure of tumors favors cells that are loaded with high amounts of pro-survival proteins, which is thought to play a role in chemoresistance as well[229]. Consequently, tumor cells are frequently on the verge of apoptosis, as they bear both high levels of pro-apoptotic and anti-apoptotic proteins[229].

2.3.4. BH3 mimetics

In that context, BH3 mimetics offer a novel and promising therapeutic strategy. BH3 mimetics are small molecules that inhibit anti-apoptotic proteins of the BCL-2 family and, thus, trigger apoptosis. These anti-apoptotic proteins inhibitors mimic the function of some BH3-only proteins[200,230].
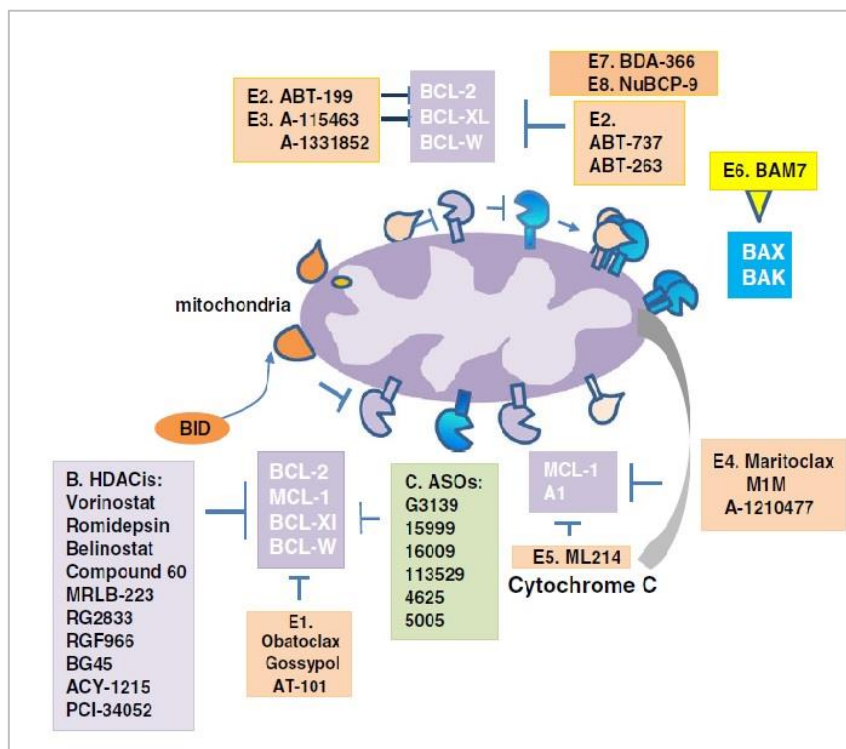

Figure 6. BCL-2 family of proteins and their inhibitors BH3 mimetics. Modified from Wu et al., 2018, Ref 197.

2.3.4.1. Pan BCL-2 family inhibitors

Obatoclax

Obatoclax (GX15-070, GeminX Pharmaceuticals, now Teva Pharmaceutical Industries) is a pan-BCL-2 family inhibitor with the ability to bind to BCL-2, BCL-X$_L$, BCL-W, BCL-B, A1 and MCL-1 with sub-micromolar affinity. It induces apoptotic characteristics in multiple myeloma (MM) and acute myeloma leukemia (AML) cells and increased chemotherapy action *in vitro*[231,232], and has been used extensively in pre-clinical studies in malignant neoplasias[232]. While obatoclax alone has failed to show clinical benefit in myelofibrosis, SCLC and NSCLC, refractory MCL, MDS and AML, obatoclax plus fluradabine and rituximab showed promising clinical activity in CLL patients[233].

Gossypol and derived compounds

Gossypol is a natural product derived from the cotton plan that acts as a BCL-2 family inhibitor[234]. Gossypol and its derivative, AT-101, exert antitumor effects on different cancer types *in vitro* and *in vivo,* and demonstrate synergistic effects with other chemo- and radio- therapeutic treatments. In addition, several nanocarriers have been designed to load gossypol or its derivatives in order to expand the range of their applications and evaluate their combination effects with other anti-tumor agents[235]. Unlike gossypol, AT-101 has been extensively explored for its efficacy in clinical trials. In particular, AT-101 with cisplatin and etoposide was effective in a variety of solid tumor patients, including ES-SCLC and was well tolerated[236]. However, in combination with chemotherapeutic agents, it has failed to show significant activity in several clinical trials.

Other known gossypol derivatives are apogossypolone (ApoG2) and ch282-5 (2-aminoethanesulfonic acid sodium-gossypolone) that have been used mostly in *in vitro* studies and experimental cancer models[237,238].

2.3.4.2. BCL-2, BCL-X$_L$ and BCL-W inhibitors

ABT-737 and **ABT-263**

One of the first BH3 mimetic that was developed was ABT-737 (Abbot Laboratories, now AbbVie) by means of NMR fragment screening, structural biology and medicinal chemistry[239]. ABT-737 showed low nanomolar affinity for BCL-2, BCL-X$_L$ and BCL-W (K$_i$

≤ 1 nM), mimicking BAD anti-apoptotic binding partners, but with insignificant binding affinity for BCL-B, MCL-1 or A1. This compound displayed anti-tumor activity in SCLC cell lines and mouse xenograft tumors and patient-derived CLL cells[240].

Since ABT-737 had poor oral absorption, ABT-263 (navitoclax) was created with better oral bioavailability. ABT-263 highly binds to BCL-X_L, BCL-2 and BCL-W (K_i ≤ 1 nM), but with low binding affinity to MCL-1 and A1. In preclinical models, ABT-263 provoked tumor regression in SCLC and acute lymphoblastic leukemia xenograft models as single agent. In combination with common chemotherapeutic agents (rituximab or bortezomib), ABT-263 enhanced their activity in B-cell lymphoma, mantle cell lymphoma (MCL) and multiple myeloma xenograft models. As ABT-737, navitoclax induced a rapid drop in platelet counts after its administration in mice and dogs, although it has proved to be reversible[241]. Of note, sorafenib-triggered apoptosis was enhanced by navitoclax co-administration in human colon cancer, hepatoma, breast cancer, gastric cancer and lung cancer cells by decreasing Akt activity and with the implication of BAX and p21[242].

Recently, ABT-263 has been identified as a senolytic drug, a compound that induces apoptosis in senescent cells, for instance in human umbilical vein endothelial cells (HUVEC), human lung fibroblasts and MEFs cells[243]. In p53-wild type breast cancer cells, navitoclax demonstrated to effectively eliminate chemotherapy-induced senescent cells[244]. In the liver, navitoclax was found to eliminate senescent HSCs and detain tumor progression[245].

ABT-263 has been tested in monotherapy in a reduced group of CLL patients with relapsed or refractory disease in a phase I clinical trial[246]. ABT-263 proved to exert efficacy, prompting phase II clinical studies. In combination with rituximab, navitoclax was well tolerated and the administration of both drugs led to higher response rates and prolonged survival in a phase II trial conducted in CLL patients[247].

Another clinical study conducted in patients with solid tumors showed the limited therapeutic potential of navitoclax in combination with carboplatin/paclitaxel, since hematological toxicities such as anemia, neutropenia and thrombocytopenia were observed[248]. On the other hand, ABT-263 together with gemcitabine displayed favorable results in a phase I study performed on advanced solid tumors patients[249].

As for hepatocellular carcinoma, there is an ongoing clinical trial in which sorafenib is being tested in combination with ABT-263 in patients with cirrhosis, hepatitis B/C

infection, metastatic or recurrent solid neoplasms and recurrent or advanced stages of HCC (NCT02143401)[250].

Other BCL-2 and BCL-X$_L$ inhibitors

Other dual inhibitors of BCL-2 and BCL-X$_L$ have been developed containing the acylsulfonamide pharmacophore, although to date they have only been tested at the preclinical level[251].

The molecule BM-1197 demonstrated high binding affinity for BCL-2 and BCL-X$_L$ ($K_i < 1$ nM) and strong anti-tumor capacity in SCLC cells and xenograft mice. Since BM-1197 also targets BCL-X$_L$, a reduction in the platelet count in mice was observed[252].

The experimental compound S44563 that inhibits BCL-2 and BCL-X$_L$ reduced tumor growth in uveal melanoma PDX-xenograft models together with fotemustine[253], and in preclinical models of SCLC showed increased the sensitivity of SCLC cells to radiotherapy[254].

The BH3 mimetic BCL2-32 targets BCL-2 and BCL-X$_L$ ($K_i = 3.3$ and 8.5 nM, respectively) and demonstrated a marked anti-tumor effect alone or in combination with chemotherapeutic agents in ALL and DLBCL xenograft models. BCL2-32 was administered on an intermittent dosing schedule in order to allow the recovery in the platelet count number[255].

AZD4320 is another novel BH3 mimetic that blocks the function of BCL-2 and BCL-X$_L$ with nanomolar affinity. AZD4320 demonstrated effectivity against hematologic cancer cell lines, AML patient derived samples and induced tumor regression without dose-limiting thrombocytopenia in xenograft AML mouse models[256]. Due to cardiovascular toxicity, AZD4320 was conjugated to a PEGylated poly-lysine dendrimer resulting in the generation of AZD0466, also a dual inhibitor of BCL-2 and BCL-X$_L$ with anti-tumor activity against ALL xenograft tumor models. This novel molecule may be a candidate for being tested in the clinical setting[257].

2.3.4.3. BCL-2 selective inhibitors

ABT-199

ABT-199, or venetoclax, is a selective inhibitor of BCL-2 with a high affinity for its target (K_i < 0.010 nM) developed by Abbot Laboratories. Since venetoclax has low affinity for BCL-X_L, no drop on the platelet count was observed *in vivo*. The dose-limiting thrombocytopenia that occurred with navitoclax administration was overcome. With its full repertoire yet to be explored, venetoclax has changed the therapeutic landscape in haematological malignancies, and most particularly chronic lymphocytic leukaemia (CLL), acute myeloid leukaemia (AML) and multiple myeloma (MM). In CLL, it has shown remarkable efficacy both as monotherapy and in combination therapy. Based on data from MURANO and CLL14 studies, fixed-duration combination therapy of venetoclax with anti-CD20 antibody is now the standard of care in numerous countries. In AML, although of limited efficacy as a single agent, venetoclax combination therapy has demonstrated encouraging outcomes including rapid, durable responses and acceptable toxicity, particularly in the older, unfit patient population[258].

An interesting work demonstrated that mutations in BCL-2 made human lymphoma cells less susceptible to ABT-199, suggesting the development of resistance to the administration of ABT-199[259]. A more recent study has suggested that BCL-2 amplicon loss and transcriptional remodeling may be drivers of the acquired venetoclax resistance in B-Cell lymphoma models[260]. Besides, the phosphorylation of BCL-2 in CLL cells abrogated the activity of ABT-199, which highlights the phosphorylation state of BCL-2 as crucial in venetoclax effectivity[261].

Beyond hematologic malignancies, ABT-199 has been tested in solid tumors in clinical trials. In metastatic breast cancer patients expressing ER and BCL-2, venetoclax proved to be safe and tolerable in combination with tamoxifen in a phase 1b clinical study[262]. Moreover, ABT-199 has also been assessed in the clinical setting in other pathologies. In a double blind, phase 1 trial, venetoclax was well tolerated in women with erythematous lupus and a reduction of total and disease-related lymphocytes was observed after its administration[263].

S55746

S55746 (BCL201 or Servier-1) is a novel BCL-2 antagonist (K_i = 1.3 nM) that induced apoptosis in hematological cell lines, including AML and B-ALL, *ex vivo* CLL and MCL patient samples and detained tumor growth in hematological xenograft murine models. Since BCL-X_L is not a target of S55746, no platelet affectation was observed *in vivo*[264]. This compound is currently being tested in a phase 1 clinical trial in patients with CLL, non-Hodgkin lymphoma or MM (NCT02920697) and in another clinical study in combination with idelalisib in patients with follicular lymphomas (FL) and mantle cell lymphomas (MCL) (NCT02603445).

2.3.4.4. BCL-X_L selective inhibitors

Navitoclax displays a strong anti-tumor effect in combination with chemotherapy, although neutropenia and thrombocytopenia appeared to be major side effects. In this context, BH3 mimetics that selectively target one member of the BCL-2 family were used to attribute the effect of BCL-2 or BCL-X_L antagonism to the development of neutropenia or thrombocytopenia[265]. This prompted the generation of the BCL-2-selective inhibitor venetoclax (ABT-199), which demonstrates robust activity but spared platelets, and of selective BCL-X_L inhibitors.

The first selective BCL-X_L inhibitor discovered was WEHI-539, which targets preferentially BCL-X_L with subnanomolar affinity (K_i= 1.1 nM)[266]. Also, A-1155463 was developed with a picomolar affinity for BCL-X_L (K_i < 0.01 nM). Of note, WEHI-539 and A-115463 alone showed tumor killing capacity in chondrosarcoma cell lines, pointing out the importance of BCL-X_L for chondrosarcoma cells survival[267].

A-1331852, developed from the previous two agents, WEHI-539 and A-1155463, through structure-based design is considered the first potent, truly selective and oral available antagonist of BCL-X_L possessing a K_i < 0.010 nM. A-1331852 has been demonstrated to disrupt the BCL-X_L-BIM complex, freeing the pro-apoptotic member BIM, provoking the release of cytochrome c, triggering capsase-3/7 activation and inducing apoptosis in leukemia cells. In addition, the selective inhibitor A-1331852 produced an increase in tumor growth inhibition in combination with docetaxel in breast cancer xenograft and NSCLC xenograft murine models than either compound alone, highlighting the ability of the BCL-X_L specific antagonist in enhancing current chemotherapy therapeutic action. BCL-X_L is crucial for platelet lifespan, since A-1331852

inoculated into healthy male Sprague-Dawley rats resulted in a reduction in platelet counts, but no neutropenia, being the BCL-2 inhibition by ABT-199 the dose-limiting factor for neutrophil survival[265].

As navitoclax, A-1331852 and also A-1155463 have been described as senolytic compounds. A-1331852 was reported to exert senolytic activity in HUVEC and IMR90 lung cells and were considered to perform better as senolytic drugs, since ABT-263 was associated to more hematological toxicities[268]. In addition, A-1331852 exhibited an anti-fibrotic effect in senescent cholangiocytes and activated fibroblasts in a mouse model lacking Mdr2$^{-/-}$[269]. BCL-X$_L$ targeting by A-1331852 also induced cell death in senescent murine biliary epithelial cells[270].

2.3.4.5. MCL-1 selective inhibitors

Tumor cells that were highly dependent on MCL-1 expression for their survival were not sensitive to the BH3 mimetics ABT-737 and ABT-263. Maritoclax, a natural compound and a marinopyrrole A, was the first compound identified to inhibit MCL-1, at the micromolar range. It selectively killed leukemia cells and enhanced ABT-737 action in hematologic malignancies cells[271].

A-1210477 (Abbvie) was developed to specifically target MCL-1 with higher binding affinity. This selective MCL-1 inhibitor (K_i = 0.000454 µM) demonstrated to disrupt MCL-1-BIM complexes and induced the mitochondrial pathway of apoptosis activation. Moreover, it showed cytotoxic activity as single agent against MM, DLBCL and NSCLC cell lines[272,273]. Of interest, the targeting of MCL-1 prevented the formation of tumor spheres in hepatocellular carcinoma cells thereby increasing apoptosis[274].

S63845 (Servier) is another small molecule with the capacity of targeting MCL-1 with 20-fold lower affinity for its target than A-1210477 (K_i = 0.19 nM). This MCL-1 antagonist potently killed hematologic cancer cells lines, while it displayed less effectivity in triggering solid tumor cancer cells death. S63845 increased the therapeutic action of other anti-cancer drugs. S63845 displayed anti-tumor activity in MM and SCLC xenograft models as single agent and was well tolerated[275]. MCL-1 inhibition was found to overcome the developed resistance to regorafenib in patient-derived organoids and PDX xenografts of colorectal cancer[276]. Similarly, the targeting of MCL-1 in vincristine-resistant rhabdomyosarcoma cells rescued their sensitivity to vincristine[277]. The blockade of both BCL-X$_L$ by A-1331852 and MCL-1 by S63845 induced the hallmarks of

apoptosis in pediatric cancer *in vitro*, including neuroblastoma, osteosarcoma, Ewing sarcoma and rhabdomyosarcoma[278,279]. Apart from tumor models, the administration of MCL-1 inhibitor S63845 or RNAi targeting MCL-1 demonstrated to deplete human hematopoietic stem and progenitor cells, being a potential side-effect of MCL-1 inhibition therapy[280].

AZD5991 is a novel antagonist of MCL-1 ($K_i = 200$ pM) developed by AstraZeneca. It provoked rapid cell death in myeloma and AML cells. AZD5991 is currently being tested in clinical trials in a phase 1 study as single agent and in combination with ABT-199 in several hematological malignancies, such as MM, AML, NHL, CLL and ALL[281].

S64315/MIK665 is another MCL-1 antagonist that showed anti-tumor effect in MM cells and xenograft mice[282]. This MCL-1 inhibitor will demonstrate its efficacy as monotherapy in AML and myelodysplastic syndrome (MDS) patients in a phase 1 study (NCT02979366) and in refractory or relapsed MM and DLBCL (NCT02992483). The safety and tolerability of S64315 is being tested in a phase 1/2 clinical study in combination with azacitidine in patients with AML (NCT04629443). Another phase 1b clinical trial conducted in AML patients will show the benefits of the co-administration of S64315 and venetoclax (NCT03672695).

AMG 176 (Amgen) inhibits MCL-1 action as well. AMG 176 elicited apoptosis in hematologic cancer cell lines, primary patient samples and mouse xenografts. Moreover, AMG 176 potentiated the therapeutic action of ABT-199 in AML mouse models and was well tolerated *in vivo*[283]. Interestingly, AMG 176 prompted CLL programmed cell death alone or in combination with venetoclax whereas no significant effect was observed on normal blood cells[284]. These early promising results have led to study AMG 176 in the clinical setting in combination with azacitidine in patients with relapsed or refractory MM/AML (NCT02675452).

AMG 397 is another MCL-1 selective blocker. Although there is few preclinical data about its efficacy, AMG 397 is currently being investigated in comparison to dexamethasone or azacitidine in patients with MM, AML, NHL, MDS in a phase 1 trial (NCT03465540).

3. Reactive oxygen species (ROS)

3.1. ROS and antioxidant defense

Reactive oxygen species (ROS) are generated as by-products of cellular metabolism. These molecular oxygen (O_2) derivatives include superoxide radical ($O_2^{\cdot-}$), hydroxyl radical ($\cdot OH$), peroxyl radical ($RO_2\cdot$) and alkoxyl radical ($RO\cdot$); as well as nonradicals like ozone (O_3), singlet oxygen ($^1O_2$), hydrogen peroxide (H_2O_2) and hypochlorous acid (HOCl). Under physiological conditions, they play a role in cellular signaling pathways at low amounts. Yet, a rise in ROS production may lead to cell damage[285]. Cellular antioxidant defense systems counteract ROS accumulation to sustain redox balance: glutathione (GSH), glutathione peroxidase (GPx), glutathione S-transferase (GST), glutathione reductase (GR), superoxide dismutases (SODs), thioredoxin peroxidases (TRXPs), thioredoxin 2 (TRX2) and glutaredoxin 2 (GRX2) can be found in mitochondria, and catalase (CAT), which neutralizes H_2O_2, is present in peroxisomes[286,287]. Nutritional antioxidants, including flavonoids, carotenoids, tocopherols and ascorbic acid, also exhibit ROS scavenging properties. Moreover, synthetic antioxidants, such as N-acetylcysteine and selenium and mitochondria-targeted antioxidants (MitoTEMPO, MitoQ, and SkQs) are effective in providing protection against mitochondrial damage[288]. An imbalance between ROS generation, specially ROS produced in mitochondria (mROS), and neutralization leads to an increase in cellular oxidative stress, which is well-known to be involved in several pathologies, including cancer, inflammation, neurodegenerative diseases, diabetes and aging[289].

3.2. ROS production by tyrosine kinase inhibitors

Cancer therapy strategies are continuously seeking better tumor response rates, disease-free survival and less associated-toxicities. More targeted therapies are pursued to diminish side-effects. Combination therapies are also being tested: regimens of different chemotherapeutic agents or chemotherapy prior to radiotherapy are also current approaches under much investigation. Immunotherapy has recently emerged as an attractive application. However, their response rates must be improved. Despite all efforts, chemoresistance and tumor relapse still occur and therefore, novel therapeutic options must be investigated[290].

Drugs that impair the action of the mitochondrial electron transport chain may increment the mitochondrial production of superoxide and other intracellular ROS. The excess of ROS levels may lead to the loss of mitochondrial membrane potential, increasing MOM permeability and finally eliciting mitochondrial cell death. Therefore, intracellular ROS production becomes essential for chemotherapeutic agents in order to induce cell death in cancer cells[291].

3.2.1. ROS production and sorafenib

Sorafenib was found to increase ROS production in human lymphoma cells U937 and the acute T cell leukemia Jurkat cells, and this effect was preceded by an augment of the cytosolic-Ca^{2+} concentration. The pretreatment of U937 cells with the antioxidant MnTBAP, a MnSOD analog, conjugated to PEG-catalase decreased ROS production by sorafenib administration[292]. Another work demonstrated that either sorafenib or arsenic trioxide, alone or combined, were capable of rising ROS generation in leukemic HL-60 cells through depleting MCL-1 protein levels[293]. Sorafenib was found to enhance radiation-induced apoptosis in colon cancer cells[294] and in renal carcinoma cells[295] by increasing ROS production. c-Met, through Nfr2-HO-1 axis was found to protect renal cancer cells against the ROS generation exerted by sorafenib. The targeting of c-Met increased oxidative stress and apoptotic markers in renal tumor xenografts[296].

In HepG2, Hep3B and HuH7 liver cancer cells, the combination of sorafenib plus vorinostat increased ROS production. Similarly, the administration of MnTBAP quenched ROS generation caused by the drug combination effect[297]. Sorafenib was found to induce cell death through a ROS-dependent mechanism in HCC, *in vitro* and *in vivo*. Besides, serum levels of sorafenib-treated patients exhibited higher levels of advanced oxidation protein products (AOPP) than before undergoing sorafenib treatment[298]. Interestingly, ABT-263 and sorafenib were discovered to augment ROS levels in HCC BEL7402 cells[242].

3.2.2. ROS production and regorafenib

Regorafenib has also been described to produce mitochondrial injury on isolated rat liver mitochondria through the decrease of membrane potential and ROS production[299].

In metastatic colorectal cancer cells, regorafenib together with the natural compound silybin triggered apoptotic cell death through a ROS-dependent mechanism[300].

Regarding hepatoma cells, regorafenib was described to stimulate ROS generation, impair the respiratory chain activity, inhibit glycolysis, increase mitophagy and produce mitochondrial toxicity in HepG2 cells[301,302]. KEAP1/Nfr2 pathway was found to be involved in the sensitivity to regorafenib of HCC cells, being KEAP1-disrupted cells more resistant to regorafenib cytotoxicity[303].

3.2.3. ROS production and cabozantinib

Few data are available concerning ROS production by cabozantinib administration in relation to its ability to induce cell death. In a study that compared 31 small-molecule kinase inhibitors on isolated mitochondria of rat liver, a ten-fold Cmax (2.58 µM) of cabozantinib showed to affect the oxygen consumption and uncoupled oxidative phosphorylation (OXPHOS). Cabozantinib was shown to decrease mitochondrial membrane potential[299].

3.3. Synthetic pro-oxidants and antioxidants as adjuncts in anti-cancer therapy

Reactive oxygen species (ROS) are known to play a dual role in cancer progression. However, their function in anticancer therapy is yet to be fully understood. While ROS seem to mediate tumorigenesis by activating proliferation and invasion pathways, oxidative stress has also been described to play a role in antitumor treatment. In this context, antioxidants may offer a therapeutic niche in oncologic patients. Antioxidants could scavenge ROS in order to impede cell transformation but also prevent ROS-mediated apoptosis[304]. Furthermore, several cancer cells bear alterations in their intracellular antioxidant system that facilitate chemoresistance[305]. Therefore, drugs that have the ability to modulate ROS generation and function may represent an interesting adjuvant therapy together with anti-cancer treatments.

3.3.1. Buthionine sulfoximine

Buthionine sulfoximine (BSO) is a potent inhibitor of gamma-glutamylcysteine synthetase (GCS), the rate-limiting enzyme in charge of GSH synthesis. Hence, the

addition of BSO depletes cells of cellular GSH, decreases GPX activity and increments ROS production. BSO decreased the level of GSH in the kidney when injected into mice[306,307]. An early work demonstrated that GSH levels are higher in HCC than in normal liver. The addition of BSO impaired HepG2 cells growth[308,309]. Arsenic trioxide (ATO) was found to cooperate with BSO in inhibiting proliferation of HCC cell lines [310,311]. The treatment with BSO elicited ferroptosis in HCC with involvement of p62-Keap1-NFR2 axis[312,313].

BSO has also been tested in the clinical setting. In a phase 1 clinical trial, intravenous BSO together with melphalan was administered to patients with refractory solid tumors, showing that the combination is safe[314]. The treatment with continuous infusion of BSO demonstrated to produce less side effects compared to the combination with melphalan in a phase 1 study conducted in advanced cancer patients[315]. On the other hand, a pilot study was performed on neuroblastoma pediatric patients and showed that the combination of BSO and melphalan had effectivity against high-risk neuroblastoma[316].

3.3.2. MnTBAP

Mn(III)tetrakis(4-benzoic acid) porphyrin, MnTBAP, is a metalloporphyrin SOD2 mimetic that has demonstrated to function as a ROS scavenger in paraquat-induced injury in endothelial cells and *in vivo* models of lung injury[317]. In ganglioside GD3-expressing Hep3B cells, the addition of MnTBAP was found to reduce ROS production under hypoxic conditions[318]. MnTBAP was discovered to limit cell death exerted by sorafenib in HepG2 cells. The SOD2 analog was also observed to increase tumor growth in mice treated with sorafenib[298]. MnTBAP diminished pro-apoptotic and anti-tumor effects of betulinic acid both *in vitro* and *in vivo* in HCC[319]. The treatment with this ROS scavenger rescued hepatoma cells from cytotoxicity induced by the combination of sorafenib and oleanolic acid[320].

3.3.3. Glutathione and Glutathione ethyl ester

Reduced glutathione (GSH) is a tripeptide (gamma-glutamyl-cysteinyl-glycine) present in the cells. GSH acts as a ROS and RNS (reactive nitrogen species) scavenger with detox power. GSH is oxidized by glutathione peroxidase to reduce H_2O_2 to water,

resulting in the glutathione oxidized form (GSSG). In the cytosol, a high ratio GSH/GSSG is maintained[287].

GSH supplementation has been explored in the context of HCC. GSH ethyl ester (GSHEE) is a permeable form of GSH that can cross lipid membranes and enter into the mitochondria[321]. HepG2 cells supplemented with GSHEE and cysteine increased their growth compared to control[309]. In HepG2 cells that overexpressed CYP2E1, the addition of GSHEE rescued cells against cell death induced by FasL and Actinomycin D[322]. The knockdown of xCT, the cystine/glutamate transporter, was found to increase ROS generation in HCC cells and block cell proliferation. The treatment with GSHEE restored ROS levels and overcame growth suppression caused by xCT silencing[323]. The disruption of the 2-oxoglutarate carrier (OGC), a known mitochondrial GSH carrier, promoted a ROS levels increase, and this effect was reversed with the addition of GSHEE in HCC cells. Mitochondrial levels of GSH were replenished with GSHEE treatment. GSHEE was also able to rescue cell viability after OGC knockdown[321]. The silencing of peroxiredoxin 2 (Prx2) produced an increase in ROS generation in HCC CSCs spheroids. The supplementation with GSHEE was able to decrease ROS levels and increase their ability to form spheres[324].

Sorafenib has been described to provoke a rise in ROS generation while depleting intracellular GSH in HepG2 cells[325–327]. Consequently, the addition of GSH to sorafenib-treated cells was shown to ameliorate oxidative stress and rescued cell viability[328].

Regarding GSH utility in the clinical setting, in a study with HCC patients who underwent hepatic arterial intervention chemotherapy, the observational group was administered GSH after treatment, resulting in higher levels of SOD, CD3+, CD4+/CD8+. Moreover, patients who were given GSH showed decreased levels of alanine transaminase (ALT), AST, alkaline phosphatase (ALP) and malondialdehyde (MDA), AOPP, with a better liver function and less oxidative stress[329].

4. Autophagy

4.1. Introduction to autophagy

Autophagy is a degradation process that occurs within cells and it is involved in nutrient starvation, recycling of damaged organelles and destruction of intracellular pathogens[330]. Three different kinds of autophagy have been described: macroautophagy, microautophagy and chaperone-mediated autophagy (CMA)[331]. In macroautophagy, two distinct processes can be identified: non-selective autophagy is stimulated by nutrient deprivation to ensure that the sufficient amount of building blocks is available, and selective autophagy degrades damaged organelles or protein aggregates. Both kinds of macroautophagy contribute to the maintenance of cell homeostasis[332].

The key feature of macroautophagy is the formation of the autophagosome, a double-membrane structure that surrounds the cargo, which fuses with the lysosome, where the degradation of the content of the vesicle takes place[333,334]. Five fundamental stages of autophagy can be described: initiation of the vesicle formation, elongation, maturation, fusion of the autophagosome and lysosome and lysosomal degradation[335]. Those steps are regulated by the autophagy-related (ATG) genes, present in both yeast and mammals[333].

4.2. Mitophagy

Mitophagy is a selective form of macroautophagy in which damaged or excessive mitochondria are removed by the autophagy machinery. Defective mitochondria cannot normally carry out OXPHOS properly, caused by a loss of membrane potential and the accumulation of ROS, contributing to a rise in cellular oxidative stress levels[336].

Mitochondria constitute a dynamic network and constantly experiment fission and fusion processes. Hence, damaged mitochondria must be isolated from the network in order to be recycled. As a consequence, mitophagy and mitochondrial dynamics (fusion and fission) are connected[336,337].

4.3. Mitophagy pathways

4.3.1. PINK1/Parkin pathway

One of the most studied mitophagy pathways is mediated by serine/threonine PTEN-induced putative kinase 1 (PINK1) and the E3 ubiquitin ligase Parkin. PINK1 is known to be the initiator and is constitutively imported to the inner mitochondrial membrane (IMM) through Translocase of the Outer Membrane (TOM) and Translocase of the Inner Membrane (TIM) complexes. Once in the IMM, presenilin-associated rhomboid-like (PARL) cleaves PINK1, which is also processed by the proteasome. As a result, PINK1 expression is kept at a low level under physiological conditions[336,338]. The loss of mitochondrial membrane potential (MMP) produces the gathering of PINK1 in the MOM, where Parkin is recruited. PINK1 phosphorylates Parkin at S65, enabling Parkin ubiquitin ligase activity[339]. Activated Parkin ubiquitinates mitochondrial substrates, such as mitofusin-1 (MFN1), MFN2, VDAC1 or Miro1. Moreover, PINK1 phosphorylates proteins ubiquitylated by Parkin, which amplifies the mitophagy process. The autophagy cargo proteins p62 and optineurin (OPTN) will recognize ubiquitylated mitochondrial proteins, which will interact with LC3 and form a complex that will be degraded by the autophagy machinery[340,341].
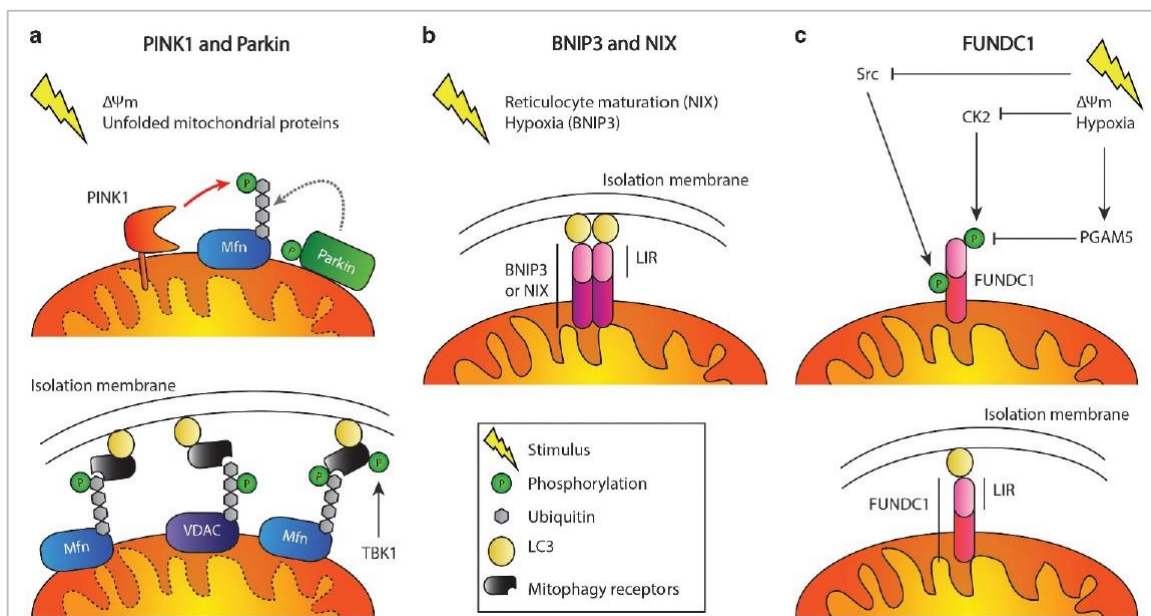
Figure 7. Main mitophagy pathways. a) PINK1 and Parkin-mediated mitophagy pathway. b) BNIP3 and NIX pathway of mitophagy. c) FUNDC1-mediated pathway. Extracted from Bernardini et al., 2017. Ref. 338.

4.3.2. BNIP3/NIX pathway

Mitophagy has also been described to occur through the BNIP3/NIX pathway in liver tissue, skeletal muscle and reticulocytes[342]. BCL-2/adenovirus E1B 19 kDa protein-interacting protein 3 (BNIP3) and BNIP3-like (BNIP3L/NIX) are found in the MOM and can bind LC3[343]. BNIP3 and NIX bear BH3 domains, although it remains unclear if they are BH3-only proteins[344]. HIF1α controls the transcription of both BNIP3 and NIX, so both are considered to take part in hypoxia-induced mitophagy[345]. Other transcriptional regulators of BNIP3 and NIX can be FOXOa3 and NF-κB[346–348]. Interestingly, BNIP3 interacts with Opa1, a mitochondrial dynamin like GTPase, to increase mitochondrial fragmentation[349]. The phosphorylation of BNIP3 may break Opa1-BNIP3 binding thereby increasing mitophagy and decreasing cell death[350]. Both NIX and BNIP3 contain a conserved LC3-binding motif, named LIR, which enhances the affinity for LC3 and functions as a receptor for recruiting mitochondria to autophagosomes[351]. The phosphorylation of the LIR domain has been suggested to control their pro-mitophagy or pro-death activity[336]. Furthermore, some works indicate that NIX could play a role in mitophagy induced by depolarization, but whether NIX acts upstream or downstream of depolarization is yet to be determined[343,352].

4.3.3. FUNDC1 pathway

FUN14 Domain Containing 1 (FUNDC1) has been identified as a mitophagy receptor. It is a MOM protein that can interact with LC3 to induce mitophagy, and is capable of triggering mitophagy through hypoxia[353]. ULK1 phosphorylates FUNDC1 on S17 in the LIR domain, thereby controlling its mitophagy activity[354]. Besides, FUNDC1 can bind to Opa1 and dynamin-related protein 1 (DRP1) after FUNDC1 phosphorylation at S13. Phosphoglycerate mutase 5 (PGAM5), which is activated by PARL cleavage once mitochondria is depolarized, dephosphorylates FUNDC1 at S13[355]. This decreases the formation of Opa1-pFUNDC1 complex, enhancing FUNDC1's binding affinity for DRP1 and triggers mitochondrial fragmentation and mitophagy[356]. Similar to NIX and BNIP3, PGAM5 was discovered to interact with BCL-X_L and necroptosis-related proteins[357].

4.3.4. Non-canonical mitophagy pathways

Beyond the canonical pathways of mitophagy described above, non-canonical pathways have also been identified[336]. Briefly, the lipid-mediated mitophagy involves cardiolipin and prohibitin 2 association[358]. AMBRA1 can also trigger mitophagy through its direct interaction with LC3[359]. BCL2L13 (BCL-RAMBO) has been shown to interact with LC3 and produce mitochondrial fragmentation via DRP1. BCL2L13 has been related to NIX/FUNDC1 mitophagy[360]. FKBP8 has been identified as another mitophagy mediator, which acts as a LC3 recruiter. FKBP8 also displayed anti-apoptotic activity[361]. Members of the Rab family GTPases have been reported to be involved in autophagosomes containing damaged mitochondria[362].

4.4. Mitophagy and cancer

There are several revision works that have delved into the connection between mitophagy and cancer extensively[336,342]. A deregulation of mitophagy proteins has been identified in cancer patients. Depending on the cancer subtype and context, mitophagy proteins appear to play a dual role, either as tumor promoters or tumor suppressors[342,363].

4.5. Mitophagy and HCC

Regarding mitophagy and hepatocellular carcinoma, it has been described that K-Ras may induce mitophagy and mitochondrial loss in HCC tissues that exhibited low glucose uptake in the early stages of tumorigenesis[364]. A study that used two different mTOR inhibitors showed that this combination was capable of triggering mitophagy in HCC cells, which is thought to exert an anti-tumor function in the liver[365]. In HCC cell lines, the blockade of the PI3K/AKT pathway provoked DNA damage-regulated autophagy modulator (DRAM)-induced apoptosis through the mediation of mitophagy[366]. Interestingly, the expression of Parkin has been related to an easier recurrence of patients with HCC with adjuvant transarterial chemoembolization[367]. Mitophagy was found to control p53 activity that regulated hepatic CSCs maintenance, and thus, has been considered to enhance hepatocarcinogenesis[368]. Under hypoxic conditions, AMPK pathway was induced and that induction led to mitophagy in HCC cells[369]. Another study described that the antifungal drug ketoconazole was able to activate mitophagy in HCC cells and murine models via PINK1 induction[370,371]. Cisplatin was found to provoke

mitophagy in HCC cells via DRP1 inhibition[372,373]. The inhibition of DRP1 was discovered to suppress mitophagy and promote apoptosis in HCC under hypoxia[374]. Hepatitis B viral x (HBx) protein has also been related to the activation of mitophagy that was restrained by the expression of E3 ubiquitin-protein ligase MARCH5 in Huh7 cells[375]. HBx has also been described to promote BNIP3L expression and mitophagy, thereby increasing cancer stemness of HCC[376]. Moreover, iron loss was identified as another mechanism that triggered mitophagy in HCC[377,378]. The lncRNA MALAT1 was described to control the metabolic reprogramming in HCC cells via the mitophagy pathway[379]. The inhibition of optineurin was found to impair mitophagy and block HCC progression[380]. In HCC senescent cells, the overexpression of PINT87aa, a peptide encoded by the long intergenic non-protein coding RNA, p53 induced transcript (LINC-PINT), was found to impair proliferation and suppress mitophagy both *in vitro* and *in vivo*, while FOXM1 expression elicited the opposite effect[381].

4.6. Mitophagy and multityrosine kinase inhibitors

A small number of research works have focused on the capacity of MKI of inducing mitophagy in HCC models. As previously reported for ROS production, sorafenib and regorafenib alone were described to induce mitophagy in HepG2 cells[302]. Sorafenib combined with melatonin potentiated mitophagy in HCC cell lines[382,383]. Hyperactivated mitophagy via ATAD3A-PINK1/Parkin pathway was found to be involved in the resistance to sorafenib of HCC cells[384]. Another study described that sorafenib activated PINK1/Parkin pathway through the targeting of the mitochondrial electron transport chain complexes and ATP synthase in HEK293T and HeLa cells[385]. The IMM protein STOML2 was reported to increase the mitophagy flux through stabilizing PINK1 and promoting HCC metastasis and modulating sensitivity towards lenvatinib[386].

Hypothesis and Objectives

Hepatocellular carcinoma is still a major health concern with a poor prognosis due to failure to respond to current chemotherapy or the development of resistance against it. For that reason, the efficacy of the systemic agents used in the clinical practice for the management of HCC, such as sorafenib, regorafenib or cabozantinib must be improved. Since sorafenib-induced mitochondrial damage is potentiated by BH3-mimetics, our working hypothesis was that the BCL-2 network could also play a role in regorafenib activity and used to enhance regorafenib efficacy.

Objective 1

Determine whether the combination of regorafenib plus the BCL-xL inhibitor A-1331852 had an additional cytotoxic effect *in vitro* and *in vivo*. We aim to know if both agents combined cooperate in inducing HCC tumor regression.

Since several multityrosine kinase inhibitors cause mitochondrial damage and ROS production in tumor cells, antioxidant supplementation may influence the ability of MKIs used in HCC therapy to exert their anti-proliferative, tumor-killing capacity.

Objective 2

Ascertain if the multikinase inhibitors sorafenib, regorafenib and cabozantinib exercise their anti-tumor function through a ROS-dependent mechanism. We intend to test how antioxidant as well as pro-oxidant compounds can alter MKIs performance in targeting HCC tumor cells.

Methodology

1. Cell cultures

Human hepatocellular carcinoma cell lines HepG2, Hep3B and PLC/PRF/5 were obtained from European Collection of Animal Cell Cultures (ECACC). LX2 human hepatic stellate cell line (HSC) was donated by Dr. Ramon Bataller and BCLC-9 cells were given by Dr. Jordi Bruix. Cells were kept inside a water jacket CO_2 incubator (Forma Series II, Thermo Scientific) at 37ºC and 5% CO_2 in Dulbecco's Modified Eagle's Medium (DMEM, with 4500 mg/L glucose, L-glutamine, and sodium bicarbonate) supplemented with 10% FBS and 1% penicillin/streptomycin. Regorafenib-resistant cell lines (HepG2 R and Hep3B R) were maintained at 2 µM regorafenib and all assays were performed with cells out of the drug for at least three days.

2. Chemicals

Sorafenib (Nexavar) and regorafenib (BAY 73-4506, Stivarga) are manufactured by Bayer. Cabozantinib was purchased from MedChem Express. A-1331852 (MedChem Express), ABT-263 (Navitoclax) and ABT-199 (Venetoclax) were purchased from Selleckchem (Houston, TX). A-1210477 was obtained from ApexBio. L-Buthionine sulfoximine, MnTBAP chloride and glutathione monoethyl ester were obtained from Santa Cruz Biotechnology, Inc.

3. Cell viability assay

Cell viability was determined by MTT (3-(4,5-dimethylthiazol-2-yl)-2,5-diphenyl tetrazolium bromide) assay. MTT reagent is converted to insoluble formazan crystals by mitochondrial dehydrogenase enzymes of living cells. Insoluble formazan is dissolved with 1-propanol and colorimetrically measured by a plate reader at a 570 nm of wavelength. Absorbance values are proportional to the amount of living cells[387].

$7.5x10^3$ or $1x10^4$ cells/well were seeded in 96-well plates and incubated at 37ºC and 5% CO_2. Cells were treated with the indicated compounds for 16-24 h at which point 10 µl of MTT reagent at a concentration of 5 mg/ml was added and incubated for 2 h. Growth media was aspirated and formazan crystals were dissolved with 100 µl of 1-propanol. Absorbance was measured in a plate reader (Multiskan® Spectrum, Thermo Fisher Scientific, Rockford, IL) at 570 nm (formazan product) and at 630 nm (background reading). The index of cell viability was calculated from the subtraction of absorbance

570 – absorbance 630. Cell viability was given as a percentage values. Wells without treatment were considered as 100% of cell viability. The relative values of the treated wells were calculated ((A570 – A630)sample/(A570-A630)control)x100.

4. Clonogenic assay

Clonogenic assay was performed with crystal violet staining. 8×10^4 cells were seeded into 12-well plates and kept at 37ºC in 5% CO_2. Cells were treated and left for three days until they were fixed with 10% formalin for 5 min. Crystal violet reagent (0.05%) was added for 30 min and after that plates were washed with water twice. Plates were drained, excess water aspirated, and photos were taken.

5. 3D tumor liver spheroids generation

Multicellular tumor spheroids were generated from a ratio 4:1 or 10:1 Hep3B or HepG2 and LX2 cells. 1×10^4 cells/well were plated in 96-well plates with a bottom coat of 1.5% agarose. Tumor liver spheroids were kept at 37ºC and 5% CO_2 for three days. Treatments were added and replaced daily. Bright field images were taken daily with Olympus IX-70 microscope equipped with the CC-12 FW camera and later analyzed with ImageJ software. Spheroid volume was calculated using the formula: Volume = L (long diameter) x S^2 (short diameter) x 0.5.

6. Caspase-3 activity assay

3×10^4 cells/well were seeded in 12-well plates. After the treatment, cells were scrapped with 50 mM Hepes (pH 7.4), 5 mM CHAPS and DTT 5mM. After centrifugation, supernatant containing the extracted proteins is collected. In order to measure Caspase-3 activity, 50 µg of protein were added to 200ul of assay buffer containing 20 mM Hepes, 5% sucrose, 0.1% CHAPS, 2 mM EDTA and 5mM DTT, pH 7.4, and 50 µM of the caspase-3 substrate Ac-DEVD-AFC (Santa Cruz Biotechnology). Fluorogenic detection of AFC after substrate cleavage was recorded at 15 min time intervals, emission 505 nm and excitation at 400 nm. A unit of caspase-3 activity is the amount of active enzyme necessary to produce an increase in 1 fluorescence unit in Spectramax Gemini XS fluorimeter. Results are usually represented as Arbitrary Unit/h/µg protein.

7. Hoechst staining

Cells were seeded at $5x10^4$ cells/well in 12-well plates and treated for 8 h. Hoechst 33258 (stock 1mg/ml) was added at 1/1000 dilution and incubated for 30 minutes. After being washed twice with PBS, images were taken with the UV filter using an Olympus IX-70 microscope with the CC-12 FW camera. Photos of twelve random fields were taken. Condensed nuclei were counted with ImageJ software.

8. Western blot assay

Cells were seeded at a density of $2x10^5$ cells/well in a 12-well or 24-well plate and treated at indicated times with indicated compounds.

Protein was collected in 250 µl of RIPA buffer containing a cocktail of protease inhibitors (cOmplete™, Roche). Bradford assay was performed in a 96-well plate to determine protein concentration. Samples were diluted ¼ and triplicates and BSA standards (0, 0.1, 0.25, 0.5, 0.75 and 1 mg/ml) were loaded. Bradford reagent was incubated for 5 min in the dark. Absorbance was read at Multiskan® Spectrum plate reader at 595 nm in order to obtain a calibration curve and determine sample protein concentration (mg/ml).

Protein samples were prepared with Laemmli Sample Buffer plus 10% β-mercaptoethanol. Samples were heated for 5 min at 95 ºC. After that, samples were kept on ice (heat shock). After a vortex and a spin, 20 µg of sample were loaded in 10-15% SDS-PAGE in a Mini-PROTEAN® Tetra System (Bio-Rad) gel electrophoresis system. 5 µl of Protein marker V (pre-stained), peqGOLD was used as molecular weight marker to monitor samples running.

Protein transfer from the gel to nitrocellulose membranes was performed using Bio Rad Trans-Blot Turbo® Transfer System. Transfer efficiency was assessed by Ponceau S staining. After removing Ponceau S dye with TBS-T washes, membranes were blocked for 1 h at room temperature or overnight at 4ºC with 5% milk in TBS-T. Three washes, 5 min/each, with TBS-T were performed prior to antibodies detection.

Primary antibodies were incubated for 3 h at room temperature or overnight at 4ºC:

PARP-1 (H-250, Santa Cruz Biotechnology, sc-7150, dilution 1:500, rabbit),

MCL-1 (S-19, Santa Cruz Biotechnology, sc-819, dilution 1:400, rabbit),

BCL-XL (H-5, Santa Cruz Biotechnology, sc-8392, dilution 1:250, mouse),

BCL-2 (C-2, Santa Cruz Biotechnology, sc-7382, dilution 1:250, mouse),

Cytochrome C (H-104, Santa Cruz Biotechnology, sc-7159, dilution 1:250, mouse),

BAX (N-20, Santa Cruz Biotechnology, sc-493, dilution 1:1000, rabbit),

Tom20 (Santa Cruz Biotechnology, sc-11415, 1:500, rabbit),

cleaved Caspase-3 (D175, #9661S Cell Signaling, 1:1000, rabbit),

MFN2 (H-68, Santa Cruz Biotechnology, sc-50331, dilution 1:1000, rabbit)

Optineurin (C-2, Santa Cruz Biotechnology, sc-166576, dilution 1:1000, mouse)

PINK1 (BC100-494, Novus Biologicals, dilution 1:2000, rabbit)

Parkin (PRK8, ab77924, Abcam, dilution 1:2000, mouse)

BNIP3L/NIX (EPR4033, ab109414, Abcam, dilution 1: 2000, rabbit)

β-Actin (Sigma-Aldrich, A3854, conjugated to HRP, dilution 1: 40,000).

Three washes with TBS-T of 5 min/wash were done to eliminate unbound primary antibody.

Secondary antibody incubation was performed for 1 h at room temperature using anti-mouse (m-IgGκ BP-HRP sc-516102, Santa Cruz Biotechnology, 1:10000) and anti-rabbit (goat anti-rabbit IgG-HRP sc-2054, Santa Cruz Biotechnology, 1:10000). After three washes with TBS-T, 5 min/wash, membranes were detected using ECL western blotting substrate (Pierce), Clarity and Clarity Max (Bio-Rad) and ChemiDoc Imaging System (Bio-Rad).

9. Gene silencing

Short interference RNA (siRNA) was used to transiently block gene expression. Cells were seeded at 70% confluence in 24-well plates. 1 µl Lipofectamine 3000™ reagent was used for Hep3B cells/well and 20 pmol siRNA/well. siRNAs were prepared in a separate tube with Opti-MEM™. Lipofectamine 3000™ and Opti-MEM™ were prepared in another Eppendorf tube. Then both tubes were mixed in order to let siRNA and Lipofectamine 3000™ to thoroughly mix for 15 min at room temperature. After that, cells were treated with siRNA coupled with Lipofectamine™ 3000 for 24 h. Experiments of cell viability were performed afterwards. The siRNA used are: Control siRNA-A (sc-37007,

Santa Cruz Biotechnology), BCL-2 siRNA (sc-29214, Santa Cruz Biotechnology), BCL-xL siRNA (sc-43630, Santa Cruz Biotechnology), BCL-2 siRNA (ID#s1915, Ambion Life technologies) and BCL-xL siRNA (ID#s1920, Ambion Life technologies).

10. Reactive Oxygen Species (ROS) measurement

Reactive oxygen species were measured using dihydroethidium (DHE) probe, that targets anion superoxide. 7.5×10^3 or 1×10^4 cells/well were seeded in 96-well plates. After treating cells with indicated drugs, DHE probe was added at a final concentration of 10 µM for 30 min. After probe internalization, two washes were performed with DMEM without phenol red to remove the unbound dye. DHE-derived red fluorescence was observed with rhodamine filter (excitation 490; emission 590 nm) and pictures of ten random fields were taken using Leica-CTR4000 microscope and LAS software.

11. Mitochondrial membrane potential assay

C5,5',6,6'-tetrachloro-1,1',3,3'-tetraethylbenzimidazolyl-carbocyanine iodide (JC-1) is a fluorescent cationic dye and used as an indicator of mitochondrial potential in cells. It Mitochondria with high membrane potential are labelled orange while mitochondria with low membrane potential are labelled green. Mitochondrial depolarization is assessed by a decrease in the red (J-aggregates)/green (J-monomers) fluorescence intensity ratio [388,389]. To determine mitochondrial membrane potential, 1×10^4 cells/well were seeded in 96-well plates. After treatments, JC-1 dye was added at a final concentration of 5 µg/ml for 15 minutes. After washes with DMEM without phenol red, fluorescence intensity was measured at 514/529 nm emission and 585/590 nm excitation with Spectramax Gemini XS fluorimeter. The ratio J-aggregates/J-monomers was calculated. The ratio of DMSO (0.05%) was used as control. Photos were taken with Leica-CTR4000 microscope and LAS software.

12. RNA Isolation

2×10^5 cells/well were seeded in 12-well plates. Cells were treated at the indicated times. After that, cells were rinsed with PBS and 0.5 ml of TRIzol® reagent was added to lysate cells. Cells were left for 5 min to dissociate nucleoproteins complex. Then 0.1 ml of

chloroform was added and samples were incubated for 2 min. Samples were centrifuged at 12,000 x g at 4ºC for 15 min. The colorless upper aqueous phase was collected into a new tube. 0.25 ml of isopropanol was added to each tube. After an incubation at room temperature for 10 min, samples were centrifuged for 10 min at 12,000 x g at 4ºC. Supernatant was discarded. After two rounds of adding 0.5 ml of 75% ethanol was added and centrifuging at 7,500 x g at 4ºC for 5 min, RNA pellets were left to air dry for 5 min and resuspended in 50 µl of RNase-free water. Samples were kept on ice until incubation at 60ºC for 10-15 min and 550 rpm. Samples were frozen and subsequently thawed prior to quantification using NanoDrop™ 1000 Spectrophotometer (Thermo Scientific).

13. Retrotranscription

Isolated RNA was reversely transcribed to cDNA. 1 µg of RNA was reverse transcribed with an iScript™ cDNA Synthesis Kit (Bio-Rad, Berkeley, CA, USA). 5x iScript Reaction Mix was added in a ratio of 4 µl per sample and iScript Reverse Transcriptase was added in a ratio of 1 µl per sample. Using MJ Mini™ Personal Thermal Cycler (Bio-Rad), the following program was performed to RNA samples: 5 min at 25 ºC, 30 min at 42 ºC, 5 min at 85ºC and after that samples were kept at 4ºC until storage. Then, cDNA concentration was adjusted at 10 ng/µl.

14. Real-time quantitative-PCR

In order to carry out qPCR and determine gene expression differences between samples, cDNA (10ng/µl) was diluted ¼ with RNase-free water. iTaq™ Universal SYBR® Green Supermix 2x (Bio-Rad) was used in a ratio of 10 µl/20 µl of reaction, forward and reverse primers were used at a 5 µM, cDNA was loaded at 2.5 ng/µl per 20 µl of reaction in 96-well or 384-well plates. Once the plate was loaded with replicates for each sample, the plate was centrifuged at 1000 rpm for 1 min. After that, plates were placed in Bio-Rad® CFX96™ or CFX384™ systems. The following protocol was applied: SYBR® only mode, 20-30 s at 95 ºC for polymerase activation and DNA denaturation, 2-5 s at 95 ºC for denaturation, 15-30 s at 60 ºC for primer annealing and extension plus plate read. 40 cycles were run for 1 min at 95 ºC. Moreover, melt-curve analysis was performed at 65-95 ºC with 0.5ºC increment for 2-5 s/step. Two housekeeping genes, β-actin and 18 S were considered as control gene expression and relative gene expression was calculated for each gene using ΔΔCt method. The primers sequences used were:

human BCL-2: Fw 5'-GGAGGATTGTGGCCTTCTTT-3'; Rv 5'-GCCGTACAGTTCCACAAAGG-3'

human BCL-XL: Fw 5'-GGATGGCCACTTACCTGA-3'; Rv 5'-CGGTTGAAGCGTTCCTG-3'

human MCL-1: Fw 5'-ATGCTTCGGAAACTGGACAT-3'; Rv 5'-TCCTGATGCCACCTTCTAGG-3'

human BCL-B: Fw 5'-GCTGGGATGGCTTTTGTCA-3'; Rv 5'-GCCTGGACCAGCTGTTTTCTC-3'

human BCL-w: Fw 5'-ACCCCAGGCTCAGCCCAACA-3'; Rv 5'-CAGCACACAGTGCAGCCCCA-3'

human BFL-1: Fw 5'-TTACAGGCTGGCTCAGGACT-3'; Rv 5'-AGCACTCTGGACGTTTTGCT-3'

human BIM: Fw 5'-TGGCAAAGCAACCTTCTGATG-3'; Rv 5'-GCAGGCTGCAATTGTCTACCT-3'

human NOXA: Fw 5'-TGGAAGTCGAGTGTGCTACTCA-3'; Rv 5'-CAGAAGAGTTTGGATATCAGATT-3'

human PUMA: Fw 5'-GCATGCCTGCCTCACCTT-3'; Rv 5'-TCACACGTCGCTCTCTCTAAACC-3'

mouse CCR2: Fw: 5'-ATCCACGGCATACTATCAACATC-3'; Rv: 5'-CAAGGCTCACCATCATCGTAG-3'

human MCP-1: Fw: 5'- TCAAACTGAAGCTCGCACTC-3'; Rv 5'-ATTGATTGCATCTGGCTGAG-3'

human β-Act: Fw 5'-AGAAAATCTGGCACCACACC-3'; Rv 5'-AGAGGCGTACAGGGATAGCA-3'

15. Tumor mice models

All animal procedures were performed according to protocols approved by the Animal Experimentation Ethics Committee from the University of Barcelona. 5-6 week old male Swiss nude mice were kept under pathogen-free conditions and fed with food and water *ad libitum*. 1×10^6 BCLC-9 or HepG2 were injected subcutaneously into the flanks of mice in 150 µl 0% FBS DMEM. Regorafenib (30 mg/kg body weight), A-1331852 (25 mg/kg body weight) or vehicle was given daily by oral gavage for 24 days. Vehicle and drugs were prepared in a mixture containing 5% DMSO, 5% absolute ethanol, 5% cremophor® and 75% physiologic serum. Tumors were measured periodically with a Vernier caliper, and the volume was calculated as length×width^2×0.5. Mice were anesthetized with pentobarbital sodium. At the time of the sacrifice, subcutaneous tumors were collected as well as peripheral blood.

16. Paraffin embedding

After collection, tumors were kept at room temperature in 10% formalin. After 48 h, samples were washed with tap water and kept at 4ºC in 70% ethanol until paraffin embedding. Samples were embedded in paraffin using Shandon Citadel 1000 tissue processor (Thermo Scientific). Tumor samples went through a dehydration process: two steps of 1:30 h in water, 1 h in 70% ethanol, another step of 70% ethanol of variable duration, two steps of 1 h in 96% ethanol, two steps of 1 h in 100% ethanol, two steps of

1 h in xylene and two steps of 2 h each in paraffin. At the end, samples were mounted in cassettes and left to cool down at 4ºC.

17. Slices

Paraffin-embedded tumor samples were cooled down with icy water and cut at 5 µm thickness with a Leica RM 2155 microtome. Slices were put on a water bath at 42 ºC and two slices from every sample were collected with each slide. Slides were left to air-dry and kept until staining.

18. Immunohistochemistry

Firstly, tumor samples were put on a basket and were heated 15 min at 60ºC to melt paraffin. Samples underwent a rehydration process prior to immunohistochemical staining at room temperature: two steps of xylene for 10 min, one step of 100% ethanol for 10 min, one step of 90% ethanol for 3 min, one step of 70% ethanol for 3 min, one step of 30% ethanol for 3 min and a step in distillated water for 5 min.

After rehydration, antigen retrieval was performed. Samples were put inside boxes containing 2% citrate buffer for 15 min in autoclave at 100ºC. Samples were left to cool down under running tap water. Then, endogenous peroxidase was blocked with 200 ml of methanol plus 6 ml of hydrogen peroxide for 15-30 min at room temperature. Three washes with PBS of 5 min/wash were performed. The excess of liquid from tumor samples was carefully dried with a paper tissue. Samples were marked with a liquid-repellent slide marker pen (Daido Sangyo, Japan). At that step, samples were placed inside a humidity and dark chamber. 10% goat serum was added for 10 min at room temperature. A rinse with PBS was performed.

Primary antibodies incubation took place overnight at 4ºC and inside the humidity and dark chamber. PCNA antibody (1:100, mouse, sc-56 Santa Cruz Biotechnology) was diluted in Dako Antibody Diluent with Background Reducing Components and 50 µl of antibody was added per sample. After three washes with PBS of 5 min/wash, the excess of liquid was carefully dried with a paper tissue. 50 µl of secondary biotinylated mouse antibody was added at 1:200 for 45 min at room temperature inside the humidity, dark chamber. After three washes with PBS of 5 min/wash, the excess of liquid was carefully dried with a paper tissue. The AB Complex/HRP was added for 30 min at room

temperature inside the humidity, dark chamber. A wash with PBS of 5 min was performed. The excess of liquid was carefully dried with a paper tissue. DAB was added for 3-5 min to samples. A quick wash with tap water was performed. After that, samples were stained with Dako hematoxylin for 5-10 s. Another quick wash with tap water was performed until mounting with Aquatex. Photos were taken with Zeiss microscope and XC50 camera.

19. Immunofluorescence

Hep3B cells were seeded at a density of 50,000 cells/well in 12-well plates on 10 mm round coverslips. After incubation with corresponding treatments, cells were rinsed with PBS and fixed with 4% PFA for 15 min. After that, three washes with PBS were performed. Fixed cells were kept at 4ºC before the immunofluorescence staining.

Cells attached to round coverslips were blocked in a solution of 1% fatty acid free BSA, 0.1% saponin and 0.5% glycine in PBS for 20 min at room temperature. After drying the excess of blocking solution, cells were incubated with primary antibodies overnight at 4ºC inside a dark chamber (LC3 antibody, #2775S, Cell Signaling Technology®, 1/300, rabbit; PDHA1 antibody, ab110330, Abcam, 1/200, mouse) in 0.05% saponin and Dako Antibody Diluent with Background Reducing Components as solvent. The next morning, three washes with PBS were performed prior to incubation with secondary antibodies for one hour at room temperature inside the dark chamber (anti-rabbit Cy3, 1/300; Alexa Fluor 488 donkey anti-mouse IgG A21202 Invitrogen, 1/300) and acid nucleic marker DRAQ5™ (DR50200, BioStatus) in 0.05% saponin and and Dako Antibody Diluent with Background Reducing Components as solvent. Three more washes with PBS were done before mounting the coverslips in 5 µl of Fluoromount-G® (0100-01, SouthernBiotech).

Preparations were left to dry overnight in the dark at room temperature. The next day photos were taken at the confocal microscope Leica TCS SPE with the 60x oil objective. Ten photos of random fields were taken per sample.

20. Synergy analysis

Synergy analysis was performed using Combenefit software and following simpler Highest Single Agent (HSA) model [390].

21. Statistical analysis

Results are expressed as mean plus or minus standard deviation of three replicates, unless indicated. Statistical comparisons were usually performed using unpaired 2-tailed Student's t test, and 1-way ANOVA followed by Newman–Keuls multiple comparison test (GraphPad Prism) was used for data quantification from patients. A p value less than 0.05 was considered significant.

22. Products

The products used to performed all techniques described are listed below.

Product	Reference
Dulbecco's Modified Eagle's Medium (DMEM)	D5796-500ML, Sigma-Aldrich
PBS	D8862-500ML, Sigma-Aldrich
FBS	10270106, Gibco
Penicillin/streptomycin	P4333, Sigma-Aldrich
Trypsin	T4049-500, Sigma-Aldrich
Sorafenib (Nexavar)	Bayer
Regorafenib (Stivarga)	Bayer
Cabozantinib	MedChem Express
A-1331852	Selleckchem
ABT-263 (Navitoclax)	Selleckchem
ABT-199 (Venetoclax)	Selleckchem
A-1210477	ApexBio
MTT (Thiazolyl Blue Tetrazolium Bromide)	M2128-1G, Sigma-Aldrich
Crystal Violet	sc-207460, Santa Cruz Biotechnology
Hoechst (bisBenzimide H 33258)	B1155-25MG, Sigma-Aldrich
RIPA (Pierce RIPA Buffer)	89900, Thermo Scientific
Protease inhibitors (Protease inhibitor cocktail tablets)	11836153001, Roche

4x Laemmli Sample Buffer	161-0747, Bio-Rad
Protein marker V (pre-stained), peqGOLD	27-2210, VWR Peqlab
BioRad Protein Assay Dye Reagent Concentrate	500-0006, Bio-Rad
Nitrocellulose Blotting Membrane (Amersham™ Protran™ Supported 0.2 µm NC)	10600015, GE Healthcare Life Sciences
Ponceau S solution	P7170-1L, Sigma-Aldrich
Milk (Nonfat dried milk powder)	A0830,0500, PanReach AppliChem
ECL western blotting substrate	Pierce Thermo Fisher Scientific
Clarity Max™ Western ECL Substrate	1705062, Bio-Rad
Clarity™ Western ECL Substrate	170-5061, Bio-Rad
TBS-T (Tris Buffered Saline, with Tween®)	T9039-10PAK, Sigma-Aldrich
Restore™ PLUS Western Blot Stripping Buffer	#46430, Thermo Scientific
10x Tris/glycine/SDS running buffer	#1610772, Bio-Rad
Trans-Blot® Turbo™ 5x Transfer Buffer	#10026938, Bio-Rad
Lipofectamine™ 3000	Invitrogen
Opti-MEM™ I	31985-070, Gibco
Dihydroethidium (DHE)	D7008, Sigma-Aldrich
DMEM without phenol red	D4947-500ML, Sigma-Aldrich
JC-1	3520-43-2, Sigma-Aldrich
TRIzol® reagent	15596018, Ambion Life Technologies
iScript™ cDNA Synthesis Kit	1708890, Bio-Rad
iTaq™ Universal SYBR® Green Supermix	1725120, Bio-Rad
Cremophor® EL	C5135, Sigma-Aldrich
Physiological serum 0.9%	Braun
DMSO (dimethyl sulfoxide)	sc-358801, Santa Cruz Biotechnology
Pentobarbital sodium 5%	Pharmacy service, Hospital Clinic
Hydrogen peroxide solution	516813-500ML, Sigma-Aldrich
10% Normal goat serum	50197Z, Invitrogen
Dako Antibody Diluent with Background Reducing Components	S3022, Dako

Vectastain ABC Kit Elite® PK-6100 Standard	Vector
DAB Substrate	11718096001, Roche
Dako Hematoxylin	CS700, Dako
Aquatex®	363123S, VWR
L-Buthionine sulfoximine	sc-200824, Santa Cruz Biotechnology
MnTBAP chloride	sc-221954, Santa Cruz Biotechnology
Glutathione monoethyl ester	sc-203974, Santa Cruz Biotechnology
Alexa Fluor 488 donkey anti-mouse IgG	A21202, Invitrogen
DRAQ5™	DR50200, BioStatus
Fluoromount-G®	0100-01, SouthernBiotech
Bovine Serum Albumin (BSA), Fatty Acid Free	sc-500949, ChemCruz®
Glycine	G7126-500G, Sigma-Aldrich
Saponin from quillaja bark	S4521-10G, Sigma-Aldrich
Paraformaldehyde solution 4% in PBS	sc-281692, ChemCruz®
Mito-TEMPO	#10-4100, Focus Biomolecules
Mitoquinone	#10-1363, Focus Biomolecules

Results

Report from the directors and the tutor

UNIVERSITAT DE
BARCELONA

Escola de Doctorat

MODEL Informe director/s /tutor sobre l'autorització del dipòsit de la tesi

El Dr. **Albert Morales Muñoz** i la Dra. **Montserrat Marí Garcia**, com a codirectors i el Dr. **Carles Enrich Bastús**, com a tutor de la tesi doctoral titulada "**Regulation of the microenvironment and chemoresistance in liver therapy**" i, d'acord amb el que s'estableix a l'article 35 Normativa reguladora del Doctorat a la Universitat de Barcelona, emeto el següent:

INFORME

(Informe detallat i motivat sobre el contingut de la tesi i sobre l'autorització de dipòsit de la tesi que s'ha demanat)

La tesi de la doctoranda Blanca Cucarull es presenta en format per articles i conté dues publicacions (Cancers 2020, factor d'impacte 6.639 i Antioxidants 2021, factor d'impacte 6.312) de les que la doctoranda es primera autora i que no han estat ni seran utilitzades en cap altre tesi doctoral.

1) **Cucarull, B.**; Tutusaus, A.; Hernáez-Alsina, T.; García de Frutos, P.; Reig, M.; Colell, A.; Marí, M.; Morales, A. Antioxidants Threaten Multikinase Inhibitor Efficacy against Liver Cancer by Blocking Mitochondrial Reactive Oxygen Species. Antioxidants 2021, 10, 1336. doi: 10.3390/antiox10091336
La doctoranda Blanca Cucarull es primera signant en solitari i la principal responsable de la feina que conté. Gràcies a ella, hem pogut identificar els productes oxidants mitocondrials com a importants efectors de la mort induïda per inhibidors multiquinasa com sorafenib o regorafenib, freqüentment utilitzats en el tractament del carcinoma hepatocelular (HCC). En models in vitro i 3D d'esferoides de tumors de fetge desenvolupats per la doctoranda, s'ha pogut caracteritzar com determinat antioxidants poden interferir amb la eficàcia de la teràpia anti-tumoral per l'HCC. Així mateix, mitjançant estudis de western blot i microscòpia confocal, també desenvolupats per la doctoranda, hem pogut identificar la mitofagia com un mecanisme activat per sorafenib i regorafenib, modulat per l'estatus redox cel·lular, i susceptible de veure's afectat per la suplementació d'antioxidants durant l'administració d'aquests agents quimioterapèutics.

2) **Cucarull, B.**; Tutusaus, A.; Subías, M.; Stefanovic, M.; Hernáez-Alsina, T.; Boix, L.; Reig, M.; García de Frutos, P.; Marí, M.; Colell, A.; Bruix, J.; Morales, A. Regorafenib Alteration of the BCL-xL/MCL-1 Ratio Provides a Therapeutic Opportunity for BH3-Mimetics in Hepatocellular Carcinoma Models. Cancers (Basel). 2020 Feb 1;12(2):332. doi: 10.3390/cancers12020332
La doctoranda Blanca Cucarull es primera signant d'aquesta publicació i la co-responsable de la feina que conté, juntament amb la doctora Anna Tutusaus que va iniciar-la en els seus primers estadis. La Dra. Tutusaus en una publicació prèvia (Tutusaus et al, Oncotarget 2016) havia identificat BCL-2 i BCL-xL com a proteïnes responsables de la toxicitat mitocondrial del sorafenib. Després de observar que BCL-xL podia jugar un paper semblant en la toxicitat induïda pel regorafenib, va deixar a la doctoranda com a responsable de tota la recerca posterior. Gràcies a ella, hem pogut identificar una alteració en el sistema de proteïnes de BCL-2, principalment de BCL-xL i MCL-1, induïda pel tractament amb regorafenib de cèl·lules de carcinoma hepatocel·lular (HCC). En models experimentals de tumors de fetge, in vitro i in vivo desenvolupats per la doctoranda, s'ha pogut caracteritzar que en la combinació de regorafenib amb l'A-1331852, inhibidor de BCL-xL, l'eficàcia de la teràpia anti-tumoral per HCC es veu clarament incrementada. Així mateix, en un model tumoral animal de resistència a regorafenib analitzat per la doctoranda, es va poder evidenciar un important increment del ratio BCL-xL/MCL-1 i l'efectivitat de la teràpia combinada de regorafenib amb l'inhibidor de BCL-xL. L'alteració del sistema de proteïnes de la família de BCL-2 va ser detectada alterada en nombrosos malalts de HCC i podria ser un bon marcador indicatiu de efectivitat del tractament amb regorafenib.

En resum, la feina desenvolupada per la doctoranda Blanca Cucarull ha contribuït a caracteritzar el dany mitocondrial induït per sorafenib i regorafenib, inhibidors multiquinasa emprats en el tractament del

UNIVERSITAT DE
BARCELONA

Escola de Doctorat

carcinoma hepatocelular, com un element crític en la seva eficàcia antitumoral. Caracteritzar aquesta via mitocondrial ens ha permès identificar que mimètics BH3 com l'A-1331852 són capaços de potenciar l'activitat de sorafenib i regorafenib, i que els suplements antioxidants poden interferir amb la efectivitat de la teràpia multiquinasa si es prenen simultàniament. Per tot això, considerem que l'aportació científica de la doctoranda Blanca Cucarull Martínez és molt rellevant i aconsellem que es procedeixi al dipòsit de la seva tesi doctoral.

Barcelona, _21_ d'/de _Setembre_ de 20 _21_.

(signat)
Dr. Albert Morales Muñoz i Dra. Montserrat Marí Garcia

Firmado digitalmente por MORALES MUÑOZ ALBERT - 43687659X
Fecha: 2021.09.21 16:01:33 +02'00'

Firmado digitalmente por MARI GARCIA MONTSERRAT - 46656698W
Fecha: 2021.09.21 16:02:40 +02'00'

Dr. Carles Enrich Bastús

Un cop s'hagi emplenat l'informe, s'ha d'adjuntar i s'ha de fer arribar al doctorand o al president de la Comissió Acadèmica del programa de doctorat responsable de la tesi.

The results that have been obtained during the completion of this doctoral thesis have been published in two original articles.

Results 1:

<u>Cucarull, B.</u>; Tutusaus, A.; Subías, M.; Stefanovic, M.; Hernáez-Alsina, T.; Boix, L.; Reig, M.; García de Frutos, P.; Marí, M.; Colell, A.; Bruix, J.; Morales, A. **Regorafenib Alteration of the BCL-xL/MCL-1 Ratio Provides a Therapeutic Opportunity for BH3-Mimetics in Hepatocellular Carcinoma Models.** Cancers 2020, 12, 332. https://doi.org/10.3390/cancers12020332

Results 2:

<u>Cucarull, B.</u>; Tutusaus, A.; Hernáez-Alsina, T.; García de Frutos, P.; Reig, M.; Colell, A.; Marí, M.; Morales, A. **Antioxidants Threaten Multikinase Inhibitor Efficacy against Liver Cancer by Blocking Mitochondrial Reactive Oxygen Species.** Antioxidants 2021, 10, 1336. https://doi.org/10.3390/antiox10091336

Results 1

The alteration of BCL-xL and MCL-1 expression by regorafenib sensibilizes hepatocellular carcinoma models towards BH3 mimetics

Cucarull, B.; Tutusaus, A.; Subías, M.; Stefanovic, M.; Hernáez-Alsina, T.; Boix, L.; Reig, M.; García de Frutos, P.; Marí, M.; Colell, A.; Bruix, J.; Morales, A. **Regorafenib Alteration of the BCL-xL/MCL-1 Ratio Provides a Therapeutic Opportunity for BH3-Mimetics in Hepatocellular Carcinoma Models.** Cancers 2020, 12, 332. https://doi.org/10.3390/cancers12020332

Novel therapeutic options for the systemic treatment of hepatocellular carcinoma have recently emerged. Sorafenib has been the standard chemotherapeutic agent used for HCC treatment during the last decade, although many patients do not tolerate sorafenib or progress after its administration. In this context, the appearance of other multityrosine kinase inhibitors, such as regorafenib or cabozantinib may provide new options for the clinical management of HCC.

Regorafenib is a multityrosine kinase inhibitor with a strong anti-antiangiogenic profile that is administered in the second line setting in HCC treatment. For that reason, we aimed to demonstrate the effectivity of regorafenib on HCC cells and xenograft mice, and analyze its mechanisms of action. On the other hand, the BCL-2 family of proteins tightly regulates apoptosis. In this context, BH3 mimetics, small molecules that closely resemble some members of the BCL-2 family may represent an attractive strategy to prompt cell death. Even though some BH3 mimetics have already been approved for the treatment of certain cancer types, the use of BH3 mimetics into the clinic has still to be widely implemented.

First, we were able to determine that regorafenib altered the pattern of BCL-2 family of proteins in a different manner compared to sorafenib in murine models of liver cancer. The transcriptomic analysis revealed that regorafenib upregulated the mRNA expression of the anti-apoptotic BCL-xL compared to sorafenib, which produced an increase in BCL-2 expression. The expression of pro-apoptotic members like BAX and BIM was upregulated at a transcriptional level in regorafenib-treated tumors in comparison with

the ones treated with sorafenib. This first data suggested that, according to this differential pattern of expression, each BH3 mimetic may be coupled with a specific MKI inhibitor.

Therefore, in order to potentiate regorafenib efficacy on HCC models, we co-administered the BH3 mimetic A-1331852, which specifically antagonizes the anti-apoptotic protein BCL-xL. We could observe that the dual treatment had a powerful anti-proliferative effect on Hep3B and HepG2 cells. However, when HCC cells were treated with the BCL-2 inhibitor ABT-199, we did not notice an increase in cell death compared to the one produced by merely using regorafenib. So, to confirm these results, we silenced with siRNA the expression of BCL-xL and BCL-2 in liver cancer cells. We detected that HCC cells highly relied on BCL-xL expression for their survival, while BCL-2 expression appeared to be far less crucial for their viability.

By administering a combined treatment with regorafenib and A-1331852, we intended to determine whether both agents interacted in a synergistic manner. To this end, we performed HSA analysis on three different HCC cell lines, which demonstrated that both compounds cooperated synergistically in killing HCC cells. As expected, when the same analysis was carried out with regorafenib and ABT-199, no synergy was observed. In addition, clonogenic assays were performed with regorafenib and A-1331852 for three days, showing the strong cytotoxic effect of this combination.

Next, we treated HCC cells for three hours with regorafenib and A-1331852 and we were able to observe a mitochondrial membrane potential loss exhibited by the shift of fluorescence of JC-1 probe. We detected a release of cytochrome c into the cytosol as well as caspase-3 activation in cells treated with both agents. PARP-1 cleavage and apoptotic nuclei were also noticeable after eight hours of the dual treatment, indicating that the combination of regorafenib and A-1331852 triggered apoptosis through the intrinsic or mitochondrial pathway.

We determined that regorafenib produced a decrease in MCL-1 protein levels as detected after two and 16 hours in hepatoma cells. An increase in BIM protein expression and BAX could also be observed. Hence, we treated HCC cells with an MCL-1 specific inhibitor together with A-1331852 to antagonize both MCL-1 and BCL-xL proteins. Consequently, a pronounced cell death could be observed with the use of the two BH3 mimetics on hepatoma cells by MTT assay.

Beyond two-dimension cell culture, we wanted to test the combination of regorafenib and A-1331852 in tumor liver spheroids. Spheroids were cultured and treated for seven days, and their growth was monitored daily. Regorafenib, at a dose of 2.5 µM, and the BCL-xL inhibitor A-1331852 (0.1-0.2 µM) greatly impeded tumor growth in comparison with A-1331852 or regorafenib alone.

To further validate this combination of chemotherapeutic drugs, we generated PDX BCLC9 murine models of HCC, which were treated with vehicle, regorafenib (30 mg/kg), A-1331852 (25 mg/kg) or the combination of both agents. The dual treatment detained tumor growth in BCLC9-tumor bearing mice, reduced tumor proliferation as shown by IHC staining of PCNA expression and altered the transcriptomic prolife of BCL-2 family of genes.

Additionally, we wanted to check the effectivity of A-1331852 in HCC models that developed resistance to long-time regorafenib administration. To do so, we studied the BCL-2 family protein profile of regorafenib-resistant HepG2 cells compared to regorafenib-sensitive cells. BCL-xL expression was found to increase while MCL-1 decreased in regorafenib-resistant cells. Moreover, regorafenib-resistant HCC cells were treated with both regorafenib and A-1331852. The BCL-xL inhibition rendered resistant cells sensitive to regorafenib again. We generated xenograft murine models of regorafenib-resistant tumors, which were treated with vehicle, A-1131852, regorafenib or the combination of both drugs. The dual treatment delayed tumor growth and reduced cell proliferation by PCNA IHC staining on regorafenib-resistant murine tumors.

Finally, in a small cohort of samples from HCC patients (n = 19), the BCL-xL/MCL-1 ratio was increased in HCC patients compared to healthy subjects using transcriptomic analysis. Furthermore, using a commercial mRNA array in I-II and IIIA-IV stages of HCC the ratio BCL-xL/MCL-1 was also detected increased. In addition, we browsed the Human Protein ATLAS, and observed that patients with higher levels of BCL-xL protein expression correlated with a worse prognosis in liver cancer.

Regorafenib Alteration of the BCL-xL/MCL-1 Ratio Provides a Therapeutic Opportunity for BH3-Mimetics in Hepatocellular Carcinoma Models

Blanca Cucarull [1,2,†], Anna Tutusaus [1,†], Miguel Subías [1], Milica Stefanovic [1,3], Tania Hernáez-Alsina [4], Loreto Boix [5], María Reig [5], Pablo García de Frutos [1,6], Montserrat Marí [1], Anna Colell [1,7], Jordi Bruix [5] and Albert Morales [1,5,*]

[1] Department of Cell Death and Proliferation, IIBB-CSIC, IDIBAPS, 08036 Barcelona, Spain; Blanca.cucarull@iibb.csic.es (B.C.); anna.tutusaus@iibb.csic.es (A.T.); msubias97@hotmail.com (M.S.); ms.milica.stefanovic@gmail.com (M.S.); pablo.garcia@iibb.csic.es (P.G.d.F.); monmari@clinic.cat (M.M.); anna.colell@iibb.csic.es (A.C.)

[2] Departament de Biomedicina, Facultat de Medicina, Universitat de Barcelona, 08036 Barcelona, Spain

[3] Department of Radiation Oncology, Catalan Institute of Oncology (ICO)-IDIBELL, L'Hospitalet, 08908 Barcelona, Spain

[4] Digestive Unit, Hospital San Pedro, Rioja Salud, 26006 La Rioja, Spain; taniahernaez@gmail.com

[5] Barcelona Clinic Liver Cancer Group, Liver Unit, Hospital Clínic of Barcelona, University of Barcelona, CIBEREHD, IDIBAPS, 08036 Barcelona, Spain; LBOIX@clinic.cat (L.B.); MREIG1@clinic.cat (M.R.); JBRUIX@clinic.cat (J.B.)

[6] Centro de Investigación Biomédica en Red sobre Enfermedades Cardiovasculares (CIBERCV), Spain

[7] Centro de Investigación Biomédica en Red sobre Enfermedades Neurodegenerativas (CIBERNED), Spain

* Correspondence: amorales@clinic.cat

† Blanca Cucarull and Anna Tutusaus contributed equally to this work.

Abstract: Background: The multikinase inhibitor regorafenib, approved as second-line treatment for hepatocellular carcinoma (HCC) after sorafenib failure, may induce mitochondrial damage. BH3-mimetics, inhibitors of specific BCL-2 proteins, are valuable drugs in cancer therapy to amplify mitochondrial-dependent cell death. Methods: In in vitro and in vivo HCC models, we tested regorafenib's effect on the BCL-2 network and the efficacy of BH3-mimetics on HCC treatment. Results: In hepatoma cell lines and Hep3B liver spheroids, regorafenib cytotoxicity was potentiated by BCL-xL siRNA transfection or pharmacological inhibition (A-1331852), while BCL-2 antagonism had no effect. Mitochondrial outer membrane permeabilization, cytochrome c release, and caspase-3 activation mediated A-1331852/regorafenib-induced cell death. In a patient-derived xenograft (PDX) HCC model, BCL-xL inhibition stimulated regorafenib activity, drastically decreasing tumor growth. Moreover, regorafenib-resistant HepG2 cells displayed increased BCL-xL and reduced MCL-1 expression, while A-1331852 reinstated regorafenib efficacy in vitro and in a xenograft mouse model. Interestingly, BCL-xL levels, associated with poor prognosis in liver and colorectal cancer, and the BCL-xL/MCL-1 ratio were detected as being increased in HCC patients. Conclusion: Regorafenib primes tumor cells to BH3-mimetic-induced cell death, allowing BCL-xL inhibition with A-1331852 or other strategies based on BCL-xL degradation to enhance regorafenib efficacy, offering a novel approach for HCC treatment, particularly for tumors with an elevated BCL-xL/MCL-1 ratio.

Keywords: liver cancer; mitochondria; apoptosis; Bcl-2 family; A-1331852; combination therapy

1. Introduction

Hepatocellular carcinoma (HCC), the most frequent primary liver cancer, is the third leading cause of cancer death and the main cause of death among patients with cirrhosis [1]. Often diagnosed at an advanced stage with poor prognosis, its incidence is expected to rise in the future due to the growing prevalence of non-alcoholic fatty liver disease associated with obesity and metabolic syndrome [2]. Despite recent advances in treatment, HCC prognosis continues to be dismal [3]. Most liver cancer patients do not benefit from immunotherapy [4] and the efficacy of the multikinase inhibitors (MKIs) sorafenib [5] and lenvatinib [6] in first-line treatment, and regorafenib [7] and cabozantinib [8] in second line, needs to be improved. Since drug effectiveness is limited by primary and acquired drug resistance [9], the identification of mechanisms enhanced by chemotherapy, particularly those susceptible to being druggable, is required to overcome treatment failure. In HCC, with a complex genetic background and without dependence on specific driver mutations for survival, vulnerabilities created by MKI treatment could provide targets to improve life expectancy [10].

Cell death-related pathways involving mitochondria are gaining interest as an alternative approach for cancer therapy [11], especially after or in combination with drug treatment that has altered mitochondrial homeostasis [10]. The BCL-2 network controls apoptosis by regulating mitochondrial outer membrane permeabilization (MOMP) via multidomain pro-apoptotic BAX and BAK [12]. MOMP triggers the release of pro-apoptotic mitochondrial intermembrane space proteins, such as cytochrome c and smac/DIABLO, activating executioner caspases and rapid cell death. In the BCL-2 system, equilibrium is established among pro-apoptotic members, such as BID, BIM, PUMA, BAD, or NOXA, and pro-survival components, mainly BCL-2, BCL-xL, and MCL-1 [13]. Cancer therapy has been described to alter the delicate balance established between activators and repressors of BAX/BAK homo-oligomerization, favoring the MOMP and leading to cell death. Upon the appearance of drug resistance, compensatory mechanisms may cause a novel BCL-2 status, which could be profited by BH3-mimetics [14–16], selective BCL-2 family member inhibitors studied in on-going clinical trials [17]. In particular, we and others have demonstrated sorafenib interaction with mitochondria [18–21], indicating the BCL-2 system has an important role in its cytotoxicity, which could be used to increase sorafenib efficacy [22,23]. Regorafenib shares a chemical structure and biological targets with sorafenib [24,25] and BCL-2 seems to participate in death-signaling pathways induced by both drugs [23]. Knowing the BCL-2 profile induced by a drug helps design a strategy based on BH3-mimetics predicted to be successful for a specific cancer [26–28]. However, unlike sorafenib, regorafenib's effect on the BCL-2 network has not been sufficiently addressed, so we aimed to evaluate this point and to test potential combination therapies in different models of liver cancer.

Our results indicate that MCL-1 reduction, as regorafenib does, allows BCL-xL antagonism to effectively eliminate HCC cells. In fact, A-1331852, a BH3-mimetic with specific anti-BCL-xL-binding capacity [29], is an effective agent to increase regorafenib efficacy and to overcome regorafenib resistance as we will demonstrate in different in vitro and in vivo HCC models. Moreover, increased BCL-xL and the BCL-xL/MCL-1 ratio are exhibited by patients with HCC, with predicted worse prognosis, suggesting that A-1331852 could be an interesting drug to combine with regorafenib during therapy.

2. Results

2.1. Mitochondrial Differences in Sorafenib vs. Regorafenib Experimental Liver Cancer Treatment

Sorafenib and regorafenib share numerous signaling pathways in their biological action, although some proteins are specifically targeted. Previous works have identified part of the cytotoxicity associated with sorafenib as mitochondrial dependent, with sorafenib activity being potentiated by mitochondrial-directed therapies. Differences in sorafenib- and regorafenib-induced pathways could provide additional targets for combination therapy and identify a mechanism that leads liver cancer cells to death.

In a patient-derived xenograft mouse model, we evaluated the effect of sorafenib and regorafenib in HCC using a microarray with a panel of cell death-related genes (Figure 1A). Although most of the mRNAs detected were similarly affected by both MKIs, changes in individual genes were detected. In particular, we observed that the alteration in BCL-2 family members was clearly different in sorafenib- and regorafenib-treated tumors. Anti-apoptotic members, such as BMF or BFL1, were mostly upregulated after both treatments. However, while the BCL-2 increase was mainly noticed after sorafenib exposure, BCL-xL, augmented more significantly in regorafenib-treated tumors (Figure 1B). Of note, the expression of pro-apoptotic members, such as BIM or BAX, was more pronounced after regorafenib treatment. These results evidenced different alterations in BCL-2 proteins induced by both MKIs, suggesting divergent mitochondrial effects and specific therapeutic opportunities for each.
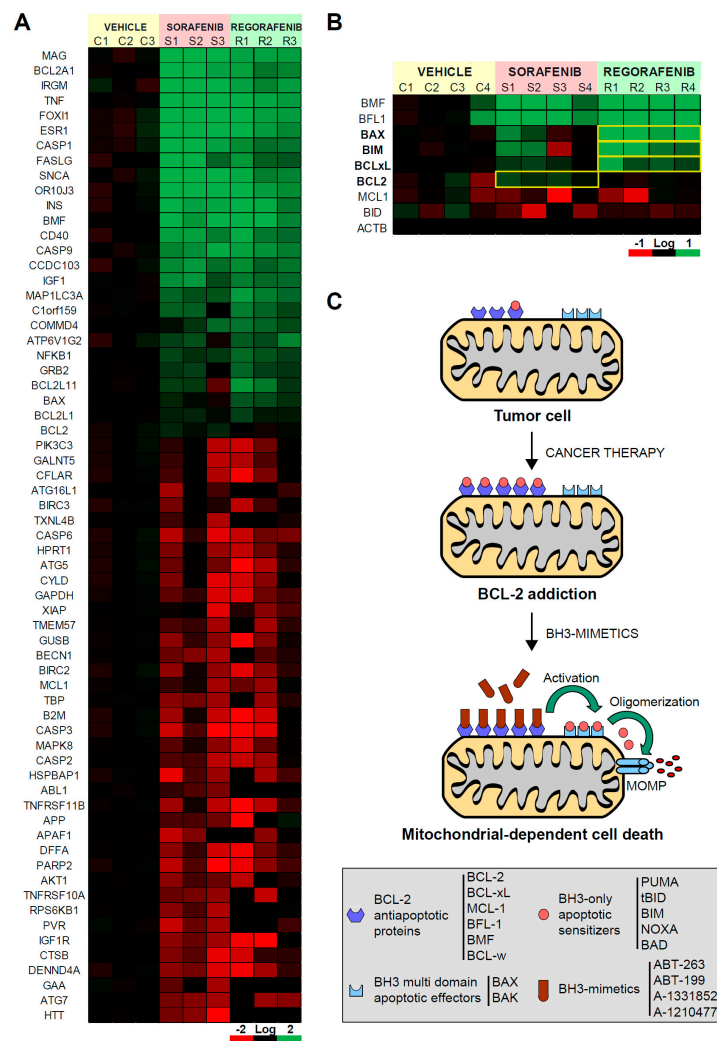

Figure 1. Sorafenib and regorafenib regulate the BCL-2 profile differently, sharing mitochondrial dependence but a distinctive therapeutic approach. (**A**) Transcriptomic analysis of genes related with liver cancer in BCLC9 tumors from nude mice treated for three weeks with vehicle (C1-3), sorafenib (S1-3), or regorafenib (R1-3). (**B**) mRNA expression of different BCL-2 proteins from treated tumors (C1-4, S1-4, and R1-4). Differences in the mRNA pattern are highlighted with yellow squares. (**C**) Cancer therapy may increase anti-apoptotic BCL-2 proteins avoiding cell death but mito-priming the cells to BH3-mimetics. Resistant hepatoma cells treated with compounds targeting BCL-2 proteins may release BH3-only proteins to bind BAX/BAK and trigger apoptotic cell death.

Several chemotherapeutic agents disturb the mitochondrial BCL-2 network, increasing both pro-apoptotic and pro-survival BCL-2 family members (Figure 1C). As a result, in surviving cancer

cells, drug therapy generates an abnormal BCL-2 balance with high levels of opposite components on each scale. This equilibrium is breakable by specific BH3-mimetics, which lead to cell death after sequestering the anti-apoptotic BCL-2 members. Since regorafenib upregulates BCL-2 expression, particularly pro-apoptotic genes, such as BIM and BAX, the priming of mitochondrial cell death should be expected. Therefore, we decided to investigate if BCL-2 addiction is created by regorafenib exposure and which proteins could be targeted to increase regorafenib efficacy.

## 2.2. BCL-xL Antagonism Is Effective to Potentiate Regorafenib Activity Against Liver Cancer Cells

We observed previously that BCL-2 and BCL-xL are the main anti-apoptotic BCL-2 proteins involved in sorafenib resistance in hepatoma liver cancer cells [23]. Since the BH3-mimetics ABT-199 [30] and A-1331852 [29] are highly effective to specifically reduce the intracellular availability of BCL-2 and BCL-xL, respectively, we tested if these compounds could modify regorafenib activity. A-1331852 greatly potentiated regorafenib toxicity in Hep3B and HepG2 cells as measured in MTT assays after 16 h (Figure 2A,B), while BCL-2 depletion with ABT-199 was not effective in increasing regorafenib action in the same hepatoma cell lines (Figure 2C,D). Of note, addition of the anti-BCL-xL BH3-mimetic A-1331852 significantly increased regorafenib-induced cell death, up to 5–6 fold (EC50: 15.1 ± 1.3 vs. 2.8 ± 0.3) in HepG2 cells and 8 to 10 times (30.7 ± 4.3 vs. 2.4 ± 0.2) in Hep3B cells.
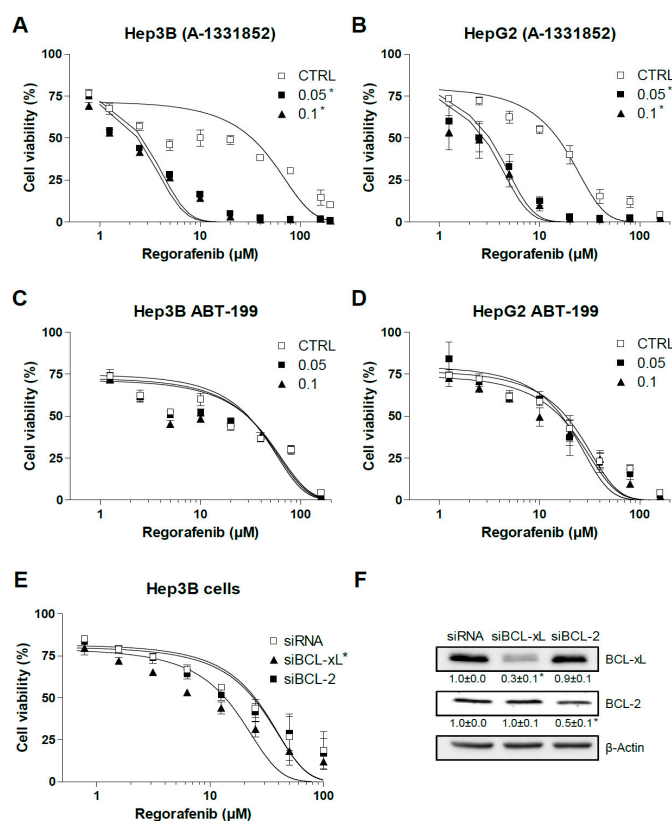
Figure 2. BCL-xL antagonism potentiates regorafenib activity on liver cancer cells. (**A**,**B**) Hep3B and HepG2 cells were treated for 16 h with the BCL-xL inhibitor A-1331852 and regorafenib at different concentrations, and cell viability was quantified by MTT. (**C**,**D**) Hep3B and HepG2 cells were treated for 16 h with the BCL-2 inhibitor ABT-199 and regorafenib at different concentrations, and cell viability was quantified by MTT. (**E**) Hep3B cells were transfected with siRNA control or against BCL-xL and BCL-2 and after 48 h treated with regorafenib at different concentrations, and cell viability was quantified by MTT. (**F**) RNA interference was confirmed and protein levels of BCL-xL, BCL-2, and β-actin are shown in parallel panels. (n = 3) * $p < 0.05$ vs. control or siCTRL cells.

To verify BCL-xL's role in the cellular protection against regorafenib, we transfected siBCL-2 and siBCL-xL in Hep3B cells (Figure 2E). Cells transfected with siBCL-2 were not sensitized against regorafenib while BCL-xL silencing potentiated cell death after 24 h of regorafenib exposure (EC50: 24.8 ± 3.5 vs. 13.6 ± 1.9). Of note, the A-1331852 efficacy of sensitizing tumor cells against regorafenib was higher than siBCL-xL reduction, probably due to A-1331852's powerful inhibition (Ki < 0.04 nM) of BCL-xL compared with the reduction obtained, up to 80% (Figure 2F), with the two siBCL-xL tested. However, in the absence of total knockdown of BCL-xL, we cannot completely discard the contribution of some off-target effect on the increased regorafenib efficacy.

To validate the capacity of A-1331852 to potentiate regorafenib toxicity, we evaluated their potential synergism in three different liver cancer cell lines, using the mathematic Highest Single Agent (HSA) model [31] and presenting heat maps of the results (Figure 3A). Synergy between both agents, regorafenib and A-1331852, was clearly observed in all three hepatoma cells, HepG2, Hep3B, and PLC/PRF/5, for concentrations of BH3-mimetic in the nanomolar range (10–200 nM) at a regorafenib concentration with therapeutic relevance in the low micromolar range (1–100 μM).
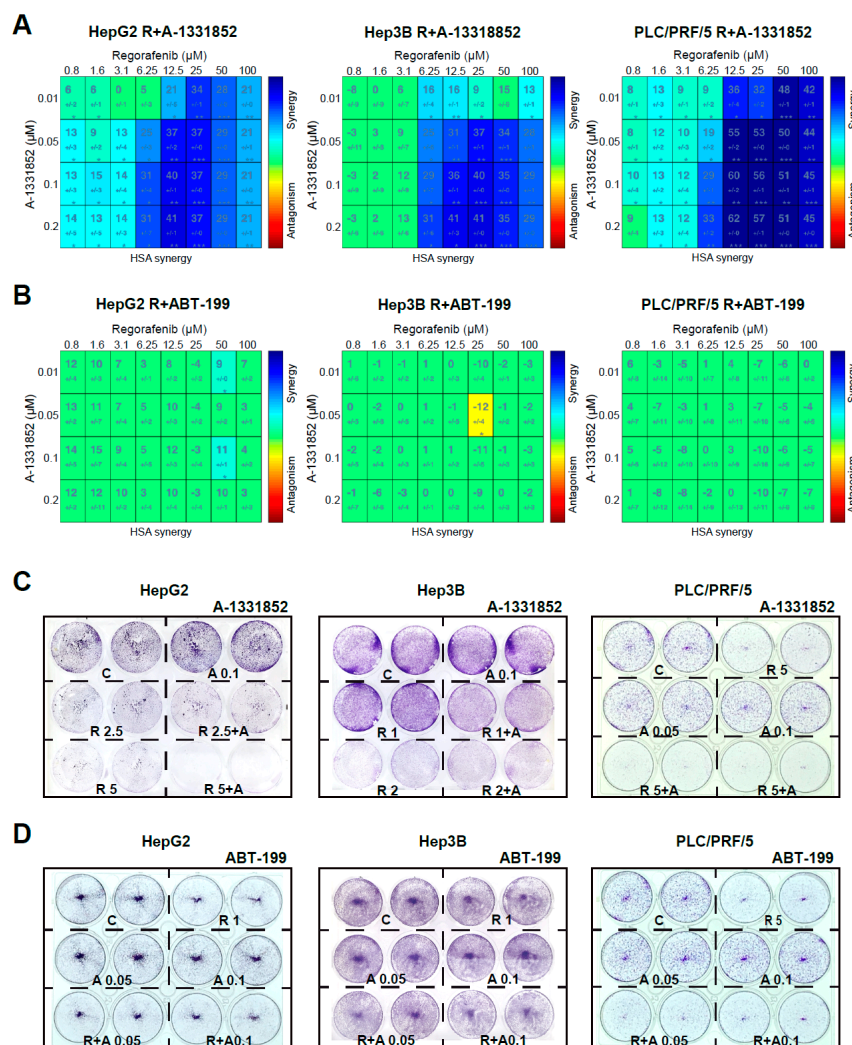
Figure 3. A-1331852 synergistically increased regorafenib cytotoxicity against different hepatoma cell lines. (**A,B**) MTT assays to test the A-1331852 and ABT-199 effect on regorafenib cytotoxicity in different liver cell lines (HepG2, Hep3B, and PLC/PRF/5) were performed, synergy calculated using HSA analysis, and results displayed with heat maps (blue synergy vs. red antagonism). (**C,D**), Crystal Violet staining was performed after 3 days of treatment with vehicle (**C**), regorafenib (R), and/or A-1331852/ABT-199 (**A**) in HepG2, Hep3B, and PLC/PRF/5 cell cultures. (n = 3) * *p* < 0.05 vs. control.

In contrast, no synergism was detected when BCL-2 was the protein targeted using ABT-199 co-administration with regorafenib in any cell line tested (Figure 3B).

In agreement with these results, the growth of HepG2, Hep3B, and PLC/PRF/5 cells was severely decreased by the combination of A-1331852 and regorafenib after three days, as denoted by Crystal Violet assays (Figure 3C). In contrast, ABT-199 was ineffective, potentiating regorafenib activity over all three hepatoma cell lines (Figure 3D). This result suggests that BCL-xL antagonism, but not BCL-2, could be an interesting mechanism to increase regorafenib efficacy in vivo.

2.3. A-1331852 Addition to Regorafenib-Treated Hepatoma Cells Triggers MMP Loss and Mitochondrial-Mediated Caspase-Dependent Apoptotic Cell Death

To verify the mitochondrial alteration induced by A-1331852 in regorafenib-treated cells, we analyzed possible changes in the mitochondrial membrane potential (MMP) by using the fluorescence probe JC-1. As soon as three hours after the drugs' co-administration, an evident decrease of the MMP was observed, denoted by the color shift observed in the cells, increasing the green mitochondrial pattern mainly in A-1331852/regorafenib-treated HepG2 and Hep3B cells (Figure 4A).

Since the decline of MMP could be associated to mitochondrial pore formation and consequent release of mitochondrial pro-apoptotic intermembrane proteins, we measured the cytosolic levels of cytochrome c at different times. As detected by Western blot, while regorafenib alone induced a minimal amount of cytochrome c presence in the cytosol (CYT), A-1331852 co-administration greatly favored its mitochondrial release (Figure 4B). In mitochondrial extracts (MITs), whereas cytochrome c levels were significantly unchanged in the combination samples, BAX exhibited mitochondrial accumulation after regorafenib treatment. Consistent with a mitochondrial-dependent apoptotic cell death, a significant increase in the active caspase-3 form is clearly visible in regorafenib-treated cells only if A-1331852 was co-administered (Figure 4B). This result was confirmed by quantification of the caspase-3 activity in cell extracts (Figure S1). As a consequence of caspase-3 activation, a cleavage of PARP-1 was detectable in A-1331852/regorafenib-treated HepG2 cells (Figure 4B).

To further analyze the early changes in BCL-2 proteins before caspase-3 triggering of cell death, we evaluated their protein levels. Once again, MCL-1 was clearly decreased in regorafenib-treated cells that was followed by BIM increases (Figure 4C). Other changes in BCL-2 proteins were not so clear, particularly due to their alteration in the levels induced by the BH3-mimetic A-1331852. Of note, while BAX mitochondrial accumulation was evident after regorafenib treatment, the BAX increase in total cell extracts was barely noticeable, emphasizing the importance of their mitochondrial analysis.

Moreover, typical apoptotic features were observed in hepatoma cells, being easily detectable by Hoechst 33258 nuclear staining after eight hours of A-1331852/regorafenib co-administration (Figure 4D). Interestingly, as previously observed with caspase-3 activation, nuclear DNA condensation was significant at time points where regorafenib alone was not inducing evident apoptotic effects, supporting a quick and relevant role of BCL-xL to modulate regorafenib anti-tumoral activity.
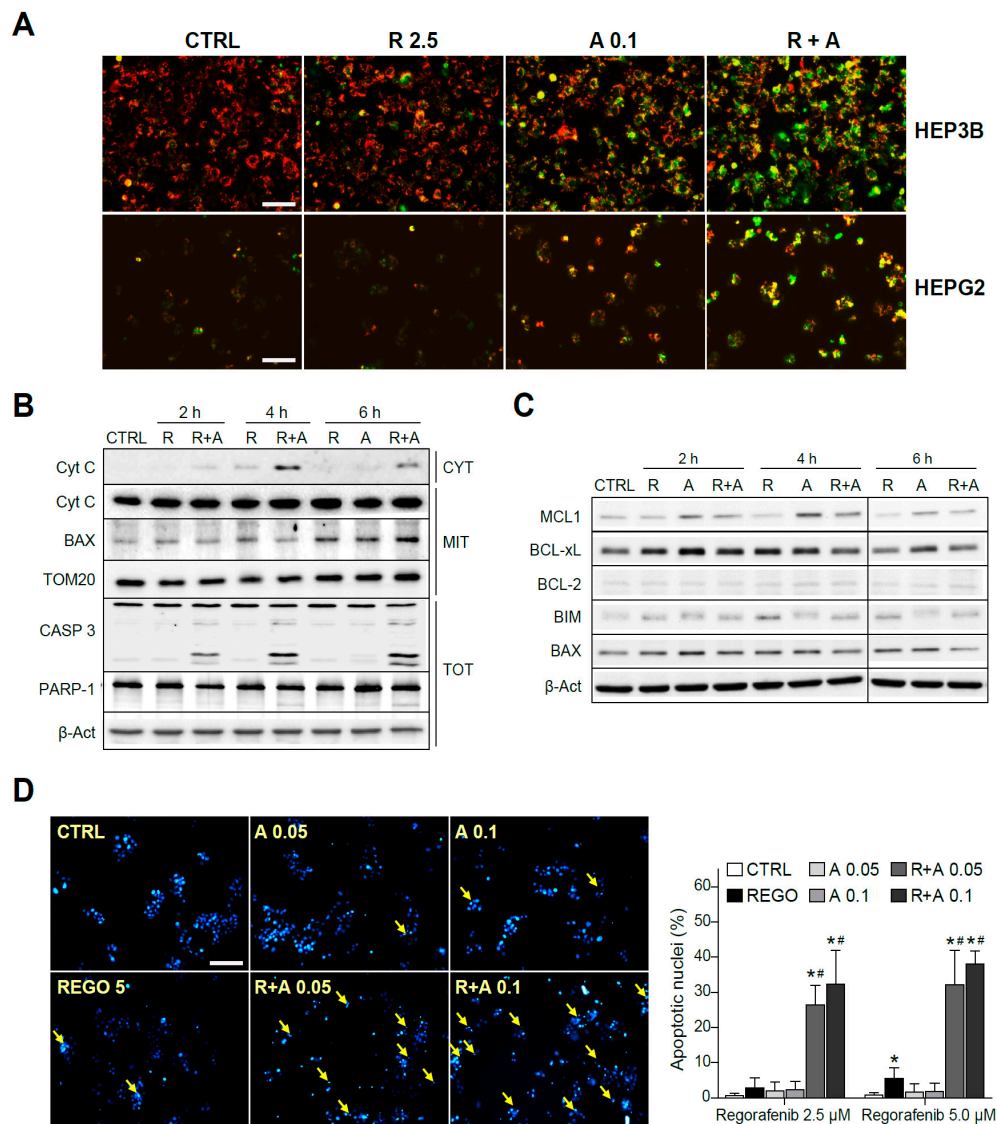
Figure 4. The regorafenib and A-1331852 combination induced apoptotic cell death via a mitochondrial caspase-dependent mechanism. (**A**) Hep3B and HepG2 cells were exposed to regorafenib (R, 2.5 μM) with or without A-1331852 (**A**, 0.1 μM) and MMP loss observed by fluorescence microscopy after 3 h (scale bar, 100 μm). (**B**) Cytochrome c release, BAX and TOM20 mitochondrial levels, caspase-3, PARP-1, and β-Actin were analyzed by Western blot in HepG2 cells. (**C**) BCL-2 proteins in cell extracts as above. (**D**) Nuclear Hoechst 33258 staining was visualized in HepG2 cells treated with regorafenib and/or A-1331852 (scale bar, 100 μm), and apoptotic cells counted (10 independent fields per condition, n = 3). * $p < 0.05$ vs. control cells, # $p < 0.05$ vs. regorafenib-treated cells.

2.4. Regorafenib Reduction of MCL-1 Facilitates A-1331852 Induction of Cell Death in Liver Cancer Cells

To better identify the mitochondrial changes induced by regorafenib that allow BCL-xL antagonism to synergistically induce cytotoxicity in hepatoma cells, we analyzed the protein levels of BCL-2 members with recognized importance in cell survival. In Hep3B and HepG2 cells treated with regorafenib, an early decrease in MCL-1 levels was consistently observed, accompanied by a progressive increase in intracellular BIM levels (Figure 5A). Of note, this MCL-1 reduction was not caused by decreased mRNA synthesis. After overnight treatment with concentrations up to 5 μM of regorafenib, no significant decreases in MCL-1 mRNA were detected (Figure S2). Besides transcriptional modulation, MCL-1 expression is also tightly controlled by post-transcriptional modification [32,33], suggesting that proteasomal degradation of MCL-1 could be taking place in regorafenib-treated hepatoma cells.

Although other mitochondrial alterations were detected, such as an increase in BCL-xL, particularly in regorafenib-treated HepG2 cells, MCL-1 reduction was presented by all cell lines tested after regorafenib treatment.
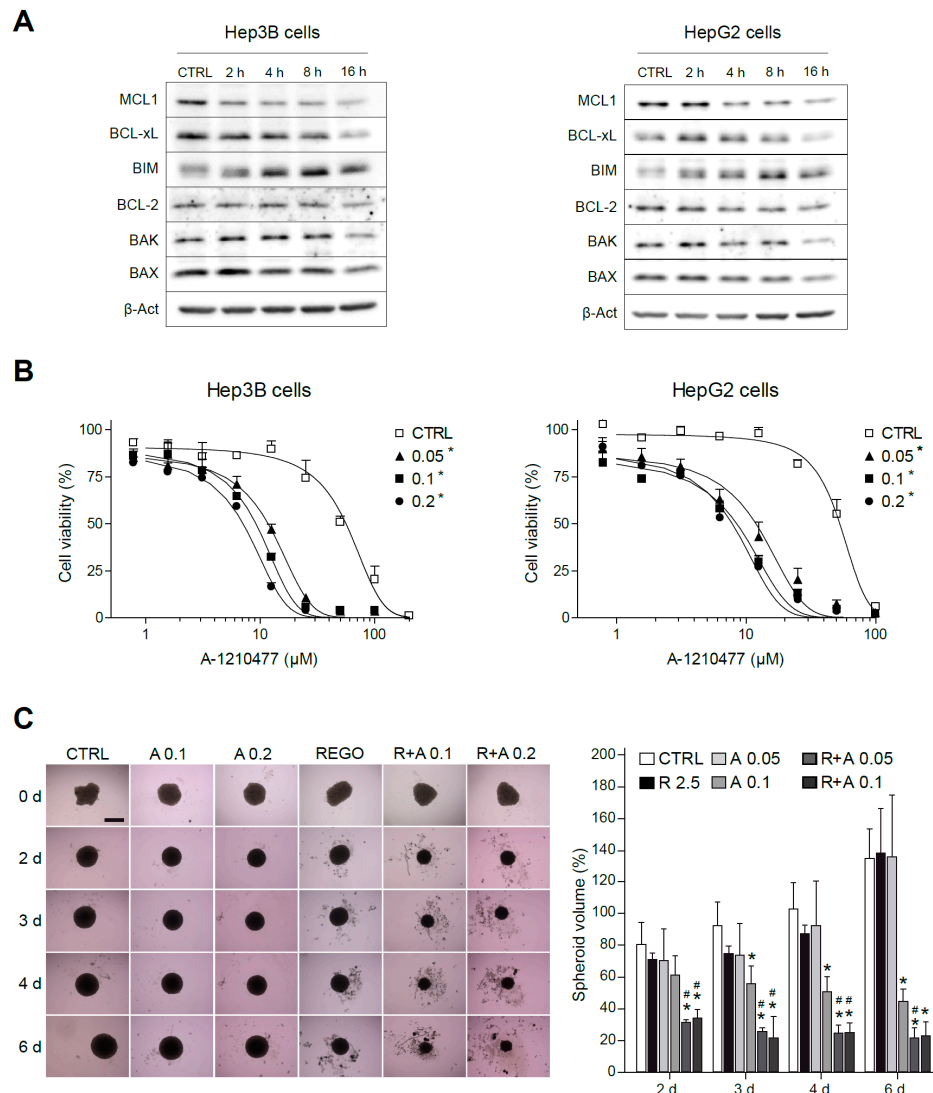

Figure 5. MCL-1 inhibition sensitizes hepatoma cells to the BCL-xL inhibitor A-1331852. (**A**) Representative Western blot images of MCL-1, BCL-xL, BIM, BCL-2, BAX, BAK, and β-Actin exhibited by Hep3B and HepG2 cells at different times (0–16 h) after regorafenib treatment (5 μM). (**B**) Effect of the MCL-1 inhibitor A-1210477 on Hep3B cells and HepG2 cells treated with A-1331852 (A, 0.05, 0.1, or 0.2 μM) for 24 h. * $p < 0.05$ vs. control cells. (**C**) Hep3B spheroids were seeded and after 24 h of aggregation treated with vehicle, regorafenib (R, 2.5 μM), and/or A-1331852 (A, 0.1 or 0.2 μM) for seven days. Spheroid growth was monitored daily (scale bar, 500 μm). (n = 3) * $p < 0.05$ vs. control cells, # $p < 0.05$ vs. regorafenib-treated cells.

Since a novel BH3-mimetic, A-1210477 [34], highly specific for MCL-1 has been recently described, we tested it, in order to deplete MCL-1 levels in hepatoma cells and combined with BCL-xL reduction using A-1331852. Interestingly, MCL-1 sequestration by A-1210477 was sufficient to induce BCL-xL-dependent cell death in liver cancer cell lines, such as HepG2 and Hep3B (Figure 5B). Therefore, this result suggests that the quick MCL-1 protein decline induced by regorafenib may be responsible for the BCL-xL addiction created in regorafenib-treated hepatoma cells, revealing a vulnerability that allows A-1331852 to be an effective anti-tumoral agent.

Before starting animal studies, we validated our results in liver spheroids, as a physiologically relevant in vitro HCC model, which resembles human liver more closely than traditional monolayer cultures. After aggregation, Hep3B spheroids were treated with regorafenib and/or A-1331852 and grown for seven days (Figure 5C). As quantified, two days after treatment, the drug combination was already effective in reducing spheroid growth while regorafenib activity was clearly minor and anti-BCL-xL-treatment alone was not significantly different from vehicle-treated spheroids.

2.5. A-1331852 in Combination with Regorafenib Is Effective to Reduce Liver Cancer Progression in a PDX Mouse Model

To test the in vivo efficacy of BCL-xL antagonism to potentiate regorafenib activity against liver cancer, we administered regorafenib and A-1331852 to mice bearing BCLC9 tumors, generated after the subcutaneous injection of this patient-derived HCC cell line. BCLC9 are anchor-free growing human hepatocellular carcinoma cells, derived from a well-differentiated human HCC, that display a stem cell phenotype and are highly effective tumor-initiating cells in nude mice. Regorafenib's capacity to decrease BCLC9 tumor growth was potentiated by A-1331852 co-administration (Figure 6A,B) while A-1331852 alone did not influence cancer progression significantly. In agreement, the proliferative capacity of the HCC cells was seriously compromised after regorafenib/A-1331852 co-administration for four weeks, as denoted by PCNA staining of tumor biopsies (Figure 5C).
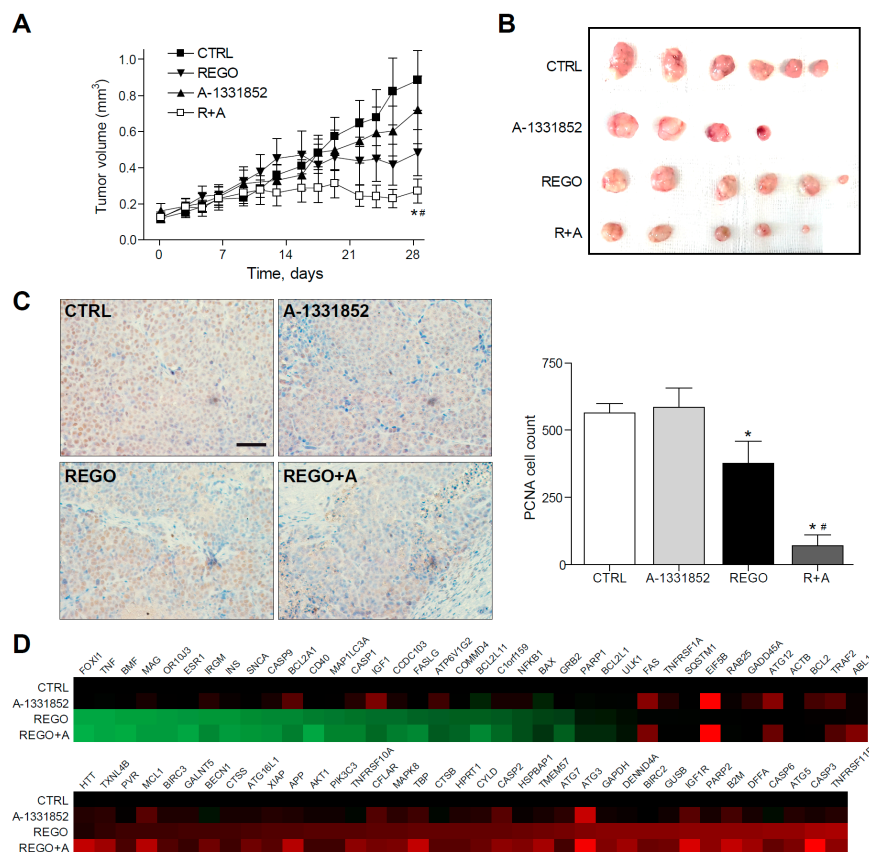
Figure 6. BCL-xL inhibitor A-1331852 remarkably reduced tumor growth in regorafenib-treated PDXs. (**A**,**B**), Subcutaneous growth quantification and images of BCLC9 tumors in mice treated with A-1331852 (25 mg/kg) and regorafenib (30 mg/kg) for 4 weeks (n = 4–6). * $p < 0.05$ vs. vehicle-treated mice. (**C**) Representative images of PCNA expression in tumor samples from BCLC9 PDXs and quantification (scale bar, 50 μm). (**D**) Transcriptomic analysis of cell death-related genes in BCLC9 tumors from nude mice treated with vehicle, regorafenib, and/or A-1331852. (n = 2).

Quantification of PCNA-positive cells by field exhibited a regorafenib reduction of tumor proliferation (377 ± 140), compared to vehicle-treated animals (563 ± 62) that was potently increased by A-1331852 co-administration (70 ± 73). In contrast, A-1331852 in monotherapy was not observed to decrease tumor development (586 ± 141). Moreover, the presence of the tumor marker Ki-67 was confirmed in the BCLC9 xenografts (Figure S3).

Of note, no changes in transaminase levels were induced by A-1331852, suggesting no hepatocellular damage induction by the BH3-mimetic to non-tumorous tissue. No major toxicity of A-1331852 was found in primary mouse hepatocytes (Figure S4) and in the human hepatic stellate cell line LX2 (Figure S5) at working concentrations, with cytotoxicity concentrations 50% (CC50s) more than 100-fold higher. Since regorafenib efficacy was clearly increased by BCL-xL inhibition in our PDX model, we evaluated the changes in regorafenib signaling introduced upon the A-1331852 combination, using a commercial microarray for cell death-related genes (Figure 6D). Interestingly, we found not only changes in BCL-2 family members, such as BFL1, BCL-xL, or BAX, but also downregulation in other genes. For instance, ATG12 and ATG3, which regulate mitochondrial homeostasis and autophagy in cell death [35], or IGF1 and IGF1R, were increased in HCC and proposed as targets for therapy [36], or the translation initiation factor EIF5B is modified by A-1331852 administration. These observations suggest an A-1331852 mitochondrial effect but also in other pathways relevant in HCC treatment.

2.6. Regorafenib Resistant Cells Are Sensitive to A-1331852 Co-Administration in Vitro and In Vivo

To know the protective mechanisms induced by regorafenib in resistant HCC tumors, a HepG2 cell line with regorafenib resistance was generated after 12 months of culture with regorafenib in the medium. An important MCL-1 reduction was accompanied by a significant BCL-xL increase in HepG2-resistant cells (R) compared to sensitive HepG2 cells (S), grown in parallel (Figure 7A).

Interestingly, BCL-xL reduction partially abrogated regorafenib resistance (Figure 7B). For instance, regorafenib cytotoxicity against HepG2 R cells (EC50: 14.2 ± 1.8 μM) was increased by A-1331852 at nanomolar concentrations (EC50: 4.5 ± 0.4 μM, at 100 nM), even lower than the activity of regorafenib alone in sensitive cells (HepG2 S EC50: 8.7 ± 1.2 μM).

To verify that A-1331852 was also effective in increasing regorafenib efficacy against regorafenib-resistant liver cancer cells in vivo, HepG2 R cells were injected subcutaneously in nude mice. As previously observed in the PDX BCLC9 model, regorafenib anti-tumoral activity was potentiated by A-1331852 administration in the HepG2 R xenograft model (Figure 7C). Accordingly, the quantification of PCNA-positive cells in the corresponding slides (Figure 7D) indicated that tumor proliferation was strongly diminished by regorafenib/A-1331852 co-administration (100 ± 88), compared to regorafenib- or vehicle-treated mice (869 ± 320 and 1573 ± 395, respectively). Moreover, to visualize cell death in the liver tumor specimens, TUNEL staining was performed. While no significant changes in TUNEL-positive cells were observed in A-1331852- and regorafenib-treated R HEPG2 tumors, mice receiving the combination treatment exhibited increased cell death (Figure S6).
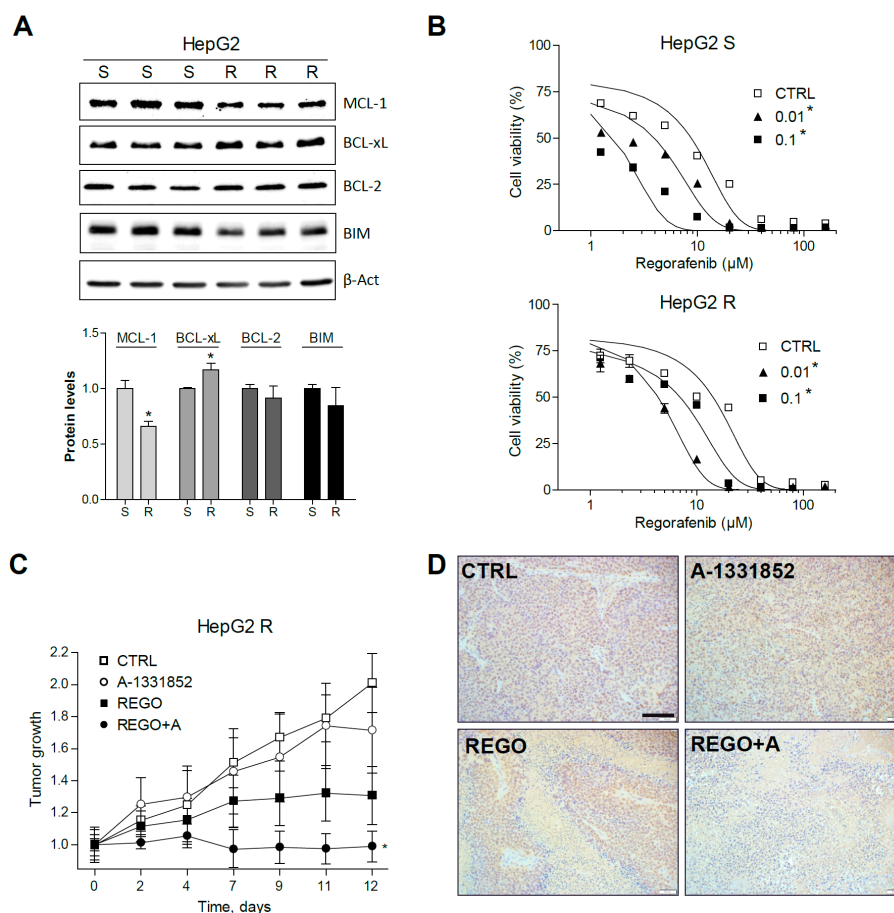
Figure 7. Regorafenib-resistant HepG2 cells, exhibiting mRNA changes in BCL-xL and MCL-1, are re-sensitized to regorafenib by A-1331582. (**A**) Representative Western blot images of MCL-1, BCL-xL, BCL-2, BIM, and β-Actin protein levels in S and R HepG2 cells. * $p < 0.05$ vs. sensitive cells. (**B**) Effect of A-1331852 (A, 0.01 or 0.1 μM) on S and R HepG2 cells. * $p < 0.05$ vs. control cells. (**C**) Subcutaneous growth of R HepG2 cells in mice treated orally with A-1331852 (25 mg/kg) and regorafenib (30 mg/kg) for 2 weeks (n = 4). (**D**) Representative images of PCNA expression in tumors from HepG2 R CDXs (scale bar, 100 μm). * $p < 0.05$ vs. vehicle-treated mice.

2.7. BCL-xL Upregulation and MCL-1 Reduction Are Present in HCC Tumor Tissue

Since our results indicate that BCL-xL reduction by A-1331852 potentiates regorafenib activity and low MCL-1 levels expose A-1331852 anti-tumoral activity against HCC tumor cells, we focused our attention on BCL-xL and MCL-1 alterations exhibited by human HCC tumors. As previously observed in a set of human biopsies from control, HCC, and surrounding non-tumorous tissue [23], BCL-xL mRNA expression was increased in some HCC samples (Figure 8A), while MCL-1 reduction was general in all tumor tissues. As a consequence, the BCL-xL/MCL-1 ratio was significantly improved in the HCC tumor group (Figure 8B).

To confirm these results, we used a commercial mRNA array with HCC tumors at different stages. Since our previously analyzed tumors were mostly small tumors (≤5 mm) in stage I-II, we wanted to compare this group with the one in stage III-IV. Once again, while BCL-xL upregulation was observed in specific tumors in both tumor groups (Figure 8C), the BCL-xL/MCL-1 ratio was significantly increased, both in stage I-II and in stage III-IV tumors (Figure 8D). These results suggest that BCL-xL upregulation is presented in HCC tumors and is frequently associated with a parallel MCL-1 reduction, a feature that could help A-1331852 anti-tumoral activity. Interestingly, no control sample exhibited a BCL-xL/MCL-1 ratio higher than 2.5, neither in our cohort (0/10) or in the commercial array (0/8).

In contrast, a BCL-xL/MCL-1 ratio over 2.5 was detected in numerous tumors in our cohort (10/19) and the commercial array (18/26).
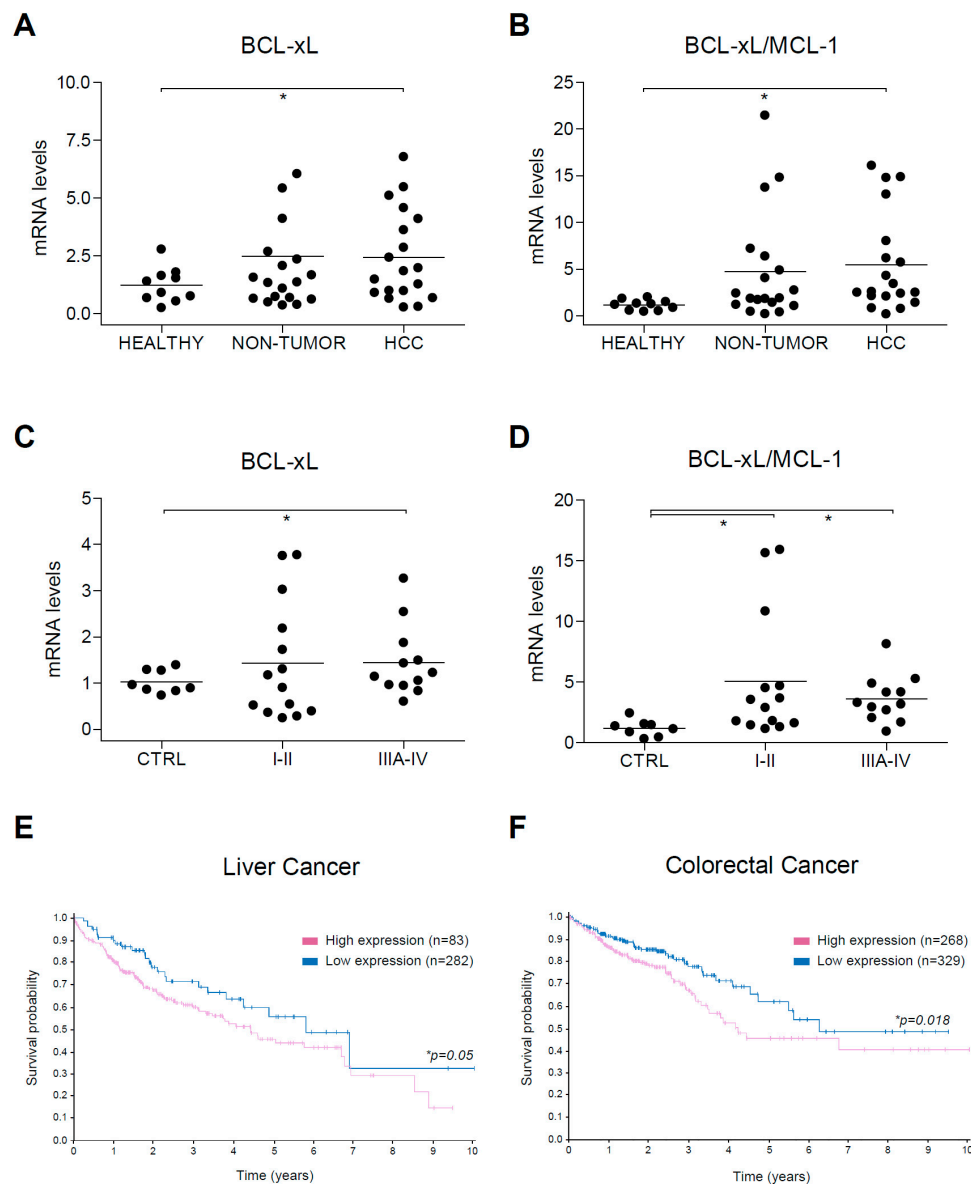
Figure 8. Alterations in BCL-xL mRNA levels and BCL-xL/MCL-1 ratio in HCC patients. (**A**) BCL-xL and (**B**) BCL-xL/MCL-1 mRNA levels were measured by qPCR in healthy liver (n = 10) and in cirrhotic and tumoral tissue from HCC patients (n = 12) with Hepatitis C virus (HCV) and/or Ethanol (EtOH) etiology. * $p < 0.05$ vs. control. (**C**) BCL-xL and (**D**) BCL-xL/MCL-1 mRNA levels were measured by qPCR in a commercial mRNA array with healthy liver (n = 8) and tumoral tissue from HCC patients in different stages (I-II, n = 14; IIIA-IV, n = 12). (**E,F**) Representation of survival probability depending on BCL-xL expression (blue, high; purple, low) in patients with liver and colorectal cancer, respectively.

Finally, since our results suggest that BCL-xL upregulation could be detrimental for HCC treatment with regorafenib, but probably also for other treatments that generate mitochondrial sensitization, such as sorafenib, we checked in the Human Protein ATLAS data [37] if BCL-xL expression could be associated with a worse prognosis in liver cancer (Figure 8E). Interestingly, high BCL-xL mRNA levels were exhibited by many tumors (n=282) and have a worst 5-year survival prognostic (45%) than low BCL-xL levels (55%, n = 83, $p = 0.05$).

Since regorafenib is also an FDA-approved drug for colorectal cancer treatment [38,39], and according to our data another potential candidate for treatment based on BCL-xL antagonism, we also analyzed BCL-xL levels in this tumor category (Figure 8F). The Atlas database analysis indicates that a BCL-xL increase in colorectal cancer is probably negative for patients having a worse 5-year survival prognosis (53%, n = 329) than low BCL-xL levels (71%, n = 268, *p* = 0.018).

Consequently, liver and colorectal patients with increased BCL-xL tumor levels seem be associated with worse prognosis and may be candidates for a combination therapy with BCL-xL antagonists, such as A-1331852.

3. Discussion

Immunotherapy is a very promising field, but its application to HCC patients seems to be an option only for a low percentage of individuals [40]. Regorafenib, a multikinase inhibitor (MKI) with a broader inhibitory profile and greater pharmacological activity than sorafenib, has been approved as second-line therapy for advanced hepatocellular carcinoma (HCC) after sorafenib failure and for advanced colorectal cancer (CRC) and gastrointestinal stromal tumors (GISTs) after standard chemotherapy [38,39]. However, MKI therapy, despite being the best treatment for hepatocellular carcinoma, is still not very effective. Further improvement of MKI activity is important to detect among the intracellular mechanisms triggered by each drug those responsible for death induction. These altered pathways may allow identification of druggable targets for combination therapy or even for use as a single agent, if the drug is effective enough and markers for patient selection can be associated. In particular, when the mitochondrial functionality is compromised, the drug creates a tumor vulnerability that could be used to promote mitochondrial-dependent cell death [10–13]. Since mitochondria, through MOMP and the release of apoptogenic intermembrane proteins, can amplify the damage leading to cell death, it is important to identify the drugs that cause mitochondrial alteration and determine the molecular mechanism involved.

In particular, if the BCL-2 network is affected, an interesting possibility arises since specific BH3-mimetics against BCL-2 proteins, such as BCL-2 (ABT-199), BCL-xL (A-1331852), or MCL-1 (A-1210477), have been designed and are tested in clinical trials. Therefore, chemotherapeutic agents that promote changes in BCL-2 proteins, once these modifications are characterized, become a probable target for combination therapy with BH3-mimetics. In fact, since the dependence on a BCL-2 protein is frequently related to its specific level, tumors with an elevated content of a specific BCL-2 family member can be treated in monotherapy with some BH3-mimetics, such as chronic and acute leukemia with ABT-199. However, what we expect to be more common is that BH3-mimetics could be administered in combination with standard chemotherapy, particularly in patients with high levels of the related protein. Of note, although the mRNA increases observed in HCCs from our cohort of patients and from the commercial array are significant, only specific individuals displayed very high levels of BCL-xL and the BCL-xL/MCL-1 ratio. It is tempting to speculate that these patients could particularly benefit from BCL-xL antagonism, mostly when, as observed in liver cancer and CRC patients, BCL-xL levels are inversely related to expected survival. Incidentally, when we separated groups depending on gender, females were much more sensitive to BCL-xL levels (*p* = 0.014, 5-year survival high 39% vs. 5-year survival low 61%). If this divergence is due to sex differences in the level of BCL-2 members, other apoptosis-related proteins in the liver, or the consequence of HCCs from different etiologies depending on each gender [41] should be further analyzed.

A-1331852 is an orally bioavailable potent and selective BCL-xL inhibitor with a Ki value in the low nanomolar range, and affinity for other BCL-2 proteins, such as BCL-2 or MCL-1, of around 600 or 15,000 times less, respectively [29]. A-1331852 has been proposed as an agent in cancer therapy [42,43] and, more recently, as a senolytic compound [44]. Interestingly, through a dual mechanism acting on senescent cholangiocytes and activated fibroblasts, A-1331852 ameliorates liver fibrosis in mice [45]. Therefore, BCL-xL inhibition, besides a direct effect on HCC survival, may change the protumoral microenvironment in which HCC develops by eliminating hepatic senescent cells and activated

fibroblasts. In this sense, experiments using liver spheroids combining liver cancer cells and activated hepatic stellate cells could be an interesting in vitro model to study this additional effect of BCL-xL inhibition. In fact, our preliminary results indicate that A-1331852 efficiently reduces tumor growth in HepG2/LX2 spheroids alone and particularly in combination with regorafenib, and in vivo mice experiments are ongoing. Moreover, other effects of BCL-xL reduction should not be discarded, since A-1331852 affects other genes important in HCC biology. The recent discovery of PUMA controlling the metabolic switch in HCC via direct interaction with the mitochondrial pyruvate carrier suggests that other actions of BCL-2 proteins could be expected [46].

Other BH3-mimetics, such as ABT-199 (venetoclax, BCL-2 inhibitor), FDA approved for chronic and acute leukemia, or ABT-263 (navitoclax, BCL-2 and BCL-xL inhibitor), are in clinical trials despite their associated hematological side effects. In particular, platelet survival is dependent on BCL-xL expression, and thrombocytopenia could be presented after administration of BCL-xL inhibitors, as observed in navitoclax studies. In addition, navitoclax-induced BCL-2 inhibition may also reduce the neutrophil count, at least in combination with other therapies [29]. In this sense, BCL-xL-selective inhibitors, such as A-1331852, will avoid dose-limiting neutropenia although its platelet effect may complicate its use as a single agent, particularly in some cirrhotic patients with HCC. However, as observed in combination with regorafenib, A-1331852 can be effective at very low concentrations, most probably before thrombocytopenia became dose limiting. In agreement, navitoclax's effect on the platelet count can be attenuated by careful dosing, as observed in clinical trials in patients with lymphoid malignancies [47].

Interestingly, a BCL-xL proteolysis-targeting chimera (PROTAC), which targets BCL-xL to the Von Hippel-Lindau (VHL) E3 ligase for degradation, has recently been designed [48]. This selective BCL-xL PROTAC degrader exhibits safe and potent antitumor activity but considerably less toxicity to platelets than ABT-263, since VHL is poorly expressed in platelets. These novel data illustrate the importance of BCL-xL in specific tumors and the possibility to circumvent the side effects related to BCL-xL deficiency in particular cells.

In summary, our data support the concept that BH3-mimetics are remarkable compounds to combine with cancer therapy when the BCL-2 network is altered. In this sense, regorafenib perturbation of the BCL-2 family creates a mitochondrial vulnerability that A-1331852 can exploit. Through MOMP and caspase activation, BCL-xL inhibition potentiates regorafenib action in in vitro and in vivo HCC models. Therefore, A-1331852 or other strategies directed to eliminate BCL-xL, such as PROTACS, should be contemplated as potential candidates for combination therapy with regorafenib in HCC treatment and probably in other cancers that exhibit BCL-xL overexpression.

4. Materials and Methods

4.1. Reagents

Dulbecco's modified eagle's medium (DMEM), trypsin-EDTA, penicillin-streptomycin and dimethyl sulfoxide (DMSO), MTT (3-(4,5-dimethylthiazol-2-yl)-2,5-diphenyl tetrazolium bromide) (M2128), Hoechst 33258 (B1155), Crystal Violet (C0755), and DCF (D6883) were purchased from Sigma-Aldrich (St. Louis, MO, USA). All tissue culture-ware was from Nunc (Roskilde, Denmark). Biotin Blocking System, peroxidase substrate (DAB), and peroxidase buffer were from DAKO (Glostrup, Denmark). Proteinase inhibitors were from Roche (Madrid, Spain). ECL Western blotting substrate was from Pierce (Thermo Fisher Scientific, Rockford, IL, USA). BCL-2 siRNA (h) (sc-29214), BCL-xL siRNA (h) (sc-43630), and scrambled controls were purchased from Santa Cruz Biotechnology (Dallas, TX, USA), while a second siRNA for BCL-2 (ID#s1915) and for BCL-xL (ID#s1920) were obtained from Ambion Life technologies (Carlsbad, CA, USA). Lipofectamine2000 (11668-027), Novex Sharp Pre-stained Protein Standard (LC5800), and JC-1 (T-3168) were from Invitrogen Life Technologies (Carlsbad, CA, USA). Sorafenib (BAY 43-9006, Nexavar) and Regorafenib (BAY 73-4506, Stivarga)

are manufactured by Bayer. A-1331852 and ABT-199 (Venetoclax) were purchased from Selleckchem (Houston, TX, USA).

4.2. Cell Culture and Biochemical Analysis

Human liver tumor cell lines Hep3B, PLC/PRF/5 and HepG2 (European Collection of Animal Cell Cultures (ECACC)), and human hepatic stellate cell line LX2 [49] were grown in DMEM (10% FBS) at 37 °C and 5% CO_2. Regorafenib-resistant hepatoma cells were maintained at 2 µM and kept without drug at least one week before experiments. Primary mouse hepatocytes were obtained after collagenase digestion [50] and cultured on collagen-coated plates one day before analysis.

4.3. MTT Assay

Cell viability was determined by MTT (3-(4,5-dimethylthiazol-2-yl)-2,5-diphenyl tetrazolium bromide) assay. In total, 1×10^4 cells/well were seeded in a 96-well plate and incubated at 37 °C and 5% CO_2. Cells were treated with regorafenib and A-1331852, ABT-199, and A-1210477 for 16–24 h before 10 µL of MTT reagent (5 mg/mL) addition and incubation for 2 h. Formazan crystals were dissolved with 100 µL of 1-propanol. Absorbance was measured in a plate reader (Multiskan®Spectrum, Thermo Fisher Scientific, Rockford, IL, USA) at 570 and 630 nm.

4.4. Crystal Violet Staining

First, 8×10^4 cells were seeded into 12-well plates and kept at 37 °C in 5% CO_2. Cells were treated and left for three days until they were fixed with 10% formalin for 5 min. Crystal violet was added for 30 min and after that they were washed twice with water. Plates were drained and photos were taken.

4.5. Caspase-3 Activity Assay

First, 3×10^4 cells were seeded in a 12-well plate. After treatments, cells were scrapped with 50 mM Hepes (pH 7.4), 5 mM CHAPS, and DTT 5mM. For Caspase-3 activity, 50 µg of protein extraction were added in 200 uL of assay buffer containing 20 mM Hepes, 5% sucrose, 0.1% CHAPS, 2 mM EDTA, and 5 mM DTT, pH 7.4, and 50 µM of the substrate Ac-DEVD-AFC (Santa Cruz Biotechnology). Detection of AFC after substrate cleavage was recorded at time intervals of 15 min, at emission 505 nm, and excitation at 400 nm. A unit of caspase-3 activity is the amount of active enzyme necessary to produce an increase in 1 fluorescence unit in Spectramax Gemini XS fluorimeter. Results are usually represented as an arbitrary unit/h/µg protein.

4.6. Hoechst Staining

Cells were seeded at 5×10^4 cells/well in 12-well plates, treated for 8 h. Hoechst 33258 was added at 1/1000 and incubated for 30 min. After being washed, images were taken using Olympus IX-70 microscope with the CC-12 FW camera. Photos of 12 random fields were taken. Condensed nuclei were counted with ImageJ software.

4.7. Mitochondrial Membrane Potential Assay

JC-1 is a fluorescent cationic dye (C5,5′,6,6′-tetrachloro-1,1′,3,3′-tetraethylbenzimidazolyl-carbocyanine iodide) used as an indicator of mitochondrial potential in cells. Mitochondrial depolarization is assessed by a decrease in the red (J-aggregates)/green (J-monomers) fluorescence intensity ratio. To determine the mitochondrial membrane potential, 1×10^4 cells/well were seeded in 96-well plates and incubated at 37 °C and 5% CO_2. Cells were treated, and after, JC-1 dye was incubated for 15 min. DMSO (0.05%) was used as the control. Photos were taken with a Leica-CTR4000 microscope and LAS software.

4.8. 3D Tumor Liver Spheroids Generation

Cellular spheroids were generated and plated in 96-well plates with a bottom coat of agarose [51,52]. Tumor liver spheroids were kept at 37 °C and 5% CO_2 for seven days and spheroid growth monitored daily.

4.9. Immunoblot Analysis

Cell lysates were prepared in RIPA buffer plus proteinase inhibitors. Samples containing 10 to 30 μg were separated by 10%–15% SDS-PAGE. Proteins were transferred to nitrocellulose membranes, blocked in 5% nonfat milk for 1 h at room temperature, and incubated overnight at 4 °C with the primary antibodies: MCL-1 (S-19, sc-819) 1:250 rabbit; BCL-2 (C-2, sc-7382) 1:250 mouse; BCL-xL (H-5, sc-8392) 1:250 mouse; PARP-1 (H-250, sc-7150) 1:250 rabbit; BIM (H-191, sc-11425) 1:250 rabbit; BAX (N-20, sc-493) 1:1000 rabbit; TOM20 (sc-11415) 1:500 rabbit; BAK (AT38E2, sc-517390) 1:250 mouse; Cytochrome C (sc-1356) 1:250 mouse were from Santa Cruz Biotechnology; Cleaved Caspase-3 (D175, #9661S) 1:1000 rabbit from Cell Signaling, and β-Actin (A3854) 1:40,000 conjugated to HRP from Sigma-Aldrich.

4.10. RNA Isolation and Real Time RT-PCR

Total RNA was isolated with TRIzol reagent. 1μg of RNA was reverse transcribed with AN iScript™ cDNA Synthesis Kit (Biorad, Berkeley, CA, USA) and real-time PCR was performed with iTaq™ Universal SYBR® Green Supermix (Biorad) following the manufacturer's instructions. The primers sequences used were:

human BCL-2: Fw 5′-GGAGGATTGTGGCCTTCTTT-3′; Rv 5′-GCCGTACAGTTCCACAAAGG-3′
human BCL-xL: Fw 5′-GGATGGCCACTTACCTGA-3′; Rv 5′-CGGTTGAAGCGTTCCTG-3′
human MCL-1: Fw 5′-ATGCTTCGGAAACTGGACAT-3′; Rv 5′-TCCTGATGCCACCTTCTAGG-3′
human ′-Act: Fw 5′-AGAAAATCTGGCACCACACC-3′ Rv 5′-AGAGGCGTACAGGGATAGCA-3′

4.11. Immunohistochemical Staining

Livers were fixed and paraffin embedded. Sections were routinely stained with Hematoxylin&Eosin (7-μm) or incubated with mAb anti-PCNA antibody (PC10) (1:200 dilution, sc-56, Santa Cruz Biotechnology) as previously indicated [53]. The slices were examined with a Zeiss Axioplan microscope equipped with a Nikon DXM1200F digital camera. The PCNA cell count was quantified in four randomly selected fields from each animal and analyzed using ImageJ software. Ki-67 staining was performed using a specific antibody (sc-23900, 1:200 mouse) from Santa Cruz Biotechnology.

4.12. Tumor Animal Models

All animal procedures were performed according to protocols approved by the Animal Experimentation Ethics Committee from the University of Barcelona (ethic code: #9850). For the subcutaneous tumor model, male Swiss nude mice, 5–6 weeks old, were kept under pathogen-free conditions with free access to standard food and water. HepG2 sorafenib-resistant cells (5×10^6) or BCLC9 cells (2.5×10^6) were injected subcutaneously into the flanks of mice in 100 μL DMEM without FBS, as previously reported [19,23,53]. Treatments with A-1331852 (25 mg/Kg body weight), regorafenib (30 mg/Kg), or vehicle (12.5% Cremophor, 12.5% ethanol, 75% sterile saline) were delivered daily via oral gavage. Tumors were measured periodically with a Vernier caliper, and the volume was calculated as length $\times$ width^2 $\times$ 0.5.

4.13. Gene Array

Predesigned 384-well human Liver cancer panel (SAB Target List, H384 Cat#10034526) and Cell Death (SAB Target List, H384 Cat#10034460) for SYBR Green detection (Bio-rad) were used following the manufacturer's instructions, as previously reported [54].

4.14. cDNA Array

TissueScan™ cDNA Array (Liver Cancer cDNA Array I, Origene) was used to quantify BCL-xL and MCL-1 levels in tumor and normal tissues. Tissue cDNAs of each array are synthesized from high quality total RNAs of pathologist verified tissues, normalized and validated with β-actin in two sequential qPCR analyses, and provided with clinical information and QC data. Our array contained cDNA from 48 samples covering 8-normal, 7-Stage I, 8-II, 8-IIIA, and 3-IV in identical plates (LVRT101). BCL-xL and MCL-1 levels were calculated by qPCR as previously indicated.

4.15. HCC Patient Study and ATLAS Database Information

Tumor and cirrhotic tissue from 19 patients diagnosed with HCC and treated at the Clinic Hospital in Barcelona, and 10 healthy liver samples from patients subjected to surgery due to colorectal cancer without any diagnosed liver disease, were included [23]. Patient data is included in Supplementary Table S1. Patients gave informed consent according to the principles embodied in the Declaration of Helsinki.

Data showing survival probability depending on the level of expression of BCL-xL were retrieved from: https://www.proteinatlas.org/ENSG00000171552-BCL2L1/pathology/liver+cancer for liver cancer; https://www.proteinatlas.org/ENSG00000171552-BCL2L1/pathology/colorectal+cancer for colorectal cancer.

4.16. Statistical Analyses

Results are expressed as mean ± standard deviation and n = 3, unless indicated. Statistical comparisons were usually performed using unpaired 2-tailed Student's t test, and 1-way ANOVA followed by Newman–Keuls multiple comparison test (GraphPad Prism) was used for data quantification from patients. A *p* value less than 0.05 was considered significant.

5. Conclusions

In HCC models, regorafenib induces changes in BCL-2 family proteins, priming mitochondrial cell death induced by BH3-mimetics, and allowing the BCL-xL inhibitor A-1331852 to enhance regorafenib efficacy.

BCL-xL increase, associated with a poor prognosis in liver and colorectal cancer, could be an interesting molecular marker for regorafenib/A-1331852 combinatory treatment in HCC patients.

References

1. Bruix, J.; Reig, M.; Sherman, M. Evidence-based diagnosis, staging, and treatment of patients with hepatocellular carcinoma. *Gastroenterology* **2016**, *150*, 835–853. [CrossRef]

2. Michelotti, G.A.; Machado, M.V.; Diehl, A.M. NAFLD, NASH and liver cancer. *Nat. Rev. Gastroenterol. Hepatol.* **2013**, *10*, 656–665. [CrossRef]

3. Yang, J.D.; Hainaut, P.; Gores, G.J.; Amadou, A.; Plymoth, A.; Roberts, L.R. A global view of hepatocellular carcinoma: Trends, risk, prevention and management. *Nat. Rev. Gastroenterol. Hepatol.* **2019**, *16*, 589–604. [CrossRef]

4. Macek Jilkova, Z.; Aspord, C.; Decaens, T. Predictive factors for response to PD-1/PD-L1 checkpoint inhibition in the field of hepatocellular carcinoma: Current status and challenges. *Cancers* **2019**, *11*, 1554. [CrossRef] [PubMed]

5. Llovet, J.M.; Ricci, S.; Mazzaferro, V.; Hilgard, P.; Gane, E.; Blanc, J.-F.; de Oliveira, A.C.; Santoro, A.; Raoul, J.-L.; Forner, A.; et al. Sorafenib in advanced hepatocellular carcinoma. *N. Engl. J. Med.* **2008**, *359*, 378–390. [CrossRef]

6. Kudo, M.; Finn, R.S.; Qin, S.; Han, K.H.; Ikeda, K.; Piscaglia, F.; Baron, A.; Park, J.W.; Han, G.; Jassem, J.; et al. Lenvatinib versus sorafenib in first-line treatment of patients with unresectable hepatocellular carcinoma: A randomised phase 3 non-inferiority trial. *Lancet* **2018**, *391*, 1163–1173. [CrossRef]

7. Bruix, J.; Qin, S.; Merle, P.; Granito, A.; Huang, Y.-H.; Bodoky, G.; Pracht, M.; Yokosuka, O.; Rosmorduc, O.; Breder, V.; et al. Regorafenib for patients with hepatocellular carcinoma who progressed on sorafenib treatment (RESORCE): A randomised, double-blind, placebo-controlled, phase 3 trial. *Lancet* **2017**, *389*, 56–66. [CrossRef]

8. Abou-Alfa, G.K.; Meyer, T.; Cheng, A.L.; El-Khoueiry, A.B.; Rimassa, L.; Ryoo, B.Y.; Cicin, I.; Merle, P.; Chen, Y.; Park, J.W.; et al. Cabozantinib in patients with advanced and progressing hepatocellular carcinoma. *N. Engl. J. Med.* **2018**, *379*, 54–63. [CrossRef] [PubMed]

9. Wörns, M.-A.; Galle, P.R. HCC therapies—lessons learned. *Nat. Revi. Gastroenterol. Hepatol.* **2014**, *11*, 447–452. [CrossRef]

10. Nguyen, C.; Pandey, S. Exploiting Mitochondrial Vulnerabilities to Trigger Apoptosis Selectively in Cancer Cells. *Cancers (Basel)* **2019**, *11*, 916. [CrossRef]

11. Bhola Patrick, D.; Letai, A. Mitochondria—Judges and Executioners of Cell Death Sentences. *Mol. Cell* **2016**, *61*, 695–704. [CrossRef] [PubMed]

12. Tait, S.W.G.; Green, D.R. Mitochondria and cell death: Outer membrane permeabilization and beyond. *Nat. Rev. Mol. Cell Biol.* **2010**, *11*, 621–632. [CrossRef] [PubMed]

13. Adams, J.M.; Cory, S. The BCL-2 arbiters of apoptosis and their growing role as cancer targets. *Cell Death Differ.* **2018**, *25*, 27–36. [CrossRef] [PubMed]

14. Punnoose, E.A.; Leverson, J.D.; Peale, F.; Boghaert, E.R.; Belmont, L.D.; Tan, N.; Young, A.; Mitten, M.; Ingalla, E.; Darbonne, W.C.; et al. Expression Profile of BCL-2, BCL-XL, and MCL-1 Predicts Pharmacological Response to the BCL-2 Selective Antagonist Venetoclax in Multiple Myeloma Models. *Mol. Cancer Ther.* **2016**, *15*, 1132–1144. [CrossRef]

15. Al-harbi, S.; Hill, B.T.; Mazumder, S.; Singh, K.; DeVecchio, J.; Choudhary, G.; Rybicki, L.A.; Kalaycio, M.; Maciejewski, J.P.; Houghton, J.A.; et al. An anti-apoptotic BCL-2 family expression index predicts the response of chronic lymphocytic leukemia to ABT-737. *Blood* **2011**, *118*, 3579–3590. [CrossRef]

16. Touzeau, C.; Ryan, J.; Guerriero, J.; Moreau, P.; Chonghaile, T.N.; Le Gouill, S.; Richardson, P.; Anderson, K.; Amiot, M.; Letai, A. BH3 profiling identifies heterogeneous dependency on Bcl-2 family members in multiple myeloma and predicts sensitivity to BH3 mimetics. *Leukemia* **2015**, *30*, 761–764. [CrossRef]

17. Merino, D.; Kelly, G.L.; Lessene, G.; Wei, A.H.; Roberts, A.W.; Strasser, A. BH3-Mimetic Drugs: Blazing the Trail for New Cancer Medicines. *Cancer Cell* **2018**, *34*, 879–891. [CrossRef]

18. Fernando, J.; Sancho, P.; Fernández-Rodriguez, C.M.; Lledó, J.L.; Caja, L.; Campbell, J.S.; Fausto, N.; Fabregat, I. Sorafenib sensitizes hepatocellular carcinoma cells to physiological apoptotic stimuli. *J. Cell. Physiol.* **2012**, *227*, 1319–1325. [CrossRef]

19. Stefanovic, M.; Tutusaus, A.; Martinez-Nieto, G.A.; Barcena, C.; de Gregorio, E.; Moutinho, C.; Barbero-Camps, E.; Villanueva, A.; Colell, A.; Mari, M.; et al. Targeting glucosylceramide synthase upregulation reverts sorafenib resistance in experimental hepatocellular carcinoma. *Oncotarget* **2016**, *7*, 8253–8267. [CrossRef]

20. Galmiche, A.; Ezzoukhry, Z.; Francois, C.; Louandre, C.; Sabbagh, C.; Nguyen-Khac, E.; Descamps, V.; Trouillet, N.; Godin, C.; Regimbeau, J.M.; et al. BAD, a Proapoptotic Member of the BCL2 Family, Is a Potential Therapeutic Target in Hepatocellular Carcinoma. *Mol. Cancer Res.* **2010**, *8*, 1116–1125. [CrossRef]

21. Chiou, J.-F.; Tai, C.-J.; Wang, Y.-H.; Liu, T.-Z.; Jen, Y.-M.; Shiau, C.-Y. Sorafenib induces preferential apoptotic killing of a drug- and radio-resistant hep G2 cells through a mitochondria-dependent oxidative stress mechanism. *Cancer Biol. Ther.* **2009**, *8*, 1904–1913. [CrossRef] [PubMed]

22. Hikita, H.; Takehara, T.; Shimizu, S.; Kodama, T.; Shigekawa, M.; Iwase, K.; Hosui, A.; Miyagi, T.; Tatsumi, T.; Ishida, H.; et al. The Bcl-xL inhibitor, ABT-737, efficiently induces apoptosis and suppresses growth of hepatoma cells in combination with sorafenib. *Hepatology* **2010**, *52*, 1310–1321. [CrossRef] [PubMed]

23. Tutusaus, A.; Stefanovic, M.; Boix, L.; Cucarull, B.; Zamora, A.; Blasco, L.; de Frutos, P.G.; Reig, M.; Fernandez-Checa, J.C.; Marí, M.; et al. Anti-apoptotic BCL-2 proteins determine sorafenib/regorafenib resistance and BH3-mimetic efficacy in hepatocellular carcinoma. *Oncotarget* **2018**, *9*, 16701–16717. [CrossRef] [PubMed]

24. Liu, S.; Du, Y.; Ma, H.; Liang, Q.; Zhu, X.; Tian, J. Preclinical comparison of regorafenib and sorafenib efficacy for hepatocellular carcinoma using multimodality molecular imaging. *Cancer Lett.* **2019**, *453*, 74–83. [CrossRef]

25. Kissel, M.; Berndt, S.; Fiebig, L.; Kling, S.; Ji, Q.; Gu, Q.; Lang, T.; Hafner, F.T.; Teufel, M.; Zopf, D. Anti-tumor effects of regorafenib and sorafenib in preclinical models of hepatocellular carcinoma. *Oncotarget* **2017**, *8*, 107096–107108. [CrossRef]

26. Butterworth, M.; Pettitt, A.; Varadarajan, S.; Cohen, G.M. BH3 profiling and a toolkit of BH3-mimetic drugs predict anti-apoptotic dependence of cancer cells. *Br. J. Cancer* **2016**, *114*, 638–641. [CrossRef]

27. Gomez-Bougie, P.; Maiga, S.; Tessoulin, B.; Bourcier, J.; Bonnet, A.; Rodriguez, M.S.; Le Gouill, S.; Touzeau, C.; Moreau, P.; Pellat-Deceunynck, C.; et al. BH3-mimetic toolkit guides the respective use of BCL2 and MCL1 BH3-mimetics in myeloma treatment. *Blood* **2018**, *132*, 2656–2669. [CrossRef]

28. Villalobos-Ortiz, M.; Ryan, J.; Mashaka, T.N.; Opferman, J.T.; Letai, A. BH3 profiling discriminates on-target small molecule BH3 mimetics from putative mimetics. *Cell Death Differ.* **2019**. [CrossRef]

29. Leverson, J.D.; Phillips, D.C.; Mitten, M.J.; Boghaert, E.R.; Diaz, D.; Tahir, S.K.; Belmont, L.D.; Nimmer, P.; Xiao, Y.; Ma, X.M.; et al. Exploiting selective BCL-2 family inhibitors to dissect cell survival dependencies and define improved strategies for cancer therapy. *Sci. Transl. Med.* **2015**. [CrossRef]

30. Souers, A.J.; Leverson, J.D.; Boghaert, E.R.; Ackler, S.L.; Catron, N.D.; Chen, J.; Dayton, B.D.; Ding, H.; Enschede, S.H.; Fairbrother, W.J.; et al. ABT-199, a potent and selective BCL-2 inhibitor, achieves anti-tumor activity while sparing platelets. *Nat. Med.* **2013**, *19*, 202–208. [CrossRef]

31. Di Veroli, G.Y.; Fornari, C.; Wang, D.; Mollard, S.; Bramhall, J.L.; Richards, F.M.; Jodrell, D.I. Combenefit: An interactive platform for the analysis and visualization of drug combinations. *Bioinformatics* **2016**, *32*, 2866–2868. [CrossRef] [PubMed]

32. Tong, J.; Tan, S.; Zou, F.; Yu, J.; Zhang, L. FBW7 mutations mediate resistance of colorectal cancer to targeted therapies by blocking Mcl-1 degradation. *Oncogene* **2017**, *36*, 787–796. [CrossRef] [PubMed]

33. Xu, J.; Huang, F.; Yao, Z.; Jia, C.; Xiong, Z.; Liang, H.; Lin, N.; Deng, M. Inhibition of cyclin E1 sensitizes hepatocellular carcinoma cells to regorafenib by mcl-1 suppression. *Cell Commun. Signal.* **2019**, *17*, 85. [CrossRef] [PubMed]

34. Leverson, J.D.; Zhang, H.; Chen, J.; Tahir, S.K.; Phillips, D.C.; Xue, J.; Nimmer, P.; Jin, S.; Smith, M.; Xiao, Y.; et al. Potent and selective small-molecule MCL-1 inhibitors demonstrate on-target cancer cell killing activity as single agents and in combination with ABT-263 (navitoclax). *Cell Death Dis.* **2015**, *6*, e1590. [CrossRef] [PubMed]

35. Radoshevich, L.; Murrow, L.; Chen, N.; Fernandez, E.; Roy, S.; Fung, C.; Debnath, J. ATG12 conjugation to ATG3 regulates mitochondrial homeostasis and cell death. *Cell* **2010**, *142*, 590–600. [CrossRef]

36. Tovar, V.; Alsinet, C.; Villanueva, A.; Hoshida, Y.; Chiang, D.Y.; Solé, M.; Thung, S.; Moyano, S.; Toffanin, S.; Mínguez, B.; et al. IGF activation in a molecular subclass of hepatocellular carcinoma and pre-clinical efficacy of IGF-1R blockage. *J. Hepatol.* **2010**, *52*, 550–559. [CrossRef]

37. Uhlen, M.; Zhang, C.; Lee, S.; Sjöstedt, E.; Fagerberg, L.; Bidkhori, G.; Benfeitas, R.; Arif, M.; Liu, Z.; Edfors, F.; et al. A pathology atlas of the human cancer transcriptome. *Science* **2017**, *357*, eaan2507. [CrossRef]

38. Arai, H.; Battaglin, F.; Wang, J.; Lo, J.H.; Soni, S.; Zhang, W.; Lenz, H.J. Molecular insight of regorafenib treatment for colorectal cancer. *Cancer Treat. Rev.* **2019**, *81*, 101912. [CrossRef]

39. Fondevila, F.; Méndez-Blanco, C.; Fernández-Palanca, P.; González-Gallego, J.; Mauriz, J.L. Anti-tumoral activity of single and combined regorafenib treatments in preclinical models of liver and gastrointestinal cancers. *Exp. Mol. Med.* **2019**, *51*, 109. [CrossRef]

40. Mahipal, A.; Tella, S.H.; Kommalapati, A.; Lim, A.; Kim, R. Immunotherapy in Hepatocellular Carcinoma: Is There a Light at the End of the Tunnel? *Cancers (Basel)* **2019**, *11*, 1078. [CrossRef]

41. Natri, H.M.; Wilson, M.A.; Buetow, K.H. Distinct molecular etiologies of male and female hepatocellular carcinoma. *BMC Cancer* **2019**, *19*, 951. [CrossRef] [PubMed]

42. Faqar-Uz-Zaman, S.F.; Heinicke, U.; Meister, M.T.; Vogler, M.; Fulda, S. BCL-xL-selective BH3 mimetic sensitizes rhabdomyosarcoma cells to chemotherapeutics by activation of the mitochondrial pathway of apoptosis. *Cancer Lett.* **2018**, *412*, 131–142. [CrossRef] [PubMed]

43. Rello-Varona, S.; Fuentes-Guirado, M.; López-Alemany, R.; Contreras-Pérez, A.; Mulet-Margalef, N.; García-Monclús, S.; Tirado, O.M.; Del Muro, X.G. Bcl-xL inhibition enhances Dinaciclib-induced cell death in soft-tissue sarcomas. *Sci. Rep.* **2019**, *9*, 3816. [CrossRef]

44. Zhu, Y.; Doornebal, E.J.; Pirtskhalava, T.; Giorgadze, N.; Wentworth, M.; Fuhrmann-Stroissnigg, H.; Niedernhofer, L.J.; Robbins, P.D.; Tchkonia, T.; Kirkland, J.L. New agents that target senescent cells: The flavone, fisetin, and the BCL-XL inhibitors, A1331852 and A1155463. *Aging (Albany NY)* **2017**, *9*, 955–963. [CrossRef] [PubMed]

45. Moncsek, A.; Al-Suraih, M.S.; Trussoni, C.E.; O'Hara, S.P.; Splinter, P.L.; Zuber, C.; Patsenker, E.; Valli, P.V.; Fingas, C.D.; Weber, A.; et al. Targeting senescent cholangiocytes and activated fibroblasts with B-cell lymphoma-extra large inhibitors ameliorates fibrosis in multidrug resistance 2 gene knockout (Mdr2−/−) mice. *Hepatology* **2018**, *67*, 247–259. [CrossRef] [PubMed]

46. Kim, J.; Yu, L.; Chen, W.; Xu, Y.; Wu, M.; Todorova, D.; Tang, Q.; Feng, B.; Jiang, L.; He, J.; et al. Wild-Type p53 Promotes Cancer Metabolic Switch by Inducing PUMA-Dependent Suppression of Oxidative Phosphorylation. *Cancer Cell* **2019**, *35*, 191–203.e8. [CrossRef]

47. Roberts, A.W.; Seymour, J.F.; Brown, J.R.; Wierda, W.G.; Kipps, T.J.; Khaw, S.L.; Carney, D.A.; He, S.Z.; Huang, D.C.; Xiong, H.; et al. Substantial susceptibility of chronic lymphocytic leukemia to BCL2 inhibition: Results of a phase I study of navitoclax in patients with relapsed or refractory disease. *J. Clin. Oncol.* **2012**, *30*, 488–496. [CrossRef]

48. Khan, S.; Zhang, X.; Lv, D.; Zhang, Q.; He, Y.; Zhang, P.; Liu, X.; Thummuri, D.; Yuan, Y.; Wiegand, J.S.; et al. A selective BCL-XL PROTAC degrader achieves safe and potent anti-tumor activity. *Nat. Med.* **2019**, *25*, 1938–1947. [CrossRef]

49. Xu, L.; Hui, A.Y.; Albanis, E.; Arthur, M.J.; O'Byrne, S.M.; Blaner, W.S.; Mukherjee, P.; Friedman, S.L.; Eng, F.J. Human hepatic stellate cell lines, LX-1 and LX-2: New tools for analysis of hepatic fibrosis. *Gut* **2005**, *54*, 142–151. [CrossRef]

50. Marí, M.; Caballero, F.; Colell, A.; Morales, A.; Caballeria, J.; Fernandez, A.; Enrich, C.; Fernandez-Checa, J.C.; García-Ruiz, C. Mitochondrial free cholesterol loading sensitizes to TNF- and Fas-mediated steatohepatitis. *Cell Metab.* **2006**, *4*, 185–198. [CrossRef]

51. May, J.E.; Morse, H.R.; Xu, J.; Donaldson, C. Development of a novel, physiologically relevant cytotoxicity model: Application to the study of chemotherapeutic damage to mesenchymal stromal cells. *Toxicol. Appl. Pharmacol.* **2012**, *263*, 374–389. [CrossRef] [PubMed]

52. Van Tienderen, G.S.; Groot Koerkamp, B.; IJzermans, J.N.M.; van der Laan, L.J.W.; Verstegen, M.M.A. Recreating Tumour Complexity in a Dish: Organoid Models to Study Liver Cancer Cells and their Extracellular Environment. *Cancers (Basel)* **2019**, *11*, 1706. [CrossRef] [PubMed]

53. Bárcena, C.; Stefanovic, M.; Tutusaus, A.; Martinez-Nieto, G.A.; Martinez, L.; García-Ruiz, C.; de Mingo, A.; Caballeria, J.; Fernandez-Checa, J.C.; Marí, M.; et al. Angiogenin secretion from hepatoma cells activates hepatic stellate cells to amplify a self-sustained cycle promoting liver cancer. *Sci. Rep.* **2015**, *5*, 7916. [CrossRef] [PubMed]

54. De Mingo, Á.; de Gregorio, E.; Moles, A.; Tarrats, N.; Tutusaus, A.; Colell, A.; Fernandez-Checa, J.C.; Morales, A.; Marí, M. Cysteine cathepsins control hepatic NF-κB-dependent inflammation via sirtuin-1 regulation. *Cell Death Dis.* **2016**, *7*, e2464. [CrossRef]

Supplementary materials: Regorafenib alteration of the BCL-xL/MCL-1 ratio provides a therapeutic opportunity for BH3-mimetics in hepatocellular carcinoma models

Blanca Cucarull, Anna Tutusaus, Miguel Subías, Milica Stefanovic, Tania Hernáez, Loreto Boix, María Reig, Pablo García de Frutos, Montserrat Marí, Anna Colell, Jordi Bruix, and Albert Morales

Table S1. Patient's data.

GENDER	AGE	Underlying liver disease	ETHIOLOGY	Virus hepatitis	AFP (ngr/mL)	TUMOR SIZE (cm)	Tumor	Vascular Invasion
M	67	cirrhosis	alcohol	NO		4,5	single	NA
M	54	cirrhosis	VHC+VHB+alcohol	VHC+VHB	15	1,3	single	NA
M	50	cirrhosis	VHC+alcohol	VHC	19	1,4	single	NA
M	61	chronic hepatitis	VHC	VHC	20	1,8	single	Yes
M	33	chronic hepatitis	VHB	VHB	4	1,1	single	No
F	61	cirrhosis	VHC	VHC	11	2,1	single	No
M	56	cirrhosis	VHC	VHC	2	5,2 (principal)	multinodular	No
M	68	cirrhosis	alcohol	No	1515	5	single	Yes, microvascular
M	61	cirrhosis	alcohol	No	2	3,5	single+1 satelite	No
M	47	cirrhosis	VHC	VHC	6	2,5	single	No
M	75	cirrhosis	VHC	VHC	23	1,1 (principal)	binodular	No
F	69	cirrhosis	VHC	VHC	7	1,2	single	Yes, microvascular
M	78	cirrhosis	VHC	VHC		4,5	single	No
M	73	cirrhosis	VHC	VHC	2	2,1	single	No
M	67	cirrhosis	VHC	VHC	22	2,1	single	No
M	63	cirrhosis	VHC	VHC	2	2,2	single	No
M	63	chronic hepatitis	VHC	VHC	9	6	single	No
M	48	cirrhosis	VHC	VHC	7	7,5	single	Yes, peritumoral
M	64	cirrhosis	alcohol	NO	6	4,5	single	No
M	68	healthy liver	NA	NO	NA	NA	NA	NA
F	70	healthy liver	NA	NO	NA	NA	NA	NA
F	47	healthy liver	NA	NO	NA	NA	NA	NA
F	50	healthy liver	NA	NO	NA	NA	NA	NA
F	55	healthy liver	NA	NO	NA	NA	NA	NA
M	36	healthy liver	NA	NO	NA	NA	NA	NA
M	36	healthy liver	NA	NO	NA	NA	NA	NA
M	55	healthy liver	NA	NO	NA	NA	NA	NA
M	37	healthy liver	NA	NO	NA	NA	NA	NA
F	73	healthy liver	NA	NO	NA	NA	NA	NA
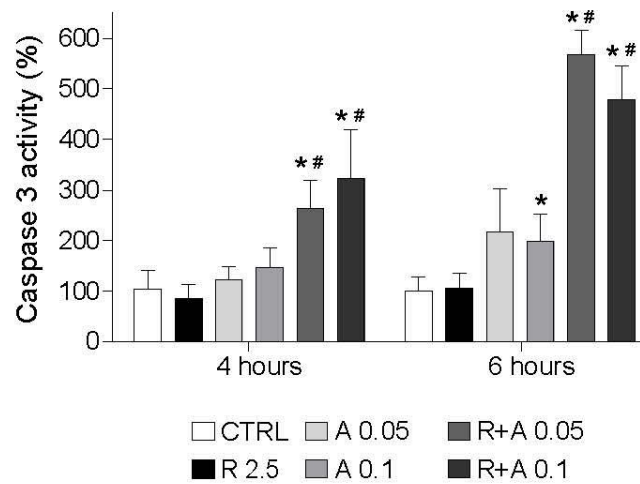
HepG2 cells were exposed to regorafenib (R, 2.5 µM) with or without A-1331852 (A, 0.1-0.05 µM) and caspase-3 activity was determined fluorimetricaly at four and six hours. *P< 0.05 vs. control cells, #P< 0.05 vs. regorafenib-treated cells. (n=3)
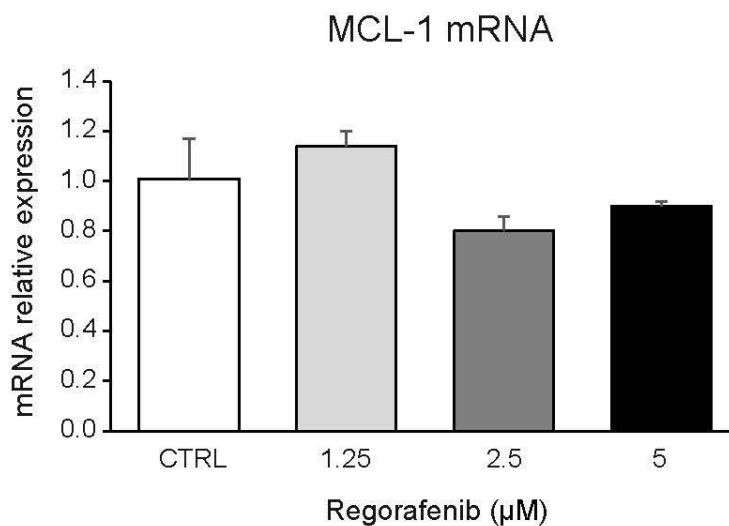
HepG2 cells were exposed to regorafenib (R, 1-5 µM) for 16 h and mRNA levels of MCL-1 were determined by qPCR. (n=2)

Supplemental Figure 3
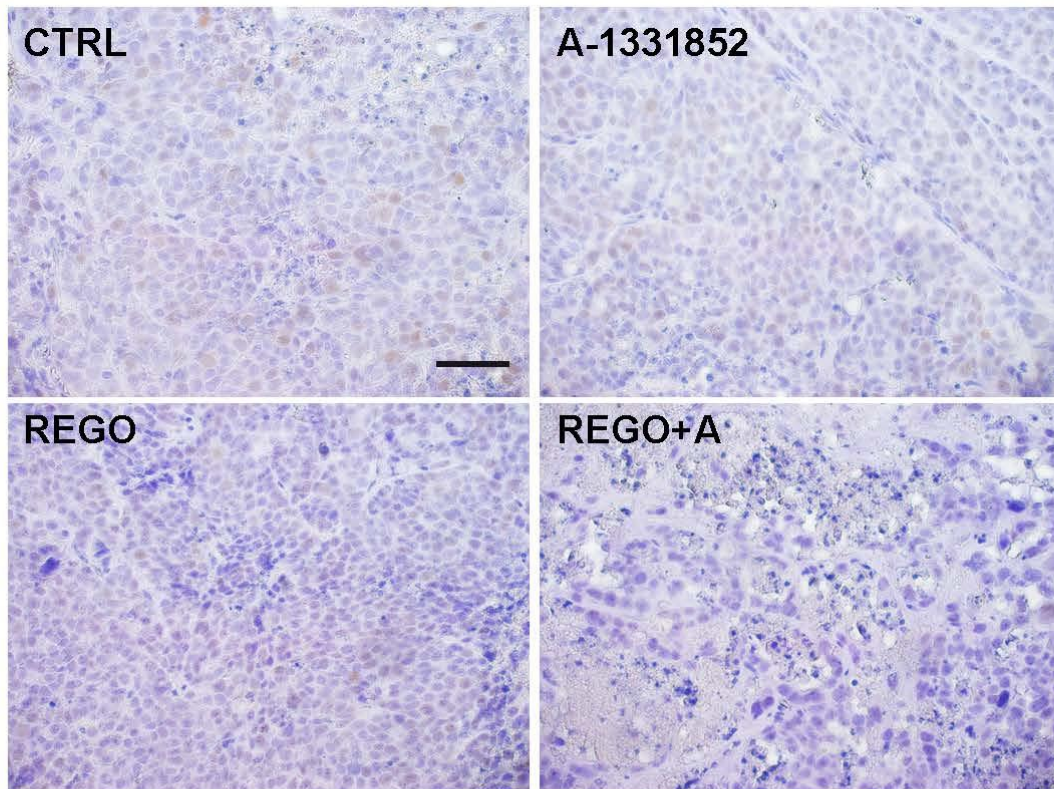
Representative images of Ki-67 expression in tumor samples from BCLC9 PDXs (scale bar, 50 μm).

Supplemental Figure 4
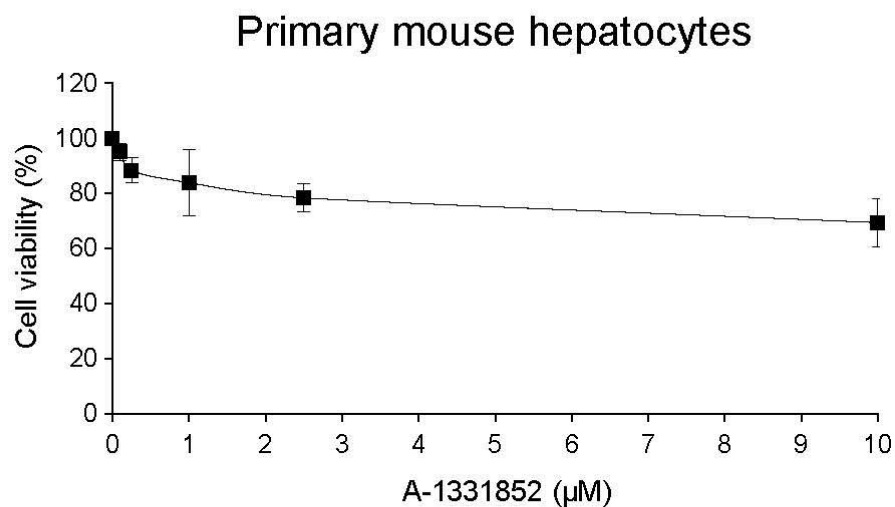
Primary mouse hepatocytes cultured on collagen plates were exposed to A-1331852 at different concentrations (up to 10 μM) and MTT assays performed 16 h. (n=4)

Human hepatic Stellate cells LX2
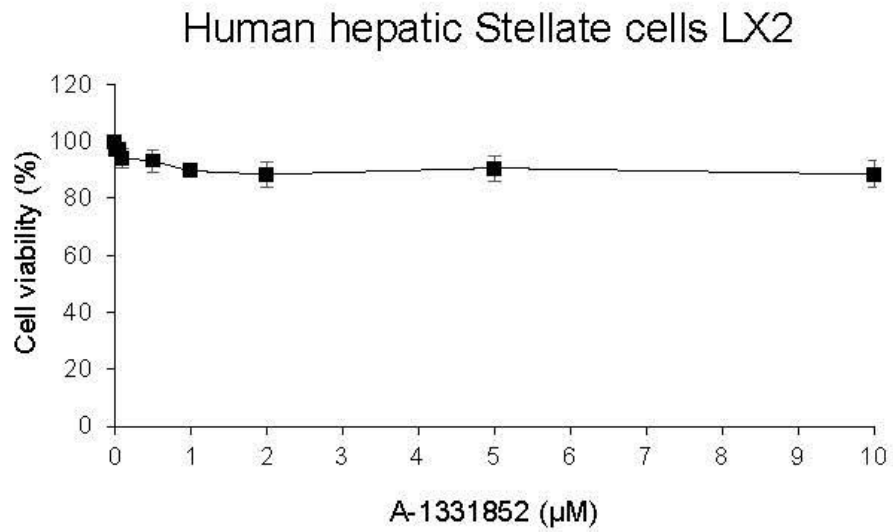
Human hepatic Stellate cells LX2 were exposed to A-1331852 at different concentrations (up to 10 µM) and MTT assays performed 16 h. (n=4)
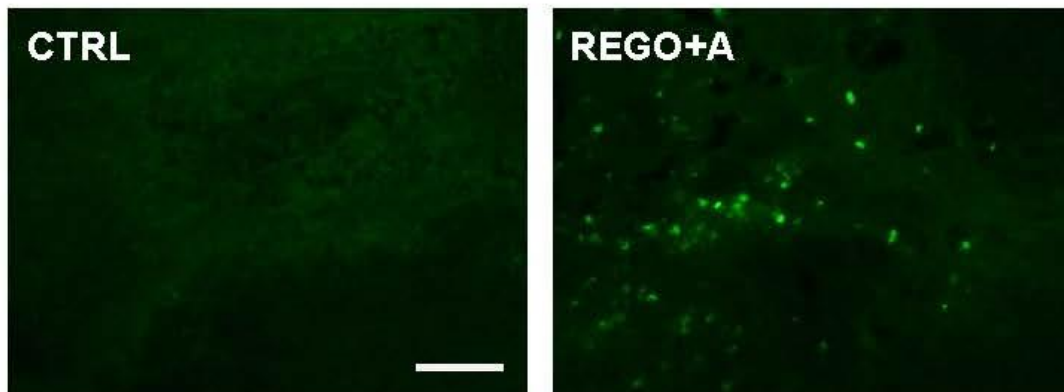
Representative images of TUNEL staining in tumor samples from R HEPG2 CDXs (scale bar, 100 µm).

Results 2

Multikinase inhibitors effect may be restrained by antioxidant supplementation in liver cancer through a ROS-dependent mechanism

Cucarull, B.; Tutusaus, A.; Hernáez-Alsina, T.; García de Frutos, P.; Reig, M.; Colell, A.; Marí, M.; Morales, A. **Antioxidants Threaten Multikinase Inhibitor Efficacy against Liver Cancer by Blocking Mitochondrial Reactive Oxygen Species.** Antioxidants 2021, 10, 1336. https://doi.org/10.3390/antiox10091336

In the last years multiple therapeutic options regarding systemic treatment of HCC have become available. Several multityrosine kinase inhibitors have been prescribed for HCC management, such as sorafenib in the first line, regorafenib in the second line and cabozantinib in the third line. In our previous work, we have assessed that MKI produce mitochondrial alterations in HCC cells that lead to apoptosis, especially in combination with BH3 mimetics. Thus, we aimed to examine the role of the oxidative stress in MKI cytotoxic action and whether antioxidants and the redox cellular status may induce differences in the efficacy of the different MKI that we have tested.

Considering that sorafenib and regorafenib have been described to produce a rise in ROS formation, three different hepatoma cell lines were pre-treated with BSO, a compound that depletes intracellular GSH levels, and incubated with sorafenib, regorafenib and cabozantinib for 20 h. Cell viability was determined by the MTT method. As a result, we could observe that cells with diminished levels of GSH were more sensitive to sorafenib and regorafenib. Of note, only HepG2 cells responded to BSO and cabozantinib administration, whereas Hep3B and PLC/PRF/5 did not. This data suggested that cabozantinib, a MKI which also targets c-Met, have less capacity than sorafenib or regorafenib to induce cell death via a ROS-dependent mechanism.

To better understand if ROS had a predominant role in MKI effectiveness, BSO was pre-administered to hepatoma cells and then treated at increasing concentrations of sorafenib, regorafenib or cabozantinib for a period of three hours. After all treatments, DHE probe was added to visualize mitochondrial superoxide anion production, one of

the main ROS generated by cells. Sorafenib and regorafenib clearly induced mitochondrial ROS production in HCC cells, whereas the superoxide anion detection with cabozantinib administration was not so evident, results that were consistent with the previous ones regarding cell viability. Cells that were pre-treated with BSO also exhibited a greater amount of ROS levels.

Besides, to test whether MKI in combination with BH3 mimetics, such as the combination of regorafenib plus A-1331852, produced cell death through mitochondrial ROS production, we treated hepatoma cells with these compounds and added the DHE probe. The dual treatment regorafenib and A-1331852 clearly induced a rise in ROS production, suggesting that at least part of their mechanism of cytotoxicity is mediated by mitochondrial ROS.

After identifying the implication of ROS in the effectivity of MKI therapy in HCC cells, we administered the antioxidant GSHe, an external supplementation of the intracellular GSH, and MnTBAP, a mimetic of the antioxidant enzyme MnSOD with either sorafenib plus ABT-263 or regorafenib and A-1331852 or sorafenib alone. The addition of GSHe or MnTBAP attenuated chemotherapy effectivity in hepatoma cells as shown by an increase in cell viability by the MTT assay.

As a closer approach to tumors, tumor liver spheroids were generated and treated for seven days with BSO, sorafenib and the combination of both agents. After that, the DHE and Hoechst probes were added. Tumor liver spheroids treated with sorafenib and BSO exhibited the greatest levels of superoxide production. Moreover, vehicle- or sorafenib-treated spheroids were exposed to the antioxidant compounds MnTBAP or GSHe, resulting in a reduction of mitochondrial ROS generation and an increase in spheroid volume. Therefore, the antioxidant supplementation interfered with MKI-triggered ROS generation in tumor liver spheroids resulting in reduced tumor growth.

Our next step was to determine the capacity of sorafenib and regorafenib of activating mitophagy in HCC cells, and if ROS had an implication in that process. To do so, Hep3B cells were treated with increasing amounts of sorafenib or regorafenib for 16 hours. After that, cells were stained with green fluorescent labelling of PDHA1, a mitochondrial matrix enzyme, and LC3, a cytosolic autophagy marker with a red fluorochrome. Immunostained cells were observed under confocal microscopy, and colocalization puncta were identified, visualized as yellow dots. These data suggested that sorafenib or regorafenib induced mitophagy in hepatoma cells and this effect was increased with the addition of BSO.

To verify these observations, Hep3B cells were treated with BSO, sorafenib or the combination of both agents for four and eight hours. Cell extracts were afterwards collected and immunoblotting technique was performed so that proteins implicated in mitochondrial dynamics and mitophagy could be detected. Being PINK1 and Parkin one of the most described mitophagy pathways, an increase in the PINK1/Parkin axis was assessed with BSO and sorafenib treatment. GSH depletion provoked by BSO resulted in a reduction of mitofusin 2 protein levels, a protein that is restrained by Parkin activity. Optineurin accumulation was detected with BSO and sorafenib dual treatment, suggesting that autophagic processes were activated. Hence, we were able to demonstrate that the anti-tumor therapy with MKI and ROS-inducing agents like BSO elicited mitophagy in HCC cells with the implication of mitochondrial ROS.

Article

Antioxidants Threaten Multikinase Inhibitor Efficacy against Liver Cancer by Blocking Mitochondrial Reactive Oxygen Species

Blanca Cucarull [1,2], Anna Tutusaus [1], Tania Hernáez-Alsina [3], Pablo García de Frutos [1,4], María Reig [5], Anna Colell [1,6], Montserrat Marí [1,*] and Albert Morales [1,5,*]

1 Department of Cell Death and Proliferation, IIBB-CSIC, IDIBAPS, 08036 Barcelona, Spain; blanca.cucarull@gmail.com (B.C.); anna.tutusaus.lopez@gmail.com (A.T.); pablo.garcia@iibb.csic.es (P.G.d.F.); anna.colell@iibb.csic.es (A.C.)
2 Departament de Biomedicina, Facultat de Medicina, Universitat de Barcelona, 08036 Barcelona, Spain
3 Digestive Unit, Hospital San Pedro, Rioja Salud, 26006 Logroño, Spain; taniahernaez@gmail.com
4 Unidad Asociada (IMIM) IIBB-CSIC, CIBERCV, 08036 Barcelona, Spain
5 Barcelona Clinic Liver Cancer (BCLC) Group, Liver Unit, Hospital Clínic of Barcelona, University of Barcelona, CIBEREHD, IDIBAPS, 08036 Barcelona, Spain; mreig1@clinic.cat
6 CIBERNED, 08036 Barcelona, Spain
* Correspondence: monmari@clinic.cat (M.M.); amorales@clinic.cat (A.M.)

Abstract: Sorafenib and regorafenib, multikinase inhibitors (MKIs) used as standard chemotherapeutic agents for hepatocellular carcinoma (HCC), generate reactive oxygen species (ROS) during cancer treatment. Antioxidant supplements are becoming popular additions to our diet, particularly glutathione derivatives and mitochondrial-directed compounds. To address their possible interference during HCC chemotherapy, we analyzed the effect of common antioxidants using hepatoma cell lines and tumor spheroids. In liver cancer cell lines, sorafenib and regorafenib induced mitochondrial ROS production and potent cell death after glutathione depletion. In contrast, cabozantinib only exhibited oxidative cell death in specific HCC cell lines. After sorafenib and regorafenib administration, antioxidants such as glutathione methyl ester and the superoxide scavenger MnTBAP decreased cell death and ROS production, precluding the MKI activity against hepatoma cells. Interestingly, sorafenib-induced mitochondrial damage caused PINK/Parkin-dependent mitophagy stimulation, altered by increased ROS production. Finally, in sorafenib-treated tumor spheroids, while ROS induction reduced tumor growth, antioxidant treatments favored tumor development. In conclusion, the anti-tumor activity of specific MKIs, such as regorafenib and sorafenib, is altered by the cellular redox status, suggesting that uncontrolled antioxidant intake during HCC treatment should be avoided or only endorsed to diminish chemotherapy-induced side effects, always under medical scrutiny.

Keywords: chemotherapy; oxidative stress; glutathione; superoxide; BCL-2; hepatocellular carcinoma; tumor spheroids; mitochondria; apoptosis; mitophagy

1. Introduction

Hepatocellular carcinoma (HCC) is often diagnosed at advanced stages with poor prognosis being the third leading cause of cancer death [1,2]. Despite recent advances in treatment, survival after HCC detection clearly needs to be improved and frequently depends on the efficacy of multikinase inhibitors (MKIs) [2,3]. In the last decade, most of the liver cancer patients have received sorafenib [4] as standard systemic therapy in first line, while regorafenib [5] and cabozantinib [6] has been prescribed for second line. Current treatments for HCC have been recently reviewed by Bruix et al. [7].

HCC has a complex genetic background, lacking specific driver mutations required for cancer cell survival. Therefore, metabolic weaknesses created in cancer cells by MKIs could be considered as an interesting opportunity for treatment in order to improve

patient's life expectancy [8]. Among them, mitochondrial alterations induced by MKIs, such as sorafenib, have received particular interest in cell death signaling [9–11]. In this sense, sorafenib, regorafenib and other MKIs have been shown to act by generating reactive oxygen species (ROS) from the mitochondrial respiratory system, inducing loss of mitochondrial membrane potential and changes in BCL-2 family proteins, which prime cancer cells to combinatory therapies with BH3-mimetics [12–15].

In clinical practice, MKIs are principally considered to act through specific tyrosine and threonine kinases and as anti-angiogenic compounds [2,3,16], while their mitochondrial effect and subsequent ROS production has been largely neglected as an important contributing mechanism until recently. For this reason, we wanted to examine if MKI-induced ROS play an important role in their anti-tumor activity and evaluate if changes in cellular antioxidants with relevant mitochondrial action may alter the response to cancer therapy in HCC treatment.

Nutrition supplements are becoming familiar components of people's diets around the world, and are most frequently used without the advice of a physician or healthcare provider [17,18]. In western countries, over-the-counter products are a common addition, particularly for individuals in special needs, such as sport practitioners, pregnant women, the elderly or those with chronic diseases [19,20]. Cancer patients are aware of their physical profile and frequently take dietary complements, principally vitamins and antioxidants. Among them, glutathione (GSH) and related precursors such as N-acetylcysteine or S-adenosylmethionine [21], antioxidant enzymes such as superoxide dismutase and mitochondrial protectors such as Coenzyme Q10 are frequently acquired for customers and individuals under cancer therapy.

Therefore, we tested the effect of modulating GSH [21], as the main antioxidant involved in mitochondrial survival, on MKI efficacy and in superoxide levels, as the principal source of free radicals in the mitochondria [22], particularly after MKI exposure [10,23]. To do so, in in vitro cellular models and in 3D tumor spheroids, we studied relevant MKIs in the presence of the superoxide dismutase (SOD) mimetic MnTBAP [24] and GSH modulators, such as the inhibitor of GSH synthesis (BSO) or the permeable GSH supplier (glutathione methyl ester, GSHe). In addition, sorafenib is a well-known inducer of autophagy/mitophagy [25,26], and the participation of mitochondrial ROS in mitophagy induction is an emerging topic in different pathological conditions [27,28]. Therefore, we analyzed the potential influence of MKI-derived ROS in autophagy/mitophagy induction and their modulation depending on the cellular redox status.

Our work reveals that MKIs exhibit differential toxicity in hepatoma cell lines, an effect that is frequently potentiated after GSH depletion, promoting mitochondrial damage and mitophagy induction. Consistent with the important role of ROS in MKI anti-cancer activity, loading with specific antioxidants, such as the SOD mimetic MnTBAP or with GSHe, reduced chemotherapy efficacy in hepatoma cell lines and enhanced tumor growth in HCC spheroids. Our results suggest that mitochondrial ROS are critical in the anti-cancer activity of MKIs frequently prescribed for HCC treatment, while antioxidant compounds may alter MKI efficacy in HCC therapy and their uncontrolled consumption should be avoided during chemotherapy treatment.

2. Materials and Methods

2.1. Reagents

Dulbecco's Modified Eagle's Medium (DMEM), trypsin-EDTA, penicillin-streptomycin and dimethyl sulfoxide (DMSO), MTT (3-(4,5-dimethylthiazol-2-yl)-2,5-diphenyl tetrazolium bromide) (M2128), Hoechst 33258 (B1155) and DCF (D6883) were purchased from Sigma–Aldrich (St. Louis, MO, USA). All tissue culture-ware was from Nunc (Roskilde, Denmark). Proteinase inhibitors were from Roche (Madrid, Spain). ECL western blotting substrate was from Pierce (Thermo Fisher Scientific, Rockford, IL, USA). Novex Sharp Pre-Stained Protein Standard (LC5800) (T-3168) were from Invitrogen Life Technologies (Carlsbad, CA, USA). Sorafenib (BAY 43-9006, Nexavar) and Regorafenib (BAY 73-4506,

Stivarga) are manufactured by Bayer. Cabozantinib and A-1331852 were purchased from MedChem Express (Monmouth Junction, NJ, USA). Buthionine sulfoximine, MnTBAP chloride and glutathione monoethyl ester were obtained from Santa Cruz Biotechnology (Dallas, TX, USA).

2.2. Cell Culture and 3D Tumor Liver Spheroid Generation

Human liver tumor cell lines Hep3B, PLC/PRF/5 and HepG2 (European Collection of Animal Cell Cultures (ECACC)) were grown in DMEM (10% FBS) at 37 °C and 5% CO_2. Hep3B cell spheroids were generated and plated in 96-well plates with a bottom coat of agarose [15], allowing spheroids to aggregate for 24 h before treatments. Tumor liver spheroids were kept at 37 °C and 5% CO_2 for 7 days and growth was monitored daily.

2.3. Cell Viability

Cell viability was determined by the MTT assay; 1×10^4 cells/well were seeded in a 96-well plate and incubated at 37 °C and 5% CO_2. After treatments, 10 μL of MTT reagent (5 mg/mL) were added and incubated for 2 h. After removal of the medium, formazan crystals from dried plates were dissolved with 100 μL of 1-propanol. Absorbance was measured in a plate reader (Multiskan® Spectrum, Thermo Fisher Scientific, Rockford, IL, USA) at 570 nm and 630 nm and cell viability calculated with untreated cells.

2.4. Reactive Oxygen Species (ROS) Measurement

Cellular ROS generation was quantified using dihydroethidium (DHE) probe that mainly targets the superoxide anion; 7.5×10^3 or 1×10^4 cells/well were seeded in 96-well plates. After treating cells with indicated drugs, DHE probe was added for 30 min. After probe internalization, 2 washes were performed with DMEM without phenol red and photos of 10 random fields taken using a Leica-CTR4000 microscope and LAS software.

2.5. Apoptotic Cell Death Detection

Cells were seeded at 5×10^4 cells/well in 12-well plates, treated for 8 h. Hoechst 33258 was added to the cell medium (10 μg/mL) for 30 min. After being washed, images of twelve random fields were taken using an Olympus IX-70 microscope with the CC-12 FW camera. After Hoechst staining, condensed nuclei were counted with ImageJ software.

2.6. Immunofluorescence

Hep3B cells were seeded at a density of 50,000 cells/well in 12-well plates on 10 mm round coverslips. After treatments, cells were rinsed with PBS, fixed with 4% PFA for 15 min, washed with PBS kept, blocked in a solution of 1% fatty acid free BSA, 0.1% saponin and 0.5% glycine in PBS for 20 min at RT and incubated with primary antibodies overnight at 4 °C inside a dark chamber (LC3 antibody, #2775S, Cell Signaling Technology®, 1/300, rabbit; PDHA1 antibody, ab110330, Abcam, 1/200, mouse) in 0.05% saponin and Dako Antibody Diluent with Background Reducing Components as solvent. After washing, samples were incubated with secondary antibodies (1 h at RT, anti-rabbit Cy3, 1/300; Alexa Fluor 488 donkey anti-mouse IgG A21202 Invitrogen, 1/300) and acid nucleic marker DRAQ5TM (DR50200, BioStatus, Leicestershire, UK), washed and mounted in 5 μL of Fluoromount-G® (0100-01, Southern Biotech, Birmingham, AL, USA). Pictures, ten random fields per sample, were taken at the confocal microscope Leica TCS SPE with the 60× oil objective.

2.7. Immunoblot Analysis

Cell lysates were prepared in RIPA buffer plus proteinase inhibitors. Samples containing (20 μg) were separated by 10–15% SDS-PAGE, transferred to nitrocellulose membranes, blocked in 5% nonfat milk for 1h at RT and incubated overnight at 4 °C with the primary antibodies: MFN2 (H-68, Santa Cruz, sc-50331, dilution 1:1000, rabbit); Optineurin (C-2, Santa Cruz, sc-166576, dilution 1:1000, mouse); PINK1 (BC100-494, Novus Biologicals, dilution 1:2000, rabbit); Parkin (PRK8, ab77924, Abcam, dilution 1:2000, mouse); β-Actin

(Sigma-Aldrich, A3854, dilution 1:40,000 conjugated to HRP). Secondary antibody incubation was performed for 1 h at RT using anti-mouse (m-IgGκ BP-HRP sc-516102, Santa Cruz, 1:10,000) and anti-rabbit (goat anti-rabbit IgG-HRP sc-2054, Santa Cruz, 1:10,000). Proteins were detected using ECL western blotting substrate (Pierce, Waltham, MA, USA), Clarity and Clarity Max (Bio-Rad, Hercules, CA, USA) and ChemiDoc Imaging System (Bio-Rad).

2.8. Statistical Analyses

Results are expressed as mean ± standard deviation and $n = 3$, unless indicated. Statistical comparisons were usually performed using unpaired 2-tailed Student's *t*-test. A *p*-value less than 0.05 was considered significant.

3. Results

3.1. Anti-Tumor Activity of Multikinase Inhibitors on Liver Cancer Cells Is Affected by Redox Status

Previous works have demonstrated that the main MKIs used in liver cancer, such as sorafenib and regorafenib, share mitochondrial-dependent cytotoxicity. Therefore, we decided to test if changes in GSH levels, a critical mitochondrial antioxidant against ROS damage in the liver, could affect the anti-tumor activity of MKIs used in HCC therapy such as sorafenib, regorafenib and cabozantinib. To do so, representative hepatoma cell lines were treated with sorafenib, MKI administered in first line for HCC patients, as well as regorafenib and cabozantinib, recommended in second- and third-line therapy (Figure 1), under regular culture conditions or after pre-treatment with BSO, an inhibitor of GSH synthesis that effectively depletes its concentration in vitro and in vivo [29,30].
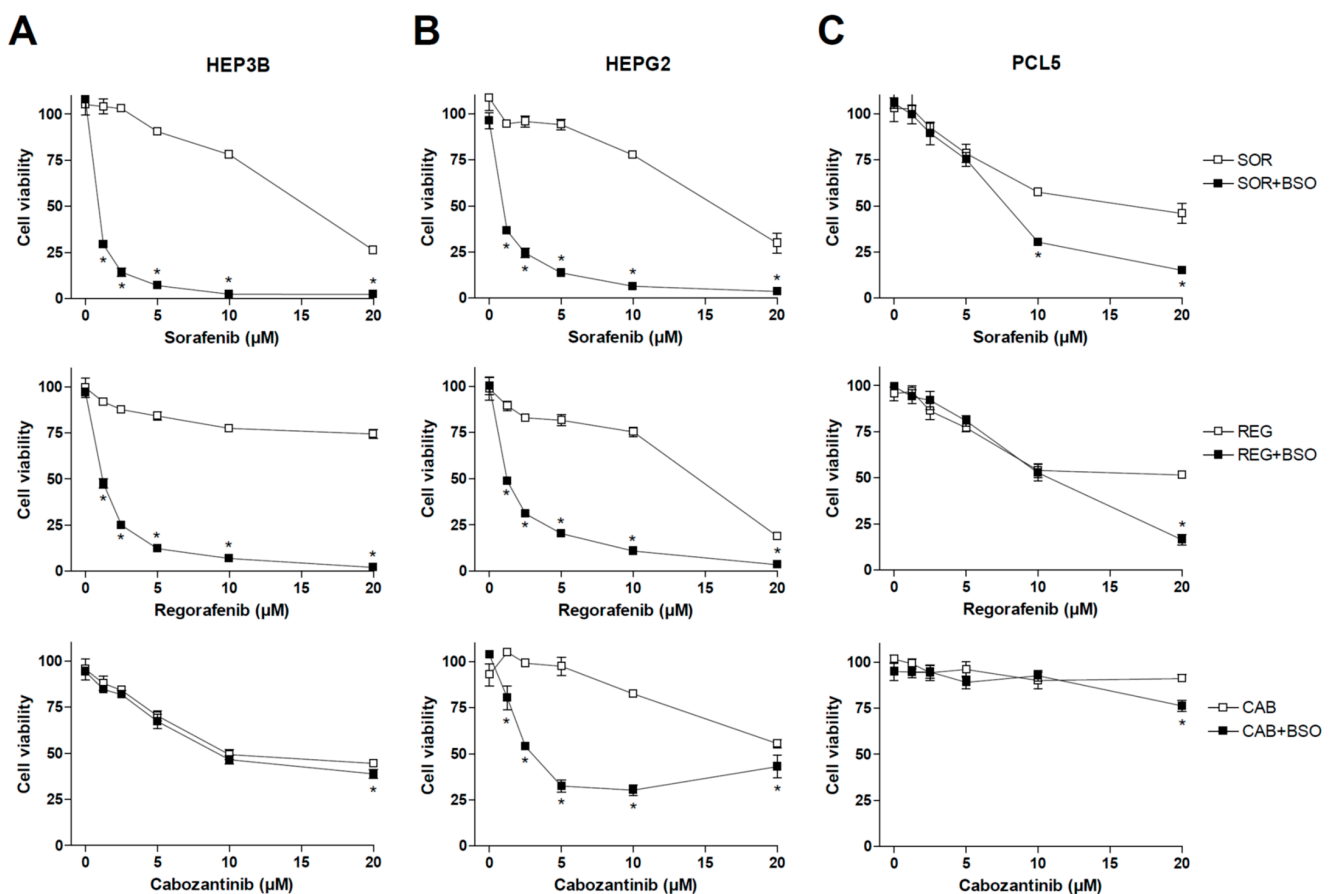
Figure 1. Effect of BSO administration on liver tumor cell lines treated with MKIs. Hep3B (A), HepG2 (B) and PLC5 (C) cells were exposed to increasing doses of sorafenib, regorafenib and cabozantinib for 20 h after incubation with vehicle (PBS) or BSO (1 mM), inhibitor of GSH synthesis, and cell viability quantified by MTT ($n = 3$). * $p < 0.05$ vs. control.

As observed above, sorafenib and regorafenib were very sensitive to GSH depletion, exhibiting cell death clearly potentiated by BSO administration. However, no significant changes were observed in cabozantinib-treated Hep3B cells after diminishing GSH levels. We also tested BSO effect on MKI efficacy in HepG2 cells, observing once again a potent synergy in sorafenib and regorafenib action. In this case, cabozantinib cytotoxicity was also potentiated by GSH reduction.

Finally, we tested MKIs and BSO in PLC5 cells, another typical hepatoma cell line, finding again sensitization to sorafenib and regorafenib by BSO addition, but at higher doses, not frequently reached in patient treatment, than previously observed in HepG2 and Hep3B cell lines. Once again, cabozantinib toxicity was not clearly affected by GSH modulation in PLC5 cells, suggesting a lower capacity of cabozantinib to generate ROS-dependent death (Figure 1).

3.2. Glutathione Reduction Potentiates Early ROS Production by Multikinase Inhibitors and BH3-Mimetics on Liver Cancer Cells

To verify that the increased anti-tumoral effect of these MKIs observed after BSO treatments was preceded by early mitochondrial ROS production, liver cancer cells were analyzed by dihydroethidium (DHE) staining. DHE oxidation, frequently used for cellular and mitochondrial $O_2^{\bullet-}$ detection, was visualized by fluorescence microscopy in HepG2 cells after three hours of MKI administration (sorafenib, regorafenib or cabozantinib) and/or previous GSH reduction with BSO (Figures 2 and 3).
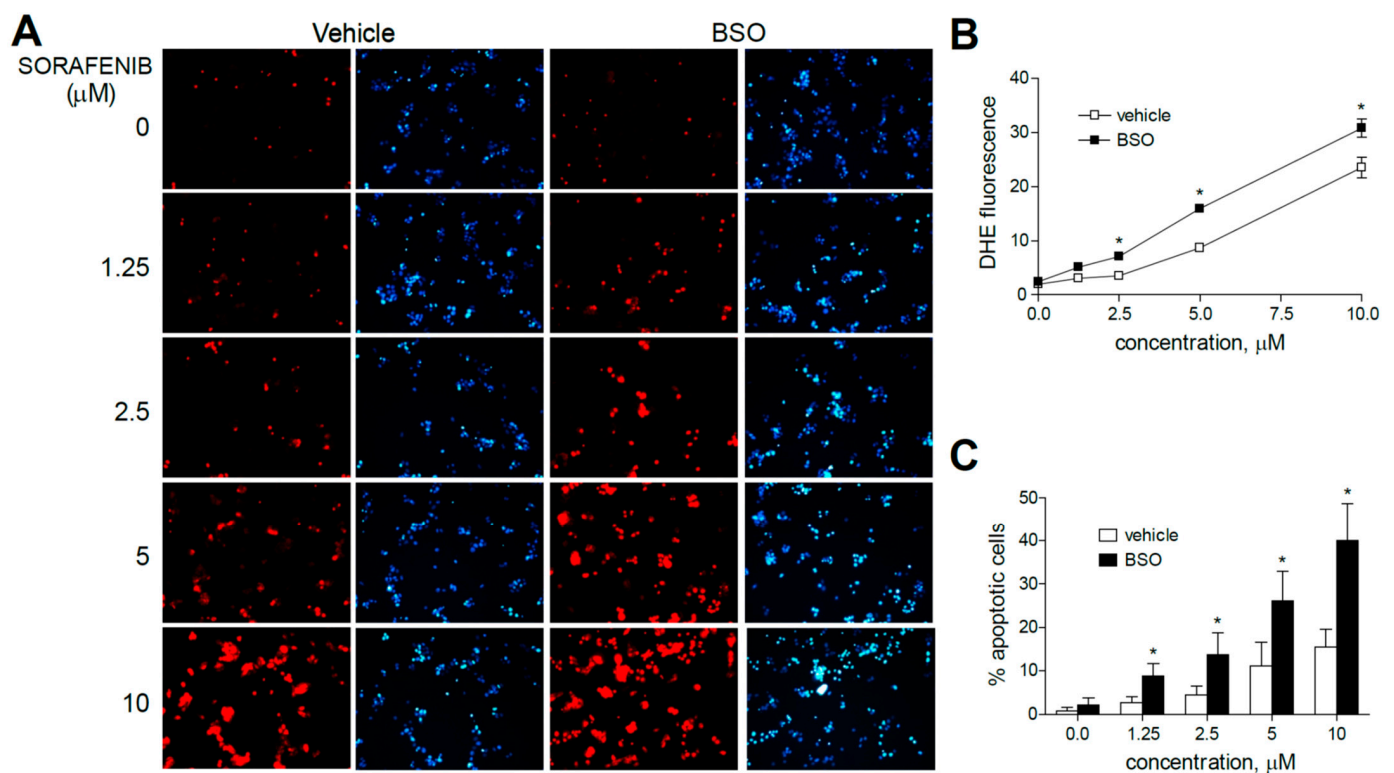
Figure 2. Superoxide production, increased by sorafenib in liver cancer cells, is enhanced by GSH reduction. (**A**) Representative fluorescence images (*n* = 10) after superoxide detection (DHE, red) and nuclear (Hoechst 33258, blue) staining of HepG2 cells at increasing concentrations of sorafenib. (**B**) Quantification of DHE fluorescence in sorafenib-treated cells was analyzed using Image J software. (**C**) Percentage of apoptotic nuclei was measured (*n* = 3). * *p* < 0.05 vs. control.
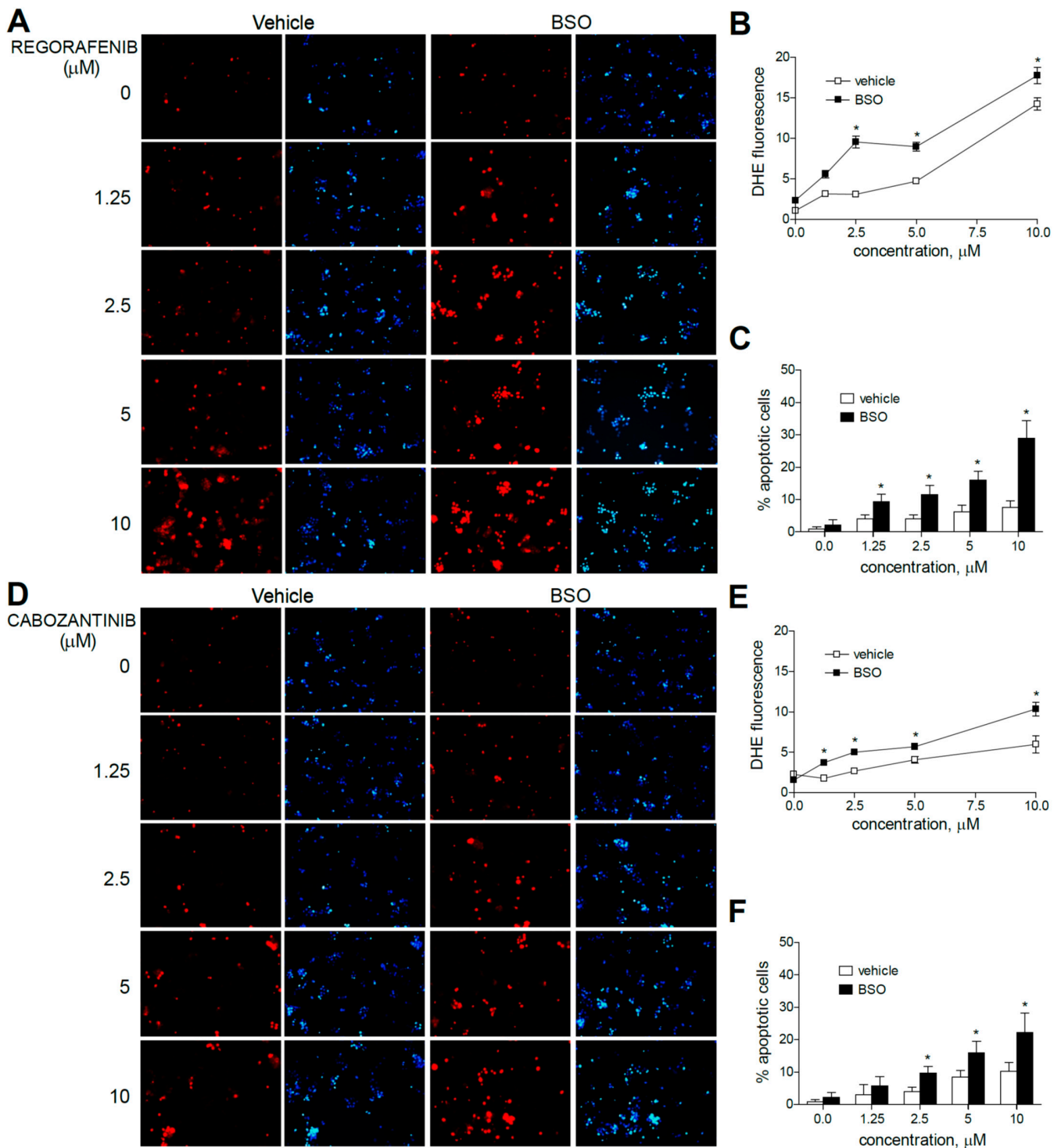
Figure 3. Superoxide production, increased by MKI treatment, is enhanced by GSH reduction. Representative fluorescence images (*n* = 10) after superoxide detection (DHE, red) and nuclear (Hoechst 33258, blue) staining of HepG2 cells after regorafenib (**A**) or cabozantinib (**D**) at increasing concentrations. (**B,E**) Quantification of DHE fluorescence in MKI-treated cells was measured using Image J software. (**C,F**) Number of apoptotic cells was counted (*n* = 3). * $p < 0.05$ vs. control.

Sorafenib increased DHE staining at all concentration (1.25 to 10 μM) ranges in HepG2 cells, even at the low micromolar levels similar to those reached during HCC systemic treatment, in agreement with the specific mitochondrial superoxide production upon sorafenib exposure previously shown [31].

Moreover, the pre-administration of BSO to deplete GSH levels clearly increased the superoxide production induced by sorafenib in all the hepatoma cell lines tested. Similar effects were observed after BSO challenge and regorafenib-treated cells, although ROS generation was mainly observed in monotherapy at the higher MKI concentrations used. As observed in sorafenib-treated cells, BSO potentiated the apoptosis induced by regorafenib treatment (Figure 3A–C).

Regarding cabozantinib, another tyrosine kinase inhibitor with anti c-MET and AXL activities [6,7], ROS production was less evident at low concentrations. However, BSO pre-treatment was effective in HepG2 cells in increasing superoxide staining, consistent with the potentiation in cabozantinib-induced cell death only observed in this specific cell line (Figure 3D–F).

Due to the mitochondrial effects of sorafenib and regorafenib, the co-administration of BH3-mimetics is now under clinical trial, and similar strategies are under biomedical scrutiny [32,33]. To identify if mitochondrial ROS production may play a role in this action, DHE staining was analyzed in hepatoma cells treated with MKI plus BCL-2 inhibitors. First, we treated liver cancer cell lines with regorafenib and the specific BCL-xL inhibitor A-1331852, a BH3-mimetic that greatly potentiates regorafenib anti-tumor activity, to verify if ROS production is modified during BH3-mimetic sensitization. As observed bellow (Figure 4), regorafenib production of mitochondrial ROS was clearly enhanced after A-1331852 addition in all liver cell lines tested.
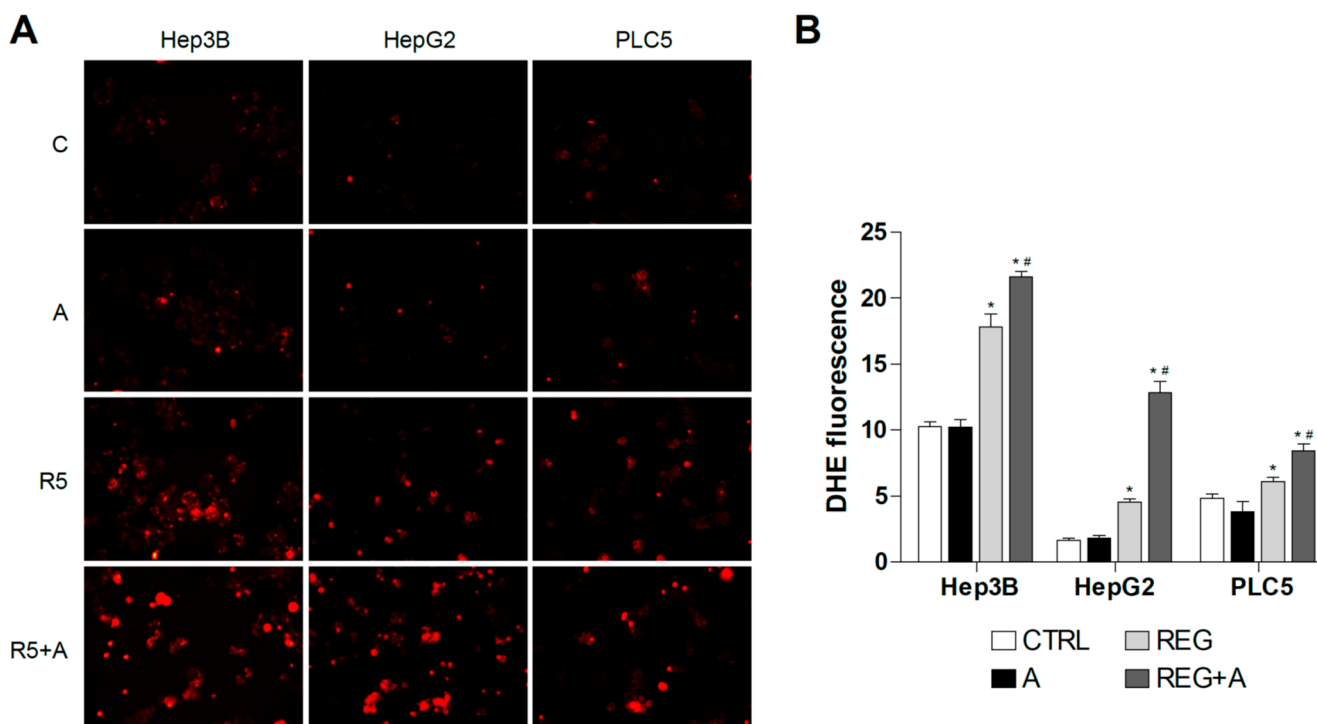
Figure 4. Superoxide production by regorafenib treatment was enhanced in liver cancer cell lines after co-administration with a BH3 mimetic. (**A**) Representative fluorescence images (*n* = 10) of DHE (red) staining in HepG2, Hep3B and PLC5 cells receiving regorafenib treatment (R, 5 μM) in combination with or without the BCL-xL inhibitor A-1331852 (A, 0.1 μM) for 4 h. (**B**) Quantification of DHE fluorescence in cells was measured using Image J software. (*n* = 3). * $p < 0.05$ vs. control, # $p < 0.05$ vs. regorafenib-treated cells.

3.3. Antioxidants May Protect Liver Cancer Cells against Sorafenib/Regorafenib-Based Anti-Cancer Therapies

After establishing that different MKIs such as sorafenib or regorafenib, alone or combined with other anti-tumor compounds such as BH3-mimetics, are generating ROS that affect tumor growth, we checked the potential influence of well-known antioxidants.

As previously observed [15], regorafenib/A-1331852 action against hepatoma cells was potent and seriously reduced in the presence of MnTBAP or GSHe (Figure 5A), suggesting that antioxidant administration may jeopardize the efficacy of this therapy.
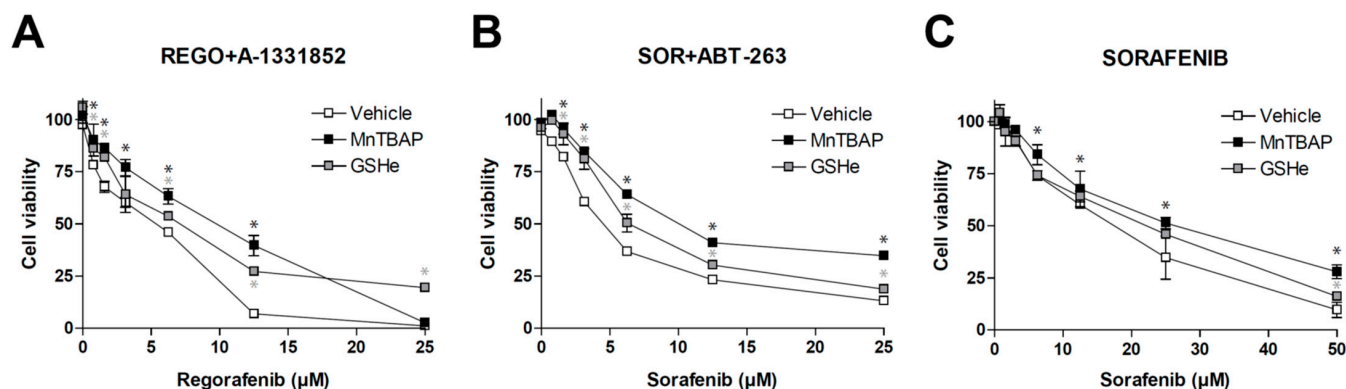
Figure 5. Antioxidants diminish the efficacy of sorafenib/regorafenib-based anti-cancer therapies. MTT assays in Hep3B cells were performed to evaluate potential cell death protection by SOD mimetic MnTBAP and GSHe, a cell permeable GSH supplier, in front of different experimental cancer therapies proposed for HCC treatment. (**A**) increasing doses of regorafenib in combination with the BCL-xL inhibitor A-1331852 (A, 0.1 μM). (**B**) increasing doses of sorafenib in combination with the BCL-2/BCL-xL inhibitor navitoclax (ABT-263) and (**C**) sorafenib alone (*n* = 3). * *p* < 0.05 vs. control cells.

As expected, the antioxidant protection was not exclusive for this therapy. ROS blockage using MnTBAP or GSHe was also effective in reducing the potent anti-tumoral effect of sorafenib plus navitoclax (Figure 5B), a chemotherapeutic combination used in an on-going clinical trial for treating US patients with relapsed or refractory solid tumors (NCT02143401).

Finally, since sorafenib was the MKI that showed the greatest capacity to generate ROS (Figure 2), we also tested if these antioxidants were able to reduce cell death caused by sorafenib in monotherapy.

As observed with the combination therapies, MnTBAP and GSHe were also able to reduce sorafenib activity against liver cancer cells (Figure 5C). Although the effect was only detected at high sorafenib doses, it confirms that this feature may be shared by other anti-cancer strategies applied in the clinic.

3.4. Mitochondrial ROS Production Controls Tumor Growth in HCC Spheroids

To validate our in vitro results in an HCC model better resembling human liver cancer than traditional monolayer cultures, we used Hep3B spheroids. Tumor spheroids were treated with sorafenib and/or ROS modulators for several days.

First, using sorafenib at a concentration in the range reached in serum during chemotherapy, we observed that treatment with the GSH synthesis inhibitor BSO reduced tumor growth, particularly in sorafenib-treated spheroids (Figure 6A,B). In fact, increased ROS production, detectable after BSO treatment, was potentiated by sorafenib addition, as visualized with DHE staining. In parallel, an increased number of apoptotic cells were detected in Hep3B spheroids under sorafenib plus BSO treatment, as denoted by in vivo Hoechst staining. Interestingly, antioxidant supplementation not only avoided tumor reduction in sorafenib/navitoclax-treated spheroids, principally after superoxide reduction with MnTBAP, but also increased tumor growth (Figure 6C), particularly after GSH supplementation using GSHe as quantified in Figure 6D.
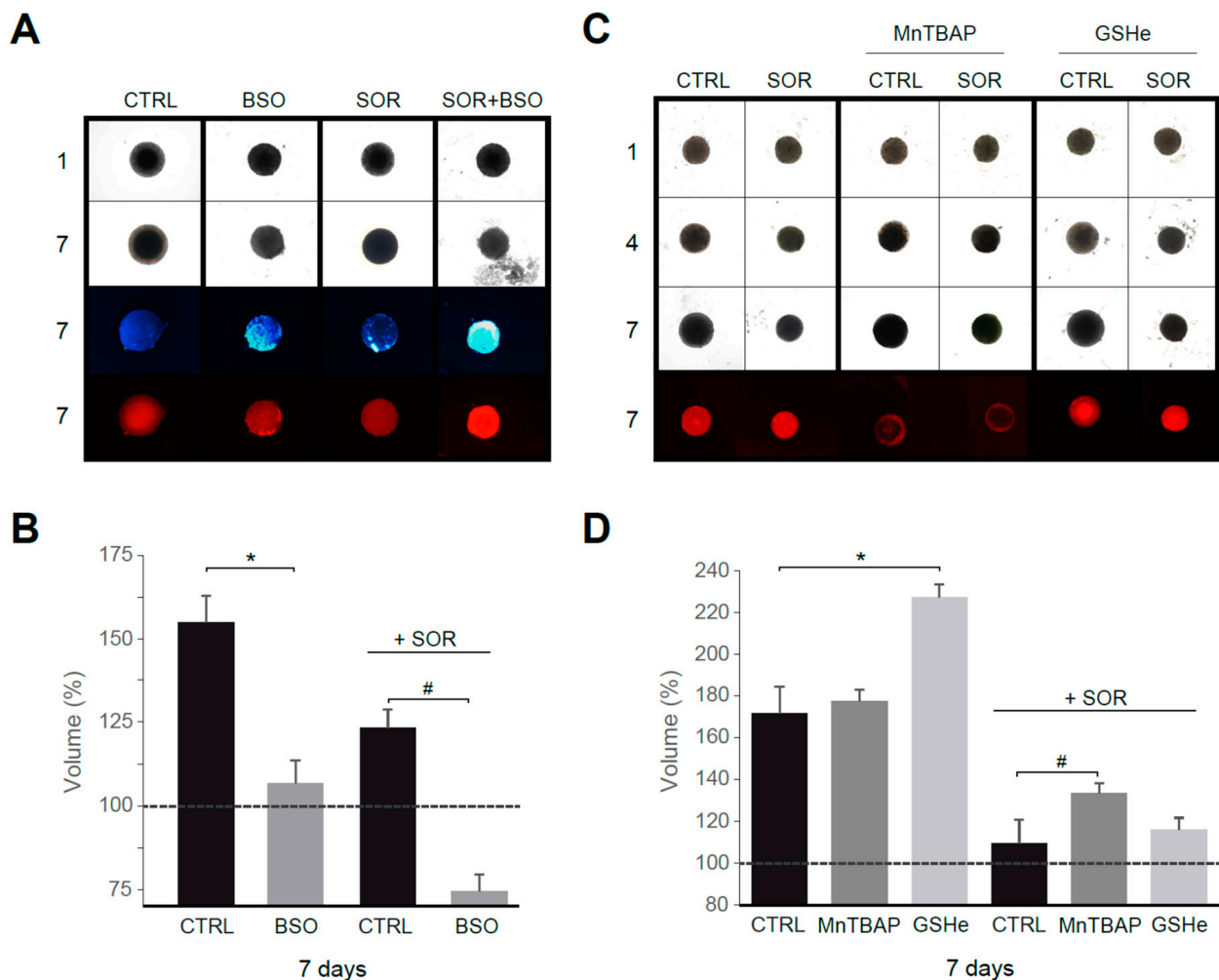
Figure 6. Superoxide reduction in sorafenib treatment favors tumor growth in a 3D spheroid model. (**A**) Hep3B spheroids were seeded (day 1) and treated with vehicle, sorafenib (S, 2.5 μM) and/or BSO (1 mM) for six days. Third row, Hoechst staining. Fourth row, DHE staining. (**B**) Spheroid growth was monitored ($n = 3$). (**C**) Effect of MnTBAP and GSHe on spheroid growth ($n = 3$). (**D**) Volume quantification. * $p < 0.05$ vs. control cells, # $p < 0.05$ vs. sorafenib-treated cells.

Therefore, the intracellular antioxidant levels modulate tumor growth under chemotherapy exposure in a 3D model of cancer that could anticipate an in vivo impact for antioxidant supplements.

3.5. MKI-Based HCC Therapy Induces Mitochondrial ROS Promoting Mitophagy

Sorafenib interaction with subunits of the mitochondrial respiratory system generates ROS that may promote mitochondrial damage and mitophagy [25,26]. To test if antioxidants and the redox status of hepatoma cells may alter chemotherapy-induced mitophagy, Hep3B cells were exposed to increasing doses of sorafenib and regorafenib, and the effects of increased mROS production were analyzed after BSO exposure. Using a mitochondrial marker such as PDHA1 (green) in combination with the autophagy protein marker LC3 (red), after sorafenib treatment we visualized a dose-dependent increase in LC3 content, consistent with autophagy induction and the appearance of yellow dots indicating co-localization of LC3 and mitochondria (Figure 7A).
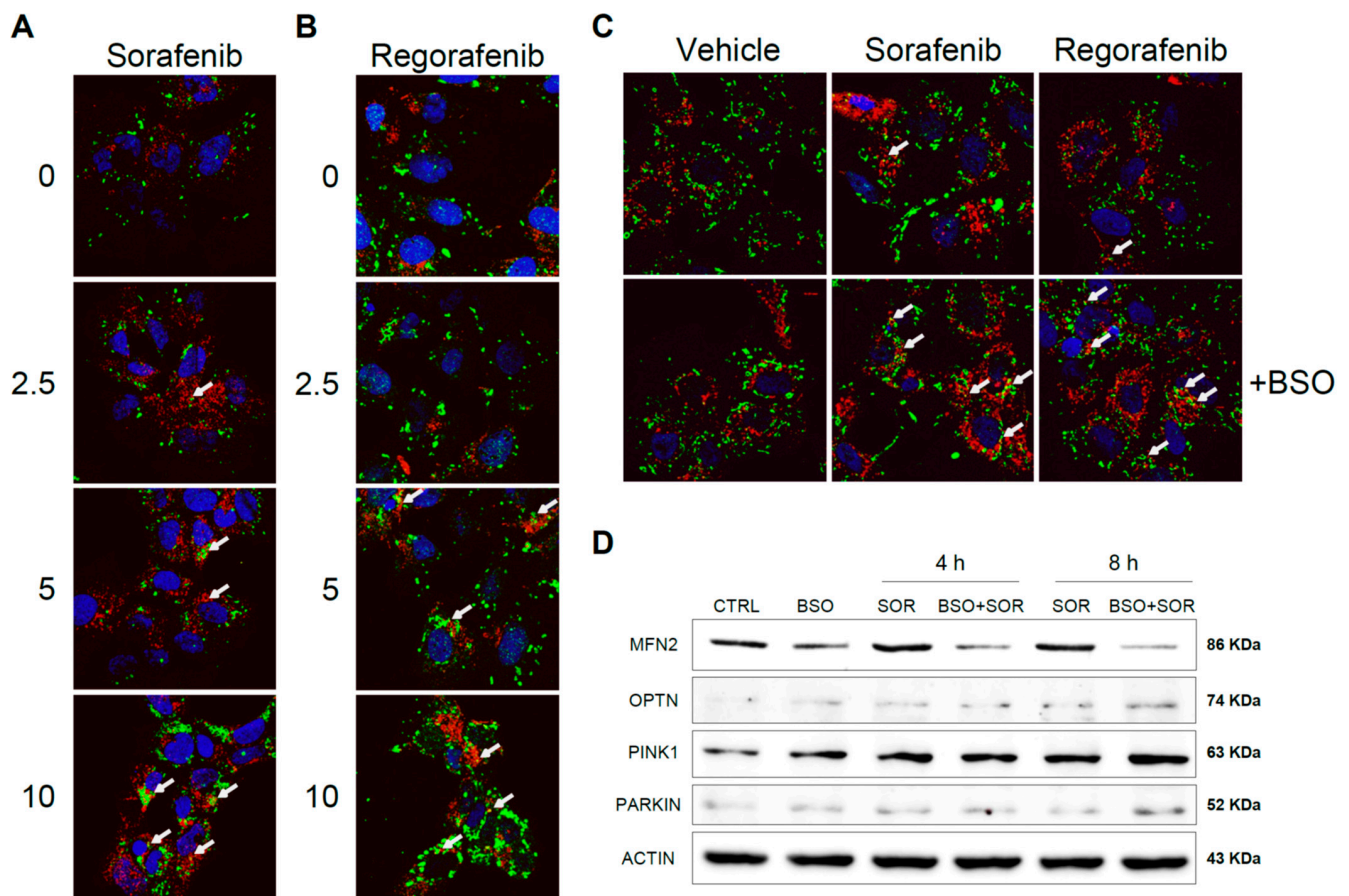
Figure 7. Sorafenib and regorafenib induced mitochondrial-ROS dependent mitophagy in hepatoma cells. Hep3B cells were treated with increasing doses of sorafenib (**A**) or regorafenib (**B**), stained with LC3 (red) and PDHA1 (green) antibodies and visualized by confocal microscopy after 16 h. Representative images of 12 independent random fields. (**C**) Hep3B cells pre-incubated with vehicle or BSO were treated with sorafenib (2.5 μM) or regorafenib (2.5 μM) and visualized as before. (**D**) Hep3B cells, incubated with vehicle or BSO, were treated with sorafenib (2.5 μM) at different times and different mitophagy-related proteins were analyzed by western blot. Representative images (*n* = 3).

Similar evidence of mitophagy was also observed in regorafenib-treated hepatoma cells (Figure 7B). Of note, the reduction in GSH by BSO pretreatment potentiated mitophagy at low micromolar sorafenib/regorafenib doses, suggesting that oxidative mitochondrial damage by MKI exposure promotes redox-dependent induction of mitophagy (Figure 7C). To verify this point, we analyzed by western blot the levels of relevant mitophagy-related proteins in Hep3B cells treated with sorafenib, evaluating changes after GSH reduction (Figure 7D).

As previously reported, sorafenib increased the cellular amount of PINK1 and Parkin [25,26], promoting the elimination of damaged mitochondria, and the pro-oxidant conditions induced in our experiments by BSO exposure potentiated this effect. Moreover, Parkin-related mitofusin 2 (MFN2) ubiquitination and proteasomal degradation [34] seem to be potentiated by GSH restriction. Stress-induced phosphorylation and proteasomal elimination of MFN2 results in mitochondrial fragmentation, a necessary event for mitophagy induction and enhanced apoptotic cell death [35]. Since MFN2 levels were decreased upon sorafenib exposure in BSO-treated cells, oxidative-induced blockage of mitochondrial fusion could be taking place. Finally, optineurin accumulation and lack of mitochondrial targeting has been described in ROS-induced mitophagy [36]. Since we found increased optineurin in sorafenib-treated hepatoma cells, particularly after BSO pre-incubation, it could be indicative of its MKI-dependent cytosolic accumulation.

Therefore, these experiments suggest that the mitochondrial damage caused by MKIs promotes mitophagy induction, while a pro-oxidative mitochondrial condition alters mitophagy progression and changes mitochondrial dynamics, in line with recent data [37]. Knowing whether this effect is an important contributor to BSO-induced cell death in chemotherapy would provide novel insights into mitochondria-dependent apoptosis and cancer therapy, a point that would require additional research.

4. Discussion

Over-the-counter dietary and nutritional supplements are commonly consumed by the general public, initially as a remedy for medical problems, but increasingly as simple additions to our diet for the alleged prevention of disease. Although nutritional supplements could be beneficial in several settings, their unrestricted intake may also have deleterious effects on human health, which are of special concern to cancer patients [38,39]. Antioxidants play an important role in maintaining cellular integrity against physiological and pathological oxidative stress, which is normally well controlled in healthy individuals [21,22,40,41]. Patients under cancer chemotherapy are conscious that their bodies are under distress and may be prone to taking supplements, particularly since no negative side-effects are expected from them. In fact, the antiangiogenic action of MKIs is well known among physicians and researchers; however, the role of ROS, and specifically of mitochondrial ROS, on MKI efficacy has not been commonly recognized. In this sense, it is important to ponder the relevance of mitochondrial oxidative stress in MKI action against liver cancer and to question the appropriateness of antioxidant supplements during MKI treatments.

Previous research has indicated that ROS are generated from the cellular action of sorafenib or regorafenib, and superoxide from mitochondria was pointed as a probable source. Our work indicates that mitochondrial ROS are common to several MKIs, including cabozantinib, in specific hepatoma cell lines as observed at higher doses and clearly evidenced after reducing antioxidant protection by BSO pre-administration. In fact, depleting GSH levels sensitized against sorafenib, regorafenib and even cabozantinib, in different hepatoma cell lines, supports the key role of ROS in MKI anti-cancer activity. Of note, the increase in mitochondrial ROS after MKI therapy is also common to other successful strategies [42–44], as we observed after regorafenib co-treatment with the BH3 mimetic A-1331852. Similarly, it may suggest that other compounds able to generate mitochondrial stress in cancer cells might be worthy of combination with MKI therapy in HCC treatment [42].

Once it was demonstrated that ROS induction by MKIs participates in the killing of cancer cells, we wanted to test if derivatives of GSH and SOD, two of the compounds more frequently recommended as antioxidant dietary supplements, could modify MKI action in hepatoma cell lines. To do so, we used the SOD mimetic MnTBAP or GSH ester (GSHe), since they both have been intensively used in vitro and in vivo [24,29,30,40,41], and they can easily target intracellular ROS even in mitochondrial compartments. Noteworthy, MnTBAP and GSHe diminished the efficacy of sorafenib and regorafenib, not only alone but also combined with BH3-mimetics, emphasizing the relevant participation of ROS in cancer therapy. Similar behavior was detected in 3D tumor spheroids, highlighting the potential problems associated with antioxidant intake during MKI therapy. It is worth remarking that this perturbing effect was fortunately not shared by all antioxidants tested. For instance, no significant protection from death was observed after administering Trolox, a vitamin E analog, or MitoQ (data not shown), a mitochondrial-targeted antioxidant that frequently protects against mitochondrial damage [45,46]. Regarding MitoQ, this TPP+-conjugated antioxidant selectively concentrates in the mitochondria and prevents mitochondrial oxidative damage, being frequently bought for sport practitioners and the public in general. However, MitoQ did not potentiate the toxicity of MKIs in liver cancer cell lines. As a possible explanation, TPP+-conjugated antioxidants penetrate the mitochondria leaded by the mitochondrial membrane potential (MMP) [47], and sorafenib

or regorafenib quickly and strongly decrease MMP in hepatoma cells, which could prevent TPP+ mitochondrial entry.

Finally, we wanted to verify mitophagy participation in MKI action since mitochondrial damage by ROS producing drugs is becoming an interesting subject modulated by the redox state, with potential antioxidant participation. Our data support that the mitochondrial damaging effect of MKIs, such as sorafenib and regorafenib, is promoting mitophagy in hepatoma cells, being the PINK1/Parkin signaling pathway clearly enhanced by modifying the antioxidant defense, as BSO pre-incubation does. Although clearance of damaged mitochondria by mitophagy is thought to mediate drug resistance in cancer cells, excessive mitochondrial clearance may induce cell metabolic disorders and cell death [48], in line with our previous results in sorafenib resistant cells [11]. Interestingly, mitochondrial fission-stimulated ROS production on chemotherapy is proposed as a reasonable target for pharmacological stimulation of mitochondrial dynamics that can benefit cancer patients with solid tumors [49]. Therefore, it is tempting to speculate that not only MKIs but also other autophagy/mitophagy-based therapies for cancer could be affected by oxidative stress and antioxidant supplementation.

5. Conclusions

Patients and physicians must be conscious that MKI-based therapies are producing mitochondrial ROS with an important role in the anti-cancer efficacy of the drugs. In particular, dietary supplements with potent antioxidant properties may not be recommended for individuals taking sorafenib or regorafenib for liver cancer treatment. This precaution should be extended for other chemotherapeutic compounds, since the absence of strong evidence indicating ROS involvement in the anti-tumor action, as it happens with cabozantinib reported studies, does not necessarily guarantee the lack of side-effects on specific cancer cells. On the other side, therapies combining pro-oxidant compounds with MKIs should be pursued since cellular redox status modulates MKI effectiveness and may affect therapies with associated autophagy/mitophagy induction.

References

1. Forner, A.; Reig, M.; Bruix, J. Hepatocellular carcinoma. *Lancet* **2018**, *391*, 1301–1314. [CrossRef]
2. Bruix, J.; da Fonseca, L.G.; Reig, M. Insights into the success and failure of systemic therapy for hepatocellular carcinoma. *Nat. Rev. Gastroenterol. Hepatol.* **2019**, *16*, 617–630. [CrossRef] [PubMed]
3. Yang, J.D.; Hainaut, P.; Gores, G.J.; Amadou, A.; Plymoth, A.; Roberts, L.R. A global view of hepatocellular carcinoma: Trends, risk, prevention and management. *Nat. Rev. Gastroenterol. Hepatol.* **2019**, *16*, 589–604. [CrossRef] [PubMed]

4. Llovet, J.M.; Ricci, S.; Mazzaferro, V.; Hilgard, P.; Gane, E.; Blanc, J.-F.; de Oliveira, A.C.; Santoro, A.; Raoul, J.-L.; Forner, A.; et al. Sorafenib in Advanced Hepatocellular Carcinoma. *N. Engl. J. Med.* **2008**, *359*, 378–390. [CrossRef]

5. Bruix, J.; Qin, S.; Merle, P.; Granito, A.; Huang, Y.-H.; Bodoky, G.; Pracht, M.; Yokosuka, O.; Rosmorduc, O.; Breder, V.; et al. Regorafenib for patients with hepatocellular carcinoma who progressed on sorafenib treatment (RESORCE): A randomised, double-blind, placebo-controlled, phase 3 trial. *Lancet* **2017**, *389*, 56–66. [CrossRef]

6. Abou-Alfa, G.K.; Meyer, T.; Cheng, A.L.; El-Khoueiry, A.B.; Rimassa, L.; Ryoo, B.Y.; Cicin, I.; Merle, P.; Chen, Y.; Park, J.W.; et al. Cabozantinib in Patients with Advanced and Progressing Hepatocellular Carcinoma. *N. Engl. J. Med.* **2018**, *379*, 54–63. [CrossRef]

7. Bruix, J.; Chan, S.L.; Galle, P.R.; Rimassa, L.; Sangro, B. Systemic treatment of hepatocellular carcinoma: An EASL position paper. *J. Hepatol.* **2021**, in press. [CrossRef]

8. Nguyen, C.; Pandey, S. Exploiting Mitochondrial Vulnerabilities to Trigger Apoptosis Selectively in Cancer Cells. *Cancers* **2019**, *11*, 916. [CrossRef]

9. Chiou, J.F.; Tai, C.J.; Wang, Y.H.; Liu, T.Z.; Jen, Y.M.; Shiau, C.Y. Sorafenib induces preferential apoptotic killing of a drug- and radio-resistant Hep G2 cells through a mitochondria-dependent oxidative stress mechanism. *Cancer Biol. Ther.* **2009**, *8*, 1904–1913. [CrossRef]

10. Heslop, K.A.; Rovini, A.; Hunt, E.G.; Fang, D.; Morris, M.E.; Christie, C.F.; Gooz, M.B.; DeHart, D.N.; Dang, Y.; Lemasters, J.J.; et al. JNK activation and translocation to mitochondria mediates mitochondrial dysfunction and cell death induced by VDAC opening and sorafenib in hepatocarcinoma cells. *Biochem. Pharmacol.* **2020**, *171*, 113728. [CrossRef]

11. Stefanovic, M.; Tutusaus, A.; Martinez-Nieto, G.A.; Barcena, C.; de Gregorio, E.; Moutinho, C.; Barbero-Camps, E.; Villanueva, A.; Colell, A.; Mari, M.; et al. Targeting glucosylceramide synthase upregulation reverts sorafenib resistance in experimental hepatocellular carcinoma. *Oncotarget* **2016**, *7*, 8253–8267. [CrossRef] [PubMed]

12. Hikita, H.; Takehara, T.; Shimizu, S.; Kodama, T.; Shigekawa, M.; Iwase, K.; Hosui, A.; Miyagi, T.; Tatsumi, T.; Ishida, H.; et al. The Bcl-xL inhibitor, ABT-737, efficiently induces apoptosis and suppresses growth of hepatoma cells in combination with sorafenib. *Hepatology* **2010**, *52*, 1310–1321. [CrossRef] [PubMed]

13. Tutusaus, A.; Stefanovic, M.; Boix, L.; Cucarull, B.; Zamora, A.; Blasco, L.; de Frutos, P.G.; Reig, M.; Fernandez-Checa, J.C.; Marí, M.; et al. Antiapoptotic BCL-2 proteins determine sorafenib/regorafenib resistance and BH3-mimetic efficacy in hepatocellular carcinoma. *Oncotarget* **2018**, *9*, 16701–16717. [CrossRef] [PubMed]

14. Song, X.; Shen, L.; Tong, J.; Kuang, C.; Zeng, S.; Schoen, R.E.; Yu, J.; Pei, H.; Zhang, L. Mcl-1 inhibition overcomes intrinsic and acquired regorafenib resistance in colorectal cancer. *Theranostics* **2020**, *10*, 8098–8110. [CrossRef] [PubMed]

15. Cucarull, B.; Tutusaus, A.; Subías, M.; Stefanovic, M.; Hernáez-Alsina, T.; Boix, L.; Reig, M.; García de Frutos, P.; Marí, M.; Colell, A.; et al. Regorafenib Alteration of the BCL-xL/MCL-1 Ratio Provides a Therapeutic Opportunity for BH3-Mimetics in Hepatocellular Carcinoma Models. *Cancers* **2020**, *12*, 332. [CrossRef] [PubMed]

16. Dong, Y.; Liu, T.H.; Yau, T.; Hsu, C. Novel systemic therapy for hepatocellular carcinoma. *Hepatol. Int.* **2020**, *14*, 638–651. [CrossRef] [PubMed]

17. Bailey, R.L.; Gahche, J.J.; Miller, P.E.; Thomas, P.R.; Dwyer, J.T. Why US adults use dietary supplements. *JAMA Intern. Med.* **2013**, *173*, 355–361. [CrossRef]

18. Dickinson, A.; MacKay, D. Health habits and other characteristics of dietary supplement users: A review. *Nutr. J.* **2014**, *13*. [CrossRef]

19. Rautiainen, S.; Manson, J.E.; Lichtenstein, A.H.; Sesso, H.D. Dietary supplements and disease prevention–a global overview. *Nat. Rev. Endocrinol.* **2016**, *12*, 407–420. [CrossRef]

20. Michaud, L.B.; Karpinski, J.P.; Jones, K.L.; Espirito, J. Dietary supplements in patients with cancer: Risks and key concepts, part 1. *Am. J. Health Syst. Pharm.* **2007**, *64*, 369–381. [CrossRef]

21. Marí, M.; de Gregorio, E.; de Dios, C.; Roca-Agujetas, V.; Cucarull, B.; Tutusaus, A.; Morales, A.; Colell, A. Mitochondrial Glutathione: Recent Insights and Role in Disease. *Antioxidants* **2020**, *9*, 909. [CrossRef]

22. Marí, M.; Colell, A.; Morales, A.; von Montfort, C.; Garcia-Ruiz, C.; Fernández-Checa, J.C. Redox control of liver function in health and disease. *Antioxid. Redox Signal.* **2010**, *12*, 1295–1331. [CrossRef] [PubMed]

23. Tesori, V.; Piscaglia, A.C.; Samengo, D.; Barba, M.; Bernardini, C.; Scatena, R.; Pontoglio, A.; Castellini, L.; Spelbrink, J.N.; Maulucci, G.; et al. The multikinase inhibitor Sorafenib enhances glycolysis and synergizes with glycolysis blockade for cancer cell killing. *Sci. Rep.* **2015**, *5*, 9149. [CrossRef] [PubMed]

24. Salvemini, D.; Wang, Z.Q.; Zweier, J.L.; Samouilov, A.; Macarthur, H.; Misko, T.P.; Currie, M.G.; Cuzzocrea, S.; Sikorski, J.A.; Riley, D.P. A nonpeptidyl mimic of superoxide dismutase with therapeutic activity in rats. *Science* **1999**, *286*, 304–306. [CrossRef] [PubMed]

25. Prieto-Domínguez, N.; Ordóñez, R.; Fernández, A.; Méndez-Blanco, C.; Baulies, A.; Garcia-Ruiz, C.; Fernández-Checa, J.C.; Mauriz, J.L.; González-Gallego, J. Melatonin-induced increase in sensitivity of human hepatocellular carcinoma cells to sorafenib is associated with reactive oxygen species production and mitophagy. *J. Pineal Res.* **2016**, *61*, 396–407. [CrossRef]

26. Zhang, C.; Liu, Z.; Bunker, E.; Ramirez, A.; Lee, S.; Peng, Y.; Tan, A.C.; Eckhardt, S.G.; Chapnick, D.A.; Liu, X. Sorafenib targets the mitochondrial electron transport chain complexes and ATP synthase to activate the PINK1-Parkin pathway and modulate cellular drug response. *J. Biol. Chem.* **2017**, *292*, 15105–15120. [CrossRef] [PubMed]

27. De Gaetano, A.; Gibellini, L.; Zanini, G.; Nasi, M.; Cossarizza, A.; Pinti, M. Mitophagy and Oxidative Stress: The Role of Aging. *Antioxidants* **2021**, *10*, 794. [CrossRef]

28. Roca-Agujetas, V.; de Dios, C.; Lestón, L.; Marí, M.; Morales, A.; Colell, A. Recent Insights into the Mitochondrial Role in Autophagy and Its Regulation by Oxidative Stress. *Oxid. Med. Cell Longev.* **2019**, *2019*, 3809308. [CrossRef]

29. Morales, A.; García-Ruiz, C.; Miranda, M.; Marí, M.; Colell, A.; Ardite, E.; Fernández-Checa, J.C. Tumor necrosis factor increases hepatocellular glutathione by transcriptional regulation of the heavy subunit chain of gamma-glutamylcysteine synthetase. *J. Biol. Chem.* **1997**, *272*, 30371–30379. [CrossRef]

30. Llacuna, L.; Marí, M.; Lluis, J.M.; García-Ruiz, C.; Fernández-Checa, J.C.; Morales, A. Reactive oxygen species mediate liver injury through parenchymal nuclear factor-kappaB inactivation in prolonged ischemia/reperfusion. *Am. J. Pathol.* **2009**, *174*, 1776–1785. [CrossRef] [PubMed]

31. González, R.; Rodríguez-Hernández, M.A.; Negrete, M.; Ranguelova, K.; Rossin, A.; Choya-Foces, C.; Cruz-Ojeda, P.; Miranda-Vizuete, A.; Martínez-Ruiz, A.; Rius-Pérez, S.; et al. Downregulation of thioredoxin-1-dependent CD95 S-nitrosation by Sorafenib reduces liver cancer. *Redox Biol.* **2020**, *34*, 101528. [CrossRef] [PubMed]

32. Leverson, J.D.; Phillips, D.C.; Mitten, M.J.; Boghaert, E.R.; Diaz, D.; Tahir, S.K.; Belmont, L.D.; Nimmer, P.; Xiao, Y.; Ma, X.M.; et al. Exploiting selective BCL-2 family inhibitors to dissect cell survival dependencies and define improved strategies for cancer therapy. *Sci. Transl. Med.* **2015**, *7*, 279ra40–ra40. [CrossRef] [PubMed]

33. Merino, D.; Kelly, G.L.; Lessene, G.; Wei, A.H.; Roberts, A.W.; Strasser, A. BH3-Mimetic Drugs: Blazing the Trail for New Cancer Medicines. *Cancer Cell* **2018**, *34*, 879–891. [CrossRef]

34. Gegg, M.E.; Cooper, J.M.; Chau, K.Y.; Rojo, M.; Schapira, A.H.; Taanman, J.W. Mitofusin 1 and mitofusin 2 are ubiquitinated in a PINK1/parkin-dependent manner upon induction of mitophagy. *Hum. Mol Genet.* **2010**, *19*, 4861–4870. [CrossRef] [PubMed]

35. Leboucher, G.P.; Tsai, Y.C.; Yang, M.; Shaw, K.C.; Zhou, M.; Veenstra, T.D.; Glickman, M.H.; Weissman, A.M. Stress-induced phosphorylation and proteasomal degradation of mitofusin 2 facilitates mitochondrial fragmentation and apoptosis. *Mol. Cell.* **2012**, *47*, 547–557. [CrossRef]

36. Roca-Agujetas, V.; Barbero-Camps, E.; de Dios, C.; Podlesniy, P.; Abadin, X.; Morales, A.; Marí, M.; Trullàs, R.; Colell, A. Cholesterol alters mitophagy by impairing optineurin recruitment and lysosomal clearance in Alzheimer's disease. *Mol. Neurodegener.* **2021**, *16*, 15. [CrossRef] [PubMed]

37. Sulkshane, P.; Ram, J.; Thakur, A.; Reis, N.; Kleifeld, O.; Glickman, M.H. Ubiquitination and receptor-mediated mitophagy converge to eliminate oxidation-damaged mitochondria during hypoxia. *Redox Biol.* **2021**, *45*, 102047. [CrossRef]

38. Lemmo, W. Potential interactions of prescription and over-the-counter medications having antioxidant capabilities with radiation and chemotherapy. *Int. J. Cancer* **2015**, *137*, 2525–2533. [CrossRef]

39. Ambrosone, C.B.; Zirpoli, G.R.; Hutson, A.D.; McCann, W.E.; McCann, S.E.; Barlow, W.E.; Kelly, K.M.; Cannioto, R.; Sucheston-Campbell, L.E.; Hershman, D.L.; et al. Dietary Supplement Use During Chemotherapy and Survival Outcomes of Patients with Breast Cancer Enrolled in a Cooperative Group Clinical Trial (SWOG S0221). *J. Clin. Oncol.* **2020**, *38*, 804–814. [CrossRef]

40. Forman, H.J.; Zhang, H. Targeting oxidative stress in disease: Promise and limitations of antioxidant therapy. *Nat. Rev. Drug Discov.* **2021**, 1–21. [CrossRef]

41. Hayes, J.D.; Dinkova-Kostova, A.T.; Tew, K.D. Oxidative Stress in Cancer. *Cancer Cell* **2020**, *38*, 167–197. [CrossRef]

42. Navarro, P.; Bueno, M.J.; Zagorac, I.; Mondejar, T.; Sanchez, J.; Mourón, S.; Muñoz, J.; Gómez-López, G.; Jimenez-Renard, V.; Mulero, F.; et al. Targeting Tumor Mitochondrial Metabolism Overcomes Resistance to Antiangiogenics. *Cell Rep.* **2016**, *15*, 2705–2718. [CrossRef]

43. López-Grueso, M.J.; González, R.; Muntané, J.; Bárcena, J.A.; Padilla, C.A. Thioredoxin Downregulation Enhances Sorafenib Effects in Hepatocarcinoma Cells. *Antioxidants* **2019**, *8*, 501. [CrossRef] [PubMed]

44. Prieto-Domínguez, N.; Méndez-Blanco, C.; Carbajo-Pescador, S.; Fondevila, F.; García-Palomo, A.; González-Gallego, J.; Mauriz, J.L. Melatonin enhances sorafenib actions in human hepatocarcinoma cells by inhibiting mTORC1/p70S6K/HIF-1α and hypoxia-mediated mitophagy. *Oncotarget* **2017**, *8*, 91402–91414. [CrossRef] [PubMed]

45. Williamson, J.; Hughes, C.M.; Cobley, J.N.; Davison, G.W. The mitochondria-targeted antioxidant MitoQ, attenuates exercise-induced mitochondrial DNA damage. *Redox Biol.* **2020**, *36*, 101673. [CrossRef]

46. Ribeiro Junior, R.F.; Dabkowski, E.R.; Shekar, K.C.; OConnell, K.A.; Hecker, P.A.; Murphy, M.P. MitoQ improves mitochondrial dysfunction in heart failure induced by pressure overload. *Free Radic. Biol. Med.* **2018**, *117*, 18–29. [CrossRef] [PubMed]

47. Cochemé, H.M.; Kelso, G.F.; James, A.M.; Ross, M.F.; Trnka, J.; Mahendiran, T.; Asin-Cayuela, J.; Blaikie, F.H.; Manas, A.R.; Porteous, C.M.; et al. Mitochondrial targeting of quinones: Therapeutic implications. *Mitochondrion* **2007**, *7*, S94–S102. [CrossRef] [PubMed]

48. Dany, M.; Gencer, S.; Nganga, R.; Thomas, R.J.; Oleinik, N.; Baron, K.D.; Szulc, Z.M.; Ruvolo, P.; Kornblau, S.; Andreeff, M.; et al. Targeting FLT3-ITD signaling mediates ceramide-dependent mitophagy and attenuates drug resistance in AML. *Blood* **2016**, *128*, 1944–1958. [CrossRef]

49. Ježek, J.; Cooper, K.F.; Strich, R. The Impact of Mitochondrial Fission-Stimulated ROS Production on Pro-Apoptotic Chemotherapy. *Biology* **2021**, *10*, 33. [CrossRef]

Discussion

Multiple therapeutic options have recently emerged as oral systemic treatments for the management of HCC[391]. Still, therapies involving monoclonal antibodies have shown promising results, although only a reduced percentage of patients could benefit from this therapeutic strategy. Multikinase inhibitors such as sorafenib, regorafenib and cabozantinib have demonstrated effectivity against HCC. However, a percentage of patients do not tolerate or develop resistance toward those inhibitors.

The dual combination of the multikinase inhibitor sorafenib together with the BCL-2/BCL-xL antagonist ABT-263 has demonstrated its capacity to potentiate cell death *in vitro* as well as produce tumor shrinkage *in vivo*. Our initial results indicated that regorafenib induced distinct changes in the expression BCL-2 family members at transcriptional level compared to sorafenib. This first evidence prompted us to examine the combinatory effect of regorafenib and BH3-mimetics in HCC preclinical models. Regorafenib and the BCL-xL inhibitor A-1331852 had a powerful cytotoxic effect against HCC cells, whereas ABT-199, the BCL-2 inhibitor, failed to enhance regorafenib action, suggesting that the targeting of BCL-xL expression was crucial to provoke cell death on regorafenib-treated hepatocarcinoma cells. We were able to confirm these results through an HSA synergy model.

Our findings showed that regorafenib and A-1331852 were capable of triggering mitochondrial membrane potential loss, caspase-3 activation and, overall, triggering cell death through the apoptotic mitochondrial pathway. We also identified the BCL-2 protein MCL-1 as one of the main targets of regorafenib. The compound A-1210477, that blocks specifically MCL-1, together with the co-treatment with A-1331852 was useful to confirm the role of MCL-1 and BCL-xL as key proteins for the survival of HCC cells.

Additionally, tumor liver spheroids were also sensitive to regorafenib and A-1331852 action. In a PDX mouse model, the co-administration of regorafenib and A-1331852 was effective in reducing tumor volume. Either in regorafenib-resistant cells or regorafenib-resistant murine tumors, the addition of A-1331852 increased their sensitivity to regorafenib. From clinical data, we could observe that HCC tumor samples displayed a BCL-xL upregulation together with an MCL-1 reduction in mRNA levels.

In line with our initial hypothesis, our results have shown that regorafenib anti-tumor effect can be improved with the use of a BH3 mimetic against BCL-xL protein in the treatment of preclinical HCC, offering a new therapeutic opportunity.

BH3 mimetics have emerged as novel compounds capable of causing cell death. Although ABT-199 has demonstrated effectivity against hematological neoplasms, we did not observe any additional effect when co-administered with regorafenib. Yet, the BCL-xL inhibition by A-1331852 was effective in killing HCC tumor cells. These results may highlight the dependency of certain tumor types on specific members of the BCL-2 family of proteins for their survival, as BCL-xL inhibition was capable of eliminating HCC cells and tumors but not the targeting of the BCL-2 protein.

The BCL-xL inhibitor A-1331852 has also displayed a synergistic effect in killing tumor cells combined with standard chemotherapy[265,392]. ABT-263, which targets BCL-2, BCL-xL and BCL-W has demonstrated to exert a strong anti-tumor effect alone and together with other chemotherapeutic agents[241,265]. Nonetheless, common side effects of ABT-263 administration are neutropenia and thrombocytopenia. Since A-1331852 has exhibited higher efficacy at a lower concentration level, the neutropenia derived from BCL-2 inhibition is avoided with its use. On the other hand, platelets rely on BCL-xL protein for their survival. Thus, BCL-xL antagonism effect on platelets could be managed by dose-escalation. Furthermore, the recently developed strategy of a BCL-xL proteolysis-targeting chimera, PROTACS, which marks BCL-xL to the Von Hippel-Lindau (VHL) E3 ligase for its degradation may be a suitable approach to spare platelets and thus, avoid thrombocytopenia[393].

Nutritional supplements have become increasingly popular as a manner to ensure that body cells are provided with all the nutrients they require. Antioxidants, either constitutive or obtained from daily intake, play an important role in maintaining cellular redox balance. For that reason, antioxidant supplementation may be seen as beneficial in aiding cells to keep their redox status. In addition, ROS have an important function in cell signaling. The excessive production of ROS may lead to oxidative stress, which can result in several pathologies, including neurodegenerative diseases, cardiovascular diseases and cancer[394]. Cancer cells often display an altered redox status. Whereas ROS may be tumor-promoting, high ROS production may activate the intrinsic or mitochondrial pathway of cell death[395]. Nevertheless, many tumor cells have adapted to high ROS levels by upregulating their antioxidant status. In this context, chemotherapy that induces an increase in ROS production appears as an attractive therapeutic option. Even so, antioxidants uptake that counteract excessive ROS generation may pose a threat to chemotherapy effectiveness.

To address this question, we treated hepatoma cells with BSO to diminish the levels of intracellular GSH. Then, we administered the multikinase inhibitors sorafenib, regorafenib or cabozantinib. Sorafenib and regorafenib effect was clearly potentiated by GSH depletion in all three cell lines of HCC. Although only in HepG2 cells the effects of cabozantinib were enhanced by the addition of BSO, this result indicates that cabozantinib is able to induce mitochondrial ROS that may participate in the elimination of specific liver tumors. In line with previous works[292,293,301,302], we determined that sorafenib and regorafenib exerted their cytotoxic effect through a mitochondrial ROS-dependent mechanism in most liver cancer cells, which was potentiated by GSH depletion. Conversely, the ability of cabozantinib to exercise its anti-tumor action via ROS production was not so evident. We were also able to observe that regorafenib together with the BH3 mimetic A-1331852 also produced a cytotoxic response with the implication of mitochondrial ROS signaling. In line with our results, BSO has demonstrated efficacy in combination therapy regimen in HCC and other solid tumors, such as glioblastoma[310,311,396,397].

The addition of MnTBAP, a MnSOD mimetic, and GSHe as antioxidant compounds has been used in several studies[398–402]. We noticed that the supplementation with GSHe or MnTBAP resulted in a reduced sensitivity to the combined therapy with sorafenib and ABT-263 or regorafenib plus A-1331852. We also detected that GSHe and MnTBAP restrained sorafenib effect as a single agent. Similarly, GSH depletion further stimulated ROS production in sorafenib-treated 3D tumor liver spheroids recapitulating the effects observed *in vitro*. The antioxidants GSHe and MnTBAP increased tumor growth as well as decreased ROS levels in sorafenib-treated spheroids, demonstrating that this ROS-dependent mechanism was involved in the development of tumor liver spheroids. On the contrary, we tested other antioxidant compounds like Trolox or MitoQ, which failed to attenuate MKI activity upon hepatoma cells and spheroids, although MitoQ has demonstrated effectivity in protecting against mitochondrial ROS[403,404]. Since we have assessed that MKI produce a mitochondrial membrane potential (MMP) destabilization, that effect could possibly interfere with the use of mitochondrial protectors that are MMP dependent, such as MitoQ.

Our data showed that sorafenib and regorafenib induced mitophagy through PINK1/Parkin pathway in HCC cells, and that mitophagy flux was potentiated with the depletion of GSH, revealing the implication of mitochondrial ROS production in that process. Other works have assessed the mitophagy-inducing capacity of sorafenib in

combination with other compounds, like melatonin[382,383]. Agents that have an impact on mitochondrial dynamics and mitochondrial ROS production have been considered as useful tools in anti-cancer therapy[405]. Hence, these agents   effectivity of the targeting of autophagy or mitophagy proteins may interfere with the anti-tumoral efficacy of MKI in liver cancer. On the other hand, it is tempting to speculate that the anti-cancer potential of specific mitophagy modulators may be altered by the intake of antioxidants or changes in the cellular redox status.

Conclusions

1. The ratio MCL-1/BCL-xL is increased in hepatocellular carcinoma (HCC) patients and modifies the therapeutic response to regorafenib..

2. The BH3 mimetic A-1331852 potentiates regorafenib cytotoxic effect in HCC cells.

3. The combination of regorafenib and A-1331852 triggers mitochondrial cell death through a loss of mitochondrial membrane potential, cytochrome c release and caspase-3 activation.

4. Regorafenib and A-1331852 reduce tumor growth and proliferation in a PDX mouse model.

5. The addition of A-1331852 together with regorafenib is also effective in regorafenib-resistant cells and murine models of HCC.

6. Regorafenib-induced changes in the BCL-2 network allow BCL-xL inhibition to enhance regorafenib efficacy in HCC treatment, particularly for tumors with an elevated BCL-xL/MCL-1 ratio

7. The multikinase inhibitors sorafenib and regorafenib exert their anti-tumor effect via a ROS-dependent mechanism in hepatoma cells.

8. The cytotoxicity caused by the dual treatment of regorafenib and A-1331852 is mediated by mitochondrial ROS production in hepatoma cells.

9. GSH depletion cooperates with MKI in inducing cell death in HCC cells and tumor liver spheroids.

10. The use of the antioxidants MnTBAP or GSHe reduces MKI efficacy against HCC cells and increases proliferation of tumor liver spheroids.

11. GSH depletion enhances MKI-induced mitochondrial-ROS dependent mitophagy in HCC cells

12. Antioxidants supplementation may affect the anti-tumor activity of specific MKIs, threatening the efficacy of sorafenib and regorafenib in HCC therapy.

Bibliography

1.   GLOBOCAN 2018. International Agency for Research on Cancer 2020. Cancer Today. http://gco.iarc.fr/.

2.   Galle, P. R. *et al.* EASL Clinical Practice Guidelines: Management of hepatocellular carcinoma. *J. Hepatol.* **69**, 182–236 (2018).

3.   Llovet, J. M. *et al.* Hepatocellular carcinoma. *Nat. Rev. Dis. Prim.* **2**, (2016).

4.   Younossi, Z. M. & Henry, L. Epidemiology of non-alcoholic fatty liver disease and hepatocellular carcinoma. *JHEP Reports* **3**, (2021).

5.   S, M. *et al.* NAFLD and MAFLD as emerging causes of HCC: A populational study. *JHEP reports Innov. Hepatol.* **3**, (2021).

6.   Chang, M.-H. *et al.* Decreased incidence of hepatocellular carcinoma in hepatitis B vaccinees: a 20-year follow-up study. *J. Natl. Cancer Inst.* **101**, 1348–1355 (2009).

7.   Waziry, R. *et al.* Hepatocellular carcinoma risk following direct-acting antiviral HCV therapy: A systematic review, meta-analyses, and meta-regression. *J. Hepatol.* **67**, 1204–1212 (2017).

8.   Singh, S., Singh, P. P., Singh, A. G., Murad, M. H. & Sanchez, W. Statins are associated with a reduced risk of hepatocellular cancer: a systematic review and meta-analysis. *Gastroenterology* **144**, 323–332 (2013).

9.   Bravi, F. *et al.* Coffee drinking and hepatocellular carcinoma risk: a meta-analysis. *Hepatology* **46**, 430–435 (2007).

10.   Marquardt, J. U., Andersen, J. B. & Thorgeirsson, S. S. Functional and genetic deconstruction of the cellular origin in liver cancer. *Nat. Rev. Cancer* **15**, 653–667 (2015).

11.   Sia, D., Villanueva, A., Friedman, S. L. & Llovet, J. M. Liver Cancer Cell of Origin, Molecular Class, and Effects on Patient Prognosis. *Gastroenterology* **152**, 745–761 (2017).

12.   Pikarsky, E. Neighbourhood deaths cause a switch in cancer subtype. *Nature* vol. 562 45–46 (2018).

13.   Llovet, J. M. *et al.* Hepatocellular carcinoma. *Nat. Rev. Dis. Prim.* **7**, 6 (2021).

14.   Zucman-Rossi, J., Villanueva, A., Nault, J.-C. & Llovet, J. M. Genetic Landscape and Biomarkers of Hepatocellular Carcinoma. *Gastroenterology* **149**, 1226-1239.e4 (2015).

15.   Villanueva, A. Hepatocellular carcinoma. *N. Engl. J. Med.* **380**, 1450–1462 (2019).

16.   Nault, J.-C. *et al.* Molecular Classification of Hepatocellular Adenoma Associates With Risk Factors, Bleeding, and Malignant Transformation. *Gastroenterology* **152**, 880-894.e6 (2017).

17.   Llovet, J. M., Montal, R., Sia, D. & Finn, R. S. Molecular therapies and precision medicine for hepatocellular carcinoma. *Nat. Rev. Clin. Oncol.* **15**, 599–616 (2018).

18. Nault, J. C. *et al.* Telomerase reverse transcriptase promoter mutation is an early somatic genetic alteration in the transformation of premalignant nodules in hepatocellular carcinoma on cirrhosis. *Hepatology* **60**, 1983–1992 (2014).

19. Schulze, K., Nault, J.-C. & Villanueva, A. Genetic profiling of hepatocellular carcinoma using next-generation sequencing. *J. Hepatol.* **65**, 1031–1042 (2016).

20. de La Coste, A. *et al.* Somatic mutations of the beta-catenin gene are frequent in mouse and human hepatocellular carcinomas. *Proc. Natl. Acad. Sci. U. S. A.* **95**, 8847–8851 (1998).

21. Audard, V. *et al.* Cholestasis is a marker for hepatocellular carcinomas displaying beta-catenin mutations. *J. Pathol.* **212**, 345–352 (2007).

22. Hsu, I. C. *et al.* Mutational hotspot in the p53 gene in human hepatocellular carcinomas. *Nature* **350**, 427–428 (1991).

23. Bressac, B., Kew, M., Wands, J. & Ozturk, M. Selective G to T mutations of p53 gene in hepatocellular carcinoma from southern Africa. *Nature* **350**, 429–431 (1991).

24. Totoki, Y. *et al.* Trans-ancestry mutational landscape of hepatocellular carcinoma genomes. *Nat. Genet.* **46**, 1267–1273 (2014).

25. Guichard, C. *et al.* Integrated analysis of somatic mutations and focal copy-number changes identifies key genes and pathways in hepatocellular carcinoma. *Nat. Genet.* **44**, 694–698 (2012).

26. Schulze, K. *et al.* Exome sequencing of hepatocellular carcinomas identifies new mutational signatures and potential therapeutic targets. *Nat. Genet.* **47**, 505–511 (2015).

27. Sporn, M. B. & Liby, K. T. NRF2 and cancer: the good, the bad and the importance of context. *Nature reviews. Cancer* vol. 12 564–571 (2012).

28. Sawey, E. T. *et al.* Identification of a therapeutic strategy targeting amplified FGF19 in liver cancer by Oncogenomic screening. *Cancer Cell* **19**, 347–358 (2011).

29. Horwitz, E. *et al.* Human and mouse VEGFA-amplified hepatocellular carcinomas are highly sensitive to sorafenib treatment. *Cancer Discov.* **4**, 730–743 (2014).

30. Zehir, A. *et al.* Mutational landscape of metastatic cancer revealed from prospective clinical sequencing of 10,000 patients. *Nat. Med.* **23**, 703–713 (2017).

31. Hoshida, Y. *et al.* Integrative transcriptome analysis reveals common molecular subclasses of human hepatocellular carcinoma. *Cancer Res.* **69**, 7385–7392 (2009).

32. Tovar, V. *et al.* Tumour initiating cells and IGF/FGF signalling contribute to sorafenib resistance in hepatocellular carcinoma. *Gut* **66**, 530–540 (2017).

33. Toffanin, S. *et al.* MicroRNA-based classification of hepatocellular carcinoma and oncogenic role of miR-517a. *Gastroenterology* **140**, 1618–28.e16 (2011).

34. Lachenmayer, A. *et al.* Wnt-pathway activation in two molecular classes of hepatocellular carcinoma and experimental modulation by sorafenib. *Clin. cancer Res. an Off. J. Am. Assoc. Cancer Res.* **18**, 4997–5007 (2012).

35.   Hanahan, D. & Weinberg, R. A. Hallmarks of cancer: the next generation. *Cell* **144**, 646–674 (2011).

36.   Sia, D. *et al.* Identification of an Immune-specific Class of Hepatocellular Carcinoma, Based on Molecular Features. *Gastroenterology* **153**, 812–826 (2017).

37.   Singal, A. G., Pillai, A. & Tiro, J. Early detection, curative treatment, and survival rates for hepatocellular carcinoma surveillance in patients with cirrhosis: a meta-analysis. *PLoS Med.* **11**, e1001624 (2014).

38.   Yang, J. D. *et al.* Impact of surveillance for hepatocellular carcinoma on survival in patients with compensated cirrhosis. *Hepatology* **68**, 78–88 (2018).

39.   Sarasin, F. P., Giostra, E. & Hadengue, A. Cost-effectiveness of screening for detection of small hepatocellular carcinoma in western patients with Child-Pugh class A cirrhosis. *Am. J. Med.* **101**, 422–434 (1996).

40.   Yang, H.-I. *et al.* Risk estimation for hepatocellular carcinoma in chronic hepatitis B (REACH-B): development and validation of a predictive score. *Lancet. Oncol.* **12**, 568–574 (2011).

41.   Singal, A. *et al.* Meta-analysis: surveillance with ultrasound for early-stage hepatocellular carcinoma in patients with cirrhosis. *Aliment. Pharmacol. Ther.* **30**, 37–47 (2009).

42.   Trevisani, F. *et al.* Serum alpha-fetoprotein for diagnosis of hepatocellular carcinoma in patients with chronic liver disease: influence of HBsAg and anti-HCV status. *J. Hepatol.* **34**, 570–575 (2001).

43.   Labgaa, I. *et al.* A pilot study of ultra-deep targeted sequencing of plasma DNA identifies driver mutations in hepatocellular carcinoma. *Oncogene* **37**, 3740–3752 (2018).

44.   Forner, A., Reig, M. & Bruix, J. Hepatocellular carcinoma. *Lancet* **391**, 1301–1314 (2018).

45.   Matsui, O. *et al.* Hepatocelluar nodules in liver cirrhosis: hemodynamic evaluation (angiography-assisted CT) with special reference to multi-step hepatocarcinogenesis. *Abdom. Imaging* **36**, 264–272 (2011).

46.   Tremosini, S. *et al.* Prospective validation of an immunohistochemical panel (glypican 3, heat shock protein 70 and glutamine synthetase) in liver biopsies for diagnosis of very early hepatocellular carcinoma. *Gut* **61**, 1481–1487 (2012).

47.   Bruix, J., Reig, M. & Sherman, M. Evidence-Based Diagnosis, Staging, and Treatment of Patients With Hepatocellular Carcinoma. *Gastroenterology* **150**, 835–853 (2016).

48.   Yau, T. *et al.* Development of Hong Kong Liver Cancer staging system with treatment stratification for patients with hepatocellular carcinoma. *Gastroenterology* **146**, 1691–700.e3 (2014).

49.   Llovet, J. M., Brú, C. & Bruix, J. Prognosis of hepatocellular carcinoma: the BCLC staging classification. *Semin. Liver Dis.* **19**, 329–338 (1999).

50.   Ikai, I. *et al.* Reevaluation of prognostic factors for survival after liver resection in patients with hepatocellular carcinoma in a Japanese nationwide survey. *Cancer* **101**, 796–802

(2004).

51.   N'Kontchou, G. *et al.* Radiofrequency ablation of hepatocellular carcinoma: long-term results and   prognostic factors in 235 Western patients with cirrhosis. *Hepatology* **50**, 1475–1483 (2009).

52.   Llovet, J. M. *et al.* Plasma biomarkers as predictors of outcome in patients with advanced hepatocellular carcinoma. *Clin. cancer Res. an Off. J. Am. Assoc. Cancer Res.* **18**, 2290–2300 (2012).

53.   Novikova, M. V., Khromova, N. V. & Kopnin, P. B. Components of the hepatocellular carcinoma microenvironment and their role in tumor progression. *Biochem.* **82**, 861–873 (2017).

54.   Qin, W., Cao, Z.-Y., Liu, S.-Y. & Xu, X.-D. Recent advances regarding tumor microenvironment and immunotherapy in hepatocellular carcinoma. *Hepatoma Res.* **6**, 24 (2020).

55.   T, T. & SL, F. Mechanisms of hepatic stellate cell activation. *Nat. Rev. Gastroenterol. Hepatol.* **14**, 397–411 (2017).

56.   Schwabe, R. F., Bataller, R. & Brenner, D. A. Human hepatic stellate cells express CCR5 and RANTES to induce proliferation and migration. *Am. J. Physiol. Gastrointest. Liver Physiol.* **285**, G949-58 (2003).

57.   Wynn, T. A. Cellular and molecular mechanisms of fibrosis. *J. Pathol.* **214**, 199–210 (2008).

58.   Forbes, S. J. & Parola, M. Liver fibrogenic cells. *Best Pract. Res. Clin. Gastroenterol.* **25**, 207–217 (2011).

59.   Faouzi, S. *et al.* Activation of cultured rat hepatic stellate cells by tumoral hepatocytes. *Lab. Invest.* **79**, 485–493 (1999).

60.   Lv, X. *et al.* Agrin para-secreted by PDGF-activated human hepatic stellate cells promotes hepatocarcinogenesis in vitro and in vivo. *Oncotarget* **8**, 105340–105355 (2017).

61.   Amann, T. *et al.* Activated hepatic stellate cells promote tumorigenicity of hepatocellular carcinoma. *Cancer Sci.* **100**, 646–653 (2009).

62.   Sancho-Bru, P. *et al.* Hepatocarcinoma cells stimulate the growth, migration and expression of pro-angiogenic genes in human hepatic stellate cells. *Liver Int. Off. J. Int. Assoc. Study Liver* **30**, 31–41 (2010).

63.   Coulouarn, C. *et al.* Hepatocyte-stellate cell cross-talk in the liver engenders a permissive inflammatory   microenvironment that drives progression in hepatocellular carcinoma. *Cancer Res.* **72**, 2533–2542 (2012).

64.   Carloni, V., Luong, T. V. & Rombouts, K. Hepatic stellate cells and extracellular matrix in hepatocellular carcinoma: more complicated than ever. *Liver Int. Off. J. Int. Assoc. Study Liver* **34**, 834–843 (2014).

65.   Bárcena, C. *et al.* Angiogenin secretion from hepatoma cells activates hepatic stellate cells

to amplify a self-sustained cycle promoting liver cancer. *Sci. Rep.* **5**, (2015).

66. Lin, N. *et al.* Activated hepatic stellate cells promote angiogenesis in hepatocellular carcinoma by secreting angiopoietin-1. *J. Cell. Biochem.* **121**, 1441–1451 (2020).

67. Zhu, B. *et al.* Activated hepatic stellate cells promote angiogenesis via interleukin-8 in hepatocellular carcinoma. *J. Transl. Med.* **13**, 365 (2015).

68. Bergers, G. & Song, S. The role of pericytes in blood-vessel formation and maintenance. *Neuro. Oncol.* **7**, 452–464 (2005).

69. Iwahasi, S. *et al.* Hepatic Stellate Cells Contribute to the Tumor Malignancy of Hepatocellular Carcinoma Through the IL-6 Pathway. *Anticancer Res.* **40**, 743–749 (2020).

70. Wen, Q. *et al.* 8-bromo-7-methoxychrysin suppress stemness of SMMC-7721 cells induced by co-culture of liver cancer stem-like cells with hepatic stellate cells. *BMC Cancer* **19**, 224 (2019).

71. Chiyonobu, N. *et al.* Fatty Acid Binding Protein 4 (FABP4) Overexpression in Intratumoral Hepatic Stellate Cells within Hepatocellular Carcinoma with Metabolic Risk Factors. *Am. J. Pathol.* **188**, 1213–1224 (2018).

72. Huang, J.-L. *et al.* Hepatic stellate cells promote the progression of hepatocellular carcinoma through microRNA-1246-RORα-Wnt/β-Catenin axis. *Cancer Lett.* **476**, 140–151 (2020).

73. Li, L.-Y. *et al.* ZEB1 regulates the activation of hepatic stellate cells through Wnt/β-catenin signaling pathway. *Eur. J. Pharmacol.* **865**, 172787 (2019).

74. Azzariti, A. *et al.* Hepatic stellate cells induce hepatocellular carcinoma cell resistance to sorafenib through the laminin-332/α3 integrin axis recovery of focal adhesion kinase ubiquitination. *Hepatology* **64**, 2103–2117 (2016).

75. Seitz, T. *et al.* Fibroblast Growth Factor 9 is expressed by activated hepatic stellate cells and promotes progression of hepatocellular carcinoma. *Sci. Rep.* **10**, 4546 (2020).

76. Mogler, C. *et al.* Hepatic stellate cells limit hepatocellular carcinoma progression through the orphan receptor endosialin. *EMBO Mol. Med.* **9**, 741–749 (2017).

77. Kalluri, R. & Zeisberg, M. Fibroblasts in cancer. *Nat. Rev. Cancer* **6**, 392–401 (2006).

78. Shimoda, M., Mellody, K. T. & Orimo, A. Carcinoma-associated fibroblasts are a rate-limiting determinant for tumour progression. *Semin. Cell Dev. Biol.* **21**, 19–25 (2010).

79. Park, S. Y. *et al.* Lysophosphatidic acid augments human hepatocellular carcinoma cell invasion through LPA1 receptor and MMP-9 expression. *Oncogene* **30**, 1351–1359 (2011).

80. Mazzocca, A. *et al.* Tumor-secreted lysophostatidic acid accelerates hepatocellular carcinoma progression by promoting differentiation of peritumoral fibroblasts in myofibroblasts. *Hepatology* **54**, 920–930 (2011).

81. Lau, E. Y. T. *et al.* Cancer-Associated Fibroblasts Regulate Tumor-Initiating Cell Plasticity

in Hepatocellular Carcinoma through c-Met/FRA1/HEY1 Signaling. *Cell Rep.* **15**, 1175–1189 (2016).

82. Pietras, K. & Ostman, A. Hallmarks of cancer: interactions with the tumor stroma. *Exp. Cell Res.* **316**, 1324–1331 (2010).

83. Jia, C.-C. *et al.* Cancer-associated fibroblasts from hepatocellular carcinoma promote malignant cell proliferation by HGF secretion. *PLoS One* **8**, e63243 (2013).

84. Liu, J. *et al.* Cancer-associated fibroblasts promote hepatocellular carcinoma metastasis through chemokine-activated hedgehog and TGF-β pathways. *Cancer Lett.* **379**, 49–59 (2016).

85. Zhang, Y., Pan, Q. & Shao, Z. Extracellular vesicle-encapsulated microRNA-1228-3p from cancer-associated fibroblasts promotes the chemoresistance of hepatocellular carcinoma cells via PLAC8. *Am. J. Physiol. Gastrointest. Liver Physiol.* (2020) doi:10.1152/ajpgi.00042.2020.

86. Yugawa, K. *et al.* Cancer-associated fibroblasts promote hepatocellular carcinoma progression through downregulation of exosomal miR-150-3p. *Eur. J. Surg. Oncol. J. Eur. Soc. Surg. Oncol. Br. Assoc. Surg. Oncol.* (2020) doi:10.1016/j.ejso.2020.08.002.

87. Wang, F., Li, L., Piontek, K., Sakaguchi, M. & Selaru, F. M. Exosome miR-335 as a novel therapeutic strategy in hepatocellular carcinoma. *Hepatology* **67**, 940–954 (2018).

88. Zhou, Y. *et al.* Hepatocellular carcinoma-derived exosomal miRNA-21 contributes to tumor progression by converting hepatocyte stellate cells to cancer-associated fibroblasts. *J. Exp. Clin. Cancer Res.* **37**, 324 (2018).

89. Liu, C. *et al.* LSD1 Stimulates Cancer-Associated Fibroblasts to Drive Notch3-Dependent Self-Renewal of Liver Cancer Stem-like Cells. *Cancer Res.* **78**, 938–949 (2018).

90. Xiong, S. *et al.* Cancer-associated fibroblasts promote stem cell-like properties of hepatocellular carcinoma cells through IL-6/STAT3/Notch signaling. *Am. J. Cancer Res.* **8**, 302–316 (2018).

91. Qian, B.-Z. & Pollard, J. W. Macrophage diversity enhances tumor progression and metastasis. *Cell* **141**, 39–51 (2010).

92. Gordon, S. & Taylor, P. R. Monocyte and macrophage heterogeneity. *Nat. Rev. Immunol.* **5**, 953–964 (2005).

93. Shirabe, K. *et al.* Role of tumor-associated macrophages in the progression of hepatocellular carcinoma. *Surg. Today* **42**, 1–7 (2012).

94. Takai, H. *et al.* Involvement of glypican-3 in the recruitment of M2-polarized tumor-associated macrophages in hepatocellular carcinoma. *Cancer Biol. Ther.* **8**, 2329–2338 (2009).

95. Fan, Q.-M. *et al.* Tumor-associated macrophages promote cancer stem cell-like properties via transforming growth factor-beta1-induced epithelial-mesenchymal transition in hepatocellular carcinoma. *Cancer Lett.* **352**, 160–168 (2014).

96. Gupta, D. K., Singh, N. & Sahu, D. K. TGF-β Mediated Crosstalk Between Malignant Hepatocyte and Tumor Microenvironment in Hepatocellular Carcinoma. *Cancer Growth Metastasis* **7**, 1–8 (2014).

97. Wan, S. *et al.* Tumor-associated macrophages produce interleukin 6 and signal via STAT3 to promote expansion of human hepatocellular carcinoma stem cells. *Gastroenterology* **147**, 1393–1404 (2014).

98. Roderfeld, M. *et al.* Innovative immunohistochemistry identifies MMP-9 expressing macrophages at the invasive front of murine HCC. *World J. Hepatol.* **2**, 175–179 (2010).

99. Fujita, N. *et al.* Role of tumor-associated macrophages in the angiogenesis of well-differentiated hepatocellular carcinoma: pathological-radiological correlation. *Oncol. Rep.* **31**, 2499–2505 (2014).

100. Wang, B. *et al.* Transition of tumor-associated macrophages from MHC class II(hi) to MHC class II(low) mediates tumor progression in mice. *BMC Immunol.* **12**, 43 (2011).

101. Wu, J. *et al.* M2 macrophage-derived exosomes facilitate hepatocarcinoma metastasis by transferring α(M) β(2) integrin to tumor cells. *Hepatology* (2020) doi:10.1002/hep.31432.

102. Yang, Y. *et al.* Crosstalk between hepatic tumor cells and macrophages via Wnt/β-catenin signaling   promotes M2-like macrophage polarization and reinforces tumor malignant behaviors. *Cell Death Dis.* **9**, 793 (2018).

103. Sprinzl, M. F. *et al.* Sorafenib perpetuates cellular anticancer effector functions by modulating the crosstalk between macrophages and natural killer cells. *Hepatology* **57**, 2358–2368 (2013).

104. Chen, J. *et al.* Upregulation of B7-H1 expression is associated with macrophage infiltration in hepatocellular carcinomas. *Cancer Immunol. Immunother.* **61**, 101–108 (2012).

105. Zong, Z. *et al.* M1 Macrophages Induce PD-L1 Expression in Hepatocellular Carcinoma Cells Through IL-1β Signaling. *Front. Immunol.* **10**, 1643 (2019).

106. Wu, K., Kryczek, I., Chen, L., Zou, W. & Welling, T. H. Kupffer cell suppression of CD8+ T cells in human hepatocellular carcinoma is mediated by B7-H1/programmed death-1 interactions. *Cancer Res.* **69**, 8067–8075 (2009).

107. Fujii, H. & Kawada, N. Fibrogenesis in alcoholic liver disease. *World J. Gastroenterol.* **20**, 8048–8054 (2014).

108. Dudley, A. C. Tumor endothelial cells. *Cold Spring Harb. Perspect. Med.* **2**, a006536 (2012).

109. Davis, G. E. & Senger, D. R. Endothelial extracellular matrix: biosynthesis, remodeling, and functions during vascular morphogenesis and neovessel stabilization. *Circ. Res.* **97**, 1093–1107 (2005).

110. Pralhad, T., Madhusudan, S. & Rajendrakumar, K. Concept, mechanisms and therapeutics of angiogenesis in cancer and other diseases. *J. Pharm. Pharmacol.* **55**, 1045–1053 (2003).

111. Baluk, P., Morikawa, S., Haskell, A., Mancuso, M. & McDonald, D. M. Abnormalities of basement membrane on blood vessels and endothelial sprouts in tumors. *Am. J. Pathol.* **163**, 1801–1815 (2003).

112. von Marschall, Z. *et al.* Dual mechanism of vascular endothelial growth factor upregulation by hypoxia in human hepatocellular carcinoma. *Gut* **48**, 87–96 (2001).

113. Kim, K.-R., Moon, H.-E. & Kim, K.-W. Hypoxia-induced angiogenesis in human hepatocellular carcinoma. *J. Mol. Med. (Berl).* **80**, 703–714 (2002).

114. Xiong, X. X., Qiu, X. Y., Hu, D. X. & Chen, X. Q. Advances in Hypoxia-Mediated Mechanisms in Hepatocellular Carcinoma. *Mol. Pharmacol.* **92**, 246–255 (2017).

115. Morse, M. A. *et al.* The role of angiogenesis in hepatocellular carcinoma. *Clin. Cancer Res.* **25**, 912–920 (2019).

116. Yamaguchi, R. *et al.* Expression of vascular endothelial growth factor in human hepatocellular carcinoma. *Hepatology* **28**, 68–77 (1998).

117. Amini, A., Masoumi Moghaddam, S., Morris, D. L. & Pourgholami, M. H. The critical role of vascular endothelial growth factor in tumor angiogenesis. *Curr. Cancer Drug Targets* **12**, 23–43 (2012).

118. Poon, R. T. P. *et al.* Prognostic significance of serum vascular endothelial growth factor and endostatin in patients with hepatocellular carcinoma. *Br. J. Surg.* **91**, 1354–1360 (2004).

119. Li, X. M., Tang, Z. Y., Qin, L. X., Zhou, J. & Sun, H. C. Serum vascular endothelial growth factor is a predictor of invasion and metastasis in hepatocellular carcinoma. *J. Exp. Clin. Cancer Res.* **18**, 511–517 (1999).

120. Heldin, C.-H. Targeting the PDGF signaling pathway in tumor treatment. *Cell Commun. Signal.* **11**, 97 (2013).

121. Zhu, K. *et al.* MiR-146a enhances angiogenic activity of endothelial cells in hepatocellular carcinoma by promoting PDGFRA expression. *Carcinogenesis* **34**, 2071–2079 (2013).

122. Cao, Y., Cao, R. & Hedlund, E.-M. R Regulation of tumor angiogenesis and metastasis by FGF and PDGF signaling pathways. *J. Mol. Med. (Berl).* **86**, 785–789 (2008).

123. Imura, S., Miyake, H., Izumi, K., Tashiro, S. & Uehara, H. Correlation of vascular endothelial cell proliferation with microvessel density and expression of vascular endothelial growth factor and basic fibroblast growth factor in hepatocellular carcinoma. *J. Med. Invest.* **51**, 202–209 (2004).

124. Bupathi, M., Kaseb, A. & Janku, F. Angiopoietin 2 as a therapeutic target in hepatocellular carcinoma treatment: current perspectives. *Onco. Targets. Ther.* **7**, 1927–1932 (2014).

125. Torimura, T. *et al.* Overexpression of angiopoietin-1 and angiopoietin-2 in hepatocellular carcinoma. *J. Hepatol.* **40**, 799–807 (2004).

126. He, Y.-F. *et al.* Tie2-Expressing Monocytes Are Associated with Identification and Prognoses of Hepatitis B Virus Related Hepatocellular Carcinoma after Resection. *PLoS*

One **10**, e0143657 (2015).

127. Scholz, A. *et al.* Angiopoietin-2 serum levels are elevated in patients with liver cirrhosis and hepatocellular carcinoma. *Am. J. Gastroenterol.* **102**, 2471–2481 (2007).

128. Kuboki, S. *et al.* Angiopoietin-2 levels in the hepatic vein as a useful predictor of tumor invasiveness and prognosis in human hepatocellular carcinoma. *J. Gastroenterol. Hepatol.* **23**, e157-64 (2008).

129. Yoshiji, H. *et al.* Angiopoietin 2 displays a vascular endothelial growth factor dependent synergistic effect in hepatocellular carcinoma development in mice. *Gut* **54**, 1768–1775 (2005).

130. Villa, E. *et al.* Neoangiogenesis-related genes are hallmarks of fast-growing hepatocellular carcinomas and worst survival. Results from a prospective study. *Gut* **65**, 861–869 (2016).

131. Gao, L. *et al.* ANGPTL2 promotes tumor metastasis in hepatocellular carcinoma. *J. Gastroenterol. Hepatol.* **30**, 396–404 (2015).

132. Yang, L., Lu, W., Huang, G. & Wang, W. Correlation between CD105 expression and postoperative recurrence and metastasis of hepatocellular carcinoma. *BMC Cancer* **6**, 110 (2006).

133. Xiong, Y.-Q. *et al.* Human hepatocellular carcinoma tumor-derived endothelial cells manifest increased angiogenesis capability and drug resistance compared with normal endothelial cells. *Clin. cancer Res. an Off. J. Am. Assoc. Cancer Res.* **15**, 4838–4846 (2009).

134. M, R., D, P., T, O., E, P. & M, H. The immunology of hepatocellular carcinoma. *Nat. Immunol.* **19**, 222–232 (2018).

135. Roderburg, C., Wree, A., Demir, M., Schmelzle, M. & Tacke, F. The role of the innate immune system in the development and treatment of hepatocellular carcinoma. *Hepatic Oncol.* **7**, HEP17 (2020).

136. S, W., N, K., I, K., W, Z. & TH, W. Myeloid cells in hepatocellular carcinoma. *Hepatology* **62**, 1304–1312 (2015).

137. TA, B. & E, A. HYPE or HOPE: the prognostic value of infiltrating immune cells in cancer. *Br. J. Cancer* **117**, 451–460 (2017).

138. SG, K. & Y, T. Natural Killer Cells and T Cells in Hepatocellular Carcinoma and Viral Hepatitis: Current Status and Perspectives for Future Immunotherapeutic Approaches. *Cells* **10**, (2021).

139. AG, B., F, W., YH, O. & SI, K. Natural Killer Cells and Regulatory T Cells Cross Talk in Hepatocellular Carcinoma: Exploring Therapeutic Options for the Next Decade. *Front. Immunol.* **12**, (2021).

140. J, B., SL, C., PR, G., L, R. & B, S. Systemic treatment of hepatocellular carcinoma: An EASL position paper. *J. Hepatol.* (2021) doi:10.1016/J.JHEP.2021.07.004.

141. Finn, R. S. *et al.* Atezolizumab plus Bevacizumab in Unresectable Hepatocellular

Carcinoma. *N. Engl. J. Med.* **382**, 1894–1905 (2020).

142. RS, H. *et al.* Predictive correlates of response to the anti-PD-L1 antibody MPDL3280A in cancer patients. *Nature* **515**, 563–567 (2014).

143. JJ, W. *et al.* Atezolizumab in combination with bevacizumab enhances antigen-specific T-cell migration in metastatic renal cell carcinoma. *Nat. Commun.* **7**, (2016).

144. Finn, R. S. *et al.* Pembrolizumab As Second-Line Therapy in Patients With Advanced Hepatocellular Carcinoma in KEYNOTE-240: A Randomized, Double-Blind, Phase III Trial. *J. Clin. Oncol. Off. J. Am. Soc. Clin. Oncol.* **38**, 193–202 (2020).

145. Yau, T. *et al.* CheckMate 459: A randomized, multi-center phase III study of nivolumab (NIVO) vs sorafenib (SOR) as first-line (1L) treatment in patients (pts) with advanced hepatocellular carcinoma (aHCC). *Ann. Oncol.* (2019) doi:10.1093/annonc/mdz394.029.

146. Lee, M. S. *et al.* Atezolizumab with or without bevacizumab in unresectable hepatocellular carcinoma (GO30140): an open-label, multicentre, phase 1b study. *Lancet. Oncol.* **21**, 808–820 (2020).

147. Liu, L. *et al.* Sorafenib blocks the RAF/MEK/ERK pathway, inhibits tumor angiogenesis, and induces tumor cell apoptosis in hepatocellular carcinoma model PLC/PRF/5. *Cancer Res.* **66**, 11851–11858 (2006).

148. Wilhelm, S. M. *et al.* BAY 43-9006 exhibits broad spectrum oral antitumor activity and targets the RAF/MEK/ERK pathway and receptor tyrosine kinases involved in tumor progression and angiogenesis. *Cancer Res.* **64**, 7099–7109 (2004).

149. Feng, Y.-X. *et al.* Sorafenib suppresses postsurgical recurrence and metastasis of hepatocellular carcinoma in an orthotopic mouse model. *Hepatology* **53**, 483–492 (2011).

150. Geng, Z. *et al.* Sorafenib inhibition of hepatic stellate cell proliferation in tumor microenvironment of hepatocellular carcinoma: a study of the sorafenib mechanisms. *Cell Biochem. Biophys.* **69**, 717–724 (2014).

151. Iyer, R. V *et al.* Dose-Dependent Sorafenib-Induced Immunosuppression Is Associated with Aberrant NFAT Activation and Expression of PD-1 in T Cells. *Cancers (Basel).* **11**, (2019).

152. Llovet, J. M. *et al.* Sorafenib in advanced hepatocellular carcinoma. *N. Engl. J. Med.* **359**, 378–390 (2008).

153. Cheng, A.-L. *et al.* Efficacy and safety of sorafenib in patients in the Asia-Pacific region with advanced hepatocellular carcinoma: a phase III randomised, double-blind, placebo-controlled trial. *Lancet. Oncol.* **10**, 25–34 (2009).

154. Reig, M. *et al.* Early dermatologic adverse events predict better outcome in HCC patients treated with sorafenib. *J. Hepatol.* **61**, 318–324 (2014).

155. Rahmani, M., Davis, E. M., Bauer, C., Dent, P. & Grant, S. Apoptosis induced by the kinase inhibitor BAY 43-9006 in human leukemia cells involves down-regulation of Mcl-1 through inhibition of translation. *J. Biol. Chem.* **280**, 35217–35227 (2005).

156. Shimizu, S. *et al.* Inhibition of autophagy potentiates the antitumor effect of the multikinase inhibitor sorafenib in hepatocellular carcinoma. *Int. J. cancer* **131**, 548–557 (2012).

157. Tai, W.-T. *et al.* Mcl-1-dependent activation of Beclin 1 mediates autophagic cell death induced by sorafenib and SC-59 in hepatocellular carcinoma cells. *Cell Death Dis.* **4**, e485 (2013).

158. van Malenstein, H. *et al.* Long-term exposure to sorafenib of liver cancer cells induces resistance with epithelial-to-mesenchymal transition, increased invasion and risk of rebound growth. *Cancer Lett.* **329**, 74–83 (2013).

159. Chow, A. K.-M. *et al.* The Enhanced metastatic potential of hepatocellular carcinoma (HCC) cells with sorafenib resistance. *PLoS One* **8**, e78675 (2013).

160. Liang, Y. *et al.* Hypoxia-mediated sorafenib resistance can be overcome by EF24 through Von Hippel-Lindau tumor suppressor-dependent HIF-1α inhibition in hepatocellular carcinoma. *Hepatology* **57**, 1847–1857 (2013).

161. Dong, N. *et al.* M2 macrophages mediate sorafenib resistance by secreting HGF in a feed-forward manner in hepatocellular carcinoma. *Br. J. Cancer* **121**, 22–33 (2019).

162. Matsui, J. *et al.* Multi-kinase inhibitor E7080 suppresses lymph node and lung metastases of human mammary breast tumor MDA-MB-231 via inhibition of vascular endothelial growth factor-receptor (VEGF-R) 2 and VEGF-R3 kinase. *Clin. cancer Res. an Off. J. Am. Assoc. Cancer Res.* **14**, 5459–5465 (2008).

163. Adachi, Y. *et al.* Antitumor and Antiangiogenic Activities of Lenvatinib in Mouse Xenograft Models of Vascular Endothelial Growth Factor-Induced Hypervascular Human Hepatocellular Carcinoma. *Cancer Invest.* **37**, 185–198 (2019).

164. Hoshi, T. *et al.* Lenvatinib induces death of human hepatocellular carcinoma cells harboring an activated FGF signaling pathway through inhibition of FGFR-MAPK cascades. *Biochem. Biophys. Res. Commun.* **513**, 1–7 (2019).

165. Kimura, T. *et al.* Immunomodulatory activity of lenvatinib contributes to antitumor activity in the Hepa1-6 hepatocellular carcinoma model. *Cancer Sci.* **109**, 3993–4002 (2018).

166. Kudo, M. *et al.* Lenvatinib versus sorafenib in first-line treatment of patients with unresectable hepatocellular carcinoma: a randomised phase 3 non-inferiority trial. *Lancet (London, England)* **391**, 1163–1173 (2018).

167. Kodama, K. *et al.* Correlation between Early Tumor Marker Response and Imaging Response in Patients with Advanced Hepatocellular Carcinoma Treated with Lenvatinib. *Oncology* **97**, 75–81 (2019).

168. Chuma, M. *et al.* Early Changes in Circulating FGF19 and Ang-2 Levels as Possible Predictive Biomarkers of Clinical Response to Lenvatinib Therapy in Hepatocellular Carcinoma. *Cancers (Basel).* **12**, (2020).

169. Saeki, I. *et al.* Early Predictors of Objective Response in Patients with Hepatocellular Carcinoma Undergoing Lenvatinib Treatment. *Cancers (Basel).* **12**, (2020).

170. Takahashi, A. *et al.* Early Tumor Shrinkage as a Predictive Factor for Outcomes in

Hepatocellular Carcinoma Patients Treated with Lenvatinib: A Multicenter Analysis. *Cancers (Basel).* **12**, (2020).

171. Fu, R., Jiang, S., Li, J., Chen, H. & Zhang, X. Activation of the HGF/c-MET axis promotes lenvatinib resistance in hepatocellular carcinoma cells with high c-MET expression. *Med. Oncol.* **37**, 24 (2020).

172. Strumberg, D. & Schultheis, B. Regorafenib for cancer. *Expert Opin. Investig. Drugs* **21**, 879–889 (2012).

173. Carr, B. I. *et al.* Effects of low concentrations of regorafenib and sorafenib on human HCC cell AFP, migration, invasion, and growth in vitro. *J. Cell. Physiol.* **228**, 1344–1350 (2013).

174. Carr, B. I. *et al.* Fluoro-Sorafenib (Regorafenib) effects on hepatoma cells: Growth inhibition, quiescence, and recovery. *J. Cell. Physiol.* **228**, 292–297 (2013).

175. Han, R. & Li, S. Regorafenib delays the proliferation of hepatocellular carcinoma by inducing autophagy. *Pharmazie* **73**, 218–222 (2018).

176. Tsai, J.-J., Pan, P.-J. & Hsu, F.-T. Regorafenib induces extrinsic and intrinsic apoptosis through inhibition of ERK/NF-κB activation in hepatocellular carcinoma cells. *Oncol. Rep.* **37**, 1036–1044 (2017).

177. Liu, Y.-C., Wu, R.-H. & Wang, W.-S. Regorafenib diminishes the expression and secretion of angiogenesis and metastasis associated proteins and inhibits cell invasion via NF-κB inactivation in SK-Hep1 cells. *Oncol. Lett.* **14**, 461–467 (2017).

178. Chen, W. *et al.* Regorafenib reverses HGF-induced sorafenib resistance by inhibiting epithelial-mesenchymal transition in hepatocellular carcinoma. *FEBS Open Bio* **9**, 335–347 (2019).

179. Bruix, J. *et al.* Regorafenib for patients with hepatocellular carcinoma who progressed on sorafenib treatment (RESORCE): a randomised, double-blind, placebo-controlled, phase 3 trial. *Lancet (London, England)* **389**, 56–66 (2017).

180. Finn, R. S. *et al.* Outcomes of sequential treatment with sorafenib followed by regorafenib for HCC: Additional analyses from the phase III RESORCE trial. *J. Hepatol.* **69**, 353–358 (2018).

181. Yakes, F. M. *et al.* Cabozantinib (XL184), a novel MET and VEGFR2 inhibitor, simultaneously suppresses metastasis, angiogenesis, and tumor growth. *Mol. Cancer Ther.* **10**, 2298–2308 (2011).

182. Xiang, Q. *et al.* Cabozantinib suppresses tumor growth and metastasis in hepatocellular carcinoma by a dual blockade of VEGFR2 and MET. *Clin. Cancer Res.* **20**, 2959–2970 (2014).

183. Kelley, R. K. *et al.* Cabozantinib in hepatocellular carcinoma: results of a phase 2 placebo-controlled randomized discontinuation study. *Ann. Oncol. Off. J. Eur. Soc. Med. Oncol.* **28**, 528–534 (2017).

184. Abou-Alfa, G. K. *et al.* Cabozantinib in patients with advanced and progressing hepatocellular carcinoma. *N. Engl. J. Med.* **379**, 54–63 (2018).

185. Brahmer, J. R. *et al.* Phase I study of single-agent anti-programmed death-1 (MDX-1106) in refractory solid tumors: safety, clinical activity, pharmacodynamics, and immunologic correlates. *J. Clin. Oncol. Off. J. Am. Soc. Clin. Oncol.* **28**, 3167–3175 (2010).

186. El-Khoueiry, A. B. *et al.* Nivolumab in patients with advanced hepatocellular carcinoma (CheckMate 040): an open-label, non-comparative, phase 1/2 dose escalation and expansion trial. *Lancet* **389**, 2492–2502 (2017).

187. Sangro, B. *et al.* Association of inflammatory biomarkers with clinical outcomes in nivolumab-treated patients with advanced hepatocellular carcinoma. *J. Hepatol.* (2020) doi:10.1016/j.jhep.2020.07.026.

188. Kim, C. G. *et al.* Hyperprogressive disease during PD-1 blockade in patients with advanced hepatocellular carcinoma. *J. Hepatol.* (2020) doi:10.1016/j.jhep.2020.08.010.

189. Yau, T. *et al.* Efficacy and Safety of Nivolumab Plus Ipilimumab in Patients With Advanced Hepatocellular Carcinoma Previously Treated With Sorafenib. *JAMA Oncol.* (2020) doi:10.1001/jamaoncol.2020.4564.

190. Zhu, A. X. *et al.* Pembrolizumab in patients with advanced hepatocellular carcinoma previously treated with sorafenib (KEYNOTE-224): a non-randomised, open-label phase 2 trial. *Lancet. Oncol.* **19**, 940–952 (2018).

191. Kudo, M. *et al.* Ramucirumab as second-line treatment in patients with advanced hepatocellular carcinoma: Japanese subgroup analysis of the REACH trial. *J. Gastroenterol.* **52**, 494–503 (2017).

192. Zhu, A. X. *et al.* Ramucirumab after sorafenib in patients with advanced hepatocellular carcinoma and increased α-fetoprotein concentrations (REACH-2): a randomised, double-blind, placebo-controlled, phase 3 trial. *Lancet Oncol.* **20**, 282–296 (2019).

193. Kudo, M. *et al.* Ramucirumab after prior sorafenib in patients with advanced hepatocellular carcinoma and elevated alpha-fetoprotein: Japanese subgroup analysis of the REACH-2 trial. *J. Gastroenterol.* **55**, 627–639 (2020).

194. Fuchs, Y. & Steller, H. Live to die another way: modes of programmed cell death and the signals emanating from dying cells. *Nat. Rev. Mol. Cell Biol.* **16**, 329–344 (2015).

195. Hengartner, M. O. The biochemistry of apoptosis. *Nature* **407**, 770–776 (2000).

196. Thornberry, N. A. & Lazebnik, Y. Caspases: enemies within. *Science* **281**, 1312–1316 (1998).

197. Kerr, J. F. R., Wyllie, A. H. & Currie, A. R. Apoptosis: A Basic Biological Phenomenon with Wideranging Implications in Tissue Kinetics. *Br. J. Cancer* **26**, 239–257 (1972).

198. Elmore, S. Apoptosis: a review of programmed cell death. *Toxicol. Pathol.* **35**, 495–516 (2007).

199. Savill, J. & Fadok, V. Corpse clearance defines the meaning of cell death. *Nature* **407**, 784–788 (2000).

200. Wu, H., Medeiros, L. J. & Young, K. H. Apoptosis signaling and BCL-2 pathways provide

opportunities for novel targeted therapeutic strategies in hematologic malignances. *Blood Rev.* **32**, 8–28 (2018).

201. Locksley, R. M., Killeen, N. & Lenardo, M. J. The TNF and TNF receptor superfamilies: integrating mammalian biology. *Cell* **104**, 487–501 (2001).

202. Ashkenazi, A. & Dixit, V. M. Death receptors: signaling and modulation. *Science* **281**, 1305–1308 (1998).

203. Schleich, K., Krammer, P. H. & Lavrik, I. N. The chains of death: a new view on caspase-8 activation at the DISC. *Cell cycle (Georgetown, Tex.)* vol. 12 193–194 (2013).

204. Scaffidi, C., Schmitz, I., Krammer, P. H. & Peter, M. E. The role of c-FLIP in modulation of CD95-induced apoptosis. *J. Biol. Chem.* **274**, 1541–1548 (1999).

205. Pfeffer, C. M. & Singh, A. T. K. Apoptosis: A Target for Anticancer Therapy. *Int. J. Mol. Sci.* **19**, (2018).

206. Singh, R., Letai, A. & Sarosiek, K. Regulation of apoptosis in health and disease: the balancing act of BCL-2 family proteins. *Nat. Rev. Mol. Cell Biol.* **20**, 175–193 (2019).

207. Garrido, C. *et al.* Mechanisms of cytochrome c release from mitochondria. *Cell Death Differ.* **13**, 1423–1433 (2006).

208. Marabese, M., Mazzoletti, M., Vikhanskaya, F. & Broggini, M. HtrA2 enhances the apoptotic functions of p73 on bax. *Cell Death Differ.* **15**, 849–858 (2008).

209. Joza, N. *et al.* Essential role of the mitochondrial apoptosis-inducing factor in programmed cell death. *Nature* **410**, 549–554 (2001).

210. Kothakota, S. *et al.* Caspase-3-generated fragment of gelsolin: effector of morphological change in apoptosis. *Science* **278**, 294–298 (1997).

211. Slee, E. A., Adrain, C. & Martin, S. J. Executioner caspase-3, -6, and -7 perform distinct, non-redundant roles during the demolition phase of apoptosis. *J. Biol. Chem.* **276**, 7320–7326 (2001).

212. Fadok, V. A., A, de C., Daleke, D. L., Henson, P. M. & Bratton, D. L. Loss of phospholipid asymmetry and surface exposure of phosphatidylserine is required for phagocytosis of apoptotic cells by macrophages and fibroblasts. *J. Biol. Chem.* **276**, 1071–1077 (2001).

213. Brunner, T. *et al.* Fas (CD95/Apo-1) ligand regulation in T cell homeostasis, cell-mediated cytotoxicity and immune pathology. *Semin. Immunol.* **15**, 167–176 (2003).

214. Trapani, J. A. & Smyth, M. J. Functional significance of the perforin/granzyme cell death pathway. *Nat. Rev. Immunol.* **2**, 735–747 (2002).

215. Pardo, J. *et al.* Apoptotic pathways are selectively activated by granzyme A and/or granzyme B in CTL-mediated target cell lysis. *J. Cell Biol.* **167**, 457–468 (2004).

216. Russell, J. H. & Ley, T. J. Lymphocyte-mediated cytotoxicity. *Annu. Rev. Immunol.* **20**, 323–370 (2002).

217. Metkar, S. S. *et al.* Granzyme B activates procaspase-3 which signals a mitochondrial

amplification loop for maximal apoptosis. *J. Cell Biol.* **160**, 875–885 (2003).

218. Martinvalet, D., Dykxhoorn, D. M., Ferrini, R. & Lieberman, J. Granzyme A cleaves a mitochondrial complex I protein to initiate caspase-independent cell death. *Cell* **133**, 681–692 (2008).

219. Nakayama, K. *et al.* Disappearance of the lymphoid system in Bcl-2 homozygous mutant chimeric mice. *Science* **261**, 1584–1588 (1993).

220. Czabotar, P. E., Lessene, G., Strasser, A. & Adams, J. M. Control of apoptosis by the BCL-2 protein family: implications for physiology and therapy. *Nat. Rev. Mol. Cell Biol.* **15**, 49–63 (2014).

221. Kvansakul, M. & Hinds, M. G. The Bcl-2 family: structures, interactions and targets for drug discovery. *Apoptosis* **20**, 136–150 (2015).

222. Certo, M. *et al.* Mitochondria primed by death signals determine cellular addiction to antiapoptotic BCL-2 family members. *Cancer Cell* **9**, 351–365 (2006).

223. Willis, S. N. *et al.* Apoptosis initiated when BH3 ligands engage multiple Bcl-2 homologs, not Bax or Bak. *Science* **315**, 856–859 (2007).

224. Kale, J., Osterlund, E. J. & Andrews, D. W. BCL-2 family proteins: Changing partners in the dance towards death. *Cell Death Differ.* **25**, 65–80 (2018).

225. Wong, W. W.-L. & Puthalakath, H. Bcl-2 family proteins: the sentinels of the mitochondrial apoptosis pathway. *IUBMB Life* **60**, 390–397 (2008).

226. Ryan, J., Montero, J., Rocco, J. & Letai, A. iBH3: simple, fixable BH3 profiling to determine apoptotic priming in primary tissue by flow cytometry. *Biol. Chem.* **397**, 671–678 (2016).

227. Montero, J. *et al.* Drug-Induced death signaling strategy rapidly predicts cancer response to chemotherapy. *Cell* **160**, 977–989 (2015).

228. Whitfield, J. R., Beaulieu, M.-E. & Soucek, L. Strategies to Inhibit Myc and Their Clinical Applicability. *Front. cell Dev. Biol.* **5**, 10 (2017).

229. Ashkenazi, A., Fairbrother, W. J., Leverson, J. D. & Souers, A. J. From basic apoptosis discoveries to advanced selective BCL-2 family inhibitors. *Nat. Rev. Drug Discov.* **16**, 273–284 (2017).

230. Montero, J. & Letai, A. Why do BCL-2 inhibitors work and where should we use them in the clinic? *Cell Death Differ.* **25**, 56–64 (2018).

231. Konopleva, M. *et al.* Mechanisms of antileukemic activity of the novel Bcl-2 homology domain-3 mimetic GX15-070 (obatoclax). *Cancer Res.* **68**, 3413–3420 (2008).

232. Trudel, S. *et al.* Preclinical studies of the pan-Bcl inhibitor obatoclax (GX015-070) in multiple myeloma. *Blood* **109**, 5430–5438 (2007).

233. Brown, J. R. *et al.* Obatoclax in combination with fludarabine and rituximab is well-tolerated and shows promising clinical activity in relapsed chronic lymphocytic leukemia. *Leuk. Lymphoma* **56**, 3336–3342 (2015).

234. Oliver, C. L. *et al.* (-)-Gossypol acts directly on the mitochondria to overcome Bcl-2- and Bcl-X(L)-mediated apoptosis resistance. *Mol. Cancer Ther.* **4**, 23–31 (2005).

235. Y, Z., J, M., L, X. & D, W. Natural Product Gossypol and its Derivatives in Precision Cancer Medicine. *Curr. Med. Chem.* **26**, 1849–1873 (2019).

236. Schelman, W. R. *et al.* A phase I study of AT-101 with cisplatin and etoposide in patients with advanced solid tumors with an expanded cohort in extensive-stage small cell lung cancer. *Invest. New Drugs* **32**, 295–302 (2014).

237. Arnold, A. A. *et al.* Preclinical studies of Apogossypolone: a new nonpeptidic pan small-molecule inhibitor of Bcl-2, Bcl-XL and Mcl-1 proteins in Follicular Small Cleaved Cell Lymphoma model. *Mol. Cancer* **7**, 20 (2008).

238. Wang, X. *et al.* A Novel Bioavailable BH3 Mimetic Efficiently Inhibits Colon Cancer via Cascade Effects of Mitochondria. *Clin. cancer Res. an Off. J. Am. Assoc. Cancer Res.* **22**, 1445–1458 (2016).

239. Oltersdorf, T. *et al.* An inhibitor of Bcl-2 family proteins induces regression of solid tumours. *Nature* **435**, 677–681 (2005).

240. Adams, J. M. & Cory, S. The BCL-2 arbiters of apoptosis and their growing role as cancer targets. *Cell Death Differ.* **25**, 27–36 (2018).

241. Tse, C. *et al.* ABT-263: a potent and orally bioavailable Bcl-2 family inhibitor. *Cancer Res.* **68**, 3421–3428 (2008).

242. Li, J. *et al.* ABT-263 enhances sorafenib-induced apoptosis associated with Akt activity and the expression of Bax and p21((CIP1/WAF1)) in human cancer cells. *Br. J. Pharmacol.* **171**, 3182–3195 (2014).

243. Zhu, Y. *et al.* Identification of a novel senolytic agent, navitoclax, targeting the Bcl-2 family of anti-apoptotic factors. *Aging Cell* **15**, 428–435 (2016).

244. Shahbandi, A. *et al.* BH3 mimetics selectively eliminate chemotherapy-induced senescent cells and improve response in TP53 wild-type breast cancer. *Cell Death Differ.* **27**, 3097–3116 (2020).

245. Li, F. *et al.* FBP1 loss disrupts liver metabolism and promotes tumorigenesis through a hepatic stellate cell senescence secretome. *Nat. Cell Biol.* **22**, 728–739 (2020).

246. Roberts, A. W. *et al.* Substantial susceptibility of chronic lymphocytic leukemia to BCL2 inhibition: results of a phase I study of navitoclax in patients with relapsed or refractory disease. *J. Clin. Oncol. Off. J. Am. Soc. Clin. Oncol.* **30**, 488–496 (2012).

247. Kipps, T. J. *et al.* A phase 2 study of the BH3 mimetic BCL2 inhibitor navitoclax (ABT-263) with or without rituximab, in previously untreated B-cell chronic lymphocytic leukemia. *Leuk. Lymphoma* **56**, 2826–2833 (2015).

248. Vlahovic, G. *et al.* A phase I safety and pharmacokinetic study of ABT-263 in combination with carboplatin/paclitaxel in the treatment of patients with solid tumors. *Invest. New Drugs* **32**, 976–984 (2014).

249. Cleary, J. M. *et al.* A phase I clinical trial of navitoclax, a targeted high-affinity Bcl-2 family inhibitor, in combination with gemcitabine in patients with solid tumors. *Invest. New Drugs* **32**, 937–945 (2014).

250. ClinicalTrials.gov, N. U. S. N. L. of M. Navitoclax and Sorafenib Tosylate in Treating Patients With Relapsed or Refractory Solid Tumors. https://www.clinicaltrials.gov/ct2/show/NCT02143401?term=abt-263&cond=hepatocellular+carcinoma&draw=2&rank=1.

251. Sleebs, B. E. *et al.* Quinazoline sulfonamides as dual binders of the proteins B-cell lymphoma 2 and B-cell lymphoma extra long with potent proapoptotic cell-based activity. *J. Med. Chem.* **54**, 1914–1926 (2011).

252. Bai, L. *et al.* BM-1197: a novel and specific Bcl-2/Bcl-xL inhibitor inducing complete and long-lasting tumor regression in vivo. *PLoS One* **9**, e99404 (2014).

253. Némati, F. *et al.* Targeting Bcl-2/Bcl-XL induces antitumor activity in uveal melanoma patient-derived xenografts. *PLoS One* **9**, e80836 (2014).

254. Loriot, Y. *et al.* Radiosensitization by a novel Bcl-2 and Bcl-XL inhibitor S44563 in small-cell lung cancer. *Cell Death Dis.* **5**, e1423 (2014).

255. Adam, A. *et al.* A Dual Bcl-2/xL Inhibitor Induces Tumor Cell Apoptosis in a Hematopoietic Xenograft Model. *Blood* **124**, 5304 (2014).

256. Balachander, S. B. *et al.* AZD4320, A Dual Inhibitor of Bcl-2 and Bcl-x(L), Induces Tumor Regression in Hematologic Cancer Models without Dose-limiting Thrombocytopenia. *Clin. cancer Res. an Off. J. Am. Assoc. Cancer Res.* **26**, 6535–6549 (2020).

257. Patterson, C. M. *et al.* Design and optimisation of dendrimer-conjugated Bcl-2/x(L) inhibitor, AZD0466, with improved therapeutic index for cancer therapy. *Commun. Biol.* **4**, 112 (2021).

258. M, L. & MA, A. Review of Venetoclax in CLL, AML and Multiple Myeloma. *J. Pers. Med.* **11**, (2021).

259. Fresquet, V., Rieger, M., Carolis, C., García-Barchino, M. J. & Martinez-Climent, J. A. Acquired mutations in BCL2 family proteins conferring resistance to the BH3 mimetic ABT-199 in lymphoma. *Blood* **123**, 4111–4119 (2014).

260. Zhao, X. *et al.* BCL2 Amplicon Loss and Transcriptional Remodeling Drives ABT-199 Resistance in B Cell Lymphoma Models. *Cancer Cell* **35**, 752-766.e9 (2019).

261. Song, T. *et al.* Bcl-2 phosphorylation confers resistance on chronic lymphocytic leukaemia cells to the BH3 mimetics ABT-737, ABT-263 and ABT-199 by impeding direct binding. *Br. J. Pharmacol.* **173**, 471–483 (2016).

262. Lok, S. W. *et al.* A Phase Ib Dose-Escalation and Expansion Study of the BCL2 Inhibitor Venetoclax Combined with Tamoxifen in ER and BCL2-Positive Metastatic Breast Cancer. *Cancer Discov.* **9**, 354–369 (2019).

263. Lu, P. *et al.* Safety and pharmacodynamics of venetoclax (ABT-199) in a randomized single and multiple ascending dose study in women with systemic lupus erythematosus.

Lupus **27**, 290–302 (2018).

264. Casara, P. *et al.* S55746 is a novel orally active BCL-2 selective and potent inhibitor that impairs hematological tumor growth. *Oncotarget* **9**, 20075–20088 (2018).

265. Leverson, J. D. *et al.* Exploiting selective BCL-2 family inhibitors to dissect cell survival dependencies and define improved strategies for cancer therapy. *Sci. Transl. Med.* **7**, 279ra40 (2015).

266. Lessene, G. *et al.* Structure-guided design of a selective BCL-X(L) inhibitor. *Nat. Chem. Biol.* **9**, 390–397 (2013).

267. de Jong, Y. *et al.* Bcl-xl as the most promising Bcl-2 family member in targeted treatment of chondrosarcoma. *Oncogenesis* **7**, 74 (2018).

268. Zhu, Y. *et al.* New agents that target senescent cells: the flavone, fisetin, and the BCL-X(L) inhibitors, A1331852 and A1155463. *Aging (Albany. NY).* **9**, 955–963 (2017).

269. Moncsek, A. *et al.* Targeting senescent cholangiocytes and activated fibroblasts with B-cell lymphoma-extra large inhibitors ameliorates fibrosis in multidrug resistance 2 gene knockout (Mdr2−/−) mice. *Hepatology* **67**, 247–259 (2018).

270. Sasaki, M., Sato, Y. & Nakanuma, Y. Increased p16INK4a-expressing senescent bile ductular cells are associated with inadequate response to ursodeoxycholic acid in primary biliary cholangitis. *J. Autoimmun.* **107**, (2019).

271. Doi, K. *et al.* Discovery of marinopyrrole A (maritoclax) as a selective Mcl-1 antagonist that overcomes ABT-737 resistance by binding to and targeting Mcl-1 for proteasomal degradation. *J. Biol. Chem.* **287**, 10224–10235 (2012).

272. Leverson, J. D. *et al.* Potent and selective small-molecule MCL-1 inhibitors demonstrate on-target cancer cell killing activity as single agents and in combination with ABT-263 (navitoclax). *Cell Death Dis.* **6**, e1590 (2015).

273. Quentmeier, H. *et al.* Diffuse Large B Cell Lymphoma Cell Line U-2946: Model for MCL1 Inhibitor Testing. *PLoS One* **11**, e0167599 (2016).

274. Zhang, H. *et al.* Targeting Mcl-1 inhibits survival and self-renewal of hepatocellular cancer stem-like cells. *Clin. Res. Hepatol. Gastroenterol.* **43**, 292–300 (2019).

275. Kotschy, A. *et al.* The MCL1 inhibitor S63845 is tolerable and effective in diverse cancer models. *Nature* **538**, 477–482 (2016).

276. Song, X. *et al.* Mcl-1 inhibition overcomes intrinsic and acquired regorafenib resistance in colorectal cancer. *Theranostics* **10**, 8098–8110 (2020).

277. Alcon, C. *et al.* Sequential combinations of chemotherapeutic agents with BH3 mimetics to treat rhabdomyosarcoma and avoid resistance. *Cell Death Dis.* **11**, 634 (2020).

278. Kehr, S. *et al.* Targeting BCL-2 proteins in pediatric cancer: Dual inhibition of BCL-X(L) and MCL-1 leads to rapid induction of intrinsic apoptosis. *Cancer Lett.* **482**, 19–32 (2020).

279. Bierbrauer, A., Jacob, M., Vogler, M. & Fulda, S. A direct comparison of selective BH3-mimetics reveals BCL-X(L), BCL-2 and MCL-1 as   promising therapeutic targets in

neuroblastoma. *Br. J. Cancer* **122**, 1544–1551 (2020).

280. Bohler, S. *et al.* Inhibition of the anti-apoptotic protein MCL-1 severely suppresses human hematopoiesis. *Haematologica* **Online ahe**, (2020).

281. ClinicalTrials.gov, N. U. S. N. L. of M. Study of AZD5991 Alone or in Combination With Venetoclax in Relapsed or Refractory Haematologic Malignancies. https://clinicaltrials.gov/ct2/show/NCT03218683?term=azd5991&draw=2&rank=1.

282. Szlavik, Z. *et al.* Discovery of S64315, a Potent and Selective Mcl-1 Inhibitor. *J. Med. Chem.* **63**, 13762–13795 (2020).

283. Caenepeel, S. *et al.* AMG 176, a Selective MCL1 Inhibitor, Is Effective in Hematologic Cancer Models Alone and in Combination with Established Therapies. *Cancer Discov.* **8**, 1582–1597 (2018).

284. Yi, X. *et al.* AMG-176, an Mcl-1 Antagonist, Shows Preclinical Efficacy in Chronic Lymphocytic Leukemia. *Clin. cancer Res. an Off. J. Am. Assoc. Cancer Res.* **26**, 3856–3867 (2020).

285. Snezhkina, A. V *et al.* ROS Generation and Antioxidant Defense Systems in Normal and Malignant Cells. *Oxid. Med. Cell. Longev.* **2019**, 6175804 (2019).

286. Marí, M. *et al.* Mitochondrial glutathione: Features, regulation and role in disease. *Biochim. Biophys. Acta - Gen. Subj.* **1830**, 3317–3328 (2013).

287. Marí, M. *et al.* Mitochondrial Glutathione: Recent Insights and Role in Disease. *Antioxidants (Basel, Switzerland)* **9**, (2020).

288. Ippolito, L., Giannoni, E., Chiarugi, P. & Parri, M. Mitochondrial Redox Hubs as Promising Targets for Anticancer Therapy. *Front. Oncol.* **10**, 1–12 (2020).

289. Snezhkina, A. V *et al.* ROS Generation and Antioxidant Defense Systems in Normal and Malignant Cells. *Oxid. Med. Cell. Longev.* **2019**, 6175804 (2019).

290. Piccolo, M. T., Menale, C. & Crispi, S. Combined anticancer therapies: an overview of the latest applications. *Anticancer. Agents Med. Chem.* **15**, 408–422 (2015).

291. H, Y. *et al.* The role of cellular reactive oxygen species in cancer chemotherapy. *J. Exp. Clin. Cancer Res.* **37**, (2018).

292. Rahmani, M. *et al.* The kinase inhibitor sorafenib induces cell death through a process involving induction of endoplasmic reticulum stress. *Mol. Cell. Biol.* **27**, 5499–5513 (2007).

293. Wang, R., Xia, L., Gabrilove, J., Waxman, S. & Jing, Y. Downregulation of Mcl-1 through GSK-3β activation contributes to arsenic trioxide-induced apoptosis in acute myeloid leukemia cells. *Leukemia* **27**, 315–324 (2013).

294. Kim, E. H., Kim, M.-S. & Jung, W.-G. The mechanisms responsible for the radiosensitizing effects of sorafenib on colon cancer cells. *Oncol. Rep.* **32**, 2421–2428 (2014).

295. Gillissen, B. *et al.* Bax/Bak-independent mitochondrial depolarization and reactive oxygen species induction by sorafenib overcome resistance to apoptosis in renal cell carcinoma. *J. Biol. Chem.* **292**, 6478–6492 (2017).

296. Chakraborty, S. *et al.* Activation of c-Met in cancer cells mediates growth-promoting signals against oxidative stress through Nrf2-HO-1. *Oncogenesis* **8**, 7 (2019).

297. Park, M. A. *et al.* Vorinostat and sorafenib increase CD95 activation in gastrointestinal tumor cells through a Ca(2+)-de novo ceramide-PP2A-reactive oxygen species-dependent signaling pathway. *Cancer Res.* **70**, 6313–6324 (2010).

298. Coriat, R. *et al.* Sorafenib-induced hepatocellular carcinoma cell death depends on reactive oxygen species production in vitro and in vivo. *Mol. Cancer Ther.* **11**, 2284–2293 (2012).

299. Zhang, J. *et al.* Effects of 31 FDA approved small-molecule kinase inhibitors on isolated rat liver mitochondria. *Arch. Toxicol.* **91**, 2921–2938 (2017).

300. Belli, V. *et al.* Regorafenib in combination with silybin as a novel potential strategy for the treatment of metastatic colorectal cancer. *Oncotarget* **8**, 68305–68316 (2017).

301. Mingard, C., Paech, F., Bouitbir, J. & Krähenbühl, S. Mechanisms of toxicity associated with six tyrosine kinase inhibitors in human hepatocyte cell lines. *J. Appl. Toxicol.* **38**, 418–431 (2018).

302. Paech, F. *et al.* Mechanisms of mitochondrial toxicity of the kinase inhibitors ponatinib, regorafenib and sorafenib in human hepatic HepG2 cells. *Toxicology* **395**, 34–44 (2018).

303. Zheng, A. *et al.* CRISPR/Cas9 genome-wide screening identifies KEAP1 as a sorafenib, lenvatinib, and regorafenib sensitivity gene in hepatocellular carcinoma. *Oncotarget* **10**, 7058–7070 (2019).

304. Prasad, S., Gupta, S. C. & Tyagi, A. K. Reactive oxygen species (ROS) and cancer: Role of antioxidative nutraceuticals. *Cancer Lett.* **387**, 95–105 (2017).

305. Cockfield, J. A. & Schafer, Z. T. Antioxidant Defenses: A Context-Specific Vulnerability of Cancer Cells. *Cancers (Basel).* **11**, (2019).

306. Griffith, O. W. & Meister, A. Potent and specific inhibition of glutathione synthesis by buthionine sulfoximine (S-n-butyl homocysteine sulfoximine). *J. Biol. Chem.* **254**, 7558–7560 (1979).

307. Oestreicher, J. & Morgan, B. Glutathione: subcellular distribution and membrane transport (1). *Biochem. Cell Biol.* **97**, 270–289 (2019).

308. Dierickx, P. J. Long-term buthionine-sulfoximine-mediated toxicity in cultured hepatoma cell lines. *Res. Commun. Chem. Pathol. Pharmacol.* **67**, 423–426 (1990).

309. Huang, Z. Z. *et al.* Mechanism and significance of increased glutathione level in human hepatocellular carcinoma and liver regeneration. *FASEB J. Off. Publ. Fed. Am. Soc. Exp. Biol.* **15**, 19–21 (2001).

310. Kito, M., Akao, Y., Ohishi, N., Yagi, K. & Nozawa, Y. Arsenic trioxide-induced apoptosis and its enhancement by buthionine sulfoximine in hepatocellular carcinoma cell lines. *Biochem. Biophys. Res. Commun.* **291**, 861–867 (2002).

311. Oketani, M. *et al.* Inhibition by arsenic trioxide of human hepatoma cell growth. *Cancer*

Lett. **183**, 147–153 (2002).

312. Sun, X. *et al.* Activation of the p62-Keap1-NRF2 pathway protects against ferroptosis in hepatocellular carcinoma cells. *Hepatology* **63**, 173–184 (2016).

313. Lippmann, J., Petri, K., Fulda, S. & Liese, J. Redox Modulation and Induction of Ferroptosis as a New Therapeutic Strategy in Hepatocellular Carcinoma. *Transl. Oncol.* **13**, 100785 (2020).

314. O'Dwyer, P. J. *et al.* Phase I trial of buthionine sulfoximine in combination with melphalan in patients with cancer. *J. Clin. Oncol. Off. J. Am. Soc. Clin. Oncol.* **14**, 249–256 (1996).

315. Bailey, H. H. *et al.* Phase I study of continuous-infusion L-S,R-buthionine sulfoximine with intravenous melphalan. *J. Natl. Cancer Inst.* **89**, 1789–1796 (1997).

316. Villablanca, J. G. *et al.* A Phase I New Approaches to Neuroblastoma Therapy Study of Buthionine Sulfoximine and Melphalan With Autologous Stem Cells for Recurrent/Refractory High-Risk Neuroblastoma. *Pediatr. Blood Cancer* **63**, 1349–1356 (2016).

317. Day, B. J. & Crapo, J. D. A metalloporphyrin superoxide dismutase mimetic protects against paraquat-induced lung injury in vivo. *Toxicol. Appl. Pharmacol.* **140**, 94–100 (1996).

318. Lluis, J. M. *et al.* GD3 synthase overexpression sensitizes hepatocarcinoma cells to hypoxia and reduces tumor growth by suppressing the cSrc/NF-kappaB survival pathway. *PLoS One* **4**, e8059 (2009).

319. Yang, J., Qiu, B., Li, X., Zhang, H. & Liu, W. p53-p66(shc)/miR-21-Sod2 signaling is critical for the inhibitory effect of betulinic acid on hepatocellular carcinoma. *Toxicol. Lett.* **238**, 1–10 (2015).

320. Liese, J., Hinrichs, T. M., Lange, M. & Fulda, S. Cotreatment with sorafenib and oleanolic acid induces reactive oxygen species-dependent and mitochondrial-mediated apoptotic cell death in hepatocellular carcinoma cells. *Anticancer. Drugs* **30**, 209–217 (2019).

321. Baulies, A. *et al.* The 2-oxoglutarate carrier promotes liver cancer by sustaining mitochondrial GSH despite cholesterol loading. *Redox Biol.* **14**, 164–177 (2018).

322. Yan, Q.-G. *et al.* Overexpression of CYP2E1 enhances sensitivity of hepG2 cells to fas-mediated cytotoxicity. *Cancer Biol. Ther.* **7**, 1280–1287 (2008).

323. Guo, W. *et al.* Disruption of xCT inhibits cell growth via the ROS/autophagy pathway in hepatocellular carcinoma. *Cancer Lett.* **312**, 55–61 (2011).

324. Son, Y. W., Cheon, M. G., Kim, Y. & Jang, H. H. Prx2 links ROS homeostasis to stemness of cancer stem cells. *Free Radic. Biol. Med.* **134**, 260–267 (2019).

325. Chiou, J.-F. *et al.* Sorafenib induces preferential apoptotic killing of a drug- and radio-resistant Hep G2 cells through a mitochondria-dependent oxidative stress mechanism. *Cancer Biol. Ther.* **8**, 1904–1913 (2009).

326. Duval, A. P., Troquier, L., de Souza Silva, O., Demartines, N. & Dormond, O. Diclofenac

Potentiates Sorafenib-Based Treatments of Hepatocellular Carcinoma by Enhancing Oxidative Stress. *Cancers (Basel).* **11**, (2019).

327. Li, Z.-J. *et al.* Artesunate synergizes with sorafenib to induce ferroptosis in hepatocellular carcinoma. *Acta Pharmacol. Sin.* **42**, 301–310 (2021).

328. Li, Y. *et al.* Sorafenib induces mitochondrial dysfunction and exhibits synergistic effect with cysteine depletion by promoting HCC cells ferroptosis. *Biochem. Biophys. Res. Commun.* **534**, 877–884 (2021).

329. Ke, Y. *et al.* Reduced glutathione ameliorates liver function, oxidative stress and inflammation after interventional therapy for hepatocellular carcinoma. *J. BUON.* **25**, 1361–1367 (2020).

330. Choi, A. M. K., Ryter, S. W. & Levine, B. Autophagy in human health and disease. *N. Engl. J. Med.* **368**, 651–662 (2013).

331. Mizushima, N. & Komatsu, M. Autophagy: renovation of cells and tissues. *Cell* **147**, 728–741 (2011).

332. Reggiori, F., Komatsu, M., Finley, K. & Simonsen, A. Autophagy: more than a nonselective pathway. *Int. J. Cell Biol.* **2012**, 219625 (2012).

333. Turco, E. & Martens, S. Insights into autophagosome biogenesis from in vitro reconstitutions. *J. Struct. Biol.* **196**, 29–36 (2016).

334. Youle, R. J. & Narendra, D. P. Mechanisms of mitophagy. *Nat. Rev. Mol. Cell Biol.* **12**, 9–14 (2011).

335. Tanida, I. Autophagy basics. *Microbiol. Immunol.* **55**, 1–11 (2011).

336. Vara-Perez, M., Felipe-Abrio, B. & Agostinis, P. Mitophagy in Cancer: A Tale of Adaptation. *Cells* **8**, (2019).

337. Ashrafi, G. & Schwarz, T. L. The pathways of mitophagy for quality control and clearance of mitochondria. *Cell Death Differ.* **20**, 31–42 (2013).

338. Greene, A. W. *et al.* Mitochondrial processing peptidase regulates PINK1 processing, import and Parkin recruitment. *EMBO Rep.* **13**, 378–385 (2012).

339. Kondapalli, C. *et al.* PINK1 is activated by mitochondrial membrane potential depolarization and stimulates Parkin E3 ligase activity by phosphorylating Serine 65. *Open Biol.* **2**, 120080 (2012).

340. Wong, Y. C. & Holzbaur, E. L. F. Optineurin is an autophagy receptor for damaged mitochondria in parkin-mediated mitophagy that is disrupted by an ALS-linked mutation. *Proc. Natl. Acad. Sci. U. S. A.* **111**, E4439-48 (2014).

341. Geisler, S. *et al.* PINK1/Parkin-mediated mitophagy is dependent on VDAC1 and p62/SQSTM1. *Nat. Cell Biol.* **12**, 119–131 (2010).

342. Bernardini, J. P., Lazarou, M. & Dewson, G. Parkin and mitophagy in cancer. *Oncogene* **36**, 1315–1327 (2017).

343. Novak, I. *et al.* Nix is a selective autophagy receptor for mitochondrial clearance. *EMBO Rep.* **11**, 45–51 (2010).

344. Ney, P. A. Mitochondrial autophagy: Origins, significance, and role of BNIP3 and NIX. *Biochim. Biophys. Acta* **1853**, 2775–2783 (2015).

345. Bellot, G. *et al.* Hypoxia-induced autophagy is mediated through hypoxia-inducible factor induction of BNIP3 and BNIP3L via their BH3 domains. *Mol. Cell. Biol.* **29**, 2570–2581 (2009).

346. Real, P. J. *et al.* Blockade of epidermal growth factor receptors chemosensitizes breast cancer cells through up-regulation of Bnip3L. *Cancer Res.* **65**, 8151–8157 (2005).

347. Dhingra, R. *et al.* Bidirectional regulation of nuclear factor-κB and mammalian target of rapamycin signaling functionally links Bnip3 gene repression and cell survival of ventricular myocytes. *Circ. Heart Fail.* **6**, 335–343 (2013).

348. Chaanine, A. H. *et al.* FOXO3a regulates BNIP3 and modulates mitochondrial calcium, dynamics, and function in cardiac stress. *Am. J. Physiol. Heart Circ. Physiol.* **311**, H1540–H1559 (2016).

349. Landes, T. *et al.* The BH3-only Bnip3 binds to the dynamin Opa1 to promote mitochondrial fragmentation and apoptosis by distinct mechanisms. *EMBO Rep.* **11**, 459–465 (2010).

350. Liu, K. E. & Frazier, W. A. Phosphorylation of the BNIP3 C-Terminus Inhibits Mitochondrial Damage and Cell Death without Blocking Autophagy. *PLoS One* **10**, e0129667 (2015).

351. Rogov, V. V *et al.* Phosphorylation of the mitochondrial autophagy receptor Nix enhances its interaction with LC3 proteins. *Sci. Rep.* **7**, 1131 (2017).

352. Kanki, T. Nix, a receptor protein for mitophagy in mammals. *Autophagy* **6**, 433–435 (2010).

353. Liu, L. *et al.* Mitochondrial outer-membrane protein FUNDC1 mediates hypoxia-induced mitophagy in mammalian cells. *Nat. Cell Biol.* **14**, 177–185 (2012).

354. Wu, W. *et al.* ULK1 translocates to mitochondria and phosphorylates FUNDC1 to regulate mitophagy. *EMBO Rep.* **15**, 566–575 (2014).

355. Sekine, S. *et al.* Rhomboid protease PARL mediates the mitochondrial membrane potential loss-induced cleavage of PGAM5. *J. Biol. Chem.* **287**, 34635–34645 (2012).

356. Chen, M. *et al.* Mitophagy receptor FUNDC1 regulates mitochondrial dynamics and mitophagy. *Autophagy* **12**, 689–702 (2016).

357. Wang, Z., Jiang, H., Chen, S., Du, F. & Wang, X. The mitochondrial phosphatase PGAM5 functions at the convergence point of multiple necrotic death pathways. *Cell* **148**, 228–243 (2012).

358. Richter-Dennerlein, R. *et al.* DNAJC19, a mitochondrial cochaperone associated with cardiomyopathy, forms a complex with prohibitins to regulate cardiolipin remodeling. *Cell Metab.* **20**, 158–171 (2014).

359. Strappazzon, F. *et al.* AMBRA1 is able to induce mitophagy via LC3 binding, regardless of PARKIN and p62/SQSTM1. *Cell Death Differ.* **22**, 419–432 (2015).

360. Lampert, M. A. *et al.* BNIP3L/NIX and FUNDC1-mediated mitophagy is required for mitochondrial network remodeling during cardiac progenitor cell differentiation. *Autophagy* **15**, 1182–1198 (2019).

361. Bhujabal, Z. *et al.* FKBP8 recruits LC3A to mediate Parkin-independent mitophagy. *EMBO Rep.* **18**, 947–961 (2017).

362. Yamano, K. *et al.* Endosomal Rab cycles regulate Parkin-mediated mitophagy. *Elife* **7**, (2018).

363. Kulikov, A. V, Luchkina, E. A., Gogvadze, V. & Zhivotovsky, B. Mitophagy: Link to cancer development and therapy. *Biochem. Biophys. Res. Commun.* **482**, 432–439 (2017).

364. Kim, J.-H. *et al.* Involvement of mitophagy in oncogenic K-Ras-induced transformation: overcoming a cellular energy deficit from glucose deficiency. *Autophagy* **7**, 1187–1198 (2011).

365. Thomas, H. E. *et al.* mTOR inhibitors synergize on regression, reversal of gene expression, and autophagy in hepatocellular carcinoma. *Sci. Transl. Med.* **4**, 139ra84 (2012).

366. Liu, K. *et al.* Phosphorylated AKT inhibits the apoptosis induced by DRAM-mediated mitophagy in hepatocellular carcinoma by preventing the translocation of DRAM to mitochondria. *Cell Death Dis.* **5**, e1078 (2014).

367. Zhang, C., Song, Z. & Yu, G. High expression of Parkin predicts easier recurrence of patients with adjuvant transarterial chemoembolization. *Biomark. Med.* **11**, 823–834 (2017).

368. Liu, K. *et al.* Mitophagy Controls the Activities of Tumor Suppressor p53 to Regulate Hepatic Cancer Stem Cells. *Mol. Cell* **68**, 281-292.e5 (2017).

369. Owada, S. *et al.* Autophagy-mediated adaptation of hepatocellular carcinoma cells to hypoxia-mimicking conditions constitutes an attractive therapeutic target. *Oncol. Rep.* **39**, 1805–1812 (2018).

370. Chen, Y. *et al.* Ketoconazole exacerbates mitophagy to induce apoptosis by downregulating cyclooxygenase-2 in hepatocellular carcinoma. *J. Hepatol.* **70**, 66–77 (2019).

371. Chen, H.-N., Chen, Y., Zhou, Z.-G., Wei, Y. & Huang, C. A novel role for ketoconazole in hepatocellular carcinoma treatment: linking PTGS2 to mitophagy machinery. *Autophagy* **15**, 733–734 (2019).

372. Sheng, J. *et al.* Inhibition of PI3K/mTOR increased the sensitivity of hepatocellular carcinoma cells to cisplatin via interference with mitochondrial-lysosomal crosstalk. *Cell Prolif.* **52**, e12609 (2019).

373. Ma, M., Lin, X.-H., Liu, H.-H., Zhang, R. & Chen, R.-X. Suppression of DRP1-mediated mitophagy increases the apoptosis of hepatocellular carcinoma cells in the setting of chemotherapy. *Oncol. Rep.* **43**, 1010–1018 (2020).

374. Lin, X.-H. *et al.* Suppressing DRP1-mediated mitochondrial fission and mitophagy

increases mitochondrial apoptosis of hepatocellular carcinoma cells in the setting of hypoxia. *Oncogenesis* **9**, 67 (2020).

375. Yoo, Y.-S. *et al.* Mitochondria ubiquitin ligase, MARCH5 resolves hepatitis B virus X protein aggregates in the liver pathogenesis. *Cell Death Dis.* **10**, 938 (2019).

376. Chen, Y.-Y. *et al.* BNIP3L-Dependent Mitophagy Promotes HBx-Induced Cancer Stemness of Hepatocellular Carcinoma Cells via Glycolysis Metabolism Reprogramming. *Cancers (Basel).* **12**, (2020).

377. Hara, Y. *et al.* Iron loss triggers mitophagy through induction of mitochondrial ferritin. *EMBO Rep.* **21**, e50202 (2020).

378. Aman, Y., Cao, S. & Fang, E. F. Iron out, mitophagy in! A way to slow down hepatocellular carcinoma. *EMBO reports* vol. 21 e51652 (2020).

379. Zhao, Y. *et al.* Nuclear-Encoded lncRNA MALAT1 Epigenetically Controls Metabolic Reprogramming in HCC Cells through the Mitophagy Pathway. *Mol. Ther. Nucleic Acids* **23**, 264–276 (2021).

380. Inokuchi, S. *et al.* Suppression of optineurin impairs the progression of hepatocellular carcinoma through regulating mitophagy. *Cancer Med.* **10**, 1501–1514 (2021).

381. Xiang, X. *et al.* Cellular senescence in hepatocellular carcinoma induced by a long non-coding RNA-encoded peptide PINT87aa by blocking FOXM1-mediated PHB2. *Theranostics* **11**, 4929–4944 (2021).

382. Prieto-Domínguez, N. *et al.* Melatonin enhances sorafenib actions in human hepatocarcinoma cells by inhibiting mTORC1/p70S6K/HIF-1α and hypoxia-mediated mitophagy. *Oncotarget* **8**, 91402–91414 (2017).

383. Prieto-Domínguez, N. *et al.* Melatonin-induced increase in sensitivity of human hepatocellular carcinoma cells to sorafenib is associated with reactive oxygen species production and mitophagy. *J. Pineal Res.* **61**, 396–407 (2016).

384. Wu, H. *et al.* Mitophagy promotes sorafenib resistance through hypoxia-inducible ATAD3A dependent Axis. *J. Exp. Clin. Cancer Res.* **39**, 274 (2020).

385. Zhang, C. *et al.* Sorafenib targets the mitochondrial electron transport chain complexes and ATP synthase to activate the PINK1-Parkin pathway and modulate cellular drug response. *J. Biol. Chem.* **292**, 15105–15120 (2017).

386. Zheng, Y. *et al.* STOML2 potentiates metastasis of hepatocellular carcinoma by promoting PINK1-mediated mitophagy and regulates sensitivity to lenvatinib. *J. Hematol. Oncol.* **14**, 16 (2021).

387. Denizot, F. & Lang, R. Rapid colorimetric assay for cell growth and survival. Modifications to the tetrazolium dye procedure giving improved sensitivity and reliability. *J. Immunol. Methods* **89**, 271–277 (1986).

388. Reers, M., Smith, T. W. & Chen, L. B. J-Aggregate Formation of a Carbocyanine as a Quantitative Fluorescent Indicator of Membrane Potential. *Biochemistry* **30**, 4480–4486 (1991).

389.   Smiley, S. T. *et al.* Intracellular heterogeneity in mitochondrial membrane potentials revealed by a J-aggregate-forming lipophilic cation JC-1. *Proc. Natl. Acad. Sci.* **88**, 3671–3675 (1991).

390.   Di Veroli, G. Y. *et al.* Combenefit: an interactive platform for the analysis and visualization of drug combinations. *Bioinformatics* **32**, 2866–2868 (2016).

391.   Bruix, J., Chan, S. L., Galle, P. R., Rimassa, L. & Sangro, B. Systemic treatment of hepatocellular carcinoma: An EASL position paper. *J. Hepatol.* (2021) doi:10.1016/j.jhep.2021.07.004.

392.   Faqar-Uz-Zaman, S. F., Heinicke, U., Meister, M. T., Vogler, M. & Fulda, S. BCL-xL-selective BH3 mimetic sensitizes rhabdomyosarcoma cells to chemotherapeutics by activation of the mitochondrial pathway of apoptosis. *Cancer Lett.* **412**, 131–142 (2018).

393.   Khan, S. *et al.* A selective BCL-XL PROTAC degrader achieves safe and potent antitumor activity. *Nat. Med.* **25**, 1938–1947 (2019).

394.   Sies, H. Oxidative stress: a concept in redox biology and medicine. *Redox Biol.* **4**, 180–183 (2015).

395.   Reczek, C. R. *et al.* A CRISPR screen identifies a pathway required for paraquat-induced cell death. *Nat. Chem. Biol.* **13**, 1274–1279 (2017).

396.   Lee, M. *et al.* 3-bromopyruvate and buthionine sulfoximine effectively kill anoikis-resistant hepatocellular carcinoma cells. *PLoS One* **12**, e0174271 (2017).

397.   Klauser, E., Gülden, M., Maser, E., Seibert, S. & Seibert, H. Additivity, antagonism, and synergy in arsenic trioxide-induced growth inhibition of C6 glioma cells: effects of genistein, quercetin and buthionine-sulfoximine. *Food Chem. Toxicol. an Int. J. Publ. Br. Ind. Biol. Res. Assoc.* **67**, 212–221 (2014).

398.   Salvemini, D. *et al.* A nonpeptidyl mimic of superoxide dismutase with therapeutic activity in rats. *Science* **286**, 304–306 (1999).

399.   Morales, A. *et al.* Tumor necrosis factor increases hepatocellular glutathione by transcriptional regulation of the heavy subunit chain of gamma-glutamylcysteine synthetase. *J. Biol. Chem.* **272**, 30371–30379 (1997).

400.   Llacuna, L. *et al.* Reactive oxygen species mediate liver injury through parenchymal nuclear factor-kappaB inactivation in prolonged ischemia/reperfusion. *Am. J. Pathol.* **174**, 1776–1785 (2009).

401.   Forman, H. J. & Zhang, H. Targeting oxidative stress in disease: promise and limitations of antioxidant therapy. *Nat. Rev. Drug Discov.* 1–21 (2021) doi:10.1038/s41573-021-00233-1.

402.   Hayes, J. D., Dinkova-Kostova, A. T. & Tew, K. D. Oxidative Stress in Cancer. *Cancer Cell* **38**, 167–197 (2020).

403.   Williamson, J., Hughes, C. M., Cobley, J. N. & Davison, G. W. The mitochondria-targeted antioxidant MitoQ, attenuates exercise-induced mitochondrial DNA damage. *Redox Biol.* **36**, 101673 (2020).

404. Ribeiro Junior, R. F. *et al.* MitoQ improves mitochondrial dysfunction in heart failure induced by pressure overload. *Free Radic. Biol. Med.* **117**, 18–29 (2018).

405. Ježek, J., Cooper, K. F. & Strich, R. The Impact of Mitochondrial Fission-Stimulated ROS Production on Pro-Apoptotic Chemotherapy. *Biology (Basel).* **10**, (2021).